NEA NUCLEAR SCIENCE COMMITTEE

TASK FORCE ON COMPUTING RADIATION DOSE AND MODELLING
OF RADIATION-INDUCED DEGRADATION OF REACTOR COMPONETS

PREDICTION OF NEUTRON EMBRITTLEMENT IN THE REACTOR PRESSURE VESSEL:

VENUS-1 AND VENUS-3 BENCHMARKS

NUCLEAR ENERGY AGENCY
ORGANISATION FOR ECONOMIC CO-OPERATION AND DEVELOPMENT

ORGANISATION FOR ECONOMIC CO-OPERATION AND DEVELOPMENT

Pursuant to Article 1 of the Convention signed in Paris on 14th December 1960, and which came into force on 30th September 1961, the Organisation for Economic Co-operation and Development (OECD) shall promote policies designed:

- to achieve the highest sustainable economic growth and employment and a rising standard of living in Member countries, while maintaining financial stability, and thus to contribute to the development of the world economy;
- to contribute to sound economic expansion in Member as well as non-member countries in the process of economic development; and
- to contribute to the expansion of world trade on a multilateral, non-discriminatory basis in accordance with international obligations.

The original Member countries of the OECD are Austria, Belgium, Canada, Denmark, France, Germany, Greece, Iceland, Ireland, Italy, Luxembourg, the Netherlands, Norway, Portugal, Spain, Sweden, Switzerland, Turkey, the United Kingdom and the United States. The following countries became Members subsequently through accession at the dates indicated hereafter: Japan (28th April 1964), Finland (28th January 1969), Australia (7th June 1971), New Zealand (29th May 1973), Mexico (18th May 1994), the Czech Republic (21st December 1995), Hungary (7th May 1996), Poland (22nd November 1996) and the Republic of Korea (12th December 1996). The Commission of the European Communities takes part in the work of the OECD (Article 13 of the OECD Convention).

NUCLEAR ENERGY AGENCY

The OECD Nuclear Energy Agency (NEA) was established on 1st February 1958 under the name of the OEEC European Nuclear Energy Agency. It received its present designation on 20th April 1972, when Japan became its first non-European full Member. NEA membership today consists of 27 OECD Member countries: Australia, Austria, Belgium, Canada, Czech Republic, Denmark, Finland, France, Germany, Greece, Hungary, Iceland, Ireland, Italy, Japan, Luxembourg, Mexico, the Netherlands, Norway, Portugal, Republic of Korea, Spain, Sweden, Switzerland, Turkey, the United Kingdom and the United States. The Commission of the European Communities also takes part in the work of the Agency.

The mission of the NEA is:

- to assist its Member countries in maintaining and further developing, through international co-operation, the scientific, technological and legal bases required for a safe, environmentally friendly and economical use of nuclear energy for peaceful purposes, as well as
- to provide authoritative assessments and to forge common understandings on key issues, as input to government decisions on nuclear energy policy and to broader OECD policy analyses in areas such as energy and sustainable development.

Specific areas of competence of the NEA include safety and regulation of nuclear activities, radioactive waste management, radiological protection, nuclear science, economic and technical analyses of the nuclear fuel cycle, nuclear law and liability, and public information. The NEA Data Bank provides nuclear data and computer program services for participating countries.

In these and related tasks, the NEA works in close collaboration with the International Atomic Energy Agency in Vienna, with which it has a Co-operation Agreement, as well as with other international organisations in the nuclear field.

FOREWORD

In response to a request from the NEA Committee on Safety of Nuclear Installations (CSNI), the NEA Nuclear Science Committee (NSC) set up an expert group to review the state of the art in the modelling of radiation-induced degradation of reactor components. The computational techniques and the claimed accuracies obtained in these calculations were also reviewed. The findings were published in a NEA report in January 1997.

As a follow-up to the above mentioned state-of-the-art report, the NSC expert group launched two blind benchmarks to verify the claimed accuracies and to validate the calculation methods used. Both benchmarks were based on the VENUS experiments performed at SCK•CEN Mol, Belgium, one being a two-dimensional (VENUS-1) and the other a three-dimensional benchmark (VENUS-3).

This report provides the detailed results from the two benchmarks. The results reveal that, in comparison with the calculations for the two-dimensional cases, a full three-dimensional calculation generally gives values much closer to the experimental values.

The conclusion is that full three-dimensional calculations provide decisive improvements in the prediction of reactor pressure vessel embrittlement due to neutron irradiation.

Acknowledgements

Special thanks to all participants who were willing to devote their time to this endeavour and to SCK•CEN (Mol) Belgium for the valuable experimental results provided for this benchmark exercise.

TABLE OF CONTENTS

List of tables

List of figures

EXECUTIVE SUMMARY

It is essential to accurately calculate neutron fluence and fluence rates at more than one location in order to assess and predict pressure vessel embrittlement and thereby ensure the safe operation of nuclear power plants.

A NEA Nuclear Science Committee Task Force on the Computing Radiation Dose and Modelling of Radiation-Induced Degradation of Reactor Components was established to review this problem. During an earlier stage of its work the task force reviewed the state of the art in calculation methodologies for neutron and gamma fluence in reactor vessels and published a report. Two blind benchmarks were then launched to verify the statements in the report.

The main objectives of these two benchmarks are:

1) To make a critical analysis and verification of each of the national methodologies.

2) To establish a clear international consensus regarding the current level of accuracy of the pressure vessel fluence predictions, using the latest nuclear data and state-of-the-art transport codes versus the experimental data.

3) To quantify the relative merits of different calculation methods and to identify a possibility to improve these methods (possible advantage of fully three-dimensional methods over two-dimensional methods).

Among the experiments available, the VENUS configurations from SCK•CEN Mol, Belgium, offered the exceptional advantage of exhibiting a realistic radial core shape and a neutron spectrum that is typical of PWRs, thus being particularly appropriate for this kind of exercise.

In the first benchmark, 2-D calculations were performed to describe the VENUS-1 configuration. In view of the results of this 2-D benchmark, it was felt that a full 3-D transport calculation was necessary, and the VENUS-3 configuration was therefore modelled in three dimensions.

Different modelling assumptions and calculation methods (deterministic and stochastic methods) were used by the participants in these benchmarks, as well as different nuclear data, both for the transport and the dosimetry calculations.

After having performed a detailed analysis of the results of the two benchmark exercises, it can be stated that the three objectives above have been achieved.

Concerning the dosimetry calculation methods, the main finding was that the calculated results of the three-dimensional benchmark (VENUS-3) are in general much closer to the experimental values than those for the two-dimensional benchmark (VENUS-1).

Chapter 1

INTRODUCTION

As many commercial light water reactors begin to approach the end of their licensed lifetime, nuclear utilities have started to investigate the possibility of extending the operating life of reactors beyond the originally licensed 30-40 years. Longer reactor operating times mean higher neutron and gamma fluence levels and/or smaller safety margins, in view of which reactor utilities/owners and regulators need to be able to ensure the integrity of reactor components and reduce still further the uncertainties in fluence estimation procedures. It is of paramount importance to be able to accurately characterise the structural integrity of reactor components so as to make correct decisions on design plant lifetime, safety margins and potential plant lifetime extension, as well to avoid controversial judgements that might prematurely shut down "still operational" nuclear power plants. Ensuring reactor pressure vessel (RPV) integrity is important for safety as well as for economical reasons, due to the possibility of plant life extensions. High energy neutron bombardment degrades the structural integrity of RPVs. In order to ensure the integrity of the RPV, therefore, neutron fluence must be predicted with a high degree of accuracy.

Because of the importance of this issue, the OECD/NEA Task Force on Computing Radiation Dose and Modelling of Radiation-Induced Degradation of Reactor Components (TFRDD) reviewed the current computation techniques for calculating neutron and gamma doses to reactor components and described in considerable detail the methods presently used in NEA Member countries for computing long-term cumulative dose rates [1].

Although the median of results reported in national calculations appeared to lie within the 20% difference between the calculated and measured values, significantly higher or lower values were also reported. Moreover, the numbers reported were very difficult to compare given that each country has its own methodology, including different reactors, computer codes, nuclear data and measurement procedures. On the basis of these country reports, the working group concluded that no firm judgement could be formed on the current international level of accuracy in pressure vessel fluence calculations.

Therefore, to verify the statement made in the report and to better identify the range of differences between calculations and measurements, the TFRDD launched an international blind intercomparison exercise.

Various methodologies are applied to predict dose rates in the Belgian VENUS test reactor [2,3], calculating in both two-dimensional (VENUS-1) and three-dimensional (VENUS-3) configurations for comparison with measured data.

Among the experiments available, the VENUS configurations offered the exceptional advantage of exhibiting a realistic radial core shape and a neutron spectrum that is typical of PWRs. The VENUS experiments are particularly suitable for benchmarking the capabilities of the calculational methodology and cross-section libraries for the prediction of fluence rates in RPVs because VENUS has a very clean structural geometry representing standard PWR pressure vessel conditions.

The task force started with two-dimensional benchmark calculations representing the VENUS-1 configuration. About 20 different calculations were presented from 10 institutions world-wide in a blind test, without the participants having any advance knowledge of the measured results.

Equivalent fission fluxes for five different threshold reactions, namely ^{58}Ni(n,p), ^{115}In(n,n′), ^{103}Rh(n,n′), ^{238}U(n,f) and ^{237}Np(n,f), were calculated at 34 detector positions at the core mid-plane level in both steel and water zones for comparison with experimental results. Fast neutron fluxes (above 1 MeV and 0.1 MeV) and DPA rates, which are needed to correlate material damage in the surveillance capsules to the pressure vessel wall in order to obtain the so-called lead factors, had also been supplied. Several 2-D S_N codes were applied, including the newest versions available [4], but use was also made of an in-house code BOXER and as well as a version of the Monte Carlo code MCNP [5,6]. The transport cross-sections were based on ENDF/B-VI [7] or JEF-2.2 [8] and the dosimetry data on IRDF-90 Version 2 [9].

Given the complex geometry of the reactor core and surrounding components, a three-dimensional neutron transport calculation was necessary in order to avoid the limitations resulting from the approximations in two-dimensional modelling and to better estimate a three-dimensional distribution of fluences.

The most challenging task was therefore to validate the latest versions of three-dimensional transport codes, given the complex configuration of VENUS-3, which contains dummy partial length elements. About 14 independent benchmark calculations were supplied by eight institutions. In order to verify the complex three-dimensional fast neutron field in detail, the number of detector positions was increased significantly to more than 200 ^{58}Ni(n,p) detectors, about 100 ^{115}In(n,n′) detectors and nearly 50 ^{27}Al(n,α) detectors. Two versions of the 3-D S_N code TORT [10], the 3-D parallel S_N code PENTRAN [11] and two versions of the Monte Carlo code MCNP were applied. Likewise the transport cross-sections were taken from ENDF/B-VI or JEF-2.2 and the dosimetry data from IRDF-90 Version 2. The energy groups in the S_N calculations were split up into the BUGLE-96 [12] structure (47 neutron groups) used for routine shielding calculations requiring modest effort and calculations to a higher degree of accuracy based on the EURLIB structure (100 neutron groups) and the VITAMIN-J structure (175 neutron groups).

For a long time it was thought that two-dimensional neutron fluence calculations and the corresponding synthesis methods were sufficient for routine applications. But the conclusion can clearly be drawn from both benchmarks that the calculated results of the three-dimensional benchmark (VENUS-3) are in general much closer to the experimental values than those of the two-dimensional benchmark (VENUS-1). This demonstrates the inherent deficiencies of two-dimensional transport calculations which suffer from approximations such as diffusion-based axial buckling corrections and proper axial averaging of the source particles or shielding materials. The powerful computers now available can easily perform full three-dimensional neutron fluence calculations, the results of which are significantly more accurate than those obtained from two-dimensional calculations.

CHAPTER 2

Objectives of the benchmarks

Based on the country reports on the state of the art in computational dosimetry, no firm judgement can be formed on:

1) The current international level of accuracy in pressure vessel fluence calculations. Compared with various reaction rates measured at surveillance positions of power reactors a large variety of differences between measurements and calculations have been reported which do not allow firm conclusions on the accuracy achieved in neutron fluence calculations.

2) The relative merits of various methodologies and hence the areas of possible improvements in various calculational schemes.

Therefore, to solve these urgent problems, two benchmark calculations were proposed and carried out world-wide. As the basis for the calculations, two well-defined and precisely measured PWR mock-ups were taken. They are:

1) VENUS-1: Two-Dimensional Benchmark on Ex-Core Dosimetry Computations.

2) VENUS-3: Three-Dimensional Benchmark on Ex-Core Dosimetry Computations.

The main objectives of these two benchmarks are:

1) To make a critical analysis and verification of each of the national methodologies used.

2) To establish an unequivocal international consensus regarding the current level of accuracy of the pressure vessel fluence predictions using the latest nuclear data and state-of-the-art transport codes versus the experimental data.

3) To quantify the relative merits of different calculation methods and to identify a possibility of improving these methods (advantage of full 3-D methods over 2-D methods).

The full specifications of benchmarks VENUS-1 and VENUS-3 can be found in Appendix A.1 and A.2, respectively.

CHAPTER 3

Participants, methods, and data

3.1 VENUS-1

A total of 20 solutions were contributed for the VENUS-1 benchmark from a total of nine countries (10 institutions). A full list of contributors is given below (see also Table 3.1), together with details of the codes and nuclear data used by the contributors.

1. ***Siemens AG, Germany***
   Participant: J. Koban
   Code: DOT4.2
   Cross-section library: EURLIB-VI/N 175 (using NJOY-91 & ENDF/B-VI Rev. 2)
   Response functions: IRDF-90 V.2
   Remarks:

2. ***SCK·CEN, Belgium***
   Participant: H. Aït Abderrahim
   Code: LEPRICON (based on DORT4.3 and ANISN)
   Cross-section library: ELXSIR (based on ENDF/B-V Rev. Mod 3)
   Response functions: ENDF/B-V
   Remarks: The synthesis available in LEPRICON is not used in this exercise because the measured results are located at core mid-plane.

3. ***VTT/ENE, Finland***
   Participant: F. Wasastjerna
   Code: DORT
   Cross-section library: BUGLE-80, BUGLE-93, BUGLE-96T
   Response functions: IRDF-90 V.2 or ENDF/B-VI
   Remarks:

4. ***IKE University of Stuttgart, Germany***
   Participant: G. Hehn, A. Sohn, M. Mattes and G. Pfister
   Code: DORT3.1
   Cross-section library: VIT-J
   Response functions: IRDF-90 V.2
   Remarks:

5. ***ENEA-Centro Ricerche "E. Clementel", Italy***
   Participant: M. Pescarini, M.G. Borgia and R. Orsi
   Code: DORT3.1
   Cross-section library: BUGLE-96
   Response functions: IRDF-90 V.2
   Remarks:

6. ***NRG (former ECN), The Netherlands***
   Participant: R. van der Stad
   Code: MCNP-4A
   Cross-section library: EJ2-MCNP based on JEF-2.2
   Response functions: IRDF-90 V.2
   Remarks:

7. ***Paul Scherrer Institute (PSI), Switzerland***
   Participant: J.M. Paratte
   Code: BOXER
   Cross-section library: ETOBOX (JEFF-1) for iron, ENDF/B-IV
   Response functions:
   Remarks:

8. ***Korea Power Engineering Co. (KOPEC), Korea***
   Participant: B.J. Moon and H.R. Hwang
   Code: DORT2.8.14
   Cross-section library: BUGLE-96
   Response functions: BUGLE-96 and IRDF-90 V.2 for Rh reaction
   Remarks:

9. ***Japan Atomic Energy Institute (JAERI) and Sumitomo Atomic Energy Industries, Japan***
   Participant: M. Suzuki, K. Kosako and Y. Sakamoto
   Code: DORT
   Cross-section library: JENDL-3.2
   Response functions: IRDF-90 V.2
   Remarks:

10. ***Centro Atómico Bariloche (CAB), Argentina***
    Participant: A.F. Albornoz and E.M. Lopasso
    Code: DORT
    Cross-section library: BUGLE-96
    Response functions: IRDF-90 V.2
    Remarks:

3.2 VENUS-3

A total of 14 solutions were contributed for the VENUS-3 benchmark from a total of seven countries (eight institutions). A full list of contributors is given below (see also Table 3.2), together with details of the codes and nuclear data used by the contributors. The results from the Oak Ridge National Laboratory were taken from the report "Analysis of the VENUS-3 Experiments" (August 1989, NUREG/CR-5338, ORNL/TM-11106) by R.E. Maerker [13].

1. ***OECD/NEA, France***
   Participant: I. Kodeli (Consultant)
   Code: TORT
   Cross-section library: BUGLE-96
   Response functions: IRDF-90 V.2
   Remarks:

2. ***CSN, UNESA, DENIM, CIEMAT, TECNATOM, Spain***
   Participant: J.M. Perlado, J. Marián and J. García Sanz
   Code: MCNP-4B
   Cross-section library: ENDF/B-VI and DLC189/MCNPXS
   Response functions: IRDF-90 V.2
   Remarks:

3. ***Korea Power Engineering Co. (KOPEC), Korea***
   Participant: B.J. Moon and H.R. Hwang
   Code: TORT
   Cross-section library: BUGLE-96
   Response functions: IRDF-90 V.2
   Remarks:

4. ***Siemens AG, Germany***
   Participant: W. Hofmann and J. Koban
   Code: TORT2.7.3
   Cross-section library: EURLIB-VI/N 175 (ENDF/B-VI)
   Response functions: IRDF-90 V.2
   Remarks:

5. ***IKE University of Stuttgart, Germany***
   Participant: G. Hehn, A. Sohn, M. Mattes and G. Pfister
   Code: TORT3.1
   Cross-section library: BUGLE-96 (low precision) and VIT-J (high precision)
   Response functions: BUGLE-96 and IRDF-90 V.2
   Remarks:

6. ***NRG (former ECN), The Netherlands***
   Participant: R. van der Stad and A. Hogenbirk
   Code: MCNP-4A
   Cross-section library: EJ2-MCNP (based on JEF-2.2)
   Response functions: IRDF-90 V.2
   Remarks:

7. ***Penn State University[1], USAF Academy[2], and SCK·CEN[3], USA and Belgium***
   Participant: A. Haghighat[1], G. Sjoden[2] and H. Aït Abderrahim[3]
   Code: PENTRAN
   Cross-section library: BUGLE-96
   Response functions: BUGLE-96 and ELXSIR for DPA cross-sections
   Remarks: PENTRAN (a 3-D parallel S_N code) has been operated on an IBM SP2 with 32 processors

8. ***Oak Ridge National Laboratory (ORNL), USA***
   Participant: R.E. Maerker
   Code: DOT4 and ANISN
   Cross-section library: ELXSIR (ENDF/B-IV and V)
   Response functions:
   Remarks:

CHAPTER 4

Benchmark results of VENUS-1

In the past, the prediction of neutron embrittlement in pressure vessel material was based mainly on one- and two-dimensional transport calculations. The results of the VENUS-1 benchmark thus reflect the degree of accuracy obtained in calculating fast neutron fluences in two-dimensional geometry. Equivalent fission fluxes had been measured for five reactions, namely ^{58}Ni(n,p), ^{115}In(n,n′), ^{103}Rh(n,n′), ^{238}U(n,f) and ^{237}Np(n,f).

The detectors were placed along the core mid-plane at 34 locations in the outer core region, the core baffle, the water reflector, the core barrel and the neutron pad (see Figure 4.1). Using this arrangement, the calculated equivalent fission fluxes could be checked from the major neutron sources in the outer core region up to the neutron pad and the second water layer on the inner side of the pressure vessel. Additionally, the theoretical quantities, i.e. fluxes above 1 MeV, above 0.1 MeV and DPA rates are investigated. The VENUS-1 measurements represent the complex structure of the vessel internals, but do not cover the vessel wall itself.

The benchmark results supplied were dominated by 2-D S_N methods, with eight contributors, one Monte Carlo application and one in-house transport code comparable to BOXER. *Calculation details supplied by participants are given in Appendix B.1.*

4.1 Comparison of calculated equivalent fission fluxes with measurements

All the benchmark calculation results supplied by contributors were correlated to the measurement and plotted as C/E values in Figures 4.2 to 4.6 separately for each type of reaction. The experimental equivalent fission fluxes are given in Tables 4.1 and 4.2 for stainless steel zones and water zones, respectively.

The Ni detector covers the flux above 3 MeV. The results for the ^{58}Ni(n,p) detector progressively deteriorate outside the core across the water and stainless steel zones. The experimental results for the Ni detector in the barrel region are suspected to be 10% too high (due to a possible error of power level re-scaling after the experiment). Even though the doubtful experimental results in the barrel region are taken into account, a decreasing trend in C/E is still observed when moving towards the outside of the core. This means that the diffusion buckling correction cannot give a valid result for the Ni detector, especially outside the core because of its high energy response.

The results for the ^{115}In(n,n′) detector are consistently good (better than for the Ni detector) and do not display any significant degradation when moving away from the core. It is worth noting this point since the In detector is a very important detector, covering the flux above 1 MeV and corresponding to the local variation of the DPA rate.

The initial results obtained for the ^{103}Rh(n,n′) detector using ENDF/B-VI and IRDF-90 Version 2 cross-sections reflect the large difference in the Rh cross-section given in these two data files.

The ENEA (Italy) made a comparative study on the basis of these two files. This study clearly shows that the ^{103}Rh cross-sections in BUGLE-96 are not good and that IRDF-90 Version 2 cross-sections yield consistent results compared with the experimental data [14].

The measurements for the ^{238}U(n,f) detector include the photo-fission effect plus approximately 4%, which is not contained in all calculations. The C/E results must therefore be adjusted by +4%.

The experimental results for the ^{237}Np(n,f) reaction also include the photo-fission effect plus approximately 3%, which is not included in the calculated results. The C/E results must therefore be adjusted by +3%. SCK·CEN (Belgium), KOPEC (Korea) [15], CAB (Argentina) [16] and ENEA (Italy) [17] subsequently took into account the thermal cut-off attributable to the Cd screen around the Np detector, which had not been stated in the original specification of the benchmark.

For detector positions at an angle $\theta = 45°$ the accuracy of calculations is lower and deteriorates as the distance from the core increases. This trend is shown in Figures 4.7 to 4.11 for each type of detector, and is mainly attributable to the lack of material symmetry which is assumed with reflective boundary condition.

4.2 Comparison of theoretical quantities

The theoretical quantities considered in the benchmarks are important parameters for the prediction of neutron embrittlement in pressure vessel material. The lead factors, expressed as the ratio of fast neutron fluence or DPA between several surveillance capsules and the crucial parts of the pressure vessel, are used to correlate the neutron damage in the pressure vessel to the measured embrittlement of the material probes in the surveillance capsules. In order to compare the calculated fast neutron fluxes or DPA rates of the benchmarks, it would be possible to plot absolute or better relative values provided that a suitable conceptual framework could be established. In a detailed diagnostic analysis of the VENUS benchmarks it has been shown that the complex spatial dependence of the In reaction rate (or equivalent fission flux) is exactly proportional to the fast neutron flux above 1 MeV and also to the DPA rate [18]. In an approximation it can also be applied to the fast neutron flux above 0.1 MeV. Therefore it was reasonable to correlate all three theoretical quantities with the same C/E values of the In equivalent fission flux and to define a divisor representing the theoretical quantity of a reference calculation (e.g. IKE 7 calculation or any other) weighted with the relevant reciprocal C/E values of In.

The absolute values of the calculated DPA rate are compared in Figure 4.12(a), showing a rather broad scatter band of ±20% over all detector positions. Further details can be obtained from the relative values of the DPA rate, as shown in Figure 4.12(b). The main difference lies in the two types of iron DPA cross-section used, the old ASTM data and current data produced from ENDF/B-VI or JEF-2.2, which differ by 20% [18].

The inherent deficiencies of two-dimensional transport calculations, which suffer from approximations such as diffusion based axial buckling corrections and proper axial averaging of sources or material configurations, have a strong influence on the comparison of fast neutron fluxes. This is shown in Figures 4.13(a) and 4.13(b) for the neutron flux above 1 MeV, and in Figures 4.14(a) and 4.14(b) for the neutron flux above 0.1 MeV.

4.3 Summary of VENUS-1 results

The results reveal that the main source of inaccuracy in the VENUS-1 results is the diffusion theory based buckling correction which works best within the reactor core but fails outside of the core, resulting in an underestimation of reaction rates by ~10% at those detector positions. This general trend might be due to the buckling correction, as for the ^{58}Ni detector case. The VENUS-1 core is very small (50 cm of axial length). Thus, the axial profile at the core mid-plane is not as flat as it is in taller cores and the buckling correction fails when it tries to represent the axial leakage, especially the fast one. This effect could be reduced with an adequate choice of the diffusion coefficient. A more or less extended practice for small cores is to take D = 1 cm for all energy groups, which reduces leakage from the higher energy groups more than that from epithermal groups. This results in a general overestimation in calculations, but this increase will be greater at positions far from the core, and then the observed underestimation of C/E at those positions will be reduced [16,18]. The main problem in 2-D dosimetry calculations is determining the right buckling correction.

KOPEC examined three different methodologies to treat axial leakage in two-dimensional calculations. These three methodologies are described in Section 8 of Appendix B.1.

ENEA compared two calculations based on plane (x,y) and polar (r,θ) geometry respectively. The most accurate global results were those obtained from the polar geometry calculation. The detailed results of the calculations for these two different geometries can be found in [14].

In transport calculations (for distances up to the pressure vessel), cross-sections approximated by a few energy group structure (e.g. BUGLE) result in the overestimation of results (about 2%) compared with the use of a fine energy group structure.

In choosing the right S_NP_L approximation, it would appear that a S_8P_3 calculation is sufficient for in-vessel dosimetry. An increased effort with $S_{12}P_5$ approximation has a negligible effect on the results. But for ex-vessel dosimetry a higher effort is to be expected concerning the S_NP_L approximation as well as the few group structure.

A further contributing factor to the deterioration of the results outside of the core region (apart from the diffusion based buckling approximation) may still be the iron cross-section in steel zones (despite recent improvements in the ENDF/B-VI data file).

An appropriate choice of the geometrical interval structure is very important. If the detector positions do not fit perfectly in the cell centre, the flux values must be interpolated.

In all the calculations certain detector positions exhibit significantly larger discrepancies with respect to the experiment than most of the detector positions. This suggests that the measurements at these few positions might not be correct and a detailed evaluation of uncertainties is therefore needed.

CHAPTER 5

Benchmark results of VENUS-3

In the three-dimensional benchmark, the number of detector positions is increased to 344. A large number of detector positions is needed to describe the streaming of fast neutrons through the complex three-dimensional geometry of the outer core region, the core baffle, the water reflector and the core barrel. The detector positions along the mid-plane of the core are shown in Figure 5.1. Axially, detectors are located at 14 different axial levels between 105 cm and 155 cm. The theoretical target quantities to be investigated are the same as for VENUS-1, i.e. fluxes above 1 MeV, above 0.1 MeV and DPA rates. The experimental target quantities, however, are reduced to three reactions with ^{58}Ni(n,p), ^{115}In(n,n′) and ^{27}Al(n,α). The Ni detector is comparable to fluxes above 3 MeV, the In detector to fluxes above 1 MeV and DPA rates, and the Al detector indicates the extreme hard end of the neutron spectrum above 8 MeV. The calculated reaction rates, or more precisely, the equivalent fission fluxes are compared with measured values directly, whereas the theoretical target quantities have been correlated to the C/E values of the In reaction. Up to eight independent results have been contributed, comprised of five 3-D S_N calculations with different degrees of detail, two Monte Carlo contributions and one flux synthesis method. *Calculation details supplied by participants can be found in Appendix B.2.*

5.1 Comparison of calculated equivalent fission fluxes with measurements

The C/E values of all contributed results of equivalent fission fluxes are plotted together for the Ni detector in Figure 5.2, for the In detector in Figure 5.3 and for the Al detector in Figure 5.4. Because of a large number of Ni detector positions, Figure 5.2 is split into four separate figures (Figures 5.2.1(a), 5.2.1(b), 5.2.2(a) and 5.2.2(b)). The experimental equivalent fission fluxes are given in Tables 5.1, 5.2 and 5.3 for Ni, In and Al detector positions, respectively. In modelling the VENUS-3, because of the partial-length shielded assemblies, the flux synthesis methodologies become inaccurate, even at the core mid-plane. Since only medium penetration depths of fast neutrons needed to be treated, this helped to improve the Monte Carlo statistics, whereas the large number of detectors increased the calculation effort appreciably. The vast majority of results were therefore produced by means of three-dimensional S_N methods comprising calculations with high and low precision as well. With few exceptions, all three-dimensional Monte Carlo and S_N results fit within a narrow band of ±10% around the measurements, which is a notable improvement on the scatter band of about ±20% shown in the VENUS-1 benchmark. The few larger deviations are concentrated within the horizontal planes at the upper and lower core edges with appreciably lower flux values, which are of minor importance with regard to pressure vessel damage.

More precise S_N calculations, especially with fine spatial mesh and multi-group structure, show deviations lower than ±5% to the experiment, mainly in the high flux region where 77% of all detectors are located, and slightly larger deviations in the low flux region at the axial core edges,

where the remaining 23% of detectors are located. Typically at the detector positions with larger C/E values, similar systematic deviations can be observed in most calculations, indicating a greater degree of uncertainty in measurements at those locations.

5.2 Comparison of theoretical quantities

The important theoretical quantities such as DPA rates and fast neutron fluxes above 1 MeV and above 0.1 MeV cannot be directly correlated to the measured values of the benchmark. Thus the calculated absolute values must be compared. However, given that the In detector is a good indicator for the spatial variation of the DPA rate and the fast neutron flux above 1 MeV, the C/E values of the In reaction were applied to construct an appropriate reference value [18]. To obtain this divisor the theoretical quantity of a reference calculation (e.g. IKE-1 calculation or any other) is weighted with the relevant reciprocal C/E value of the In reaction. In an approximation the same procedure could also be applied to the flux above 0.1 MeV.

The calculated DPA rates of the benchmark VENUS-3 exhibit a relatively large scatter band which is illustrated in Figure 5.5(a) for absolute values. Further details can be seen in the plot of Figure 5.5(b), where the DPA rates are given in relation to the C/E values of In. It is clearly apparent that two versions of DPA cross-sections differing by 20% have been applied in the S_N calculations. DPA rates calculated with the data from ASTM-82 are significantly underestimated compared with those derived from new iron data of ENDF/B-VI. A slight underestimation (2-4%) is observed in the results of IKE-2, where the energy integration is restricted to E > 0.1 MeV. A shift of 15% may be seen between both Monte Carlo results.

The intercomparison of the calculated fast neutron fluxes above 1 MeV is given in Figure 5.6(a) for the absolute values showing a reduced scatter band compared to the DPA rate. With the improved diagnostic possibilities of the relative values shown in Figure 5.6(b), the calculated results of fast neutron fluxes can be classified as follows:

The major group of the S_N calculations has a scatter band of ±5% or better. There is a smaller group of S_N calculations with a broader band of ±10%. The Monte Carlo results belong to this group. In each group there are a few larger deviations, which coincide very well with the minima in Figure 5.6(a), indicating a higher uncertainty of the In measurements at these detector positions.

Finally, similar conclusions can be drawn for the fast neutron flux above 0.1 MeV as shown in Figures 5.7(a) and 5.7(b).

5.3 Summary of VENUS-3 results

From the three-dimensional VENUS-3 benchmark two main conclusions can be drawn:

- Overall the 3-D VENUS-3 results are far superior to the 2-D VENUS-1 results. This is mainly due to the lack of any buckling approximation in 3-D calculations.

- The 3-D results of the TORT, PENTRAN and MCNP codes are within the target accuracy of ±10% desired for dosimetry calculations. If necessary, more precise calculations are possible with deviations of ±5% with regard to the measurements.

It was discussed that presenting dosimetry calculations in the form of “equivalent fission fluxes” can adversely affect results by introducing an additional uncertainty due to calculation of the “fission averaged dosimeter cross-section”, because the reaction rate is the primary quantity calculated. Ideally, the fission averaged dosimeter cross-section should be provided by the experiment. In the absence of this experimental constant, the fission averaged dosimeter cross-section has to be calculated. In the benchmark each participant calculated the fission averaged dosimeter cross-section from the basic fine group detector response cross-sections contained in the IRDF-90 V.2 and ENDF/B-VI (BUGLE-96) data files. These calculated values differ up to 8% due to the different number of energy groups that each participant used in the calculations. The possible improvement or deterioration of results will be analysed in the following chapter.

KOPEC carried out two different calculations: the synthesising calculation using 2-D DORT and the 3-D TORT calculation. While the synthesising calculation provides unsatisfactory results for the detectors located far from the selected azimuthal angle for the DORT XZ model, the TORT calculation shows a good level of consistency within ±10% with the experimental data and gives consistent results for all regions and all detectors [19].

It is worth noting that the PSU group performed their calculation with the PENTRAN code in a parallel environment using an IBM SP2 computer with 32 processors. This calculation required only 1.5 hours, while resulting in a similar accuracy (within ±10% of the experimental data) as that achieved by the TORT code using the same few group library BUGLE-96.

CHAPTER 6

Uncertainties of benchmark calculations and measurements

Every calculated or measured value of a given physical quantity possesses uncertainties, which can be summarised by error bars around the point values shown in all figures mentioned previously. As is well known from the statistical standard deviations of Monte Carlo results, an uncertainty band has to be attributed to each curve representing mean values of the quantity calculated.

It is the existence of all relevant uncertainties which requires that the calculation procedures of fast neutron fluence in the reactor pressure vessel be benchmarked to measured results in clean experimental configurations designed specifically for RPV situations.

The uncertainties involved in reactor fluence determination can be classified into several distinct types: generic uncertainties (such as in cross-sections) which will apply to fluence determination in general, and specific uncertainties (such as reactor dimensions) which apply to individual cases. Specific uncertainties only affect a single or a few cases of fluence evaluation and therefore are not defined by measurements in benchmark fields. Generic uncertainties can be divided into random uncertainties and systematic uncertainties. The generic uncertainties can be determined from uncertainty estimate parameters and by gathering data from benchmarks in order to investigate systematic bias and scatter of both measurements and calculations. Random uncertainties will introduce scatter in the results, and data correlation enables this scatter to be defined and provides a check on the assessment of the random component of the assumed errors. Systematic uncertainties will bias the result in the same direction in each application. These biases can be identified through a comparison of calculations and measurements, but these comparisons cannot necessarily identify the source of the bias in order to eliminate it. Thus the impact of known biases when applied in new situations (e.g. geometries that have not been benchmarked) will remain a source of uncertainty [20].

Results of calculations are subject to many uncertainties relating, for example, to geometrical and computational variables, nuclear constants characteristics, modelling assumptions, mathematical approximations, fine energy structure in the neutron spectrum, etc. In general, given the complexity of the physical phenomena involved, on the one hand, and the variety of measurement and computational methods currently used to address the same phenomena on the other, further standardisation and discipline is felt necessary to increase data comparability in all aspects of reactor safety with the result that the use of in-house codes will be finally abandoned.

6.1 Uncertainties in the calculated benchmark results

Sensitivity and uncertainty analyses have been performed by the OECD/NEA to correlate the uncertainties of fast neutron flux and reaction rates calculated at detector positions in the reactor barrel of VENUS-3. This was done with the given uncertainties of input quantities such as source spectrum, spatial distribution, and absolute power as well as transport cross-sections and detector activation cross-sections [21]. The relative uncertainty of the calculated fast neutron flux above 1 MeV amounts to 7%, as shown in Table 6.1. Compared to the fast flux in a surveillance probe position in a real

PWR, only the uncertainty resulting from the iron cross-sections is underestimated in VENUS-3 by about a factor of 2, since the surveillance capsules are placed outside the reactor barrel, whereas all other contributions to the total uncertainty are properly covered in the benchmark. With regard to the reaction rates in the reactor barrel, the relative uncertainty of ^{115}In(n,n′) amounts to 7%, of ^{58}Ni(n,p) to 9%, and of ^{27}Al(n,α) to 14%. This holds for the reaction rates as target quantities. If for the derived quantity of equivalent fission fluxes a full cross-correlation of the denominator (fission spectrum and response function) is assumed, the relative uncertainties are significantly reduced to about 6% for the In detector, 6% for the Ni detector, and 7% for the Al detector. These uncertainties represent upper boundaries for all detectors placed nearer to the reactor core.

The fission spectrum (^{235}U) averaged detector cross-sections, used by each contributor to convert the primary calculated reaction rates into equivalent fission fluxes, are presented in Tables 6.2 and 6.3 for VENUS-1 and VENUS-3, respectively, and have been compared in Tables 6.4 to 6.6. There are two different origins for the detector cross-sections from IRDF-90 Version 2 and from ENDF/B-VI/V. To show the relative deviations, in Table 6.4 a mean value is produced from continuous energy and multi-group representations. These reference values are applied in the few group approximations of Tables 6.5 and 6.6. With regard to the IRDF-90 Version 2 data, the variation in the denominator is relatively small and shows the largest deviations of -3% for the NEA result of In and -2.7% for the JAERI result of Ni. This results in In reaction rates of the NEA being lower by 3% compared to the equivalent fission fluxes of Figure 5.3 and the Ni reaction rates of JAERI being lower by 2.7% compared to Figure 4.2.

There are larger deviations of the denominator in Table 6.6 if the original BUGLE-96 detector cross-sections are used based on ENDF/B-VI. The KOPEC and PSU denominators for the Al reaction are higher by 8%, which means that their Al reaction rates are higher by 8% compared to their equivalent fission fluxes of Figure 5.4. This large deviation is observed for high energetic neutrons. For the total energy range of fast neutrons the ^{155}In(n,n′) reaction is more appropriate. Here we get in Table 6.6 a small underestimation of the denominator of about -3%, which means that the In reaction rates of KOPEC and PSU are reduced by 3% compared to the pertaining equivalent fission fluxes shown in Figure 5.3 for VENUS-3. The same holds true for the KOPEC results in Figures 4.3 and 4.8 of VENUS-1.

In Maerker's ORNL publication, measured values of the fission averaged detector cross-sections are given, which deviate slightly between -2% and +3% from the chosen theoretical references [13]. The equivalent fission fluxes of ORNL/Maerker were derived from the measured fission averaged detector cross-sections of Mol. For the reaction rates the old BUGLE data from ENDF/B-V were applied. Such ORNL results cannot profit from the uncertainty reduction by anti-correlation of the denominator quantities, and must additionally include the uncertainty of the measured fission averaged detector cross-sections.

One particular problem with the Monte Carlo results lies in their inherent statistical fluctuations, with the result that besides the calculated mean values of the quantities their standard deviations also have to be supplied. The three Monte Carlo applications supplied by NRG (for VENUS-1 and VENUS-3) and Spain (for VENUS-3) used two different versions of the MCNP code. The standard deviations of the calculated benchmark results for VENUS-3 are included in the C/E plots, as shown in Figures 6.1 to 6.3 for each detector type. There are commonly some larger underestimations, which are independently produced by S_N calculations, as well. These special detector positions should be discussed with the experimental uncertainties in detail. There is a slight tendency of underestimation observed in NRG's In and Al results. So far the uncertainties treated were mainly related to the benchmark results of VENUS-3.

The results of VENUS-1 are dominated by principal approximations of two-dimensional transport calculations. It has been shown that the diffusion based buckling correction of the axial neutron streaming in the material layers outside the reactor core overestimates the axial flow, resulting in a radially increasing underestimation [18]. Therefore a better fit of the axial buckling correction had been proposed and applied. There are further problems with appropriate averaging of the axial variation of the neutron source in the reactor core and averaging of material configurations outside the core. In both multi-dimensional S_NP_L approximations the accuracy of the results depends on the spatial mesh, the details of the energy group structure and the anisotropy of fluxes and cross-sections taken in the calculational effort [18]. For in-vessel dosimetry S_8P_3 approximations are adequate. Interpolation of reaction rates to the exact position of the detectors is required normally. For routine fast fluence calculations the few group structure of BUGLE-96 is sufficient.

6.2 Uncertainties given for the benchmark experiments

The PWR mock-up, the VENUS facility at SCK·CEN, Mol in Belgium carefully represents the pressure vessel internals of a Westinghouse three-loop reactor with two core loading configurations: VENUS-1, simulating a fresh PWR core, and VENUS-3, simulating a partial length shielded assembly in which the fuel is partially replaced by steel in the outermost fuel rows. The dimensions and composition of materials are measured and specified precisely, which is not possible in a real PWR in operation. The same holds for the measurements of fast neutrons, with various threshold detectors at several hundred positions inside the pressure vessel. Furthermore the carefully measured reaction rates were related directly to the reaction rates in a given pure fission spectrum of ^{235}U, resulting in highly accurate values of equivalent fission fluxes, also unthinkable in real PWR configurations.

The relevant literature cites the relative uncertainty of the neutron fission source with regard to absolute power below 4% and the source space distribution between 1.5% and 4%. The relative uncertainty of the individual measured reaction rates is given as 3% and the estimated composite of all measurement uncertainties of the equivalent fission fluxes is below 5%. In high precision calculations of the complex three-dimensional neutron field of VENUS-3 about 77% of all detectors concur within 5% with the measured equivalent fission fluxes, which is a perfect fit between the measurements and the calculated values. On the other hand, the largest deviations between measurements and calculations accumulate at the extreme top and bottom locations of the active core region. At these “poor” detector positions nearly all calculations demonstrate a common large underestimation in the C/E values of the equivalent fission fluxes, as well as in the relative values of the important theoretical quantities such as DPA rates and fast neutron fluxes. These “poor” detector positions correspond exactly to the sharp minima in the curves of the absolute theoretical quantities. This comparison of measurements and calculations clearly indicates a systematic overestimation of the measurements (more than 5%) for the detector positions with extremely low reaction rates.

CHAPTER 7

Conclusions

With an increasing number of power reactors world-wide now approaching the end of their design life, decisions must be made with regard to final shutdown or possible plant life extension. Thus, benchmarks for ex-core neutron fluence determination are urgently needed.

The benchmark calculations obtained from the PWR mock-up experiment VENUS-1 have made it possible to clarify the capabilities and limits of two-dimensional neutron transport calculations. For over twenty years, two-dimensional transport calculations have been the principal method used to determine the fast neutron fluence responsible for the neutron embrittlement of reactor pressure vessel walls. Mainly due to the diffusion based axial buckling correction, it has been demonstrated that a relative difference between measurement and calculation of ±20% has to be taken into account. A given uncertainty of the measurement amounts to ±5%. This has been shown by about 20 independent calculations contributed to the VENUS-1 benchmark from around the world. For more than 15 years two-dimensional transport calculations have been the basis of the flux synthesis method for routine calculation of the so-called lead factors used to correlate the neutron embrittlement at critical locations (weld seams) in the pressure vessel to the measured embrittlement of the surveillance probes.

In determining the fast neutron fluence in the pressure vessel of large power reactors, the influence of the axial buckling correction is smaller than in the VENUS-1 benchmark. However, in two-dimensional calculations, there still remains a problem in treatment of axial core power variation. Furthermore, the axial coolant density changes in the reactor core have to be properly approximated. This fact becomes more important in boiling water reactors. These two effects are not present in the VENUS-1 benchmark.

To improve neutron fluence determination the more complex three-dimensional PWR mock-up experiment, VENUS-3, has been studied with 14 independent benchmark calculations. The latest versions of three-dimensional transport codes such as TORT, PENTRAN and MCNP have been validated and in a decisive finding it has been shown that the results for the three-dimensional benchmark VENUS-3 are in general appreciably closer to the experimental values than for the two-dimensional benchmark VENUS-1. In more than 200 positions of threshold detectors the difference, which has to be regarded between measurement and calculation, amounts to ±10%. This can be reached by three-dimensional S_8P_3 calculations, even with the few group library BUGLE-96, which meets the present routine requirements of in-vessel dosimetry. The same uncertainty is observed with regard to the Monte Carlo results based on two versions of the MCNP. As a result of major advances in hardware development, it is now possible to carry out three-dimensional calculations with S_N codes for neutron fluence calculations in multi-group versions, e.g. with the energy details of VITAMIN-J (175) or EURLIB (100) group structures. In 77% of all detector positions in VENUS-3 the concordance between high-precision calculations and measurements was improved to better than ±5%, the figure quoted for the overall uncertainty of experimental results. Transferring the transport codes to the latest massive parallel computers will significantly reduce the long computing times required for three-dimensional calculations.

As a follow-up to these benchmark exercises, a comprehensive analysis with uncertainties of some exceptional experimental values would be necessary, as soon as they become available, to better understand the origin of systematic discrepancies for certain detector positions. The use of MOX fuel in LWRs presents different neutron characteristics and it would therefore be of interest to develop a benchmark for MOX fuelled reactors.

REFERENCES

[1] "Computing Radiation Dose to Reactor Pressure Vessel and Internals"- State-of-the-Art Report, NSC/DOC(96)5, OECD NEA, Paris, 1997.

[2] A. Fabry, *et al*., "VENUS PWR Engineering Mock-Up: Core Qualification, Neutron and Gamma Field Characterisation", Proc. of the 5th ASTM-EURATOM Symposium on Reactor Dosimetry, Geesthacht, Germany, 24-28 September 1984, pp. 771-782.

[3] L. Leenders, "LWR-PVS Benchmark Experiment VENUS-3 (With Partial Length Shielded Assemblies)", FCP/VEN/01, SCK·CEN, Mol, Belgium, September 1988.

[4] W.A. Rhoades and R.L. Childs, "The DORT Two-Dimensional Discrete Ordinates Transport Code", *Nucl. Sci. Eng.*, Vol. 99, 1, 1988, pp. 88-89.

[5] "MCNP – A General Monte Carlo N-Particle Transport Code, Version 4A", J.F. Briesmeister, ed., LA-12625-M, Version 4A, UC 705 and UC 700, Los Alamos National Laboratory, Los Alamos, NM, November 1993.

[6] "MCNP – A General Monte Carlo N-Particle Transport Code, Version 4B," J.F. Briesmeister, ed., LA-12625-M, Version 4B, UC 705 and UC 700, Los Alamos National Laboratory, Los Alamos, NM, March 1997.

[7] P.F. Rose, "ENDF/B-VI Summary Documentation", BNL-NCS-17541 (ENDF-201) 4th Edition, October 1991.

[8] C. Nordborg and M. Salvatores, "Status of the JEF Evaluated Data Library", *Nuclear Data for Science and Technology*, J.K. Dickens, ed., American Nuclear Society, LaGrange, IL, 1994.

[9] N.P. Kocherov and P.K. McLaughlin, "The International Reactor Dosimetry File (IRDF-90 Version 2)", IAEA-NDS-141, International Atomic Energy Agency, October 1993.

[10] W.A. Rhoades and R.L. Childs, "The TORT Three-Dimensional Discrete Ordinates Neutron/ Photon Transport Code", Oak Ridge National Laboratory, Oak Ridge, TN, ORNL-6268, April 1987.

[11] G.E. Sjoden and A. Haghighat, "PENTRAN – Parallel Environment Neutral-Particle TRANsport Version 4.33", Manual, Nuclear Engineering Program, Penn State University, University Park, September 1996. Also, G.E. Sjoden and A. Haghighat, "PENTRAN – A 3-D Cartesian Parallel S_N Code with Angular, Energy, and Spatial Decomposition", Proceedings of the Joint International Conference on Mathematical Methods and Supercomputing in Nuclear Applications, Vol. II, 1267-1276, Saratoga Springs, NY, 6-10 October 1997.

[12] "BUGLE-96: Coupled 47 Neutron, 20 Gamma-Ray Group Cross-Section Library Derived from ENDF/B-VI for LWR Shielding and Pressure Vessel Dosimetry Applications", Oak Ridge National Laboratory, Oak Ridge, TN, RSIC Data Library Collection, DLC-185/BUGLE-96, March 1996.

[13] R.E. Maerker, "Analysis of the VENUS-3 Experiments", NUREG/CR-5338 ORNL/TM-11106, Oak Ridge National Laboratory, August 1989.

[14] M. Pescarini, *et al*., "ENEA-Bologna Validation of the BUGLE-96 ENDF/B-VI Library on the VENUS-1 Neutron Shielding Benchmark Experiment – A Synthesis of the Final Results", OECD NEA, JEF/DOC-778.

[15] H.R. Hwang, *et al*., "Advanced Methodology Development for Radiation Physics and Criticality Safety Analysis (in Korean)", KOPEC Report, June 1999.

[16] A.F. Albornoz and E.M. Lopasso, "CAB Calculations of the VENUS-1 Two-Dimensional Benchmark on Ex-Core Dosimetry Computations", Report CNEA-CAB 47/08/98, Centro Atómico Bariloche, April 1998.

[17] M. Pescarini, M.G. Borgia and R. Orsi, "VENUS-1 Shielding Benchmark Experiment: ENEA-Bologna Results of a Neutron Transport Analysis with the BUGLE-96 ENDF/B-VI Library and the DORT-3.1 S_N Code in Plane Geometry", ENEA-Report, Bologna, Sept. 1998.

[18] G. Hehn, A. Sohn, M. Mattes and G. Pfister, "IKE Calculations of the OECD NEA Benchmarks VENUS-1 and VENUS-3 for Computing Radiation Dose to Reactor Pressure Vessel and Intenals", IKE 6 NEA 2, December 1997.

[19] B.J. Moon, H.H. Kim and H.R. Hwang, "Analysis of the VENUS-3 Benchmark Experiment Using DORT and TORT", Proc. of the Int. Conf. on the Physics of Nuclear Science and Technology, Long Island, New York, USA, 5-8 October 1998, pp. 931-938.

[20] J. Bros, *et al*., "Dosimetry and Neutron Transport Methods for Reactor Pressure Vessels", AMES Report No. 8, European Commission, EUR 16470 EN, November 1996.

[21] I. Kodeli and E. Sartori, "Use of Benchmark Experiments Database for Pressure Vessel Dosimetry", ANS Radiation Protection and Shielding Division Topical Conf. Technologies for the New Century, Nashville, TN, USA, 19-23 April 1998, pp. I-287-I-294.

TABLES AND FIGURES

Table 3.1. Summary table of two-dimensional benchmark calculations: VENUS-1

Contributor	Method	Spatial mesh	Energy groups	Cross-sections	Neutron source	Axial leakage treatment	Response functions (barn)
J. Koban Siemens Germany	DOT4.2 S_8	(r,θ) = 165×98	100	EURLIB-VI/ N175 (using NJOY-91 & ENDF/B-VI Rev.2)	For spectral shape of the neutron source, ^{235}U fission spectrum based on ENDF/B-VI was adopted	DB^2 correction Thermal neutron: $DB^2 = 2.4 \times 10^{-3}$ Neutrons above thermal energy: $DB^2 = 2.12 \sim 2.40 \times 10^{-3}$ (depending on zones)	IRDF-90 V.2 Ni = 0.105 In = 0.1852 Rh = 0.7027 ^{238}U = 0.3043 ^{237}Np = 1.349
H Aït Abderrahim SCK·CEN Belgium	LEPRICON (DORT/ANISN) S_8P_3	(r,θ) = 165×66	56	ELXSIR Based on ENDF/B-V Rev. Mod 3	ENDF/B-V ^{235}U fission spectrum	DB^2 correction Given B^2 values were used. D for each group and zone was determined ($D=1/3\Sigma_{tr}$)	ENDF/B-V Ni = 0.1053 In = 0.1795 ^{238}U = 0.3048 ^{237}Np = 1.3479
F. Wasastjerna VTT/ENE Finland	DORT S_8 or S_{16} P_3 or P_7	(r,θ) = 41 or 91 $\times$ 28 or 60	17 or 47	BUGLE-80 BUGLE-93 BUGLE-96T	"Harwell 1975" (a Watt spectrum) spectrum was used to determine the energy dependence	DB^2 correction Given B^2 values were used. D for each group and zone was determined.	IRDF-90 V.2 or ENDF/B-VI
G. Hehn A. Sohn M. Mattes G. Pfister IKE Germany	DORT3.1 $S_{12}P_5$	(r,θ) = 93×53 (x,y) = 62×62	175	VIT-J	Transfer the relative pin power distribution in (x,y) into (r,θ) mesh system. ^{235}U fission spectrum was used: normalisation factor = 3.264×10^{11} n/cm/sec in the total core quadrant	DB^2 correction Group and zone dependent DB^2 → underestimation B = 0 → overestimation D = 1 & given B^2 → results in between	IRDF-90 V.2 Ni: 0.1053 In: 0.1853 Al: 7.279E-4 Rh: 0.7031 ^{238}U: 0.3046 ^{237}Np: 1.3498
M. Pescarini M.G. Borgia R. Orsi ENEA Italy	DORT 3.1 S_8P_3	(x,y) = 113×113 and 162×163 (r,θ) = 172×143	47	BUGLE-96	Normalisation factor = 3.2584×10^{11} n/cm/sec	DB^2 correction Thermal (groups 46 & 47): D = 0.159 cm, $B^2 = 2.401 \times 10^{-3} cm^{-2}$ Fast (groups 1 to 45): *In-core region* D = 1.13 cm, $B^2 = 2.401 \times 10^{-3} cm^{-2}$ *Ex-core region* D = 1.13 cm, $B^2 = 2.278 \times 10^{-3} cm^{-2}$	IRDF-90 V.2 (flat weighting) Ni: 0.1072 In: 0.1865 Rh: 0.7068 ^{238}U: 0.3074 ^{237}Np: 1.3555

Table 3.1. Summary table of two-dimensional benchmark calculations: VENUS-1 (*cont.*)

Contributor	Method	Spatial mesh	Energy groups	Cross-sections	Neutron source	Axial leakage treatment	Response functions (barn)
R. van der Stad NRG The Netherlands	MCNP4A		Continuous	EJ2-MCNP based on JEF2.2		Finite geometry	IRDF-90 V.2 Ni: 0.1069 In: 0.1855 Rh: 0.7035 ^{238}U: 0.3039 ^{237}Np: 1.3411
J.M. Paratte PSI Switzerland	BOXER (transport code) P_1	(x,y) $= 60 \times 60$	36 (> 1 MeV) 44 (> 0.1 MeV)	ETOBOX (JEFF-1), for iron, ENDF/B-IV	Normalisation factor $= 3.2552 \times 10^{8}$ n/cm^3 sec	DB^2 correction $B^2 = 2.4 \times 10^{-3}$ cm^{-2}	
B.J. Moon H.R. Hwang KOPEC Korea	DORT 2.8.14 S_8P_5	(x,y) $= 104 \times 93$ (r,θ) $= 92 \times 122$	47	BUGLE-96	The reference core average fission rate 2.10×10^{-8} fiss/cm/sec was used for source normalisation	DB^2 approximation (xy model) and synthesis method (xy and r-theta models)	BUGLE-96 Ni: 0.1070 In: 0.1802 Rh: 0.7075 (IRDF-90 V.2) ^{238}U: 0.3070 ^{237}Np: 1.330
M. Suzuki K. Kosako Y. Sakamoto JAERI/SAEI Japan	DORT $S_{16}P_5$	(r,θ) $= 109 \times 90$	86	JENDL-3.2	Normalised to 3.255×10^{-11} in 1/4 core and full power	DB^2 correction using VENUS-1 experimental B^2 values	IRDF-90 V.2 Ni: 0.1027 In: 0.1823 Rh: 0.6951 ^{238}U: 0.2985 ^{237}Np: 1.3372
A.F. Albornoz E.M. Lopasso CAB Argentina	DORT S_8P_3	(r,θ) $= 220/235 \times 63$ or $= 253 \times 63$	47	BUGLE-96	A reference core average fission rate at 100% power equal to 2.1×10^{8} fiss/cm/sec was used for source normalisation.	DB^2 correction Given B^2 values are used. D was calculated for each material zone from data BUGLE-96 (that is, $D=1/3\Sigma tr$)	IRDF-90 V.2 Ni: 0.1067 In: 0.1854 Rh: 0.7 ^{238}U: 0.3045 ^{237}Np: 1.3437 DPA Fe-ASTM: 862.88

Table 3.2. Summary table of three-dimensional benchmark calculations: VENUS-3

Contributor	Methods	Spatial mesh	Energy groups	Cross-sections	Neutron source	Response functions (barn)
I. Kodeli (consultant) NEA France	TORT S_4P_1 and S_8P_3	(xyz) $= 51 \times 52 \times 22$	47	BUGLE-96	A complete 3-D map of the neutron source from the measured power distribution (using an interpolation procedure RECOG-ORNL) was prepared.	IRDF-90 V.2 Ni: 0.1063 In: 0.1797 Al: 7.323E-4
J.M. Perlado J. Marián J. García Sanz DENIM Spain	MCNP-4B	Full 3-D geometry description	Continuous	ENDF/B-VI (NJOY91 & ACER) DLC189/MCNPXS		IRDF-90 V.2 Ni: 0.105 In: 0.185 Al: 0.72E-3
B.J. Moon H.R. Hwang KOPEC Korea	TORT S_8P_5	(xyz) $= 56 \times 45 \times 26$	47	BUGLE-96	The measured 3-D pinwise source distribution and the interpolated values by NEA were used. Normalised to the reference measured fission rate 5.652×10^{-12} fiss/sec/quadrant at 100% power and 2.432 n/thermal fission	IRDF-90 V.2 Ni: 0.107 In: 0.1802 Al: 7.82E-4
W. Hofmann J. Koban Siemens Germany	TORT 2.7.3 (PC version) S_8P_3	(xyz) $=55 \times 55 \times 32$	100	EURLIB-VI/N175 (ENDF/B-VI)	^{235}U fission spectrum normalised to 1.0 and pin by pin relative source distribution for 14 axial zones provided by NEA were used. Normalisation factor = 2.697×10^8	IRDF-90 V.2 Ni: 0.105 In: 0.1852 Al: 7.2E-4
G. Hehn A. Sohn M. Mattes G. Pfister IKE Germany	TORT3.1 S_8P_3 (low) to $S_{12}P_5$ (high)	(xyz) $= 62 \times 62 \times 62$ (r,θ,z) $= 93 \times 53 \times 62$ or $= 71 \times 53 \times 62$	47 175	BUGLE-96 (low precision) VIT-J (high precision)	Relative pin power distribution in Cartesian co-ordinates was transferred into the cylindrical mesh system in conserving the source strength. The neutron source rate has been normalised to 1.551×10^3/sec in the total core quadrant.	BUGLE-96 Ni: 0.107 In: 0.1802 Al: 7.821E-4 IRDF-90 V.2 Ni: 0.1053 In: 0.1853 Al: 7.279E-4

Table 3.2. Summary table of three-dimensional benchmark calculations: VENUS-3 (*cont.*)

Contributor	Methods	Spatial mesh	Energy groups	Cross-sections	Neutron source	Response functions (barn)
R. van der Stad A. Hogenbirk NRG The Netherlands	MCNP4A	1/4 core, full 3-D geometry	Continuous	EJ2-MCNP (based on JEF 2.2)	From the given "normalised pin power density" density, a fixed neutron source distribution for MCNP can be deduced. In the MCNP fixed source calculations a standard Watt's fission spectrum was taken for the energy distribution of the source neutrons.	IRDF-90 V.2 Ni: 0.1069 In: 0.1855 Al: 7.19E-4
A. Haghighat G. Sjoden H. Aït Abderrahim PSU/USAFA/ SCK·CEN USA/Belgium	PENTRAN S_8P_3	Coarse mesh (xyz) $= 7 \times 7 \times 4$ These coarse meshes are partitioned for a total of 84 784 fine meshes	47	BUGLE-96	For the source spectrum, ENDF/B-VI ^{235}U spectrum is collapsed based on the 47-group BUGLE-96 energy group structure. The flux distribution is normalised based on a total fission source of 1.375×10^{12} (fission neutrons/sec/quadrant). This total fission source is determined using a reference measured fission rate of 5.652×10^{12} (fission/sec/quadrant) and an average number of fission neutrons per fission ν of 2.43.	BUGLE-96 Ni: 0.1079 In: 0.1793 Al: 7.765E-4
R.E. Maerker ORNL USA	DOT 4+ANISN (synthesis) DOT 4: S_6P_3 ANISN: S_8P_3	DOT 4 (2-D) (xy) $= 65 \times (36\text{-}101)$ (xz) $= 65 \times 77$		ELXSIR (ENDF/B-IV + V)	Both measured and interpolated source distribution data were used to produce a complete pin-by-pin radial distribution at two levels (114.05 cm and 145.5 cm) and a complete pin-by-pin radial distribution at all 14 levels between 105 cm and 155 cm for all pin locations in the west by south-west octant of the core lying to the left of the 45° direction.	Ni: 0.1085 In: 0.1903 Al: 7.06E-4

Table 4.1. VENUS-1: Experimental equivalent fission fluxes in stainless steel zones (n/cm^2/s)

Measurement position	No.	Radius [cm]	Angle	^{58}Ni(n,p)	^{115}In(n,n′)	^{103}Rh(n,n′)	^{238}U(n,f)	^{237}Np(n,f)
Inner baffle	2	4.454	8.1	1.51E+09	1.90E+09	2.22E+09	1.91E+09	2.52E+09
	3	6.237	45.0	1.82E+09	2.30E+09	2.64E+09	2.28E+09	2.95E+09
Outer baffle	4	39.696	0.9	6.38E+08	7.83E+08		7.96E+08	1.10E+09
	5	40.093	8.1	6.06E+08	7.37E+08	8.63E+08	7.37E+08	
	6	41.456	16.8	4.97E+08	5.98E+08	6.91E+08	6.12E+08	8.21E+08
	7	43.693	24.7	2.93E+08	3.52E+08	4.16E+08		4.91E+08
	8	42.589	29.2	3.07E+08	3.64E+08	4.30E+08	3.64E+08	5.08E+08
	9	37.218	34.0	5.72E+08	7.16E+08	8.29E+08	7.26E+08	9.67E+08
	10	32.186	40.2	9.31E+08	1.18E+09	1.39E+09	1.15E+09	1.60E+09
Barrel	11	49.774	0.7	9.01E+07	9.72E+07		1.00E+08	1.21E+08
	12	50.659	10.8	7.81E+07	8.50E+07		8.72E+07	1.12E+08
	13	50.659	21.1	7.46E+07	8.40E+07	9.80E+07	8.65E+07	1.23E+08
	14	51.003	25.6	6.37E+07	7.20E+07		7.23E+07	1.08E+08
	15	51.034	28.8	5.88E+07	6.45E+07		6.76E+07	9.58E+07
	16	50.847	33.9	5.47E+07	5.60E+07		6.01E+07	7.60E+07
	17	50.909	41.0	4.79E+07	4.65E+07		4.72E+07	6.26E+07
	18	50.784	45.0	4.84E+07	4.55E+07	5.27E+07	4.75E+07	6.08E+07
Neutron pad	28	62.700	21.1		8.89E+06			
	29	62.700	42.0		5.95E+06			

Table 4.2. VENUS-1: Experimental equivalent fission fluxes in water zones (n/cm^2/s)

Measurement position	No.	Radius [cm]	Angle	^{58}Ni(n,p)	^{115}In(n,n′)	^{103}Rh(n,n′)	^{238}U(n,f)	^{237}Np(n,f)
Central hole	1	0.000	0.00	1.13E+09	1.24E+09	1.38E+09	1.35E+09	
Water gap I	30	32.965	45.00		8.07E+08	9.31E+08	8.18E+08	
	31	36.529	45.00		4.08E+08	4.51E+08		4.82E+08
	32	40.093	45.00		2.14E+08	2.34E+08	2.30E+08	2.43E+08
	33	43.657	45.00		1.17E+08	1.16E+08		1.30E+08
	34	47.221	45.00		6.80E+07	7.39E+07	7.34E+07	
Water gap II	19	55.260	10.75		2.85E+07		3.02E+07	3.64E+07
	20	55.260	16.63		2.80E+07		2.90E+07	3.82E+07
	21	55.260	21.14		2.72E+07		2.98E+07	
	22	55.260	25.62		2.46E+07		2.51E+07	3.33E+07
	23	55.260	28.78		2.33E+07		2.38E+07	3.20E+07
	24	55.260	33.89		1.97E+07		2.08E+07	2.59E+07
	25	55.260	37.44				1.97E+07	2.44E+07
	26	55.260	40.99		1.73E+07			
	27	55.260	45.00		1.64E+07		1.77E+07	2.22E+07

Table 5.1.1. VENUS-3: Experimental equivalent fission fluxes of nickel detectors at inner and outer baffle locations

Measurement position	Angle	Axial level (cm)	^{58}Ni(n,p)
Inner baffle			
(-1,+2)	8.1°	114.50	1.233E+09
		131.45	1.743E+09
		131.55	1.760E+09
		145.50	1.248E+09
(-1,-1)	45.0°	114.50	1.474E+09
		131.45	2.086E+09
		131.55	2.097E+09
		145.50	1.523E+09
Outer baffle			
(-29,+2)	0.9°	106.50	9.802E+07
		110.50	1.360E+08
		114.50	1.750E+08
		118.50	2.106E+08
		122.50	2.576E+08
		125.50	3.085E+08
		128.50	3.880E+08
		131.50	5.003E+08
		134.50	5.571E+08
		137.50	5.731E+08
		141.50	5.544E+08
		145.50	4.945E+08
		149.50	4.052E+08
		153.50	2.912E+08
(-29,-2)	8.1°	114.50	1.636E+08
		131.50	4.639E+08
		145.50	4.638E+08
(-29,-7)	16.8°	114.50	1.362E+08
		131.50	3.803E+08
		145.50	3.778E+08
(-29,-12)	24.7°	114.50	9.002E+07
		131.50	2.211E+08
		145.50	2.167E+08
(-27,-14)	29.2°	114.50	1.059E+08
		131.50	2.395E+08
		145.50	2.220E+08
(-22,-14)	34.0°	114.50	3.080E+08
		131.50	5.194E+08
		145.50	4.341E+08
(-17,-14)	40.2°	114.50	6.242E+08
		131.50	9.238E+08
		145.50	7.106E+08

Table 5.1.2. VENUS-3: Experimental equivalent fission fluxes of nickel detectors at core barrel locations

Measurement position	Angle	Axial level (cm)	^{58}Ni(n,p)
Core barrel			
(-37,+2)	0.7°	106.50	1.694E+07
		110.50	2.221E+07
		114.50	2.824E+07
		118.50	3.597E+07
		122.50	4.388E+07
		125.50	4.936E+07
		128.50	5.539E+07
		131.50	6.090E+07
		134.50	6.453E+07
		137.50	6.676E+07
		141.50	6.438E+07
		145.50	5.873E+07
		149.50	4.932E+07
		153.50	3.757E+07
(-37,-5)	10.8°	114.50	2.486E+07
		131.50	5.210E+07
		145.50	5.039E+07
(-35,-12)	21.1°	106.50	1.415E+07
		110.50	1.923E+07
		114.50	2.383E+07
		118.50	2.960E+07
		122.50	3.559E+07
		125.50	4.042E+07
		128.50	4.540E+07
		131.50	5.030E+07
		134.50	5.411E+07
		137.50	5.520E+07
		141.50	5.348E+07
		145.50	4.780E+07
		149.50	4.042E+07
		153.50	3.071E+07
(-34,-15)	25.6°	114.50	2.187E+07
		131.50	4.348E+07
		145.50	4.092E+07
(-33,-17)	28.8°	114.50	2.108E+07
		131.50	3.942E+07
		145.50	3.673E+07
(-31,-20)	33.9°	114.50	2.880E+07
		131.50	4.480E+07
		145.50	3.927E+07
(-28,-24)	41.0°	114.50	2.534E+07
		131.50	3.764E+07
		145.50	3.059E+07

Table 5.1.3. VENUS-3: Experimental equivalent fission fluxes of nickel detectors at core barrel locations

Measurement position	Angle	Axial level (cm)	^{58}Ni(n,p)
Core barrel			
(-26,-26)	45.0°	106.50	1.749E+07
		110.50	2.249E+07
		114.50	2.743E+07
		118.50	3.162E+07
		122.50	3.529E+07
		125.50	3.743E+07
		128.50	3.848E+07
		131.50	3.864E+07
		134.50	3.843E+07
		137.50	3.811E+07
		141.50	3.508E+07
		145.50	3.090E+07
		149.50	2.545E+07
		153.50	1.974E+07
(-12,-35)	68.9°	106.50	3.421E+07
		110.50	4.652E+07
		114.50	5.720E+07
		118.50	6.502E+07
		122.50	7.095E+07
		125.50	7.478E+07
		128.50	7.515E+07
		131.50	7.681E+07
		134.50	7.491E+07
		137.50	7.236E+07
		141.50	6.641E+07
		145.50	5.715E+07
		149.50	4.667E+07
		153.50	3.445E+07
(+2,-37)	89.3°	106.50	4.321E+07
		110.50	5.814E+07
		114.50	7.080E+07
		118.50	8.203E+07
		122.50	8.938E+07
		125.50	9.403E+07
		128.50	9.540E+07
		131.50	9.618E+07
		134.50	9.429E+07
		137.50	9.057E+07
		141.50	8.207E+07
		145.50	7.174E+07
		149.50	5.807E+07
		153.50	4.317E+07

Table 5.1.4. VENUS-3: Experimental equivalent fission fluxes of nickel detectors at water gap locations

Measurement position	Angle	Axial level (cm)	^{58}Ni(n,p)
Water gap			
(-33,+2)	0.81°	106.50	3.736E+07
		110.50	5.027E+07
		114.50	6.366E+07
		118.50	7.684E+07
		122.50	9.566E+07
		125.50	1.124E+08
		128.50	1.330E+08
		131.50	1.509E+08
		134.50	1.646E+08
		137.50	1.680E+08
		141.50	1.636E+08
		145.50	1.448E+08
		149.50	1.207E+08
		153.50	8.650E+07

Table 5.1.5. VENUS-3: Experimental equivalent fission fluxes of nickel detectors at partial length shielded assembly (PLSA) locations

Measurement position	Angle	Axial level (cm)	^{58}Ni(n,p)
PLSA			
(-27,+3)	0.97°	106.50	1.648E+08
		110.50	2.296E+08
		114.50	2.947E+08
		118.50	3.548E+08
		122.50	4.275E+08
		125.50	5.062E+08
		128.50	6.752E+08
(-27,+2)	0.97°	131.05	1.084E+09
		134.15	1.234E+09
		137.25	1.280E+09
		141.35	1.227E+09
		145.45	1.108E+09
		149.55	9.125E+08
		153.65	7.026E+08

Table 5.1.5. VENUS-3: Experimental equivalent fission fluxes of nickel detectors at partial length shielded assembly (PLSA) locations (*cont.*)

Measurement position	Angle	Axial level (cm)	^{58}Ni(n,p)
PLSA			
(-25,+3)	1.04°	106.50	2.713E+08
		110.50	3.843E+08
		114.50	4.896E+08
		118.50	5.899E+08
		122.50	6.947E+08
		125.50	7.980E+08
		128.50	1.025E+09
		131.05	1.617E+09
		134.15	1.846E+09
		137.25	1.897E+09
		141.35	1.846E+09
		145.45	1.628E+09
		149.55	1.354E+09
		153.65	1.033E+09
(-23,+2)	1.12°	131.05	2.280E+09
		134.15	2.426E+09
		137.25	2.443E+09
		141.35	2.309E+09
		145.45	2.030E+09
		149.55	1.656E+09
		153.65	1.250E+09
(-23,+3)	1.12°	106.50	5.115E+08
		110.50	7.161E+08
		114.50	9.113E+08
		118.50	1.094E+09
		122.50	1.264E+09
		125.50	1.400E+09
		128.50	1.624E+09
(-27,-9)	21.3°	106.50	1.141E+08
		110.50	1.480E+08
		114.50	1.793E+08
		118.50	2.212E+08
		122.50	2.646E+08
		125.50	3.204E+08
		128.50	4.479E+08

Table 5.1.6. VENUS-3: Experimental equivalent fission fluxes of nickel detectors at 3.3% fuel locations

Measurement position	Angle	Axial level (cm)	^{58}Ni(n,p)
3.3% fuel			
(-21,+2)	1.2°	106.05	9.316E+08
		110.15	1.282E+09
		114.25	1.644E+09
		118.35	1.986E+09
		122.45	2.276E+09
		125.55	2.494E+09
		128.65	2.683E+09
		131.75	2.860E+09
		134.85	2.925E+09
		137.95	2.855E+09
		141.05	2.744E+09
		145.15	2.406E+09
		149.25	1.967E+09
		153.35	1.473E+09
(-19,+3)	1.3°	106.05	1.141E+09
		110.15	1.589E+09
		114.25	2.014E+09
		118.35	2.424E+09
		122.45	2.774E+09
		125.55	2.988E+09
		128.65	3.160E+09
		131.75	3.267E+09
		134.85	3.295E+09
		137.95	3.218E+09
		141.05	3.046E+09
		145.15	2.679E+09
		149.25	2.195E+09
		153.35	1.651E+09
(-22,+0)	5.8°	106.05	7.661E+08
		110.15	1.057E+09
		114.25	1.350E+09
		118.35	1.620E+09
		122.45	1.876E+09
		125.55	2.067E+09
		128.65	2.280E+09
		131.75	2.527E+09
		134.85	2.628E+09
		137.95	2.622E+09
		141.05	2.495E+09
		145.15	2.209E+09
		149.25	1.829E+09
		153.35	1.376E+09

Table 5.1.6. VENUS-3: Experimental equivalent fission fluxes of nickel detectors at 3.3% fuel locations (*cont.*)

Measurement position	Angle	Axial level (cm)	^{58}Ni(n,p)
3.3% fuel (+2,-23)	88.6°	106.05	1.285E+09
		110.15	1.768E+09
		114.25	2.210E+09
		118.35	2.606E+09
		122.45	2.898E+09
		125.55	3.045E+09
		128.65	3.120E+09
		131.75	3.118E+09
		134.85	3.047E+09
		137.95	2.894E+09
		141.05	2.706E+09
		145.15	2.333E+09
		149.25	1.888E+09
		153.35	1.403E+09

Table 5.2.1. VENUS-3: Experimental equivalent fission fluxes of indium detectors at inner baffle, outer baffle and water gap locations

Measurement position	Angle	Axial level (cm)	^{115}In (n,n′)
Inner baffle			
(-1,+2)	8.1°	131.50	2.249E+09
(-1,-1)	45.0°	131.50	2.713E+09
Outer baffle			
(-29,+2)	0.9°	106.50	1.189E+08
		110.50	1.698E+08
		114.50	2.181E+08
		118.50	2.657E+08
		122.50	3.256E+08
		125.50	3.871E+08
		128.50	4.859E+08
		131.50	6.112E+08
		134.50	6.915E+08
		137.50	7.196E+08
		141.50	6.894E+08
		145.50	6.182E+08
		149.50	5.062E+08
		153.50	3.614E+08
Water gap			
(-33,+2)	0.8°	106.50	3.767E+07
		110.50	5.187E+07
		114.50	6.610E+07
		118.50	8.268E+07
		122.50	9.990E+07
		125.50	1.187E+08
		128.50	1.405E+08
		131.50	1.553E+08
		134.50	1.725E+08
		137.50	1.835E+08
		141.50	1.786E+08
		145.50	1.596E+08
		149.50	1.344E+08
		153.50	1.003E+08

Table 5.2.2. VENUS-3: Experimental equivalent fission fluxes of indium detectors at core barrel locations

Measurement position	Angle	Axial level (cm)	$^{115}In(n,n')$
Core barrel			
(-37,+2)	0.7°	106.50	1.898E+07
		110.50	2.632E+07
		114.50	3.364E+07
		118.50	4.168E+07
		122.50	5.081E+07
		125.50	5.862E+07
		128.50	6.611E+07
		131.50	7.527E+07
		134.50	7.857E+07
		137.50	8.181E+07
		141.50	7.946E+07
		145.50	7.187E+07
		149.50	6.074E+07
		153.50	4.538E+07
(-37,-5)	10.8°	114.50	3.114E+07
		131.50	6.647E+07
		145.50	6.490E+07
(-35,-12)	21.1°	114.50	3.145E+07
		131.50	6.527E+07
		145.50	6.317E+07
(-34,-15)	25.6°	114.50	2.916E+07
		131.50	5.782E+07
		145.50	5.406E+07
(-33,-17)	28.8°	106.50	1.616E+07
		110.50	2.251E+07
		114.50	2.843E+07
		118.50	3.422E+07
		122.50	4.037E+07
		125.50	4.450E+07
		128.50	4.936E+07
		131.50	5.326E+07
		134.50	5.578E+07
		137.50	5.706E+07
		141.50	5.482E+07
		145.50	4.892E+07
		149.50	4.325E+07
		153.50	3.041E+07

Table 5.2.3. VENUS-3: Experimental equivalent fission fluxes of indium detectors at core barrel locations

Measurement position	Angle	Axial level (cm)	$^{115}In(n,n')$
Core barrel			
(-31,-20)	33.9°	106.50	1.696E+07
		110.50	2.323E+07
		114.50	2.884E+07
		118.50	3.446E+07
		122.50	3.955E+07
		125.50	4.336E+07
		128.50	4.667E+07
		131.50	4.954E+07
		134.50	5.079E+07
		137.50	5.121E+07
		141.50	4.861E+07
		145.50	4.393E+07
		149.50	3.846E+07
		153.50	2.700E+07
(-28,-24)	41.0°	114.50	2.928E+07
		131.50	4.457E+07
		145.50	3.611E+07
(-26,-26)	45.0°	114.50	3.187E+07
		131.50	4.601E+07
		145.50	3.651E+07
(-12,-35)	68.9°	114.50	7.292E+07
		131.50	1.001E+08
		145.50	7.480E+07
(+2,-37)	89.3°	106.50	5.576E+07
		110.50	7.180E+07
		114.50	8.627E+07
		118.50	9.990E+07
		122.50	1.101E+08
		125.50	1.140E+08
		128.50	1.168E+08
		131.50	1.159E+08
		134.50	1.154E+08
		137.50	1.111E+08
		141.50	1.006E+08
		145.50	8.685E+07
		149.50	7.624E+07
		153.50	5.050E+07

Table 5.3. VENUS-3: Experimental equivalent fission fluxes of aluminium detectors at various locations

Measurement position	Angle	Axial level (cm)	$^{27}Al(n,\alpha)$
Inner baffle			
(-1,-1)	45.0°	131.50	1.927E+09
(-1,+2)	8.1°	131.50	1.561E+09
Outer baffle			
(-29,+2)	0.9°	114.50	1.852E+08
		131.50	4.788E+08
		145.50	4.765E+08
Water gap			
(-33,+2)	0.8°	114.50	8.376E+07
		131.50	1.871E+08
		145.50	1.782E+08
Core barrel			
(-37,+2)	0.7°	114.50	4.110E+07
		131.50	7.669E+07
		145.50	7.270E+07
(-37,-5)	10.8°	114.50	3.197E+07
		131.50	6.316E+07
		145.50	6.026E+07
(-35,-12)	21.1°	114.50	3.159E+07
		131.50	6.022E+07
		145.50	5.705E+07
(-34,-15)	25.6°	114.50	3.051E+07
		131.50	5.328E+07
		145.50	4.801E+07
(-33,-17)	28.8°	114.50	2.753E+07
		131.50	4.977E+07
		145.50	4.330E+07
(-31,-20)	33.9°	114.50	3.168E+07
		131.50	5.149E+07
		145.50	4.350E+07
(-28,-24)	41.0°	114.50	3.683E+07
		131.50	5.481E+07
		145.50	4.279E+07
(-26,-26)	45.0°	114.50	3.807E+07
		131.50	5.532E+07
		145.50	4.231E+07
(-12,-35)	68.9°	114.50	6.806E+07
		131.50	8.915E+07
		145.50	6.547E+07
(+2,-37)	89.3°	114.50	9.554E+07
		131.50	1.202E+08
		145.50	8.848E+07

Table 6.1. Uncertainty results of VENUS-3

Source of uncertainty		Uncertainty (%)			
Neutron source		$\phi > 1$ MeV	$^{27}Al(n,\alpha)$	$^{58}Ni(n,p)$	$^{115}In(n,n')$
Fission spectrum		4.4	12	6.5	4.4
Source space distribution		1.5-4			
Absolute power		4			
Detector					
Response function		0	1.4	2.5	2.2
Cross-sections	H	1.9	1.1	1.4	1.6
	O	0.6	1.6	0.7	0.5
	Fe	2	5	2.5	2.1
Total for reaction rates		7.1	14.1	9.0	7.4
Total for equivalent fission fluxes		–	7.2	5.7	5.5

Table 6.2. VENUS-1: Detector cross-sections averaged with the fission spectrum of ^{235}U

	Siemens	**SCK·CEN**	**VTT**	**IKE**	**ENEA**
Library basic data groups	IRDF-90 V.2 EURLIB 100 g	ELXSIR ENDF/B-V 56 g	IRDF-90 V.2 BUGLE-96 47 g	IRDF-90 V.2 VITAMIN 175 g	IRDF-90 V.2 BUGLE-96 47 g
Ni	0.1050	0.1053		0.1053	0.1072
In	0.1852	0.1795		0.1853	0.1865
Rh	0.7027			0.7031	0.7068
^{238}U	0.3043	0.3048		0.3046	0.3074
^{237}Np	1.3490	1.3479		1.3498	1.3555
	NRG	**PSI**	**KOPEC**	**JAERI**	**CAB**
Library basic data groups	IRDF-90 V.2 – cont.	JEFF-1 – 45g	ENDF/B-VI BUGLE-96 47 g	IRDF-90 V.2 BUGLE-96 47 g	IRDF-90 V.2 BUGLE-96 47 g
Ni	0.1069		0.1070	0.1027	0.1067
In	0.1855		0.1802	0.1823	0.1854
Rh	0.7035		0.7057 (IRDF 90 V.2)	0.6951	0.7000
^{238}U	0.3039		0.3070	0.2985	0.3045
^{237}Np	1.3411		1.330	1.3372	1.3437

Table 6.3. VENUS-3: Detector cross-sections averaged with the fission spectrum of ^{235}U

	VTT	NEA	SPAIN	KOPEC
Library basic data groups	IRDF-90 V.2 BUGLE-96 47 g	IRDF-90 V.2 BUGLE-96 47 g	IRDF-90 V.2 – –	ENDF/B-VI BUGLE-96 47 g
Ni	0.105	0.1063	0.105	0.107
In	0.184	0.1797	0.185	0.1802
Al	7.087E-4	7.32E-4	0.72E-3	7.82E-4

	Siemens	IKE	IKE	PSU	ORNL
Library basic data groups	IRDF-90 V.2 EURLIB 100 g	IRDF-90 V.2 VITAMIN 175 g	ENDF/B-VI BUGLE-96 47 g	ENDF/B-VI BUGLE-96 47 g	ENDF/B-V E>0.1MeV 38 g
Ni	0.105	0.1053	0.107	0.1079	0.1085
In	0.1852	0.1853	0.1802	0.1793	0.1903
Al	7.2E-4	7.279E-4	7.821E-4	7.765E-4	7.06E-4

Table 6.4. Fission averaged detector cross-section σ[b] in continuous energy or multi-group representation with data from IRDF-90 V.2

Detector	Institutions:	NRG	SPAIN	IKE	Siemens	Mean value
	Groups:	cont.	cont.	175	100	
Ni	σ_{Ni}[b]	0.1069	0.105	0.1053	0.105	0.10555
In	σ_{In}[b]	0.1855	0.185	0.1853	0.1852	0.18525
Al	σ_{Al}[b]	0.719E–3	0.720E–3	0.7279E–3	0.720E–3	0.72173E–3
Rh	σ_{Rh}[b]	0.7035	–	0.7031	0.7027	0.7031
^{238}U	σ_{U}[b]	0.3039	–	0.3046	0.3043	0.30427
^{237}Np	σ_{Np}[b]	1.341	–	1.3498	1.349	1.3466

Table 6.5. Relative deviation Δσ/σ[%] of fission averaged detector cross-section σ in few group representation of BUGLE-96 with data from IRDF-90 V.2

Detector	Reference σ-value of Table. 6.4	Institutions:	CAB	ENEA	NEA	VTT	JAERI
Ni	0.10555	σ[b] Δσ/σ[%]	0.1067 +1.09	0.1072 +1.56	0.1063 +0.71	0.105 -0.52	0.1027 -2.70
In	0.18525	σ[b] Δσ/σ[%]	0.1854 +0.08	0.1865 +0.67	0.1797 -3.00	0.184 -0.67	0.1823 -1.59
Al	0.72173E–3	σ[b] Δσ/σ[%]	– –	– –	0.7323E-3 +1.46	0.7087E-3 -1.80	– –
Rh	0.7031	σ[b] Δσ/σ[%]	0.700 -0.44	0.7068 +0.53	– –	– –	0.6951 -1.14
^{238}U	0.30427	σ[b] Δσ/σ[%]	0.3045 +0.08	0.3074 +1.03	– –	– –	0.2985 -1.90
^{237}Np	1.3466	σ[b] Δσ/σ[%]	1.3437 -0.22	1.3555 -0.66	– –	– –	1.3372 -0.70

Table 6.6. Relative deviation Δσ/σ[%] of fission averaged detector cross-section σ in few group representation of BUGLE-96 with data from ENDF/B-VI/V

Detector	Reference σ-value of Table 6.4	Institutions:	IKE	ENEA	KOPEC	ORNL (Mol exp.)	ORNL (B-V)	PSU
Ni	0.10555	σ[b]	0.1070	0.1070	0.1070	0.1085	0.1054	0.1079
		Δσ/σ[%]	+1.37	+1.37	+1.37	+2.79	-0.14	+2.22
In	0.18525	σ[b]	0.1802	0.1802	0.1802	0.1903	0.1803	0.1793
		Δσ/σ[%]	-2.73	-2.73	-2.73	+2.73	-2.67	-3.21
Al	0.72173E–3	σ[b]	0.7821E-3	–	0.782E-3	0.706E-3	0.67E-3	0.7763E-3
		Δσ/σ[%]	+8.36	–	+8.35	-2.18	-7.17	+7.59
Rh	0.7031	σ[b]	0.1194	0.1195	0.7057	–	–	–
		Δσ/σ[%]	–	–	+0.37	–	–	–
^{238}U	0.30427	σ[b]	0.3073	0.3073	0.3070	–	–	–
		Δσ/σ[%]	+1.00	+1.00	+0.90	–	–	–
^{237}Np	1.3466	σ[b]	1.3305	1.3305	1.330	–	–	–
		Δσ/σ[%]	-1.20	-1.20	-1.24	–	–	–

Figure 4.1. VENUS-1: Detector positions

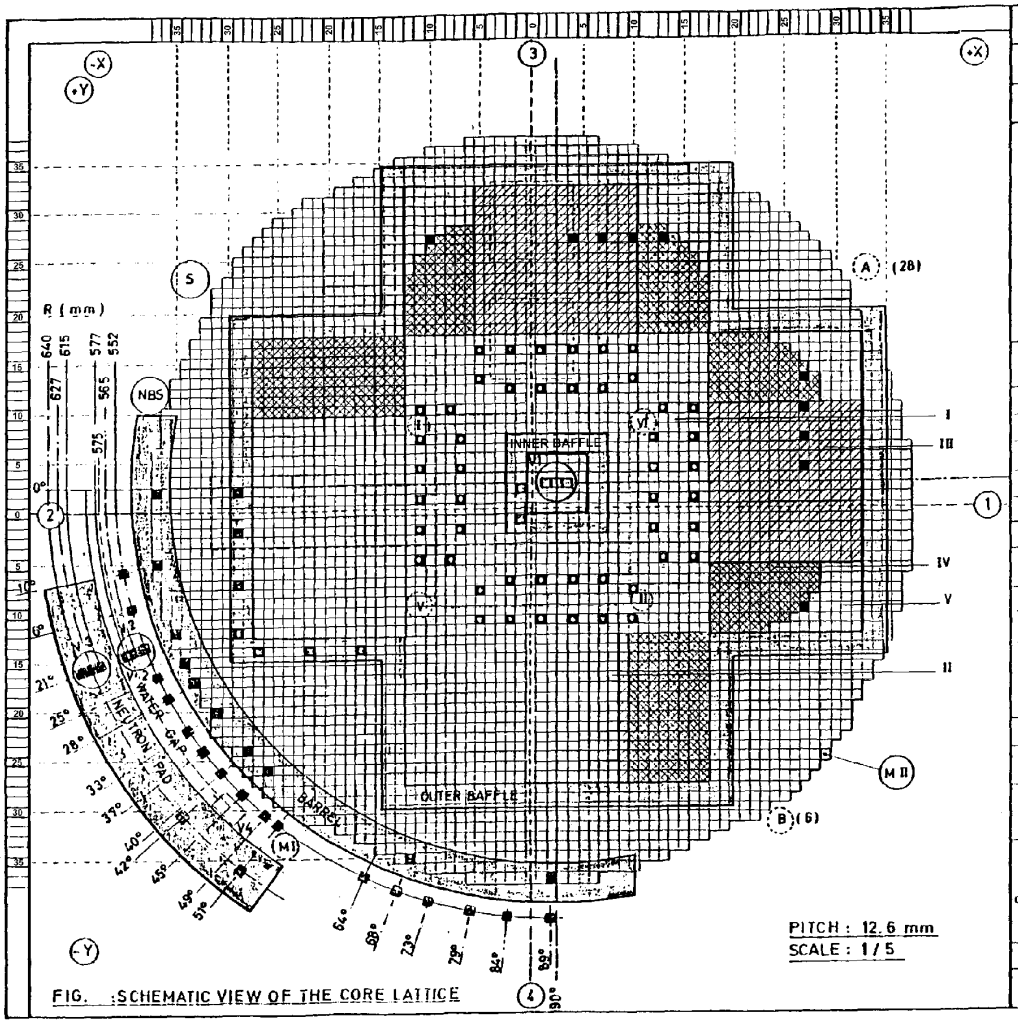

FIG. : SCHEMATIC VIEW OF THE CORE LATTICE

C.E.N-S.C.K | VENUS CRITICAL EXPERIMENT

EXPERIMENT : LWR-PVS - BENCHMARK

DATE : from 24.01.83 to 23.06.83

CONFIGURATION N° 29/16

DENSITY RODS : NONE

BORON CONCENTRATION (p.p.m.) : NONE

START-UP SOURCE (S) YES

NEUTRON GENERATOR (N) NONE

ABSORBING ROD ■ BR + 2M

PYREX ROD □ 48

FUEL REGIONS TOTAL : (2600 - 58) pins

DESIGNAT.	%U5/%Pu (1)	COLOUR OR SYMBOL	NUMBER OF FUEL PINS	EQ. RADIUS OR X . Y	INVESTIGATED CELL
I	3/0		800-48		
II	4/0 (3d)		645		
III	4/0 (1st)		495 - 6		
IV	4/0 (2d)		504 - 2		
V	3/0 (2)		156 - 2		

MONITORING DETECTORS

DESIGNAT.	DIAMET.	SYMBOL	N° CABLE	LOCATION	LEVEL	CHANNEL
PROPORTIONAL BF3 COUNTER						
FISSION CHAMBER	1/8"	M I		R=552 θ=75°	Bottom	C
	1/4"	M II		X=+29 Y=-25	Bottom	D
	1"	NBS				

CONTROL DETECTORS

DESIGNAT.	DIAMET.	SYMBOL	N°	LOCATION	LEVEL	CHANNEL
PROPORTIONAL COUNTER	1"	(A)		28	mid-pl.	A
	1"	(B)		6	mid-pl.	B
ION CHAMBER (NON-COMPENSATED)		(I)		X=-11 Y=+9	under reactor	I
		(II)		X=+11 Y=-9	under reactor	II
		(V)		X=-11 Y=-9	under reactor	V
		(VI)		X=+11 Y=+9	under reactor	VI

REMARK :

VERIFIED BY: APPROVED BY:

Figure 4.2. VENUS-1: C/E comparison of equivalent fission fluxes at Ni detector positions

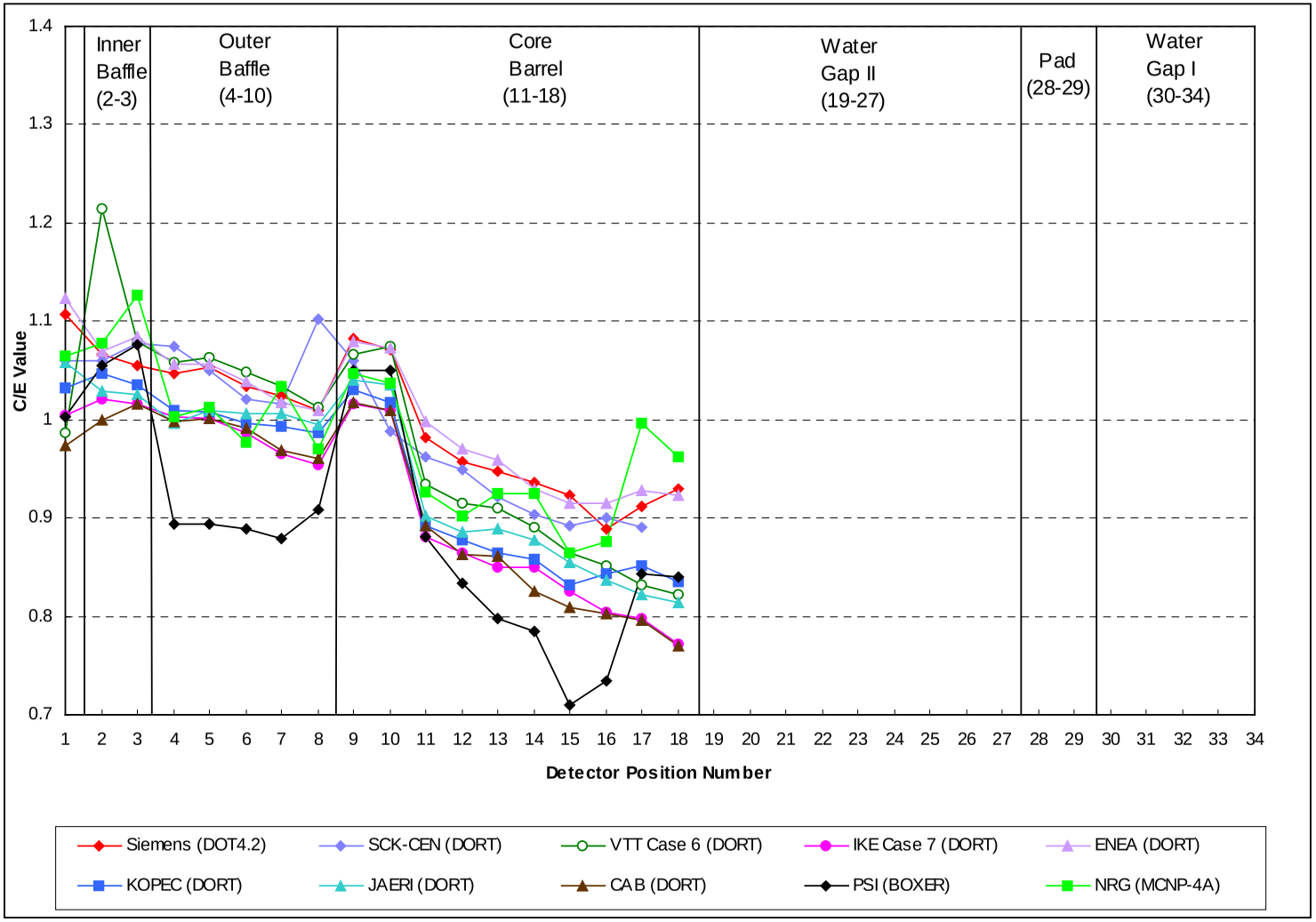

Figure 4.3. VENUS-1: C/E comparison of equivalent fission fluxes at In detector positions

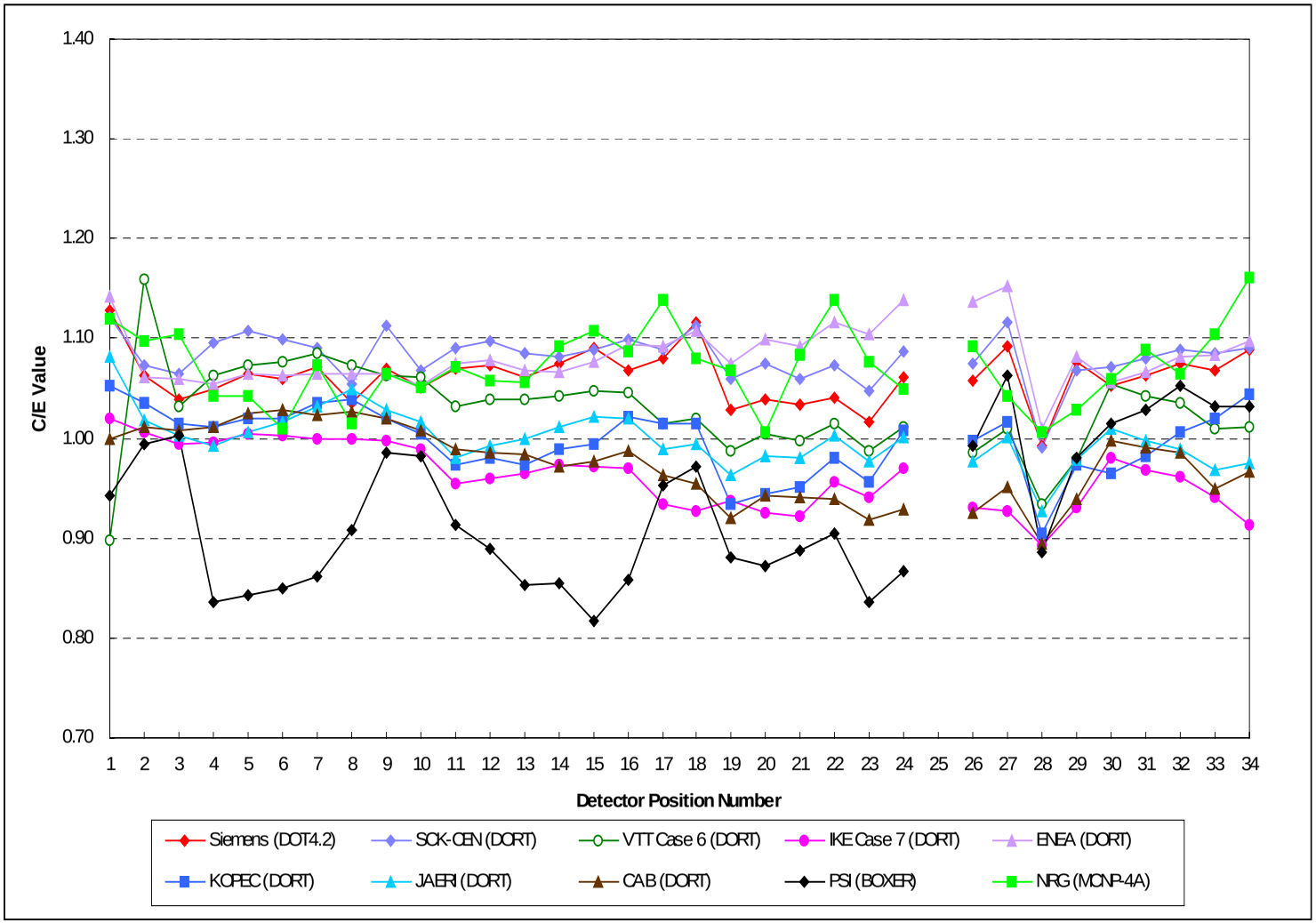

Figure 4.4. VENUS-1: C/E comparison of equivalent fission fluxes at Rh detector positions

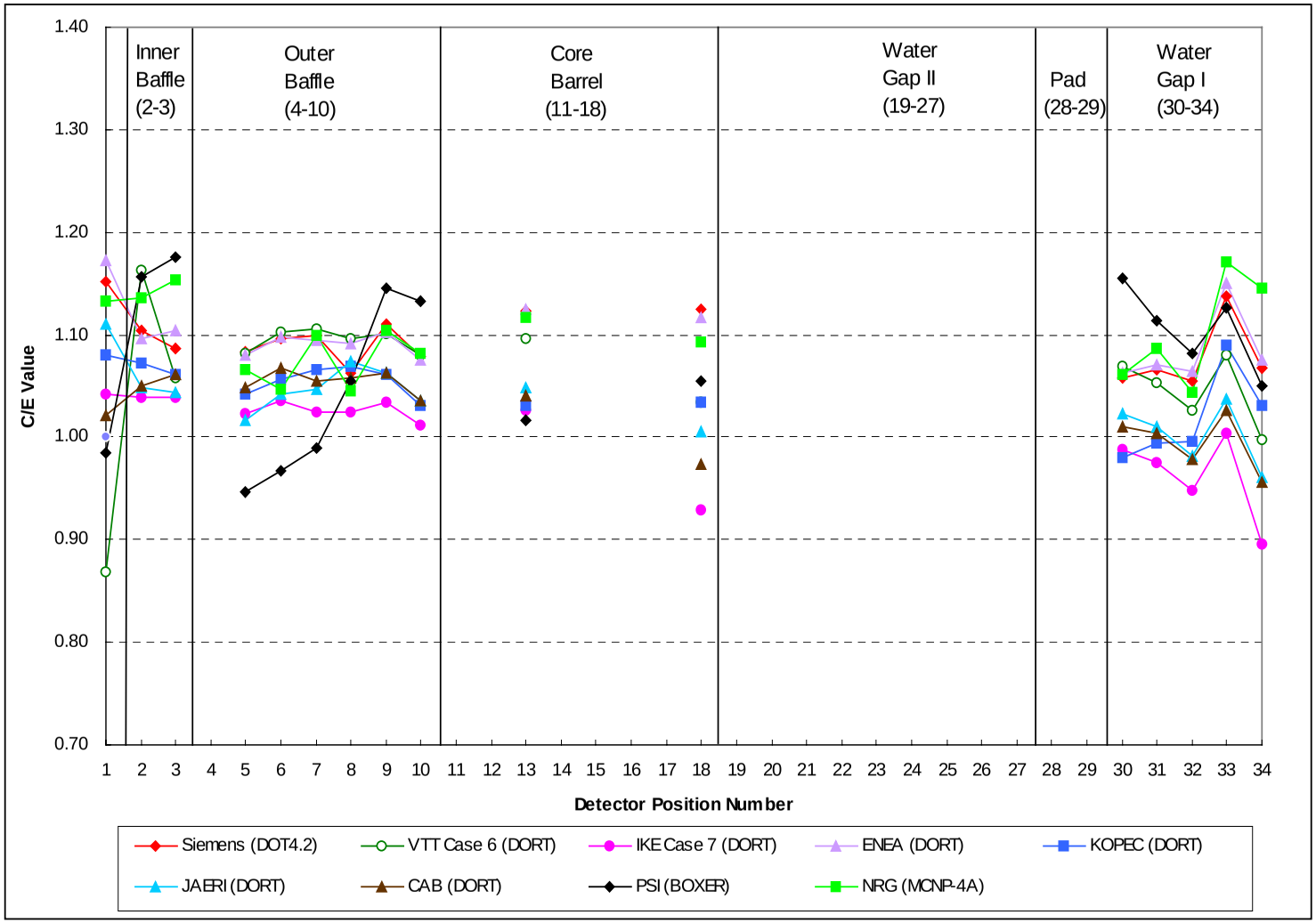

Figure 4.5. VENUS-1: C/E comparison of equivalent fission fluxes at ^{238}U detector positions

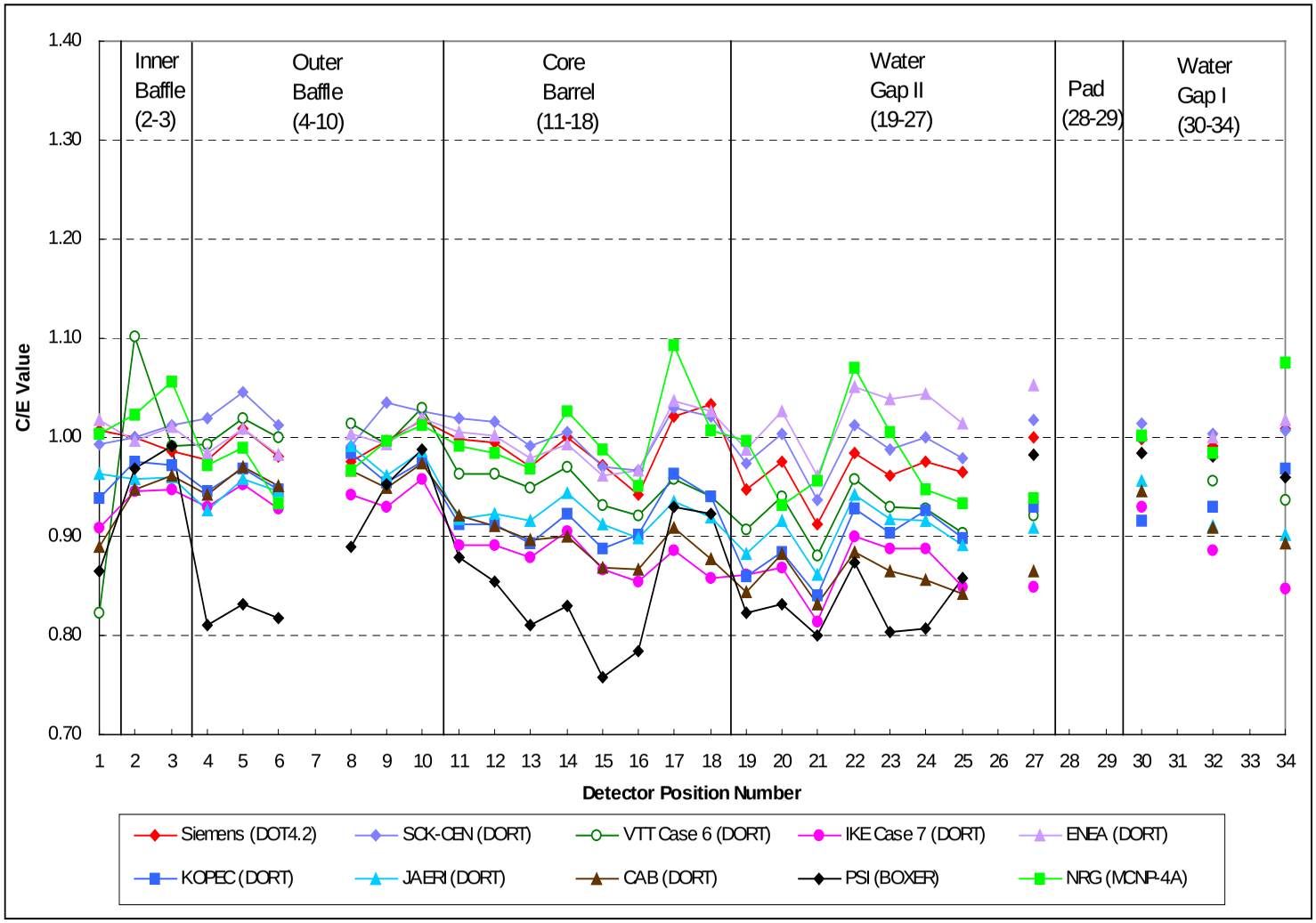

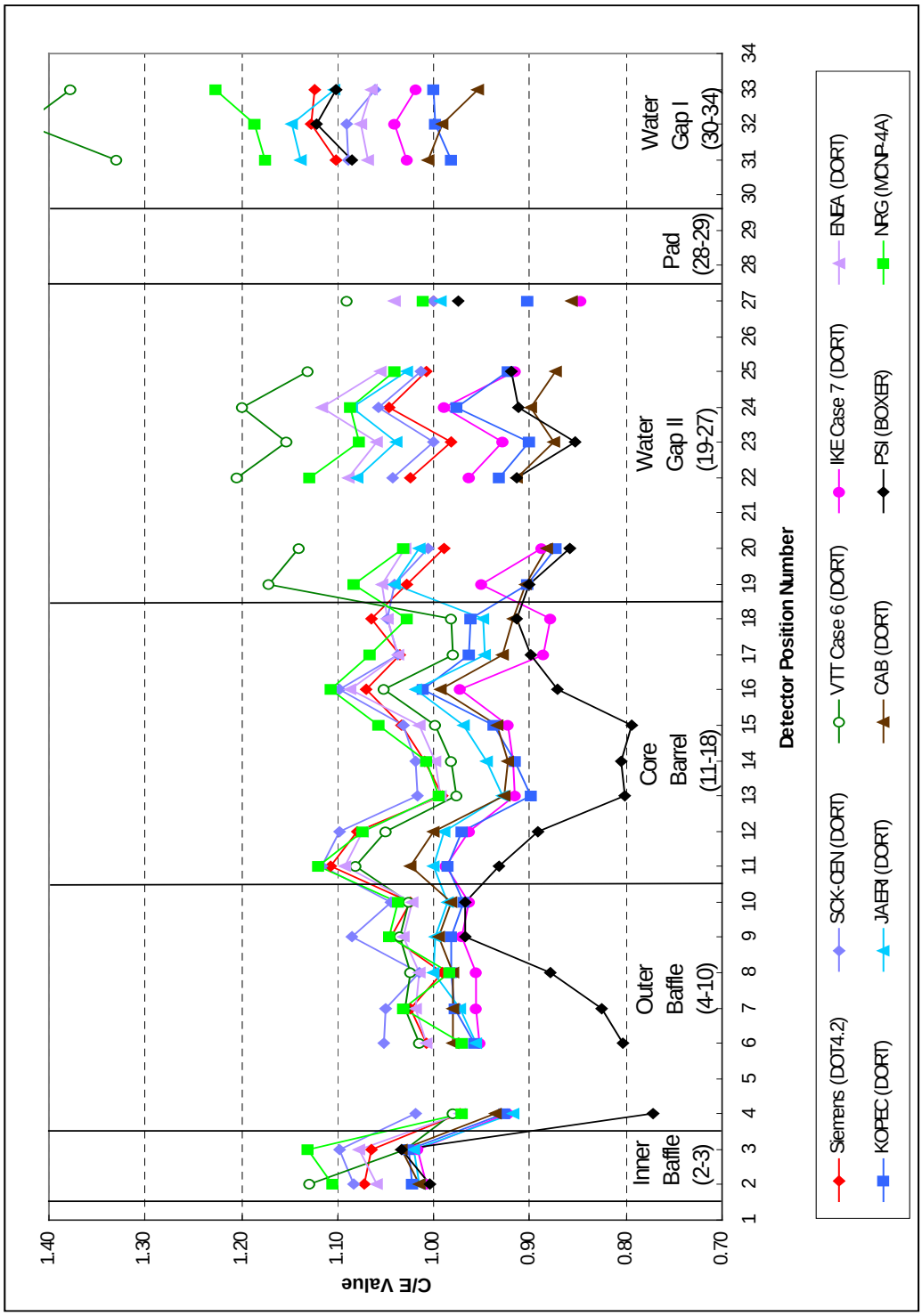

Figure 4.6. VENUS-1: C/E comparison of equivalent fission fluxes at ^{237}Np detector positions

Figure 4.7. VENUS-1: C/E comparison of equivalent fission fluxes at Ni detector positions at an angle of 45°

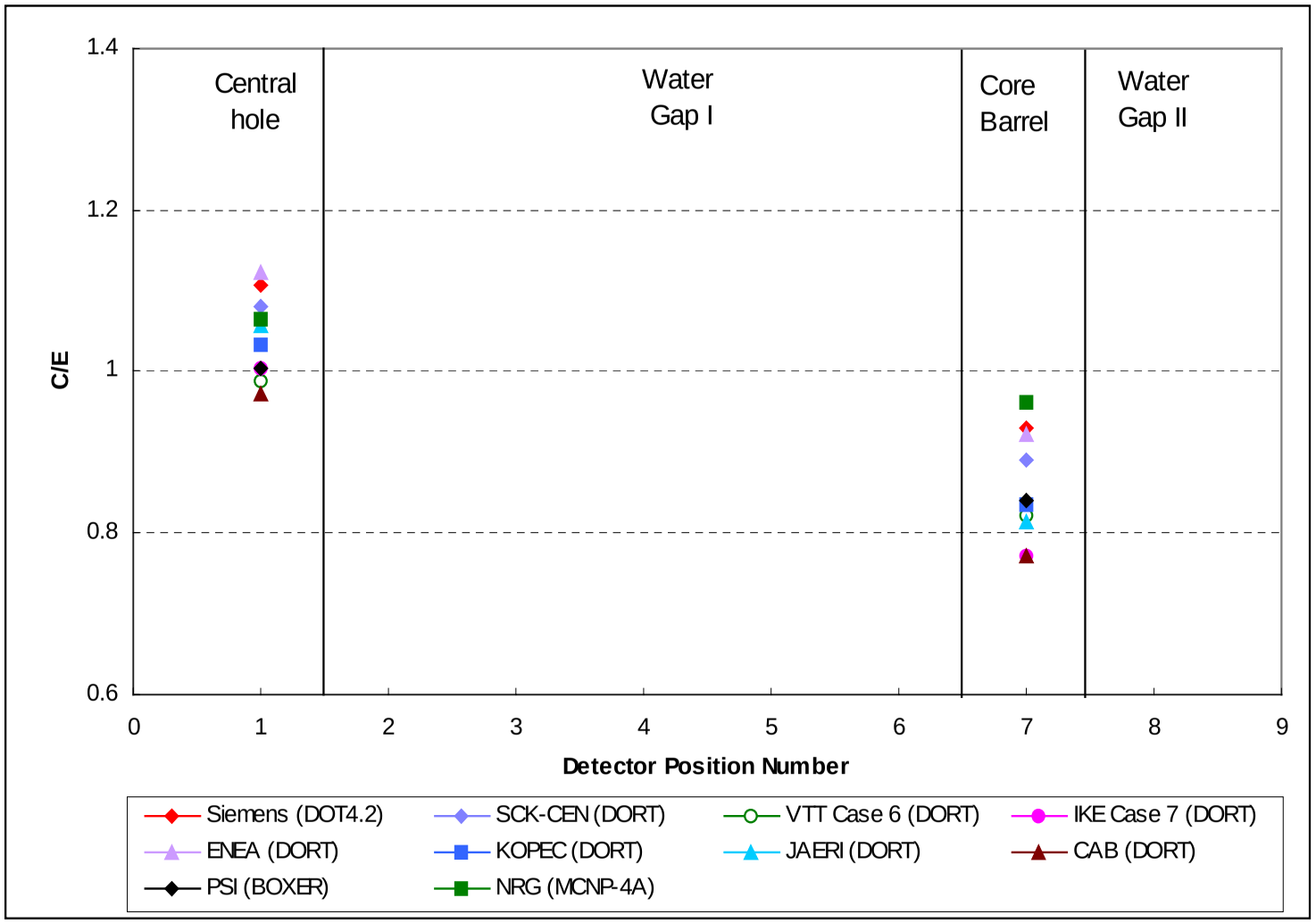

Figure 4.8. VENUS-1: C/E comparison of equivalent fission fluxes at In detector positions at an angle of 45°

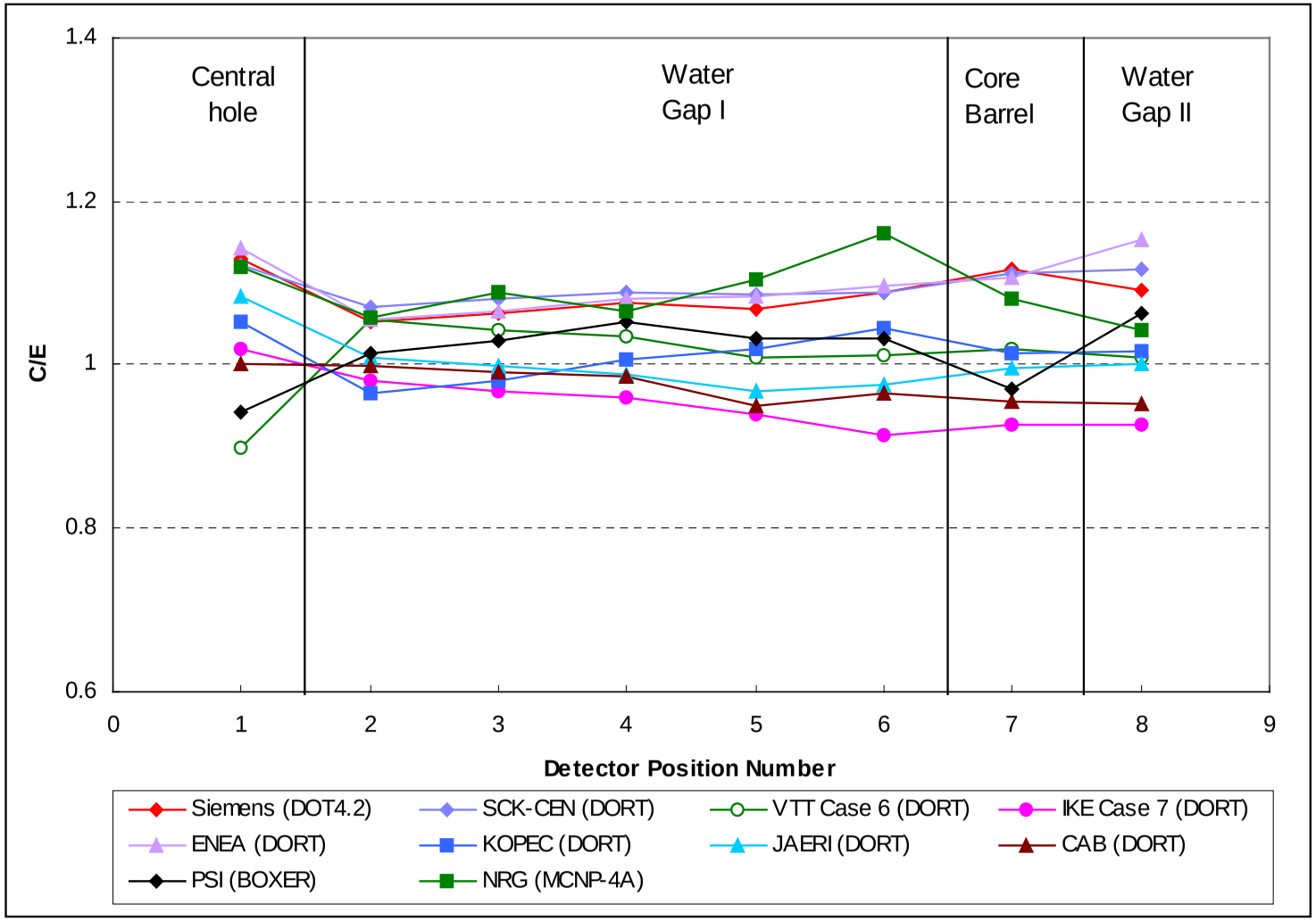

Figure 4.9. VENUS-1: C/E comparison of equivalent fission fluxes at Rh detector positions at an angle of 45°

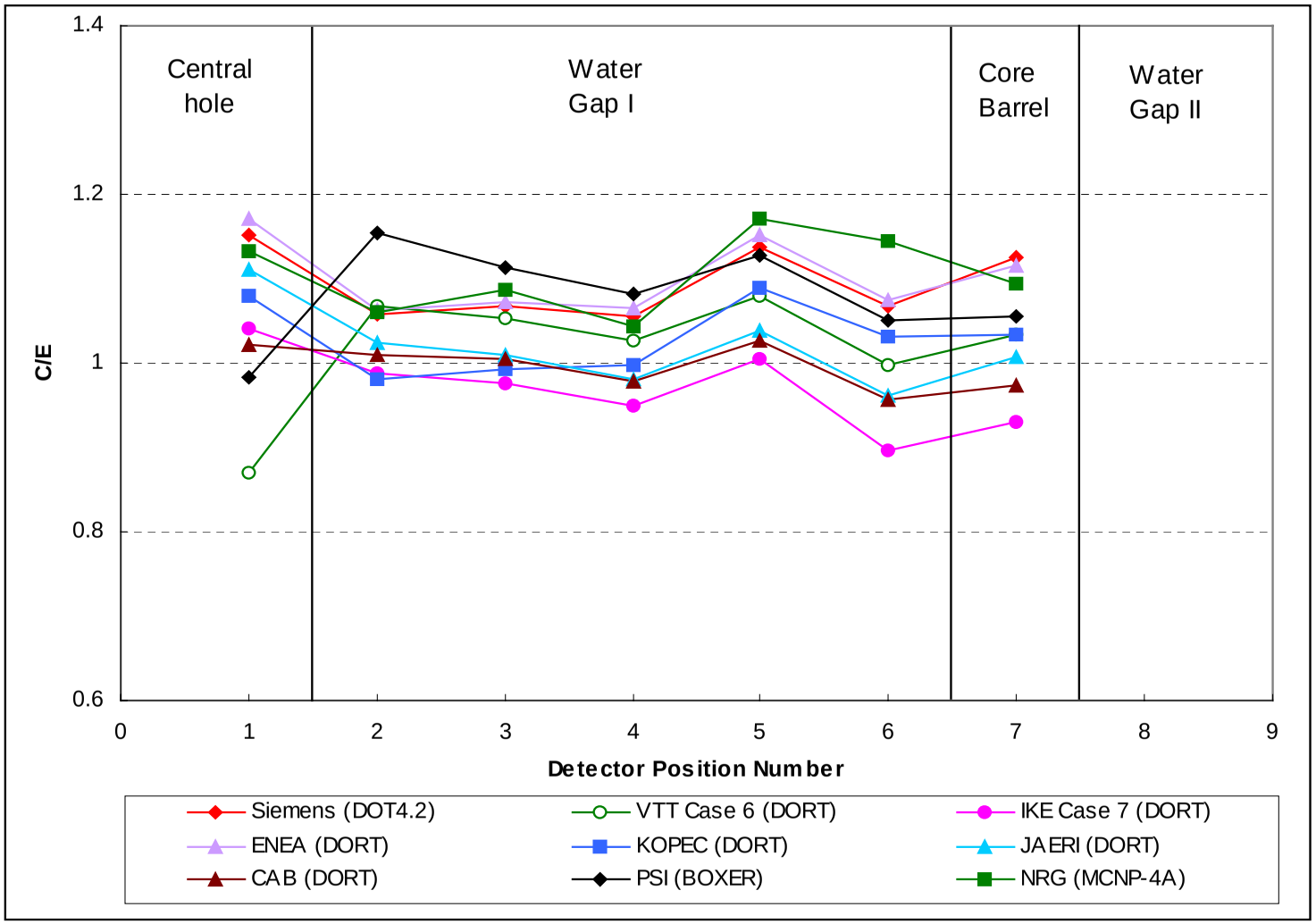

Figure 4.10. VENUS-1: C/E comparison of equivalent fission fluxes at ^{238}U detector positions at an angle of 45°

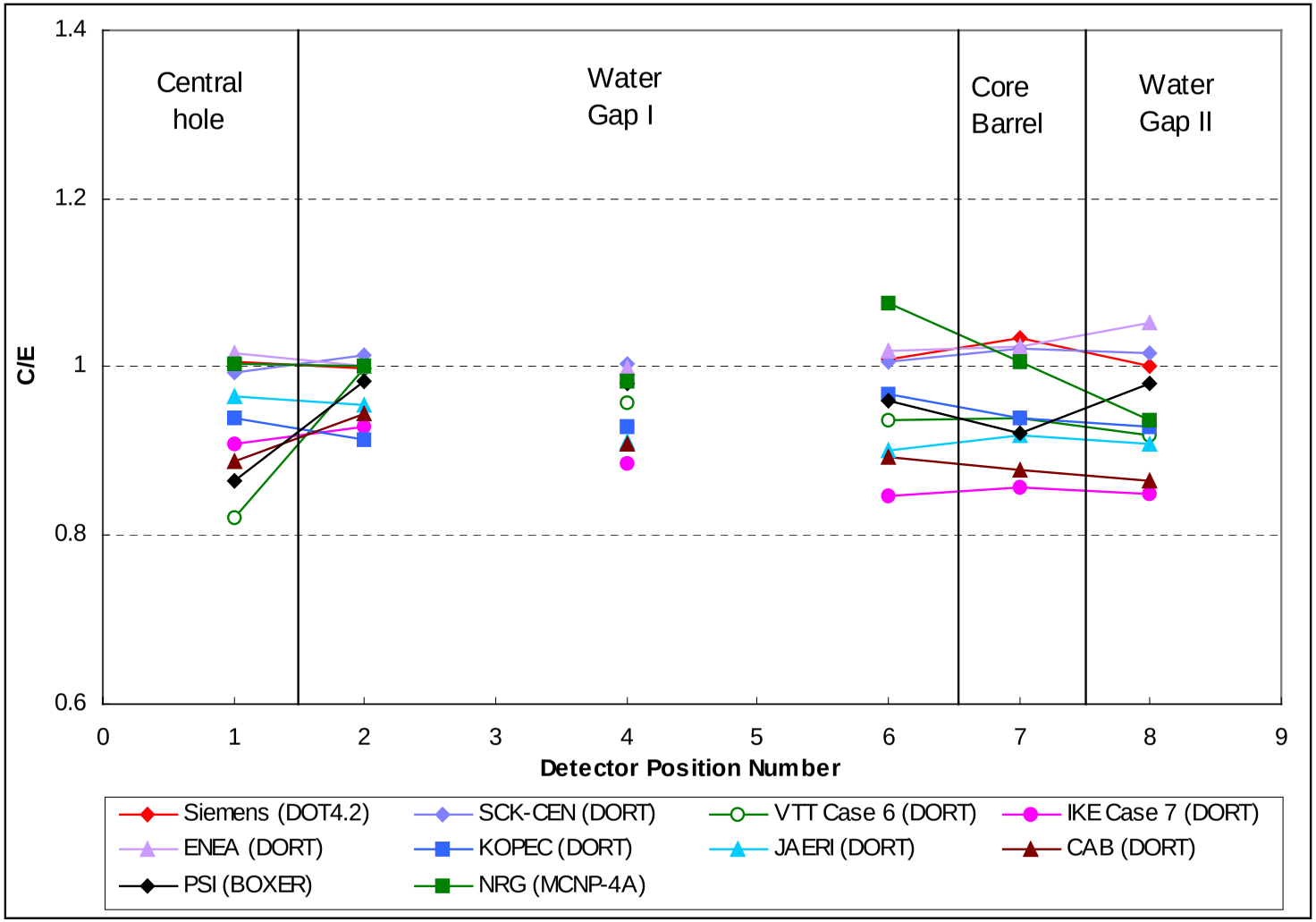

Figure 4.11. VENUS-1: C/E comparison of equivalent fission fluxes at ^{237}Np detector positions at an angle of 45°

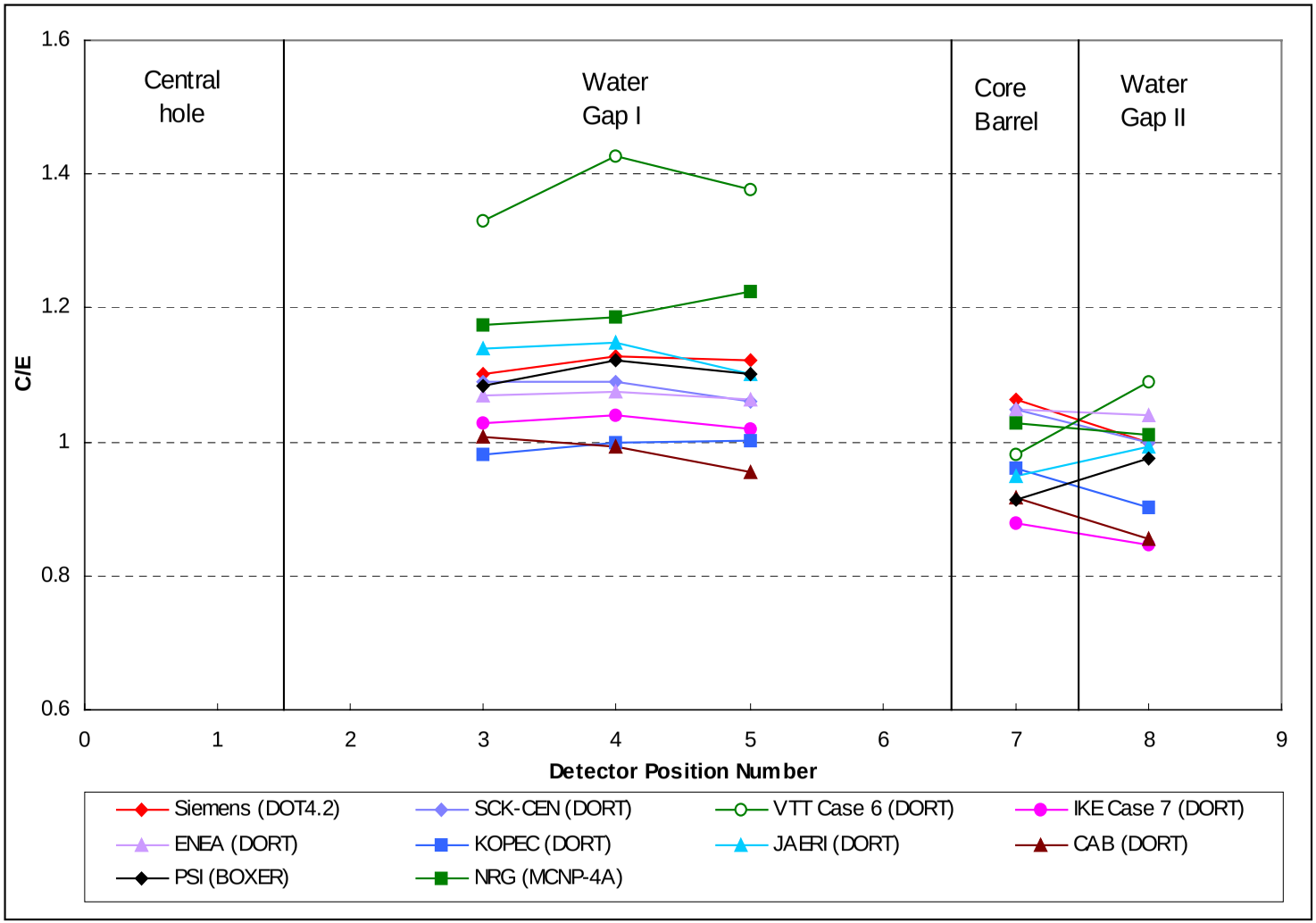

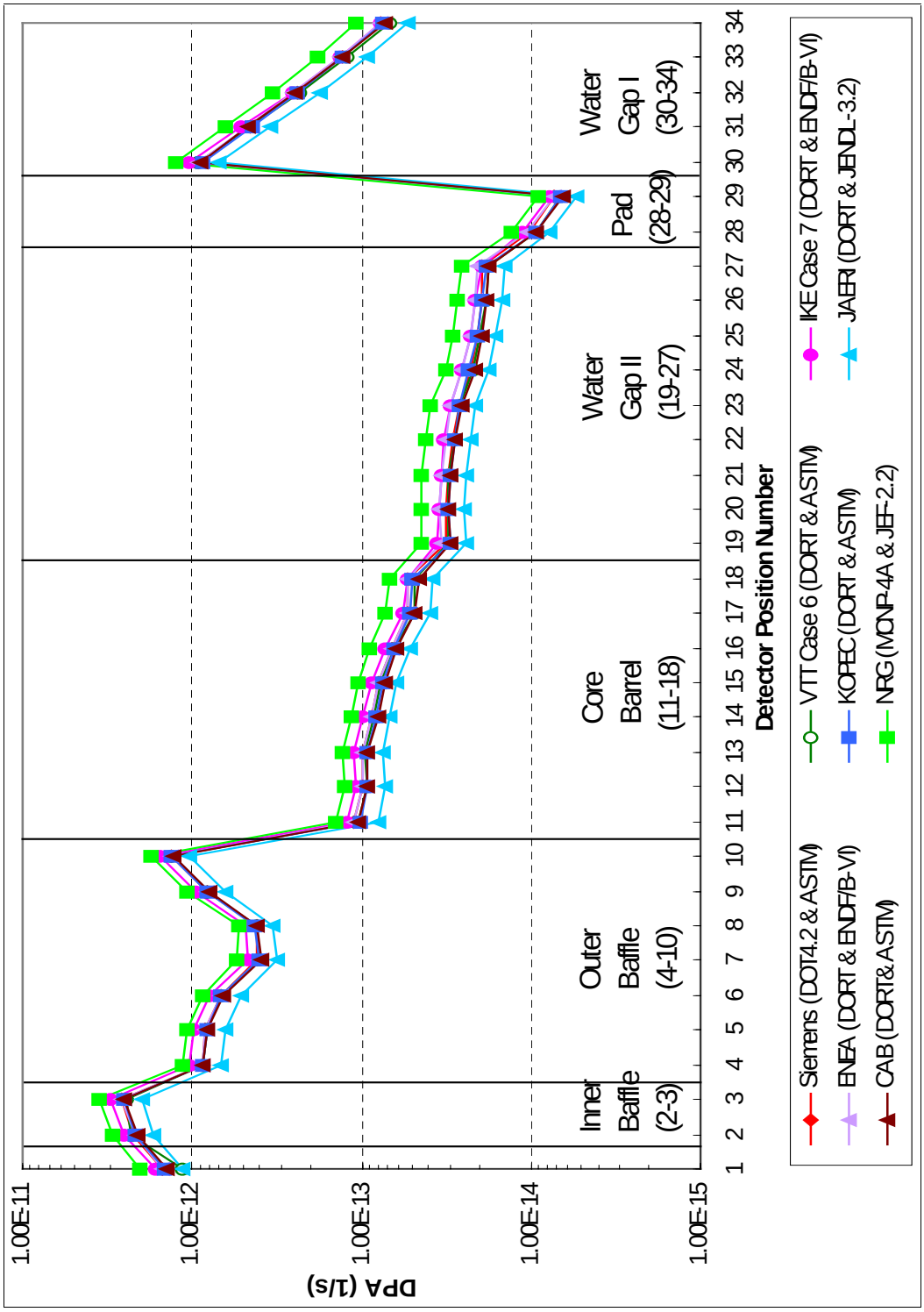

Figure 4.12(a). VENUS-1: Absolute DPA rates

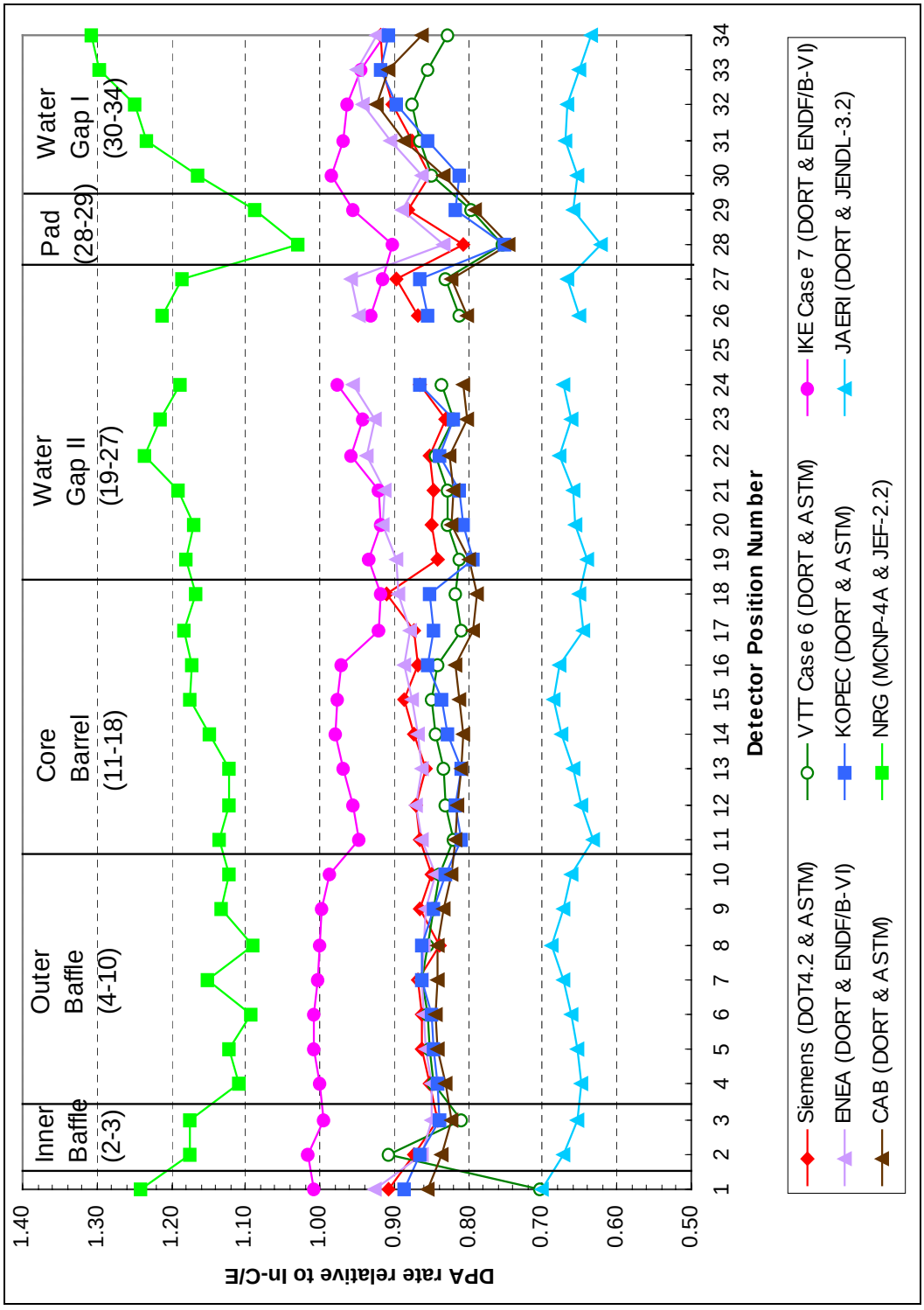

Figure 4.12(b). VENUS-1: Relative DPA rates

Figure 4.13(a). VENUS-1: Absolute fast neutron flux above 1.0 MeV

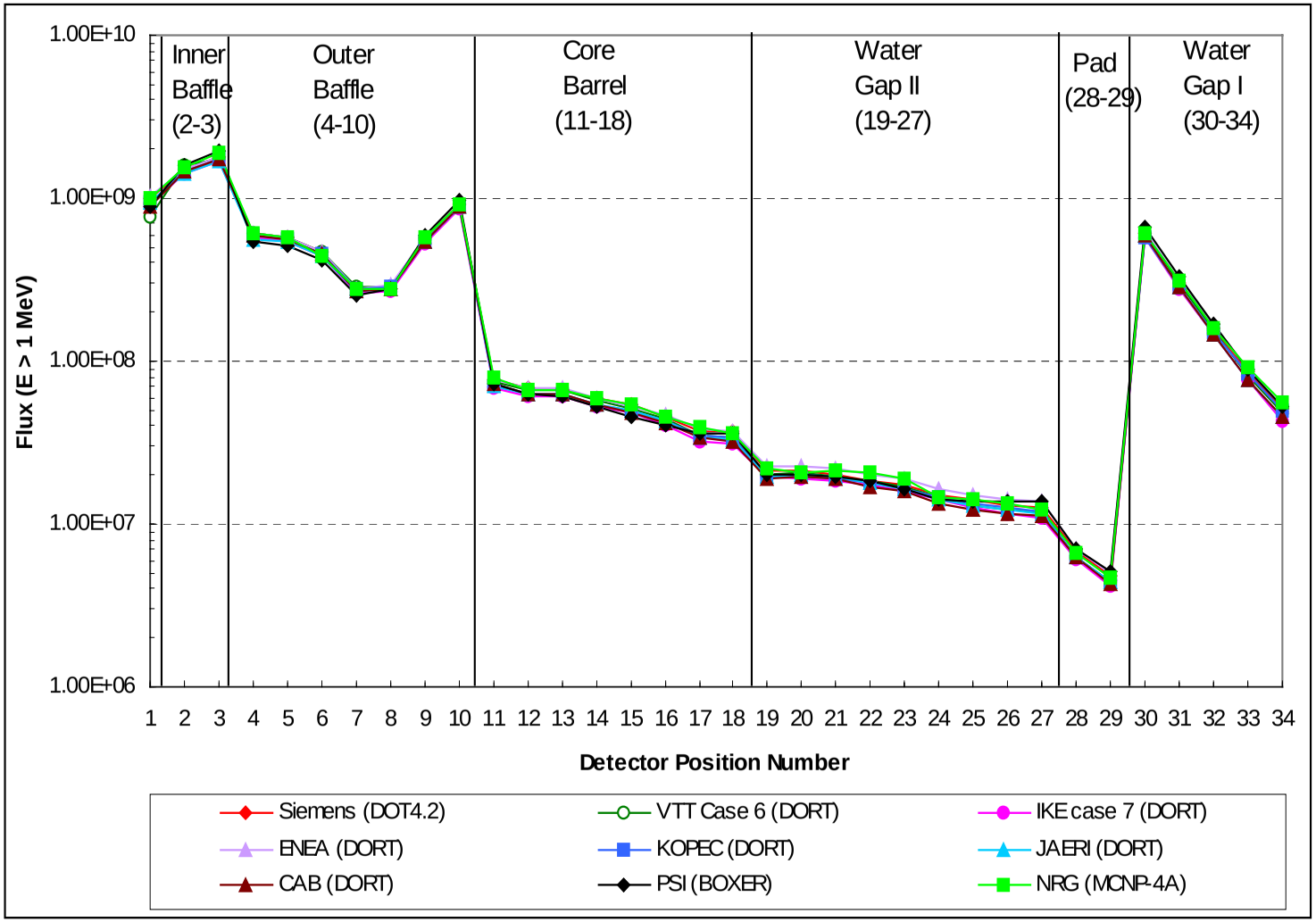

Figure 4.13(b). VENUS-1: Relative fast neutron flux above 1.0 MeV

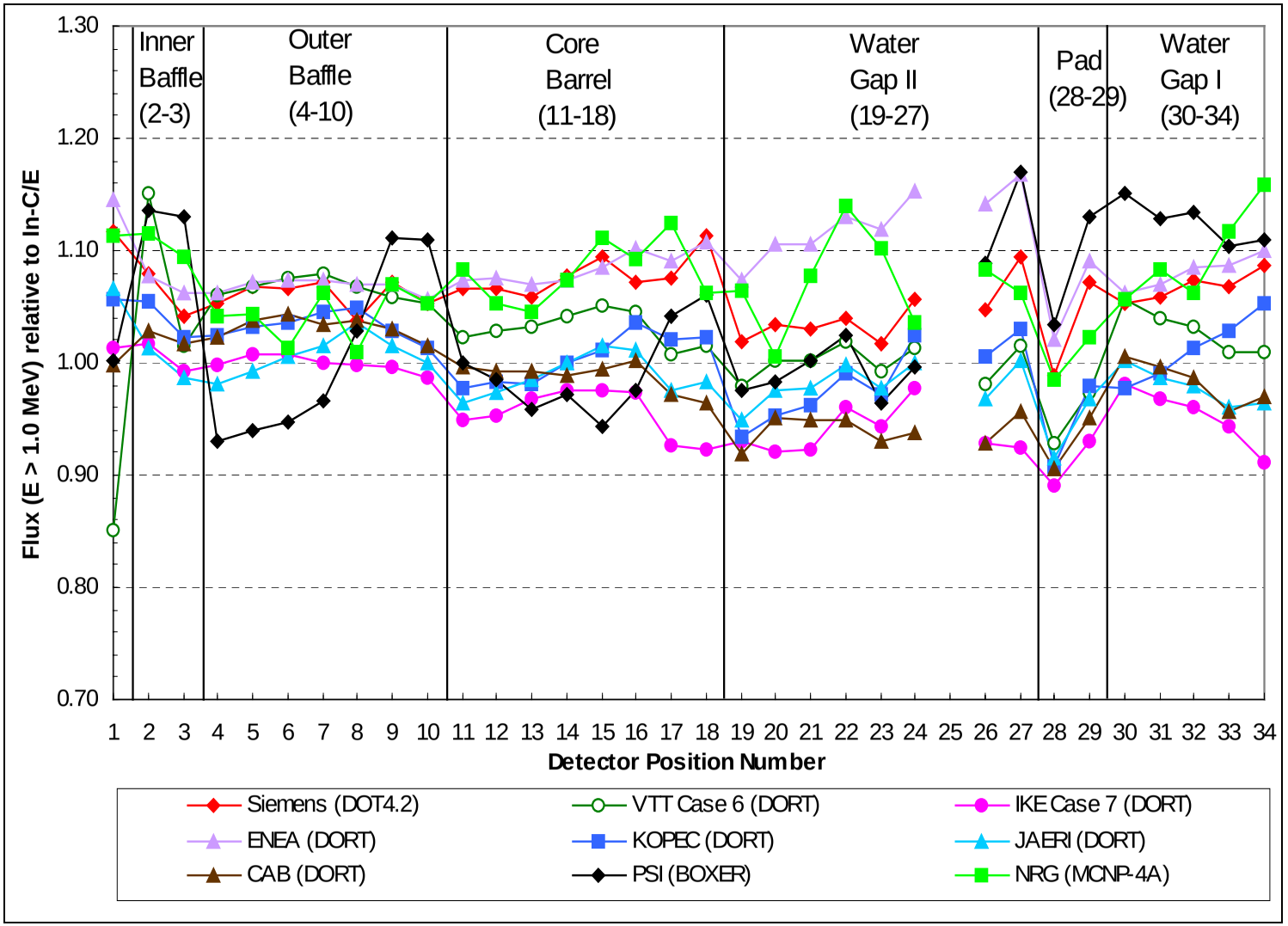

Figure 4.14(a). VENUS-1: Absolute neutron flux above 0.1 MeV

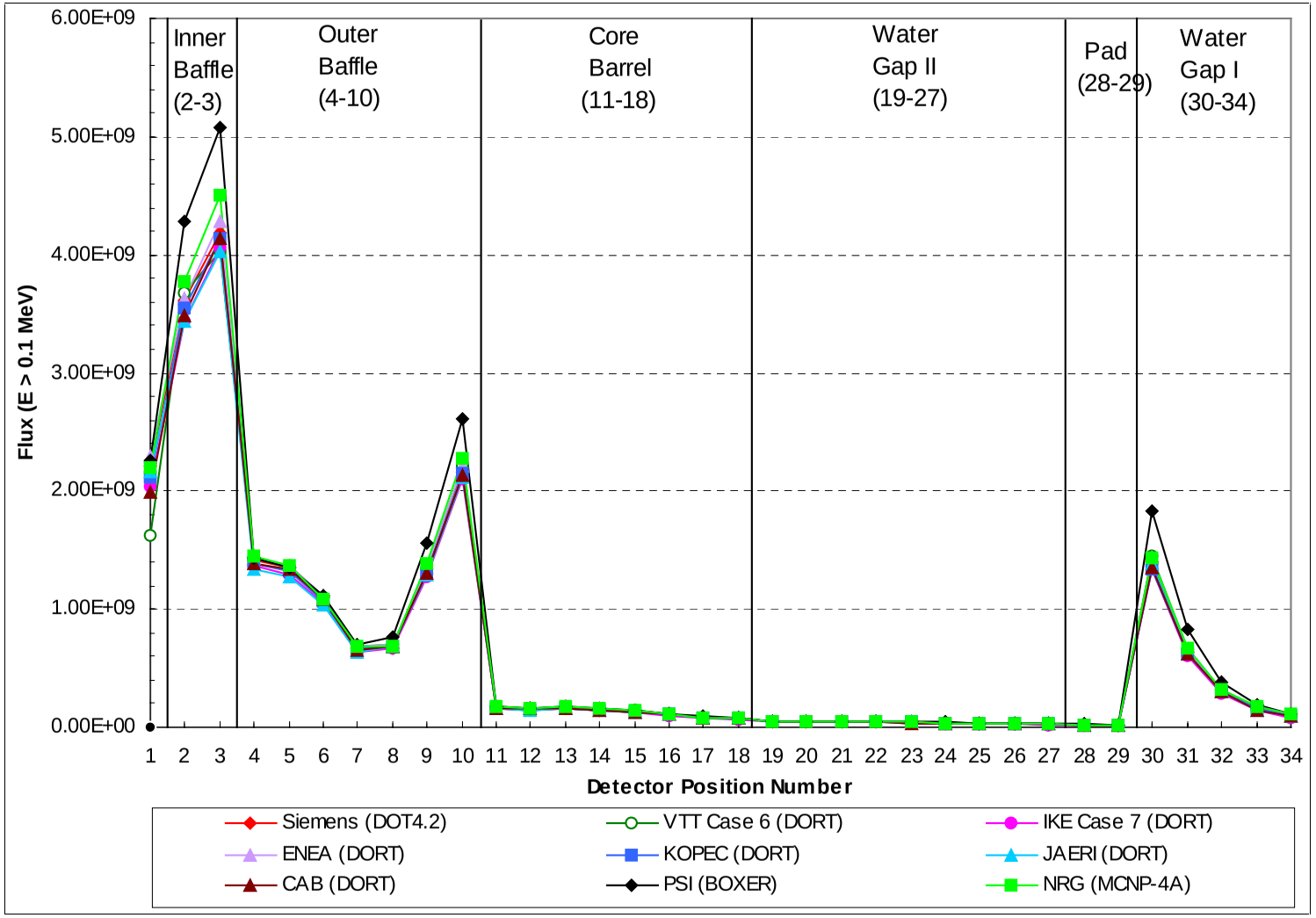

Figure 4.14(b). VENUS-1: Relative neutron flux above 0.1 MeV

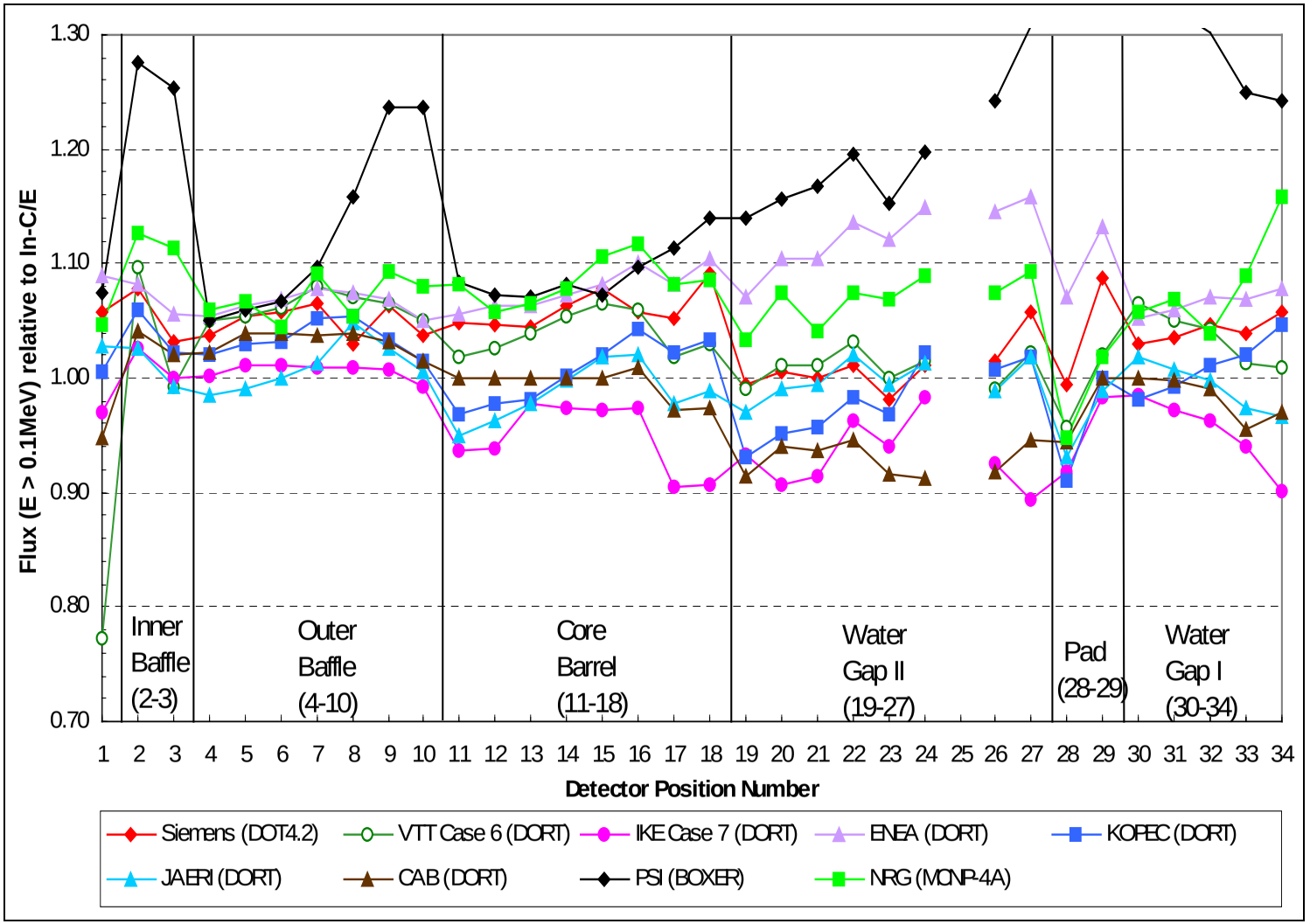

Figure 5.1. VENUS-3: Detector positions

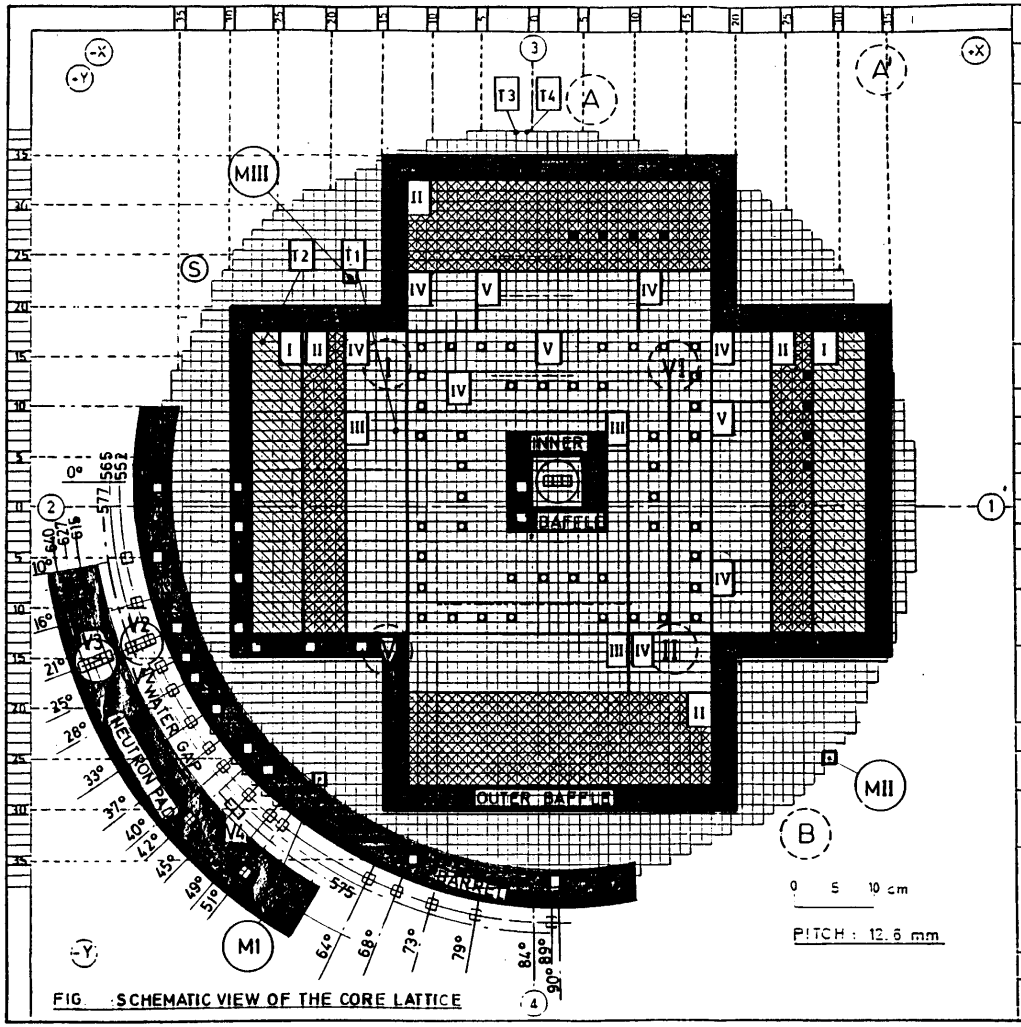

FIG : SCHEMATIC VIEW OF THE CORE LATTICE

C.E.N-S.C.K | VENUS CRITICAL FACILITY

EXPERIMENT : VENUS-3 : WR-PVS - BENCHMARK (PLSA)

DATE : from 28 03 88 to

CONFIGURATION N° 31 / 08

DENSITY RODS : NONE

BORON CONCENTRATION (p.p.m) : NONE

START-UP SOURCE (S) YES

NEUTRON GENERATOR (N) NONE

ABSORBING ROD ■ 8R Level ≈ 3/4 fuel height

PYREX ROD □ 44

FUEL REGIONS TOTAL : (2600-52) PINS

DESIGNAT.	%US/%Pu	COLOUR OR SYMBOL	NUMBER OF FUEL PINS	EQ. RADIUS OR X . Y	INVESTIGATED CELL
I	SS-3/0		300		
II	3/0		780-8		
III	4/0 (3)		648-17		
IV	4/0 (2)		456-12		
V	4/0 (1)		416-15		

MONITORING DETECTORS :

DESIGNAT.	DIAMET.	SYMBOL	N° CABLE	LOCATION X/y	LEVEL	CHANNEL
PROPORTIONAL BF_3 COUNTER						
FISSION CHAMBER	1/8" ^{5}U	MI	-	-21 / -27	Bottom	C
	1/4" ^{5}U	MII	-	+29 / -25	Bottom	E
	1mm ^{5}U	MIII	-	-18 / +23	Mid. pl. Nim-rack	

CONTROL DETECTORS

DESIGNAT.	DIAMET.	SYMBOL	N°	LOCATION	LEVEL	CHANNEL
PROPORTIONAL COUNTER	1"	(A)		wall	-	A
	1"	(B)		6	Bottom	B
ION CHAMBER UNCOMPENSATED		(I)		-	under reactor	log I
		(II)		-		log II
		(V)		-		lin V
		(VI)		-		lin VI

REMARK : K_{eff} = 1 for water at 1680 mm & R_2 ≈ 1400 mm

VERIFIED BY : APPROVED BY :

Figure 5.2. VENUS-3: C/E comparison of equivalent fission fluxes at Ni detector positions

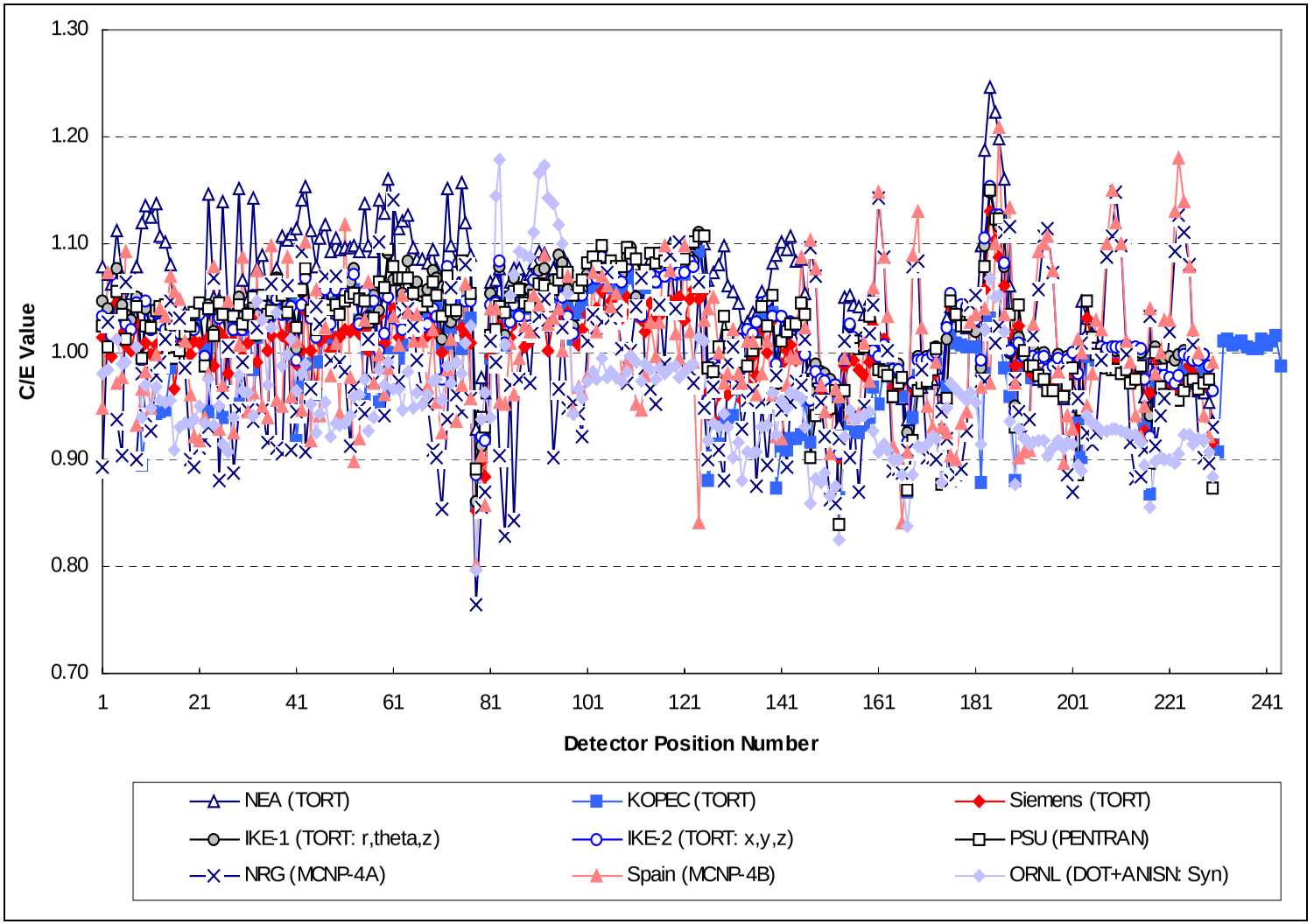

Figure 5.2(a). VENUS-3: C/E comparison of equivalent fission fluxes at Ni detector positions (1 to 126)

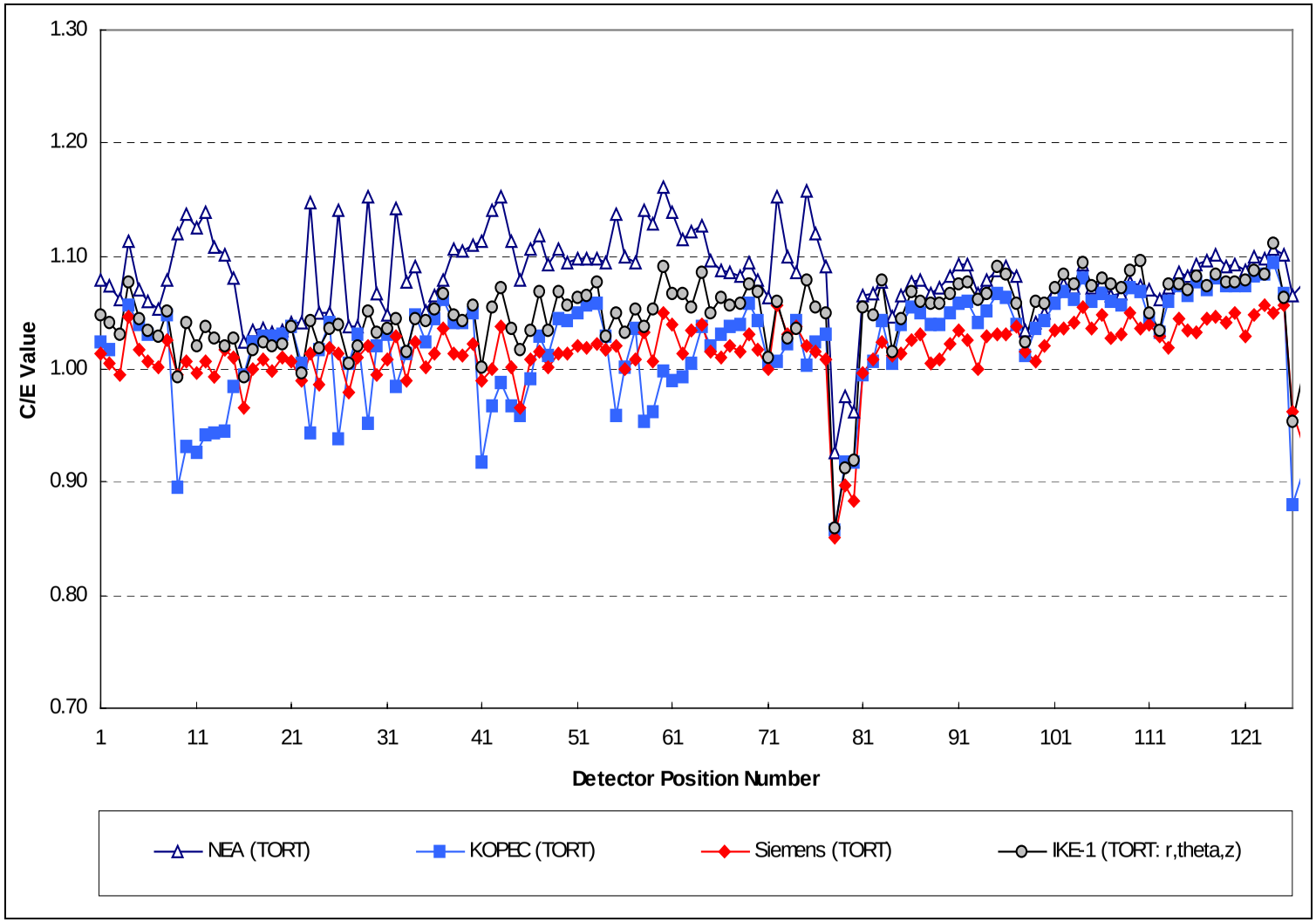

Figure 5.2(b). VENUS-3: C/E comparison of equivalent fission fluxes at Ni detector positions (127 to 244)

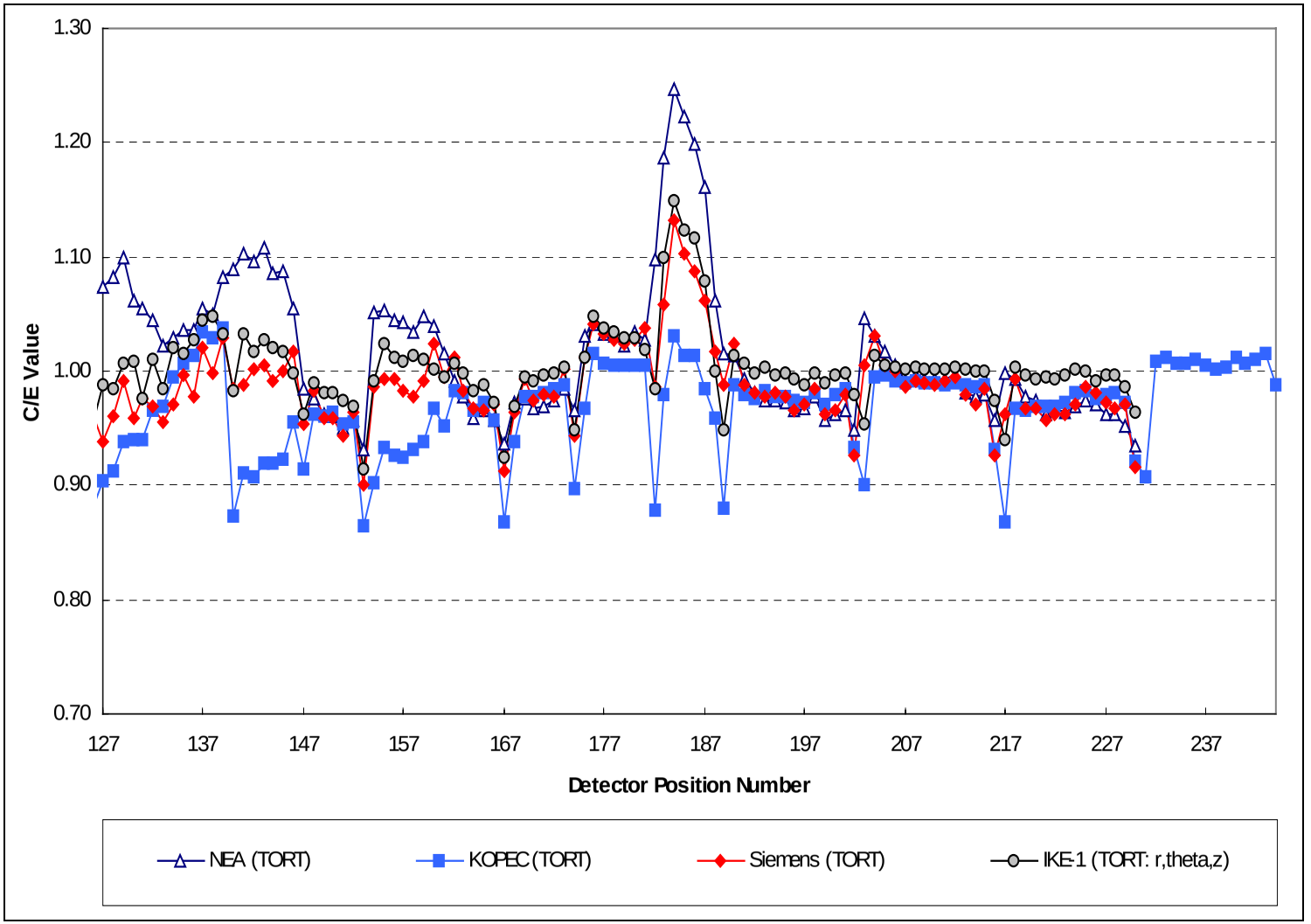

Figure 5.2(c). VENUS-3: C/E comparison of equivalent fission fluxes at Ni detector positions (1 to 126)

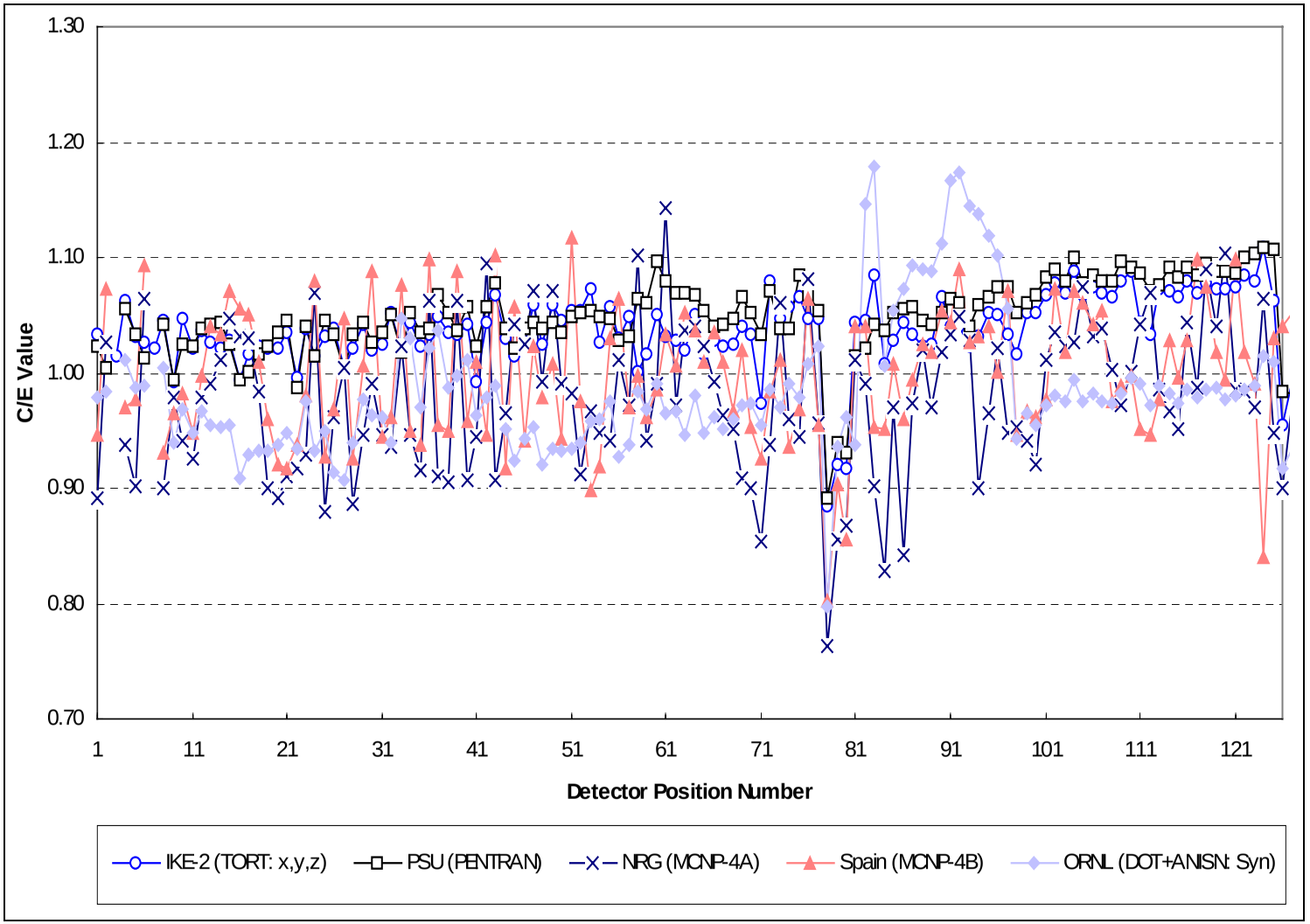

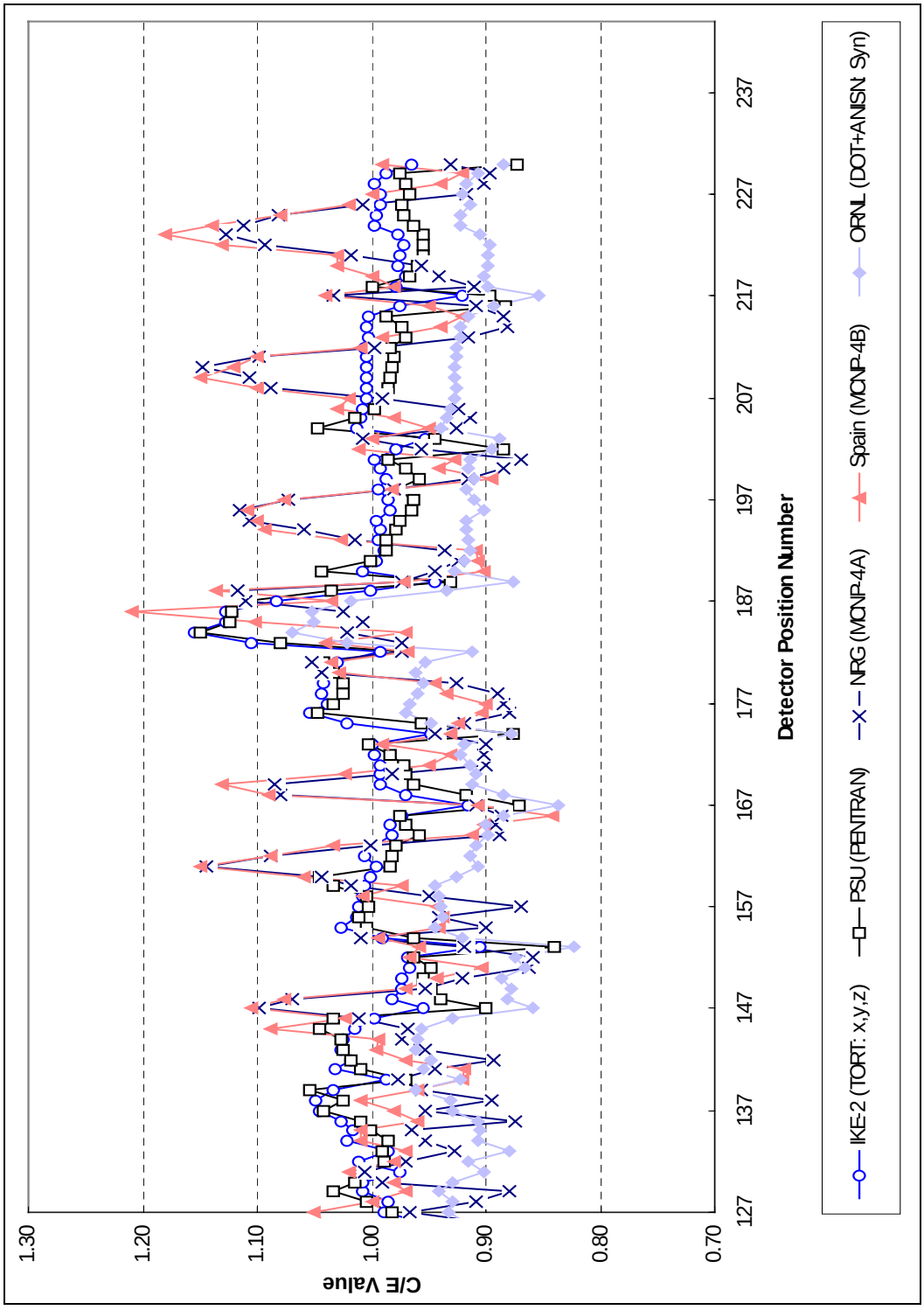

Figure 5.2(d). VENUS-3: C/E comparison of equivalent fission fluxes at Ni detector positions (127 to 244)

Figure 5.3. VENUS-3: C/E comparison of equivalent fission fluxes at In detector positions

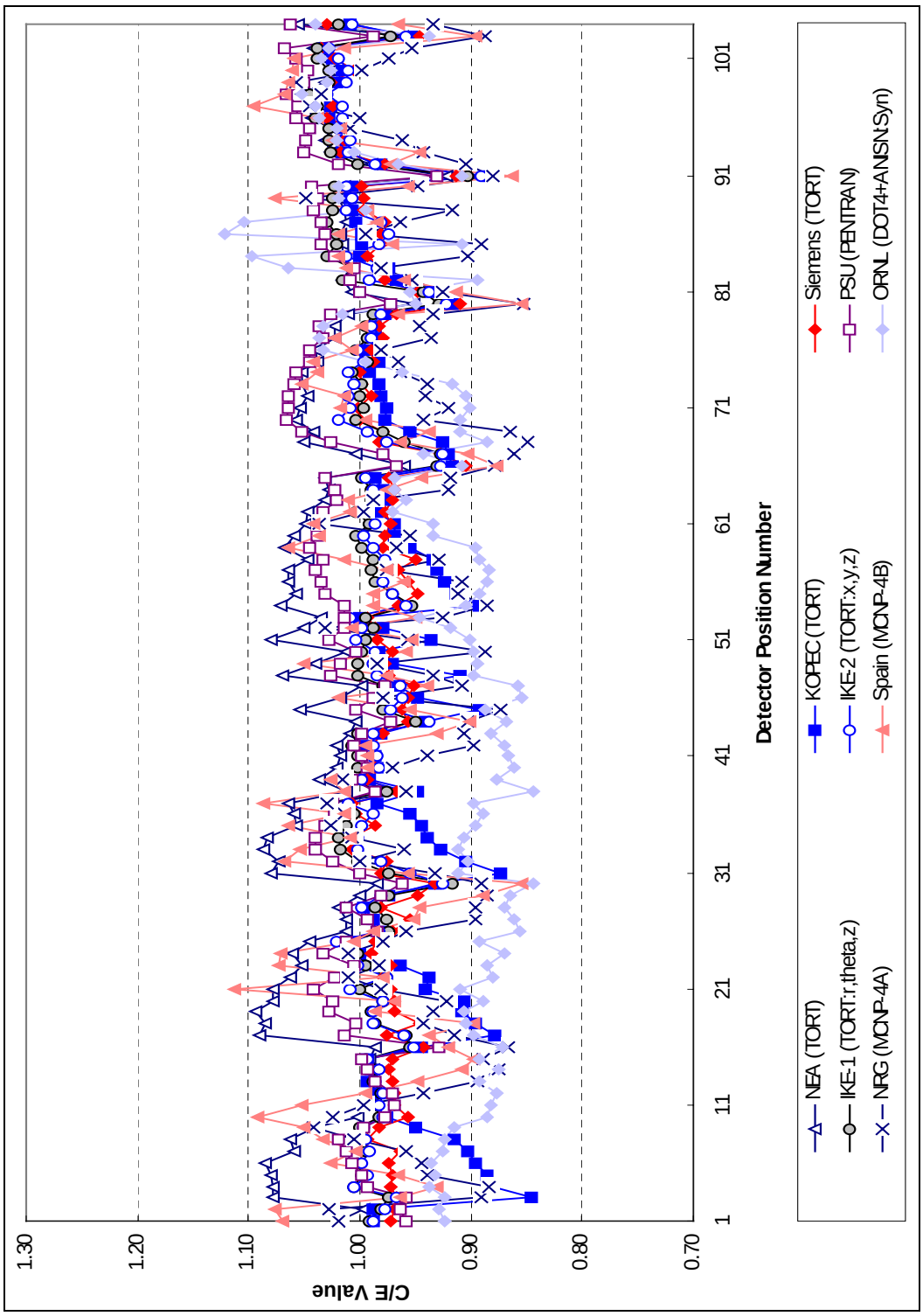

Figure 5.4. VENUS-3: C/E comparison of equivalent fission fluxes at Al detector positions

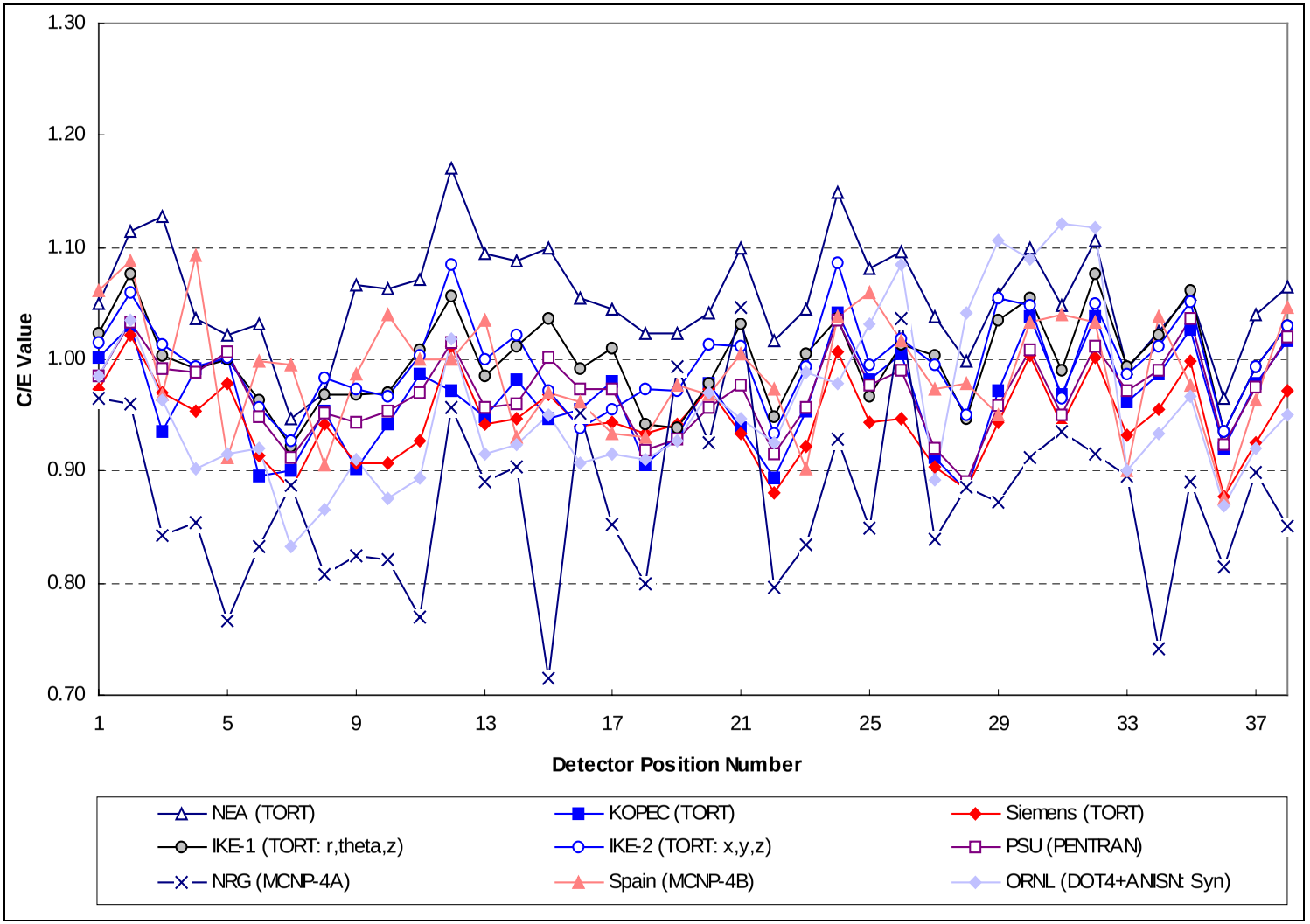

Figure 5.5(a). VENUS-3: Absolute DPA rates at In detector positions

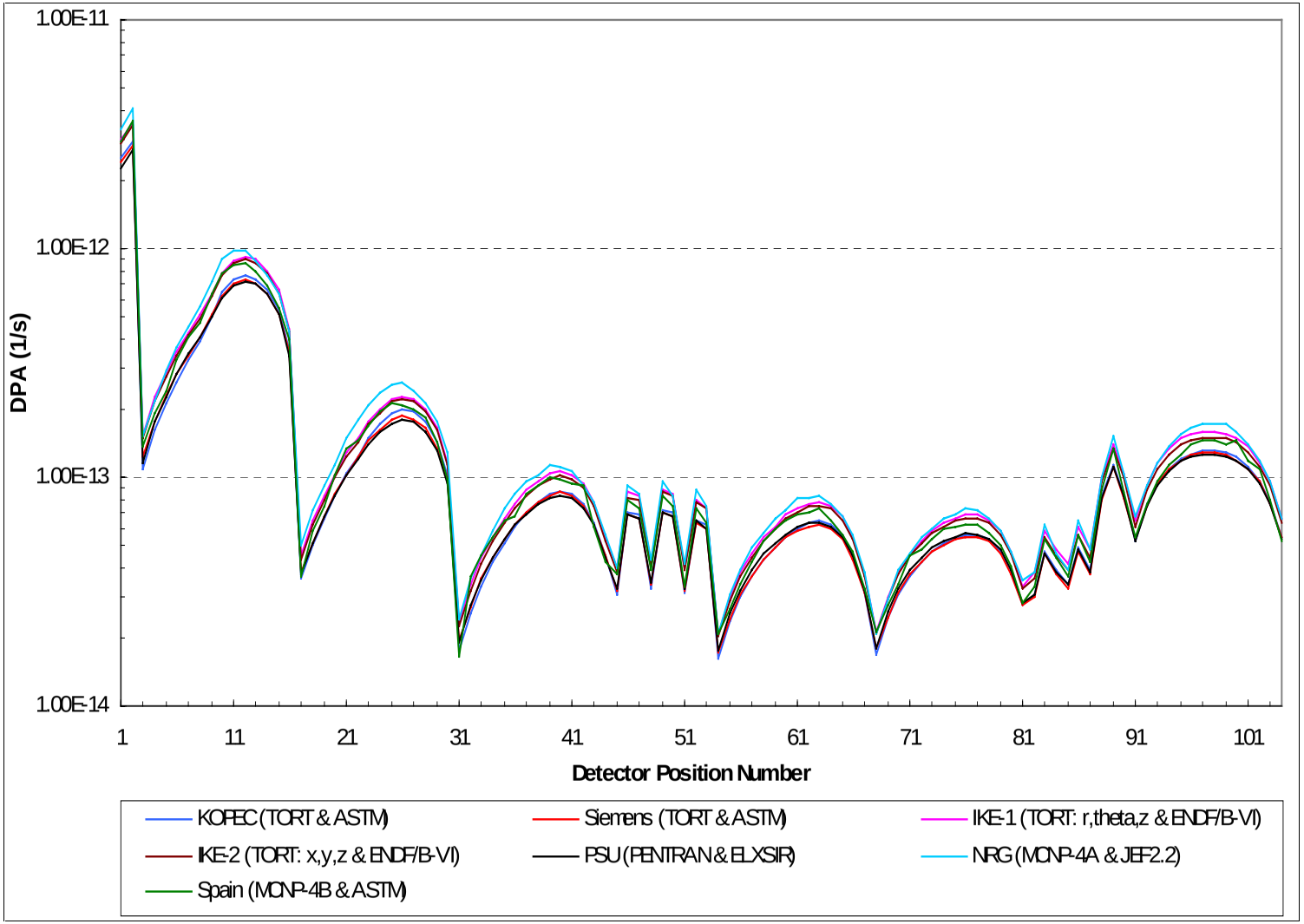

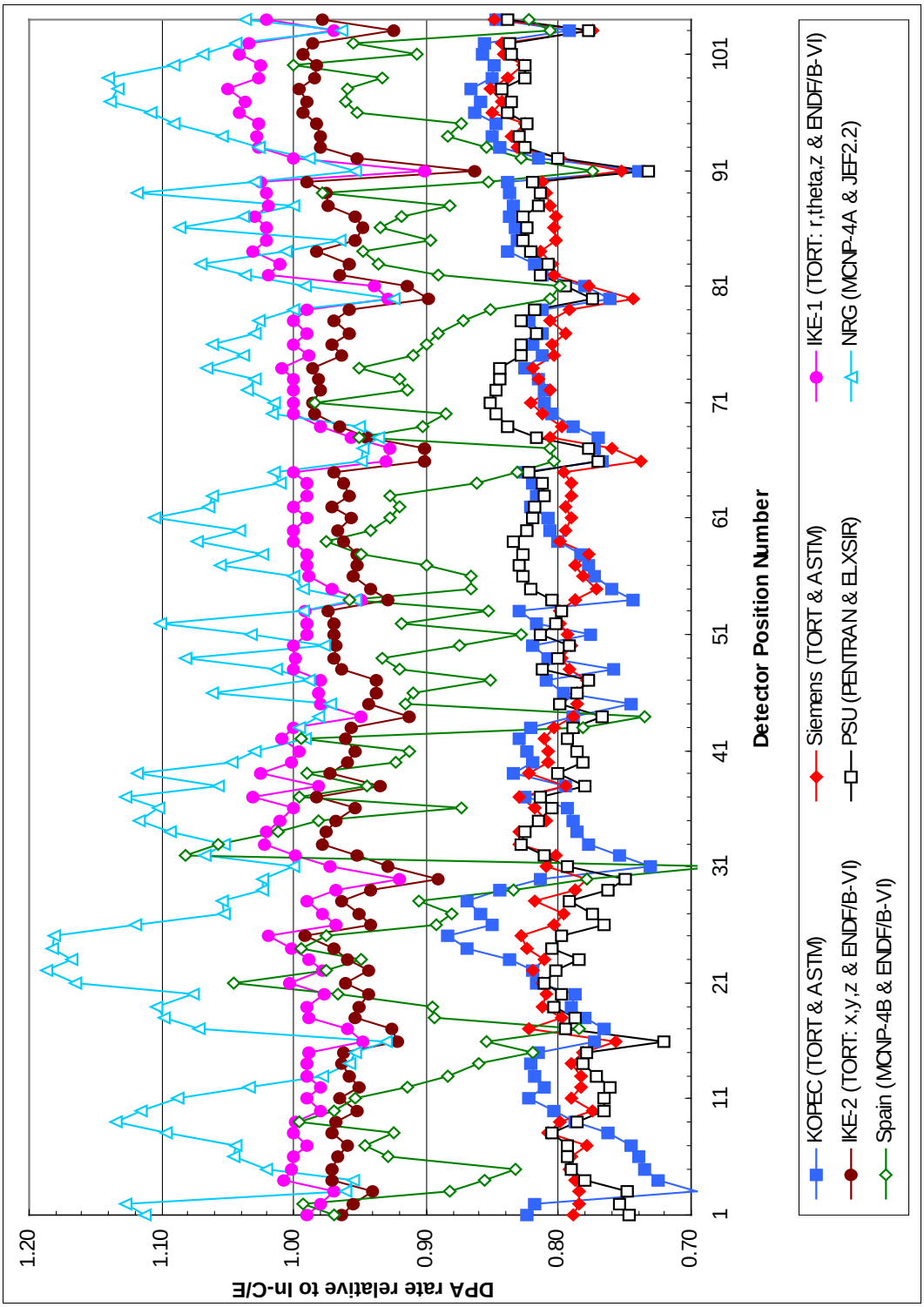

Figure 5.5(b). VENUS-3: Relative DPA rates at In detector positions

Figure 5.6(a). VENUS-3: Absolute fast neutron flux above 1.0 MeV at In detector positions

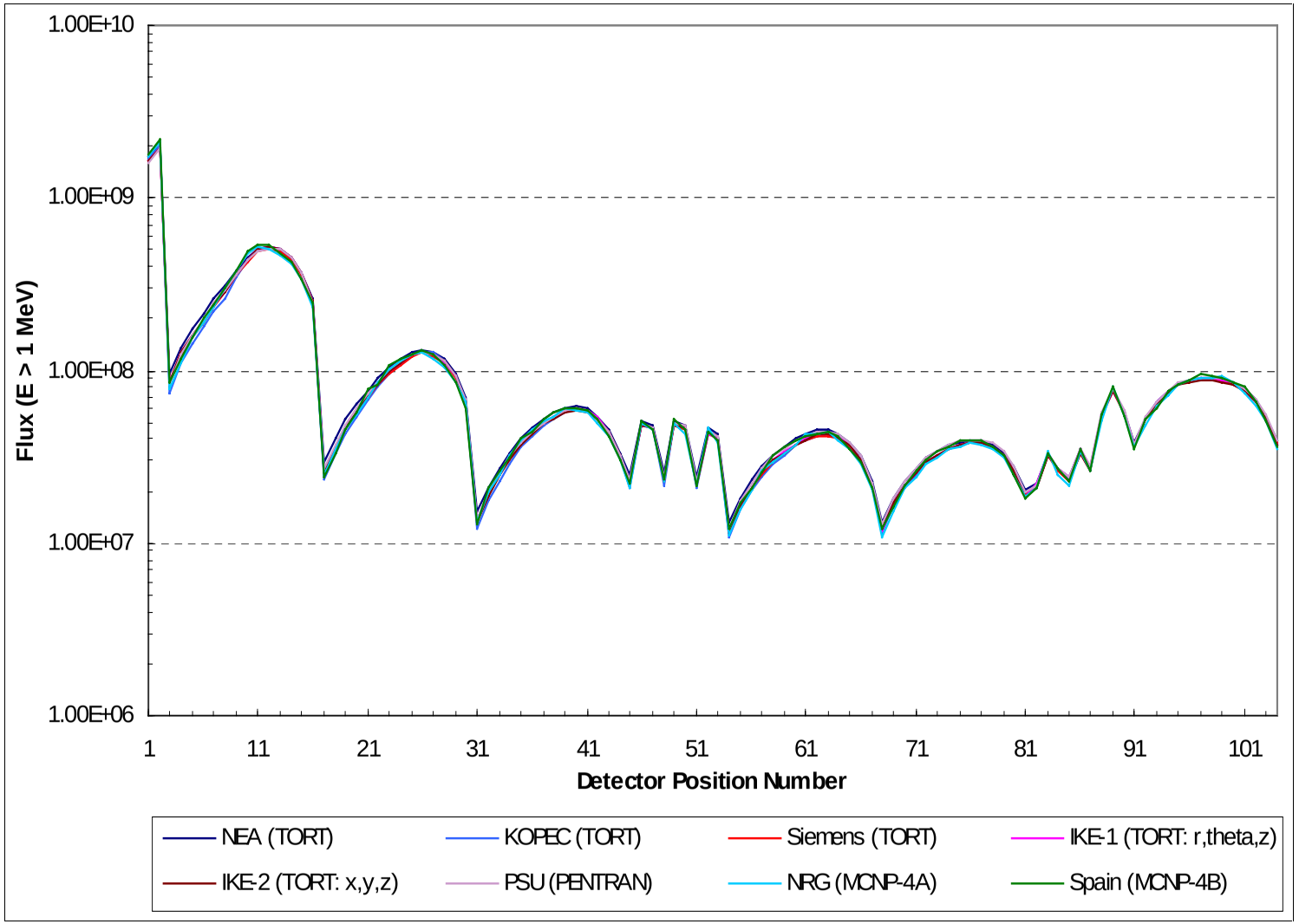

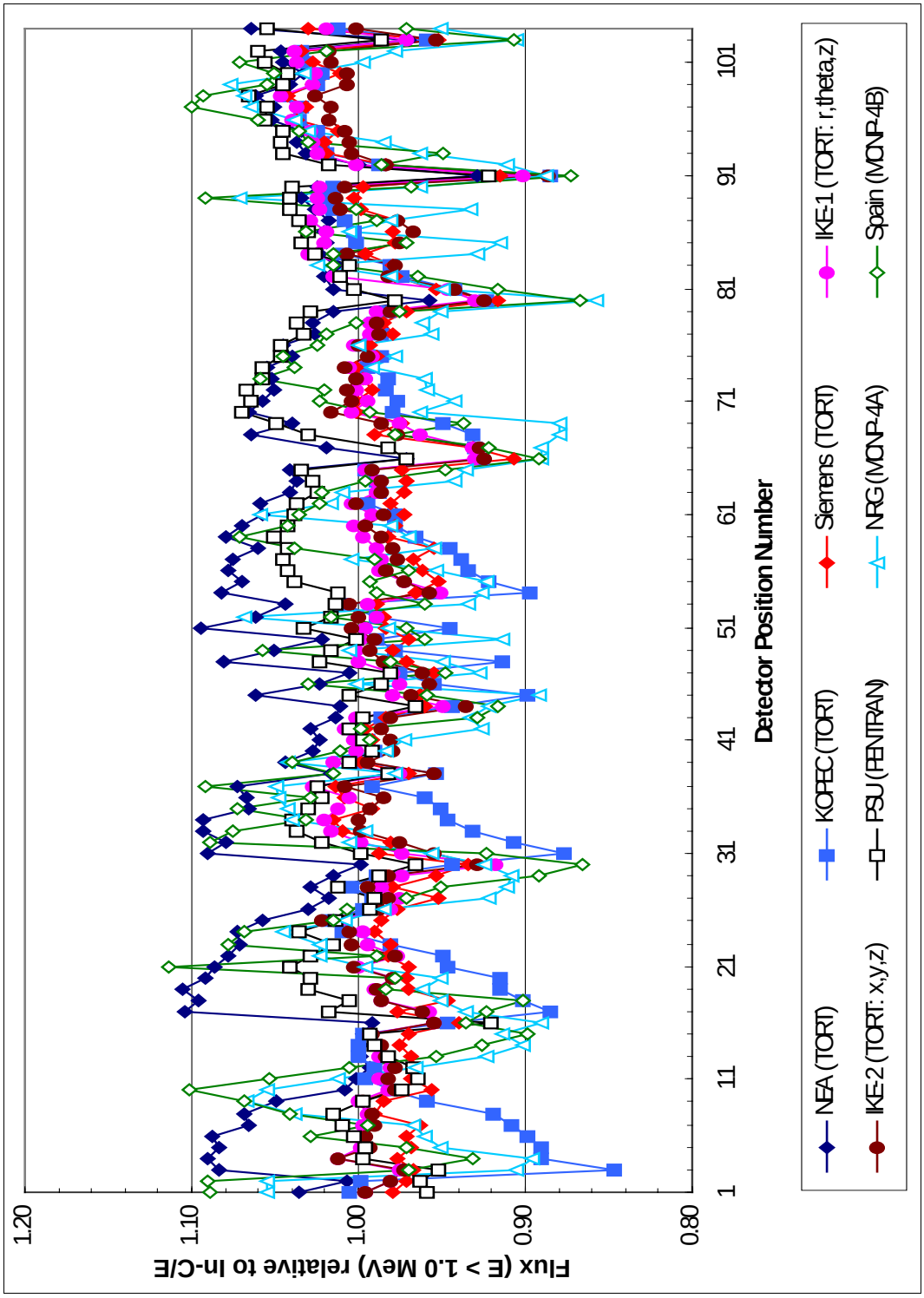

Figure 5.6(b). VENUS-3: Relative fast neutron flux above 1.0 MeV at In detector positions

Figure 5.7(a). VENUS-3: Absolute neutron flux above 0.1 MeV at In detector positions

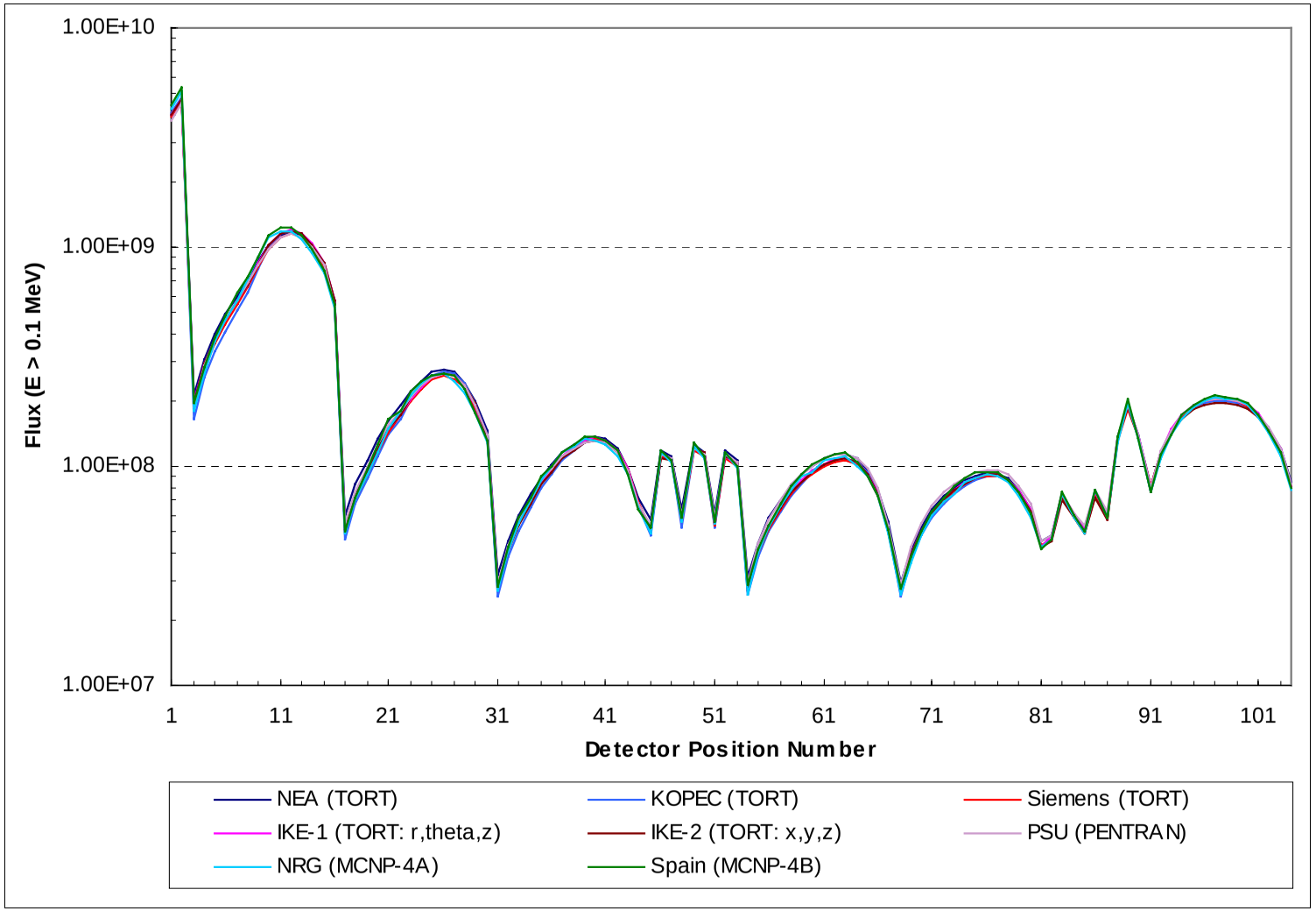

Figure 5.7(b). VENUS-3: Relative neutron flux above 0.1 MeV at In detector positions

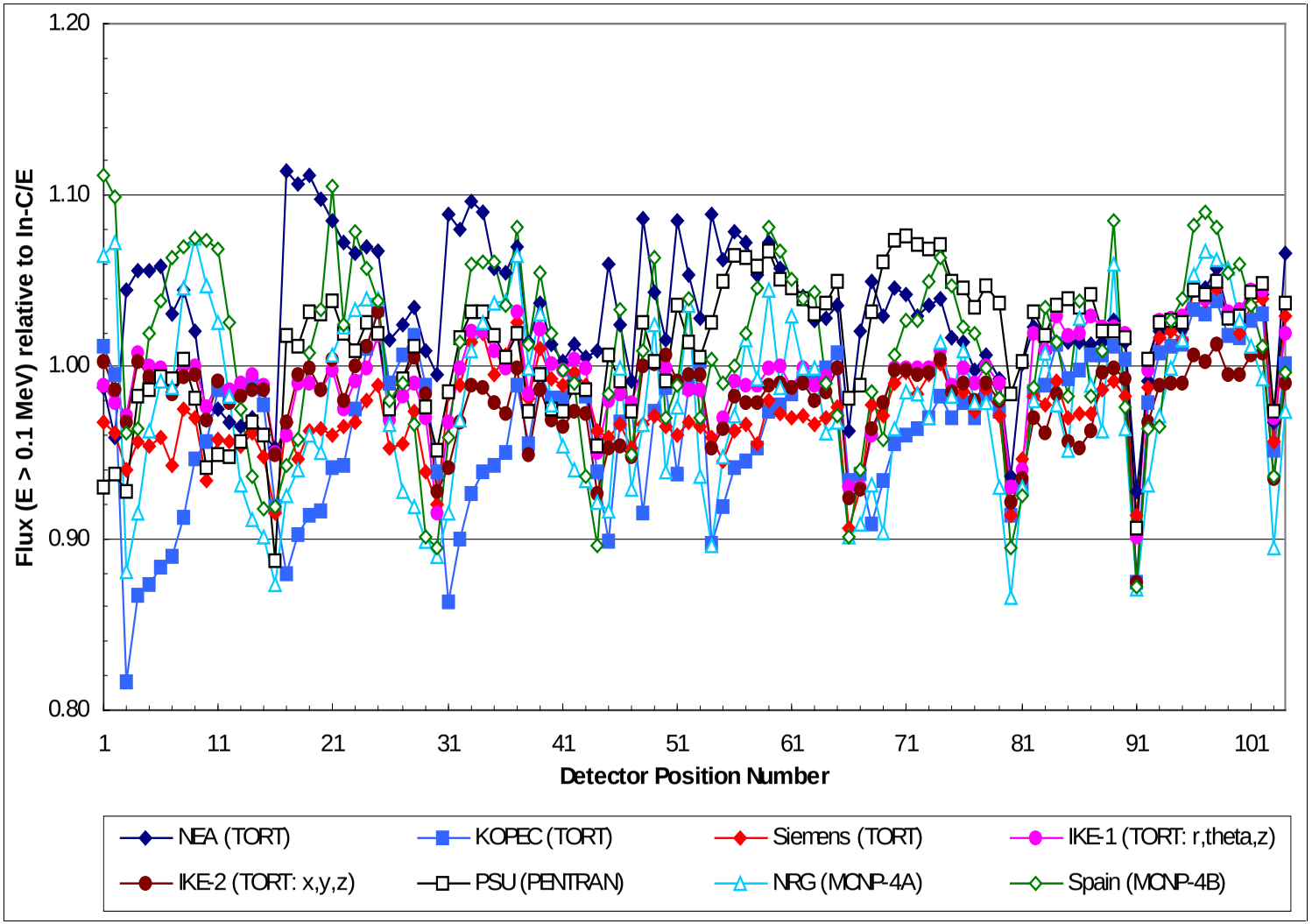

Figure 6.1. VENUS-3: Standard deviations of Monte Carlo calculation results at Ni detector positions

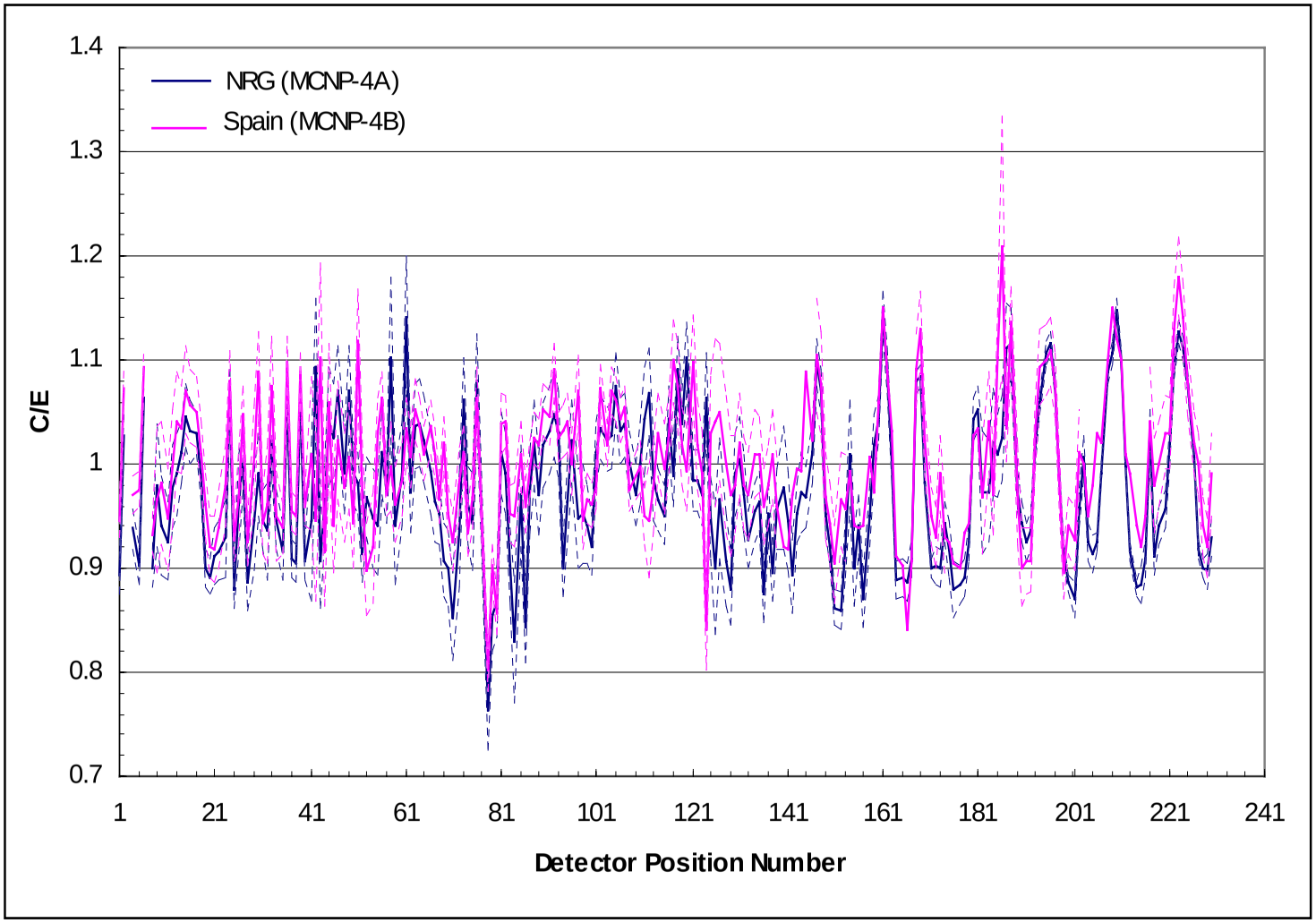

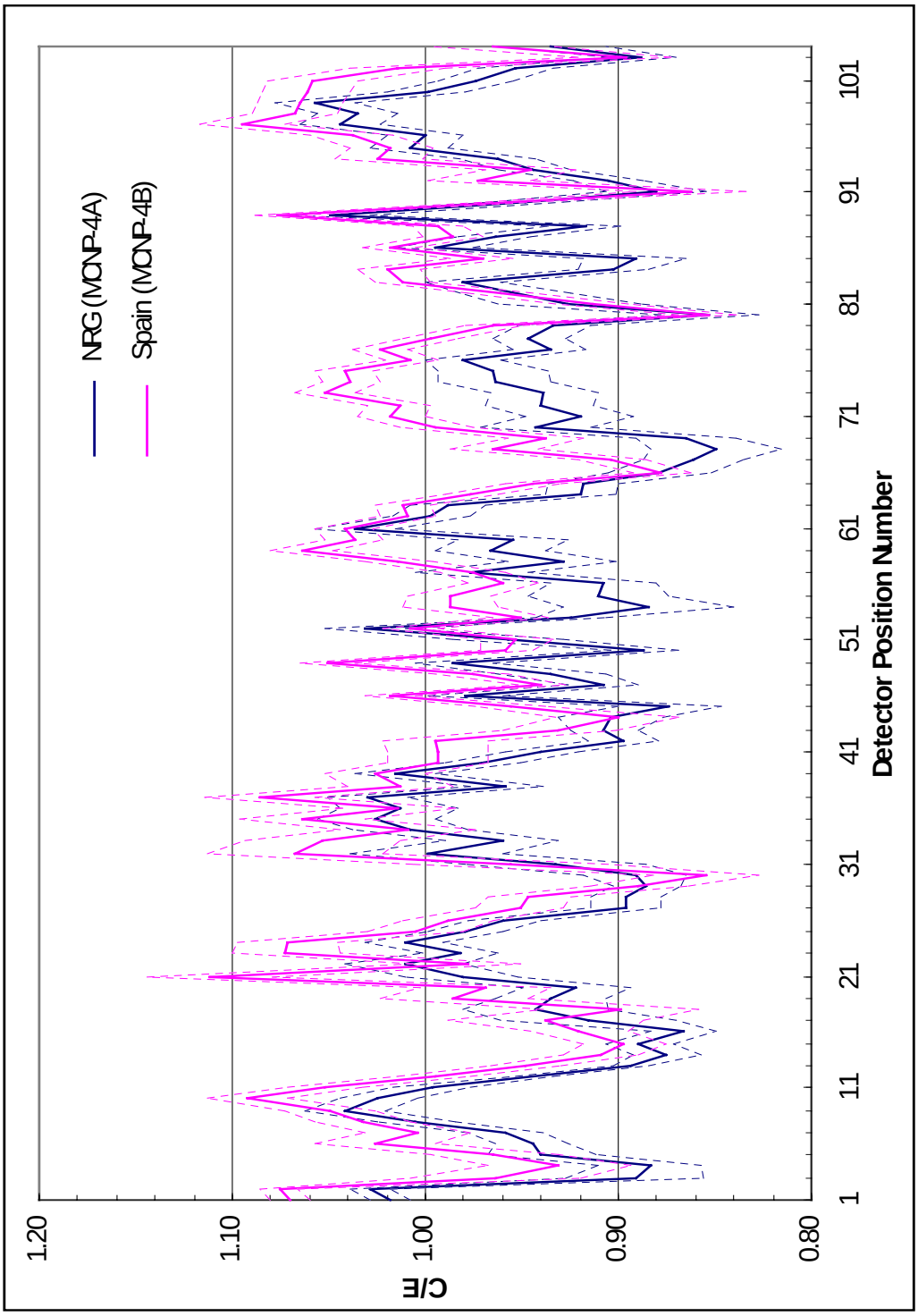

Figure 6.2. VENUS-3: Standard deviations of Monte Carlo calculation results at In detector positions

Figure 6.3. VENUS-3: Standard deviations of Monte Carlo calculation results at Al detector positions

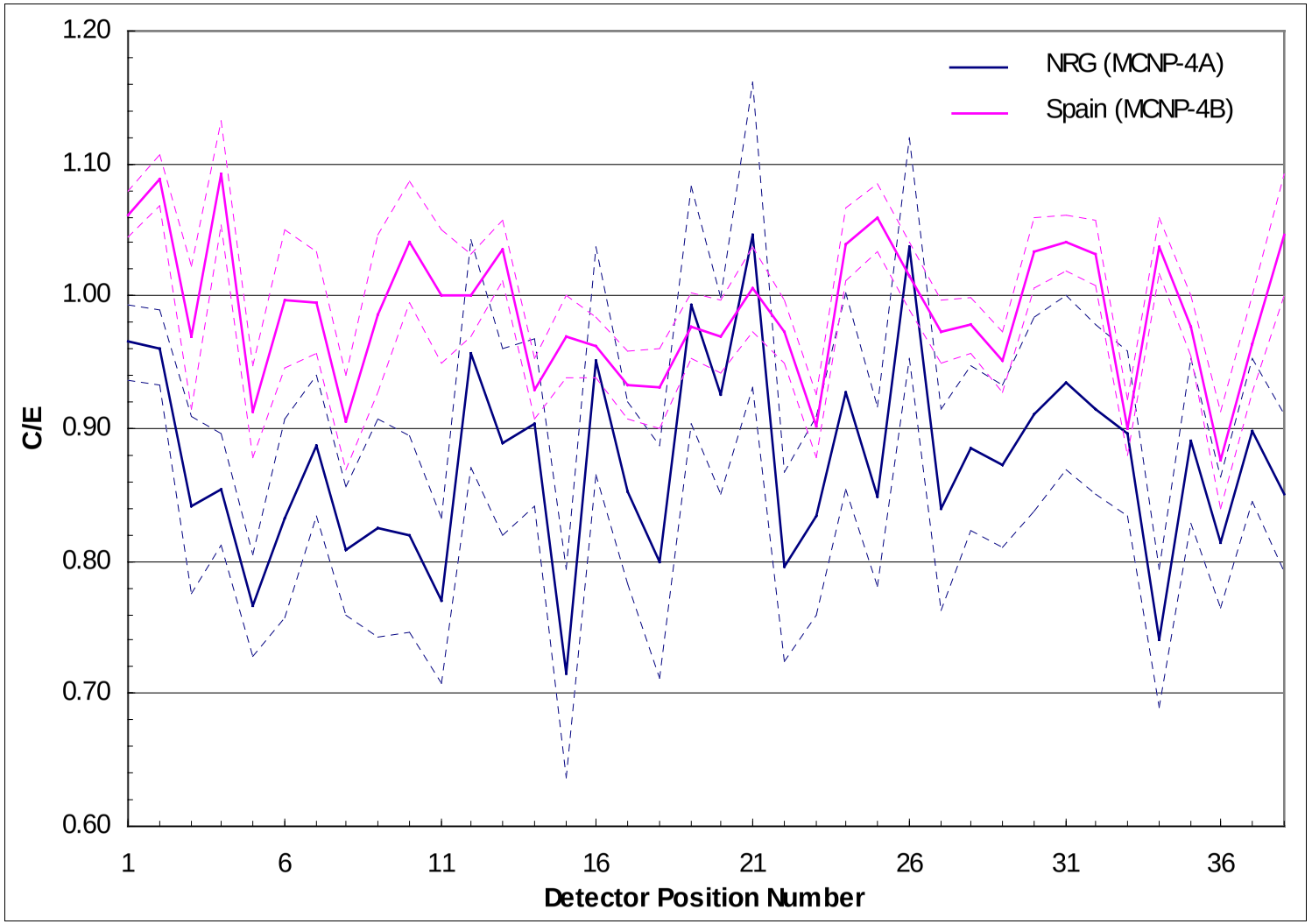

APPENDIX A

Benchmark specifications

A.1. VENUS-1

I. General comments

In this benchmark exercise the goal is to test the current state-of-the-art two-dimensional methods of calculating neutron flux to reactor components against the measured data of the VENUS-1 critical experiment.

This is a "blind" test hence the measured values of the equivalent fission flux at specified VENUS locations are not revealed to the participants *a priori* but will be provided when benchmark results are analysed.

The following documents are included in this distribution package:

- "VENUS-1: Description of Geometry and Composition of Different Materials".
- "VENUS-1: Results of Experimental Determination of Relative Power Distribution and Absolute Level of Reference Power".
- "Results of Experimental Measurement of Vertical Bucklings in the Core and Outside".

The content of these documents is briefly characterised in the following sections.

II. Document No. 1: "VENUS-1: Description of Geometry and Composition of Different Materials"

Detailed descriptions of the VENUS-1 experiment and the VENUS-1 reactor configuration are given in the first document. The information given fully specifies all geometry and material data required in developing the detailed computational model of the 1/8 fraction of the VENUS reactor.

All elements of the VENUS reactor specified in this document should be modelled in the calculations.

III. Document No. 2: "VENUS-1: Results of Experimental Determination of Relative Power Distribution and Absolute Level of Reference Power"

In this second document the measured values of pin power in the units of *fiss/s/cell* in the 1/8 of the VENUS core to be modelled in calculations are provided. The pin power distribution entries in the table are given as numbers normalised to the core average value of 1 *fiss/s/cell*.

The provided normalised pin power distributions should be used by the participants to define the fission source for neutron transport calculations.

The reference core average fission rate at 100% power is given at 2.1×10^8 (±1.8%) *fiss/cm/s* and should be used in any normalisations that may be required in the calculations.

IV. Document No. 3: "Results of Experimental Measurement of Vertical Bucklings in the Core and Outside"

This document provides values of experimentally measured axial bucklings in the VENUS-1 configuration of the VENUS reactor. These axial bucklings should be used as input data in the 2-D neutron transport calculations of the benchmark.

V. Results to be provided and their format

The fission flux measurement points as well as the reactor zones in which they are placed in the VENUS reactor are defined in Table 1 below. The co-ordinates of the measurement points are given in three different co-ordinate systems:

- (x,y) co-ordinates with respect to the reactor grid (used in the experiments).
- (x,y) co-ordinates with respect to the core centre (for use in calculational model).
- (r,θ) co-ordinates with respect to the core centre (for use in calculational model).

IMPORTANT!!!

The dimensioning data of the VENUS reactor are given in two different co-ordinate systems: partially in the (r,θ) co-ordinates and partially in the (x,y) co-ordinates. When developing the geometrical model of the VENUS reactor for the benchmark transport calculations in either co-ordinate system [i.e. (r,θ) or (x,y)], a need will arise to transform the VENUS geometrical data from one co-ordinate system to another. For example, in the (r,θ) model of the VENUS reactor a transformation of dimensioning data from (x,y) co-ordinate system to (r,θ) co-ordinate system will be necessary when modelling neutron sources and some material zones. **Extreme care** is advised in performing the co-ordinate system transformation. In addition, **when reporting** your results, **please describe** your co-ordinate system **transformation procedure** and **criteria/ principles applied** as these **can affect** the results.

For the measurement points in Table 1 the "equivalent fission flux" and neutron fluxes at threshold energies E_{th} > 1.0 MeV and E_{th} > 0.1 MeV should be calculated and reported in Table 2 and Table 3, defined below. The "equivalent fission flux" is defined as a ratio of calculated reaction rate (five different reactions to be considered are defined in Tables 2 and 3) and the average dosimeter cross-section.

In the calculations, the participants are kindly requested to use the **IRDF-90 *Version* 2** dosimeter cross-section data in order to assure comparability between different results.

The following information should be included when reporting the results of the benchmark:

- Description of the calculations procedure (all important information about modelling assumptions and codes/methods used); if S_N method is used then the quadrature set order should be reported (a symmetric or not quadrature is used?), etc.
- Grid/mesh structure of the model.

- The name and version of the point library neutron transport cross-section data and the energy group structure.

- Method/model used in cross-section collapsing.

- The name and version of the dosimeter cross-sections data.

- Any other information not listed above but judged by the participant as important in interpreting this benchmark should be included.

VI. Optional calculations

Three additional but **optional** calculations are suggested:

1) The participants who wish are kindly invited to calculate the DPA using pre-calculated neutron spectra. Those DPAs should be reported in columns marked "**Optional DPA**" in Tables 2 and 3.

2) Those participants who wish to test their pin power calculations techniques may compute the pin power distribution map as given in the Document No. 2 "VENUS-1: Results of Experimental Determination of Relative Power Distribution and Absolute Level of Reference Power". In such a case the results should be reported using an identical format to that of Figure 2 in this document.

3) The participants who wish to perform the uncertainty analysis of their benchmark calculations are encouraged to do so as an additional option.

Table 1. Co-ordinates of VENUS-1 measurement positions

No.	Measurement point zone	(x,y) co-ordinates with respect to reactor grid	(r,θ) in (cm,°) co-ordinates with respect to core centre	(x,y) in (cm,cm) co-ordinates with respect to core centre
	Central hole			
1		(+2.5,+2.5)		(0.,0.)
	Interior baffle			
2		(-1,+2)	(–,8.1°)	(-4.41,-0.63)
3		(-1,-1)	(–,45.0°)	(-4.41,-4.41)
	Exterior baffle			
4		(-29,+2)	(–,0.9°)	(-39.69,-0.69)
5		(-29,-2)	(–,8.1°)	(-39.69,-5.67)
6		(-29,-7)	(–,16.8°)	(-39.69,-11.97)
7		(-29,-12)	(–,24.7°)	(-39.69,-18.27)
8		(-27,-14)	(–,29.2°)	(-37.17,-20.79)
9		(-22,-14)	(–,34.0°)	(-30.87,-20.79)
10		(-17,-14)	(–,40.2°)	(-24.57,-20.79)
	Barrel			
11		(-37,+2)	(–,0.7°)	(-49.77,-0.63)
12		(-37,-5)	(–,10.8°)	(-49.77,-9.45)
13		(-35,-12)	(–,21.1°)	(-47.25,-18.27)
14		(-34,-15)	(–,25.6°)	(-45.99,-22.05)
15		(-33,-17)	(–,28.8°)	(-44.73,-24.57)
16		(-31,-20)	(–,33.9°)	(-42.21,-28.35)
17		(-28,-24)	(–,41.0°)	(-38.43,-33.39)
18		(-26,-26)	(–,45.0°)	(-35.91,-35.91)
	Water between barrel and neutron pad (WATER GAP II)			
19		(–,–)	(55.2,10.8°)	(-54.36,-9.59)
20		(–,–)	(55.2,16.6°)	(-52.89,-15.80)
21		(–,–)	(55.2,21.1°)	(-51.53,-19.78)
22		(–,–)	(55.2,25.6°)	(-50.03,-23.33)
23		(–,–)	(55.2,28.8°)	(-48.74,-25.91)
24		(–,–)	(55.2,33.9°)	(-46.29,-30.06)
25		(–,–)	(55.2,37.4°)	(-44.08,-33.22)
26		(–,–)	(55.2,41.0°)	(-42.29,-35.48)
27		(–,–)	(55.2,45.0°)	(-39.03,-39.03)
	Thermal shield (neutron pad)			
28		(–,–)	(62.7,21.1°)	(-58.54,-22.47)
29		(–,–)	(62.7,42.0°)	(-46.60,-41.95)
	Reflector (WATER GAP I)			
30		(-16,-16)	(–,45°)	(-23.31,-23.31)
31		(-18,-18)	(–,45°)	(-25.83,-25.83)
32		(-20,-20)	(–,45°)	(-28.35,-28.35)
33		(-22,-22)	(–,45°)	(-30.87,-30.87)
34		(-24,-24)	(–,45°)	(-33.39,-33.39)

Table 2. Ex-vessel equivalent fission flux in stainless steel zones: VENUS-1

Measure position	^{58}Ni(n,p)	^{115}In(n,n′)	^{103}Rh(n,n′)	^{238}U(n,f)	^{237}Np(n,f)	Flux at E > 0.1 MeV	Flux at E > 1.0 MeV	Optional DPA
Int. baffle								
(-1,+2)								
(-1,-1)								
Ext. baffle								
(-29,+2)								
(-29,-2)								
(-29,-7)								
(-29,-12)								
(-27,-14)								
(-22,-14)								
(-17,-14)								
Barrel								
(-37,+2)								
(-37,-5)								
(-35,-12)								
(-34,-15)								
(-33,-17)								
(-31,-20)								
(-28,-24)								
(-26,-26)								
Neutron pad								
21°								
42°								

Table 3. Ex-vessel equivalent fission flux in water zones: VENUS-1

Measure position	^{58}Ni(n,p)	^{115}In(n,n′)	^{103}Rh(n,n′)	^{238}U(n,f)	^{237}Np(n,f)	Flux at E > 0.1 MeV	Flux at E > 1.0 MeV	Optional DPA
Central hole:								
(+2.5,+2.5)								
Water I:								
(-16,-16)								
(-18,-18)								
(-20,-20)								
(-22,-22)								
(-24,-24)								
Water II								
(R = 55.26):								
10.75								
16.63°								
21.14°								
25.62°								
28.78°								
33.89°								
37.44°								
40.99°								
45.00°								

VENUS-1: Description of Geometry and Composition of Different materials

(*Issued 18.10.83*)

LWR-PV SURVEILLANCE DOSIMETRY IMPROVEMENT PROGRAMME: VENUS PWR CORE SOURCE AND AZIMUTHAL LEAD FACTOR EXPERIMENTS AND CALCULATIONAL TESTS

1.0 Facility description and quality assurance (L. Leenders)

1.1. General

The VENUS critical facility is a zero power reactor located at SCK·CEN, Mol (Belgium). This facility was built in 1963-1964, as a nuclear mock-up of a projected marine reactor called VULCAIN; hence the name VENUS which means "Vulcain Experimental NUclear Study".

In 1967, this facility was adapted and improved in order to study LWR core designs and to provide experimental data for nuclear code validation. A great flexibility was looked for, as well as an easy handling of the fuel pins, handled one by one, while a great precision of the results had to be achieved.

In 1980, additional material was purchased with a view to studying typical 17×17 PWR fuel assemblies. Such an adaptation is easy: only new reactor grids and small devices adapted to the new fuel geometry are necessary.

In 1982, special stainless steel pieces were manufactured in order to built a pressure vessel mock-up representative of a three-loop Westinghouse power plant. This first stainless steel pieces were delivered at the beginning of December 1982 and the reactor, loaded with this mock-up core, was made critical on 20 December 1982.

1.2. Description of the facility

The facility comprises a reactor shielded room and several associated facilities: the control room, the fuel storage area , the gamma scanning device, the counting room and the plutonium laboratory.

The shielded room is partly illustrated in Figure 1.1. Under the floor, it contains:

- The reactor vessel (~ 2.6 m^3).
- The reactor grids (1 m diameter).
- The safety neutron detectors.
- The safety system (moderator fast dump).
- The water and compressed air circuitries (not shown in the figure).

The working room (6, above the floor) gives a direct access to the reactor core for loading and unloading fuel pins or experimental thimbles. This room contains:

- The start-up neutron source.
- The reactor and health physics controls.
- The regulating rod or fission chamber mechanisms.
- The handling tools.

Due to the direct access to the fuel, the reactor is shutdown when the shielded room is open. The neutron flux level in operation is limited to 10^9 nv, with a view to limiting the irradiation level of the core and the radioactivity of unloaded fuel pins.

1.3. Core design

The LWR-PVS benchmark experiment in VENUS is aimed at validating the analytical methods needed to predict the azimuthal variation of the fluence in the pressure vessel. The VENUS core was designed with the following objectives:

a) *It had to be representative of typical irradiation conditions of a modern PWR vessel*. From exploratory calculations [Ref. 1.1], it appeared that a three-loop Westinghouse plant presents a higher azimuthal gradient of the fluence; this gradient has moreover a higher sensitivity to fuel pattern modification. For this reason, the VENUS mock-up had preferably to simulate the corner assembly environment of such a plant, i.e.:

   - Core baffle thickness: 2.858 cm.
   - Reflector minimum thickness: 2.169 cm.
   - Core barrel thickness: 5.161 cm.
   - First water gap thickness: 5.952 cm.
   - Thermal shield thickness: 6.825 cm.
   - Second water gap thickness: 11.431 cm.
   - Pressure vessel thickness: 20.003 cm.

b) *It had to fit the grid and the vessel geometries of VENUS*. This led to a limitation of the core size and of the amount of simulated internals. In fact:

   - The core is made of sixteen "15×15" subassemblies, instead of "17×17" ones (the pin-to-pin pitch remains typical of the "17×17" subassembly).
   - The second water gap and the pressure vessel are not simulated. A validation of the calculation up to the thermal shield was considered as acceptable; the complete simulation in the radial direction was indeed investigated in a slab geometry with the PCA mock-up.

- Except for the baffle and the reflector minimum thickness, the thicknesses have been somewhat reduced to fit the VENUS geometry.

c) The core size being defined by a) and b), the core loading was adjusted on the basis of preliminary calculations [Ref. 1.2] with the following objectives:

- A pure uranium core (instead of uranium/plutonium) was preferred as being simpler both experimentally and analytically [Ref. 1.3].

- The gamma-heating experiments had to be performed with a low boron content, thus preferably without boron poisoning of the water [Ref. l.3].

- The power shape factor had to be as low as possible, in order to reach, in the different stainless steel pieces, fast flux levels high enough to perform accurate measurements.

- The azimuthal flux variations had to be as high as possible to allow a valuable test of the analytical methods.

- An octagonal symmetry was desirable, to reduce computing costs.

All these objectives were attained with the actual core configuration as given in Figure 1.2; acceptable power flattening and azimuthal flux ratio (~ 2 at half thickness of core barrel) were obtained by a lower fuel enrichment, a central hole and a given amount of Pyrex poison rods in the inner core.

Note: During the approach to criticality, some fixed and mechanised absorbing rods had to be added, far from the region of interest, to adjust the reactivity balance.

d) The core being completely defined, the preliminary calculations were useful to choose the measurement locations of interest. The 21° and 45° angles, which correspond to the maximum and minimum fast fluxes respectively, were provided with experimental holes. In particular, access holes are accommodated at 21° and at the centre with a view to performing neutron and gamma spectrometry.

Notes: The angular shape of the core barrel is such that both quadrant and octagonal symmetries are achieved with acceptable reflecting conditions (in stainless steel) at 0°, 45° and 90° respectively.

The angular shape of the thermal shield, so-called neutron pad, was limited by the available space (it is moreover removable); the quadrant and octagonal symmetries are also achieved with reflecting conditions in water at 0° and 90° and with reflecting conditions in stainless at 45°. This geometry was moreover considered as representative of some Babcock & Wilcox designs.

1.4. Core description

Figure 1.2 gives a horizontal cross-section and Figure 1.3 a top view of the actual core. For experimental and analytical purposes, it should be regarded as a perfect symmetrical core reproducing four times the quadrant between 0° and 90°. The other quadrants are loaded with fuel pins

"quasi" identical to the fuel pins of the first quadrant (due to fuel inventory limitations) and with some absorbing rods for criticality balance adjustment.

Starting from the centre, the core may be divided in 10 regions:

- The *central hole* (water).
- The *inner baffle* (stainless steel: 2.858 cm thick).
- The 3/0 *fuel region*, containing zircaloy clad UO_2 rods, with 3.3% enriched uranium, in a "17×17" type lattice; 12 PYREX-rods, typical of PWR poison clusters are loaded per quadrant (in VENUS language: 3/0 means 3% ^{235}U and 0% PuO_2).
- The 4/0 *fuel region*, containing stainless steel clad UO_2 rods, with 4% enriched uranium, the rods are typical of a "15×15" lattice (first generation of Westinghouse plants), and are loaded with the same pin-to-pin pitch typical of the "17×17" type lattice.
- The *outer baffle* (stainless steel: 2.858 cm thick).
- The *reflector* (minimum thickness: 2.169 cm).
- The *barrel* (stainless steel: 4.99 cm thick).
- The *water gap* (water: 5.80 cm thick).
- The *neutron pad* (stainless steel, average thickness: 6.72 cm).
- The *VENUS environment*, i.e. the jacket (air filled), the reactor vessel (stainless steel) and the reactor room (air).

Figure 1.4 shows a vertical cross-section of the core. The figure shows clearly that, whatever the region is, the material of interest (i.e. fuel or stainless steel) is located from level 105 cm to level 155 cm (50 cm length). To ensure proper axial buckling conditions, both lower and upper axial reflectors are "quasi" infinite for all the regions (the effective extrapolation length is about 7 cm); where necessary water is replaced by Plexiglas.

These details are nevertheless not important for the analytical model, as the experimental axial bucklings are used in the calculation.

1.5. Qualified data on the core materials

- The core materials are qualified in several ways. For the stainless steels, for instance, the qualification is based on a comparison between the corresponding standard, the certificate delivered by the supplier and, at least one analysis carried out by SCK·CEN. The adopted value is generally the average of the consistent data (if necessary a weighted average is made) and the given error is the range defined by the extreme values ($\varepsilon = \pm$ (max.-min.)/2).
- For most materials, there is at least one more sample for documentation or later cross-check.
- For the fuel cladding and the Pyrex tubes, the linear specific weight was determined instead of the volume specific weight as the accuracy of checking the tube thickness is too small.

- The impurities of water were checked in the worst conditions, i.e. when the water resistivity reached its lowest value (250 kΩcm); the water temperature is the median value for the experimental period (from 24.01.83 to 23.06.83) and the range is defined by the extreme recorded values.

- For the VENUS internals being outside the LWR-PVS benchmark mock-up, no qualification was made so that average stainless steel characteristics are given.

The detailed qualification is given in a work document [Ref. 1.4], and the results are as follows.

1.5.1. Central hole

1.5.1.1. Water composition: H_2O, impurities lower than given hereafter

- Diluted oxygen: O 8.6 ppm (saturation for air-water contact)

- Detected impurities:

B	12 ppb (1.E-9 g/l) ~ ppm (weight)
Si	46
Mn	2.5
Fe	.7
Mg	5
Cu	5
Ca	75
Al	8
Sr	.5
Zn	25
V	5
Ag	2
Ba	15

- Non-detected impurities: Li, Zr, Ti, Be, Nb, Ga, Hf, Co, In, Bi, Ni, Pb, Cd, Te, P, Ge, W, Sb, Cr, Mo, Hg, As, Tl, Sn

1.5.1.2. Water temperature

- (23.0 ± 1.5)°C

1.5.2. Inner baffle

1.5.2.1. Chemical composition: AISI 304 stainless steel

C	(.059 ± .020) w/o
Mn	(1.651 ± .053)
P	(.030 ± .015)
S	(.013 ± .013)
Si	(.285 ± .129)
Cr	(16.370 ± .327)
Ni	(8.720 ± .185)

Mo (.454 ± .075)
Co (.138 ± .070)
Fe (72.281 ± .231)
Check 100.001

Detected impurities: – < 10 ppm: Cd, Ta, Au, B
– < 100 ppm: Sm, Eu, Dy, Ir, Gd
Non-detected impurity: Cu

1.5.2.2. Specific weight

- (7.902 ± .002) g/cm^3

1.5.3. 3/0 fuel cell (with standard VENUS fuel pins)

1.5.3.1. Fuel composition: UO_2

1.5.3.2. Fuel stoichiometry [O/U]

- 1.997 ± .005

1.5.3.3. Fuel isotopic composition of U

^{234}U (.029 ± .001) w/o
^{235}U (3.306 ± .010)
^{236}U (.016 ± .001)
^{238}U (96.649 ± .012)
Check 100.000

Total impurities: .8 ppm B equivalent in U

1.5.3.4. Fuel linear specific weight

- (5.40 ± .05) g/cm

1.5.3.5. Fuel diameter

- (.819 ± .002) cm

1.5.3.6. Fuel pellet length

- (.992 ± .040) cm

1.5.3.7. Fuel length

- (50.0 ± .1) cm

1.5.3.8. Cladding composition: Zircaloy 4

Sn (1.41 ± .06) w/o
Fe (.20 ± .01)
Cr (.10 ± .01)
O (.12 ± .01)
Zr (98.17 ± .06)
Check 100.00

Detected impurities:
– < 1 ppm: B, Cd, U
– < 10 ppm: C1, Co, Cu, H, Mg, Mn, Ti, Zn
– < 50 ppm: Al, Hf, N, Nb, Ni, V, W, Au, Ir, Mo, Pb
– < 100 ppm: Ta, Si, Sm, Eu, Dy, Gd, Lu
– 146 ppm: C

1.5.3.9. Cladding linear specific weight

- (1.0627 ± .0004) g/cm

1.5.3.10. Cladding outer diameter

- (.950 ± .001) cm

1.5.3.11. Cladding inner diameter

- (.836 ± .001) cm

1.5.3.12. Fuel cell pitch

- (1.260 ± .001) cm

1.5.3.13. Moderator

- Water, see Section 1.5.1

1.5.4. Pyrex cell

1.5.4.1. Pyrex composition: Corning glass code 7740

SiO_2 78.53 w/o
B_2O_3 (14.65 ± .15)

Al_2O_3 2.21
Fe_2O_3 .05
Na_2O 3.44
K_2O 1.13
Check 100.01

1.5.4.2. Isotopic composition of B

^{10}B: (19.775 ± .005) at %
^{11}B: (80.225 ± .005)

1.5.4.3. Pyrex outer diameter

- (.9048 ± .0043) cm

1.5.4.4. Pyrex inner diameter

- (.6058 ± .0031) cm

1.5.4.5. Pyrex linear specific weight

- (.7886 ± .0052) g/cm

1.5.4.6. Cladding composition: AISI 304 stainless steel

C (.03 ± .03) w/o
Mn (.87 ± .42)
Si (.29 ± .16)
Cr (18.40 ± .10)
Ni (9.50 ± .50)
Mo (.07 ± .07)
Fe (70.84 ± 1.28)
Check 100.00

1.5.4.7. Cladding specific weight

- (7.9 ± .1) g/cm^3

1.5.4.8. Cladding outer diameter

- (.978 ± .005) cm

1.5.4.9. Cladding inner diameter

- (.940 ± .003) cm

1.5.4.10. Pyrex cell pitch

- (1.260 ± .001) cm

1.5.4.11. Moderator

- Water, see Section 1.5.1

1.5.5. 4/0 fuel cell (with standard VENUS fuel pins, third delivery)

1.5.5.1. Fuel composition: UO_2

1.5.5.2. Fuel stoichiometry [O/U]

- 2.00 ± .01

1.5.5.3. Isotopic composition of U

^{234}U (.031 ± .009) w/o
^{235}U (4.022 ± .008)
^{236}U (.023 ± .006)
^{238}U (95.924 ± .010)

Impurities: not available

1.5.5.4. Fuel linear specific weight

- (6.39 ± .70) g/cm

1.5.5.5. Fuel diameter

- (.8926 ± .0005) cm

1.5.5.6. Fuel pellet length

- (1.114 ± .115) cm

1.5.5.7. Fuel length

- (50.0 ± .5) cm

1.5.5.8. Cladding composition: AISI 304 stainless steel

C (.040 ± .040) w/o
Mn (1.290 ± .030)
P (.020 ± .020)
S (.015 ± .015)
Si (.135 ± .003)
Cr (18.300 ± .400)
Ni (10.030 ± .200)
Mo (.132 ± .003)
Fe (70.038 ± .711)

Detected impurities: – < 10 ppm: Cd, Ta, Au, B, Co
– < 100 ppm: Sm, Eu, Dy, Ir, Gd

1.5.5.9. Cladding linear specific weight

- (.8855 ± .0007) g/cm

1.5.5.10. Cladding outer diameter

- (.978 ± .002) cm

1.5.5.11. Cladding inner diameter

- (.902 ± .004) cm

1.5.5.12. Fuel cell pitch

- (1.260 ± .001) cm

1.5.5.13. Moderator

- Water, see Section 1.5.1

1.5.6. Outer baffle

- Stainless steel, see Section 1.5.2

1.5.7. Reflector

- Water, see Section 1.5.1

1.5.8. Barrel

1.5.8.1. Chemical composition: AISI 304 stainless steel

C .015 w/o
Mn (1.303 ± .430)
P .028
S .005
Si .513
Cr (18.464 ± .200)
Ni (10.199 ± .380)
Mo .474
Co .097
Fe (68.819 ± 1.010)
N .080
Check 99.997

Not-detected impurities: Cd, Sm, Eu, Dy, Ir, Gd, Ta, Cu, Au, B

1.5.8.2. Specific weight

- (7.9 ± .1) g/cm^3 (not qualified so far)

1.5.9. Water gap

- Water, see Section 1.5.1

1.5.10. Neutron pad

1.5.10.1. Chemical composition: AISI 304 stainless steel

C .016 w/o
Mn (.830 ± .280)
P .026
S .004
Si .395
Cr (18.022 ± .030)
Ni (10.588 ± .360)
Mo .425
Co .196
Fe (69.498 ± .670)
Check 100.000

Non-detected impurities: Cd, Sm, Eu, Dy, Ir, Gd, Ta, Cu, Au, B

1.5.10.2. Specific weight

- (7.9 ± .1) g/cm^3 (not qualified so far)

1.5.11. Space between neutron pad and jacket

- Water, see Section 1.5.1

1.5.12. Jacket inner wall

1.5.12.1. Chemical composition: AISI 304 stainless steel (not qualified)

C (.024 ± .012) w/o
Mn (1.168 ± .270)
P (.025 ± .003)
S (.008 ± .005)
Si (.374 ± .150)
Ce (17.619 ± 1.047)
Ni (9.836 ± .934)
Mo (.452 ± .024)
Co (.113 ± .074)
Fe (70.354 ± 1.963)
N (.027 ± .040)
Check 100.000

1.5.12.2. Specific weight

- (7.9 ± .1) g/cm^3 (not qualified)

1.5.13. Jacket volume

- Air with 100% relative humidity

1.5.14. Jacket outer wall

- Stainless steel, see Section 1.5.12

1.5.15. Space between jacket and reactor vessel

- Water, see Section 1.5.1

1.5.16. Reactor vessel wall

- Stainless steel, see Section 1.5.12

1.5.17. Around the reactor vessel

- Dry air

1.6. Qualified data on the core geometry

The components of the mock-up were qualified in sizes during fabrication and before loading in the core, special attention was paid to the stainless steel thicknesses.

Some data, particularly sensitive for the fast neutron depletion, were checked in the core as built, for instance, the minimum outer baffle-barrel distance, the water gap thickness and the azimuthal location of the neutron pad. All the recorded data were combined to describe the mock-up as given in Figure 1.5. Where no qualification was possible, the data were deduced from the fabrication specifications.

Notes: During the mounting, it was stated that the neutron pad did not take its designed azimuthal location, probably due to some machining mistake; it has been decided, on site, to adjust the V3 hole (foreseen at the highest azimuthal fast neutron flux and accommodated for spectrometry) at the angle 21.1°.

Up to the inner diameter of the neutron pad, all the components are concentric with respect to the core centre, they are defined by distances or radii d1 to d8; the VENUS internals (jacket and reactor vessel) are concentric with respect to a point located at X′= -3.15 cm, Y′= -3.15 cm in the core mode. Consequently, their locations are no longer given by radii but by thicknesses t4 to t9 and the neutron pad has a variable thickness.

As the calculational model will include experimental bucklings, the vertical sizes are not important, they were qualified in order to make a complete package. When limited in height, the components are 50 cm high and the following data are given: LL = lower level, UL = upper level, h = height (see Figure 1.4); otherwise the regions are quasi infinite in height and are actually located from level 0 to 168 cm.

The detailed qualification is given in a work document [Ref. 1.5], the data are as follows:

1.6.1. Central hole (I)

d1 = (3.442 ± .021) cm

1.6.2. Inner baffle (II)

d2 = (6.300 ± .013) cm
t1 = (2.858 ± .003) cm
LL II = (104.849 ± .032) cm
UL II = (154.856 ± .036) cm
h II = (50.006 ± .004) cm

1.6.3. 3/0 fuel region (III)

d3 = (18.900 ± .005) cm
LL III = (105.00 ± .05) cm
UL III = (155.00 ± .15) cm
h III = (50.0 ± .1) cm

1.6.4. 4/0 fuel region (IV)

d4 = (37.800 ± .013) cm
d9 = (18.900 ± .013) cm
LL IV = (105.00 ± .05) cm
UL IV = (155.00 ± .55) cm
h IV = (50.0 ± .5) cm

1.6.5. Outer baffle (V)

d5 = (40.658 ± .021) cm
d10 = (21.758 ± .021) cm
t2 = (2.858 ± .003) cm
LL V = (104.850 ± .033) cm
UL V = (154.850 ± .039) cm
h V = (50.000 ± .006) cm

1.6.6. Reflector (VI)

t14 (distance between baffle corner and barrel) = (2.169 ± .080) cm
t14 bis (idem, but taking account of broken corners) = (2.251 ± .080) cm
d6 (barrel inner radius) = (48.283 ± 0.050) cm

1.6.7. Barrel (VII)

d6 = (48.283 ± 0.050) cm
d7 = (53.273 ± .060) cm
t3 = (4.99 ± .01) cm
LL VII = (105.00 ± .06) cm
UL VII = (155.00 ± .16) cm
h VII = (50.0 ± .1) cm

1.6.8. Water gap (VIII)

t15 = (5.800 ± .060) cm

1.6.9. Neutron pad (IX)

d8 = (59.073 ± .120) cm
t10 = (6.300 ± .030) cm
t11 = (6.690 ± .030) cm
t12 = (7.050 ± .030) cm
t13 = (6.900 ± .030) cm
a1 = (11.25 ± .25)°
a2 = (21.10 ± .10)°
a3 = 45°

a4 = (54.75 ± .25)°
LL IX = (105.00 ± .26) cm
UL IX = (155.00 ± .16) cm
h IX = (50.0 ± .1) cm

1.6.10. Space between neutron pad and jacket

e10 = (.3 ± .3) cm at 11.25°
e11 = (.3 ± .3) cm at 21.10°
e12 = (.332 ± .310) cm at 45°
e13 = (.3 ± .3) cm at 54.75°

1.6.11. Jacket inner wall (X)

t4 = (11.80 ± .21) cm
t5 = .5 cm

Note: The inner radius of the jacket inner wall is (62.0 ± .15) cm with respect to a centre being at (X′ = -3.15 cm, Y′ = -3.15 cm) from the core centre, all the next internals are concentric with this jacket inner wall.

1.6.12. Jacket volume (XI)

t6 = (15.0 ± .3) cm

1.6.13. Jacket outer wall (XII)

t5 = .5 cm

1.6.14. Space between jacket and reactor vessel (XIII)

t9 = (2.0 ± .3) cm

1.6.15. Reactor vessel wall (XIV)

t7 = .4 cm

1.6.16. Reactor room (XV)

Infinite medium filled by air.

REFERENCES

Ref. 1.1. LWR Pressure Vessel Surveillance Dosimetry Improvement Program Review Meeting, NBS, Maryland, 26-30 Oct. 1981: Exploratory Calculations Carried out at Westinghouse, S. Anderson in co-operation with G. Guthrie (HEDL).

Ref. 1.2. LWR Pressure Vessel Surveillance Dosimetry Improvement Program Review Meeting, NBS, Maryland, 11-15 Oct. 1982: Design Study of the Core Loading for the VENUS PWR Pressure Vessel Benchmark Facility, G. Minsart (SCK·CEN).

Ref. 1.3. LWR Pressure Vessel Surveillance Dosimetry Program, "Activities, Status and Scheduling", 29 March-2 April 1982.

Ref. 1.4. Letters to Dr. Kam and Dr. Williams (ORNL), dated 22 June 1983 and 7 September 1983: VENUS Core: Definition and Qualifications of the Materials, and Up-Dating. L. Leenders.

Ref. 1.5. Letters to Dr. Kam and Dr. Williams (ORNL), dated 7 July 1983: VENUS LWR-PVS Benchmark: Definition and Qualifications of the Geometry. L. Leenders.

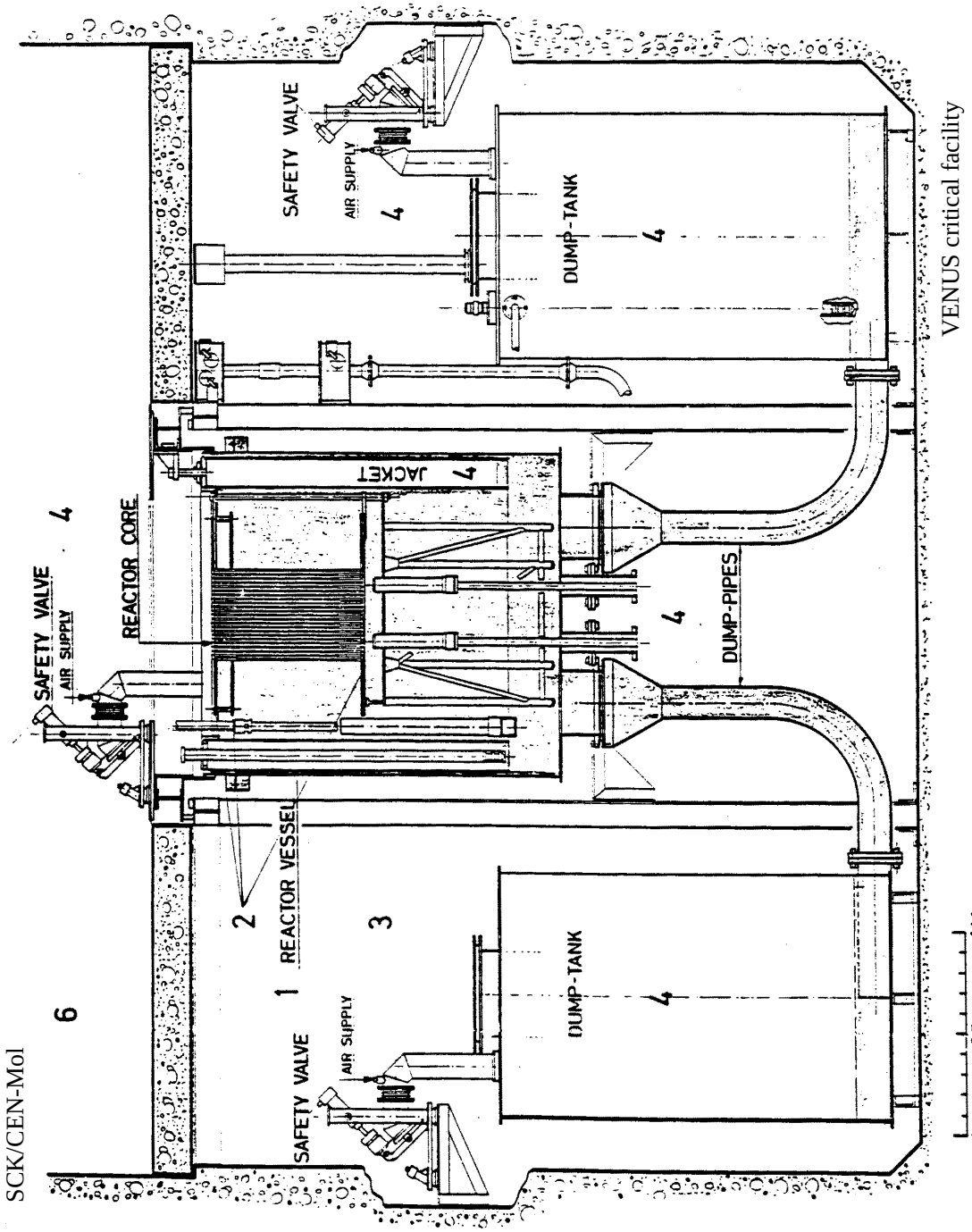

Figure 1.1. Vertical cross-section of the facility

Figure 1.2. Core description (horizontal cross-section)

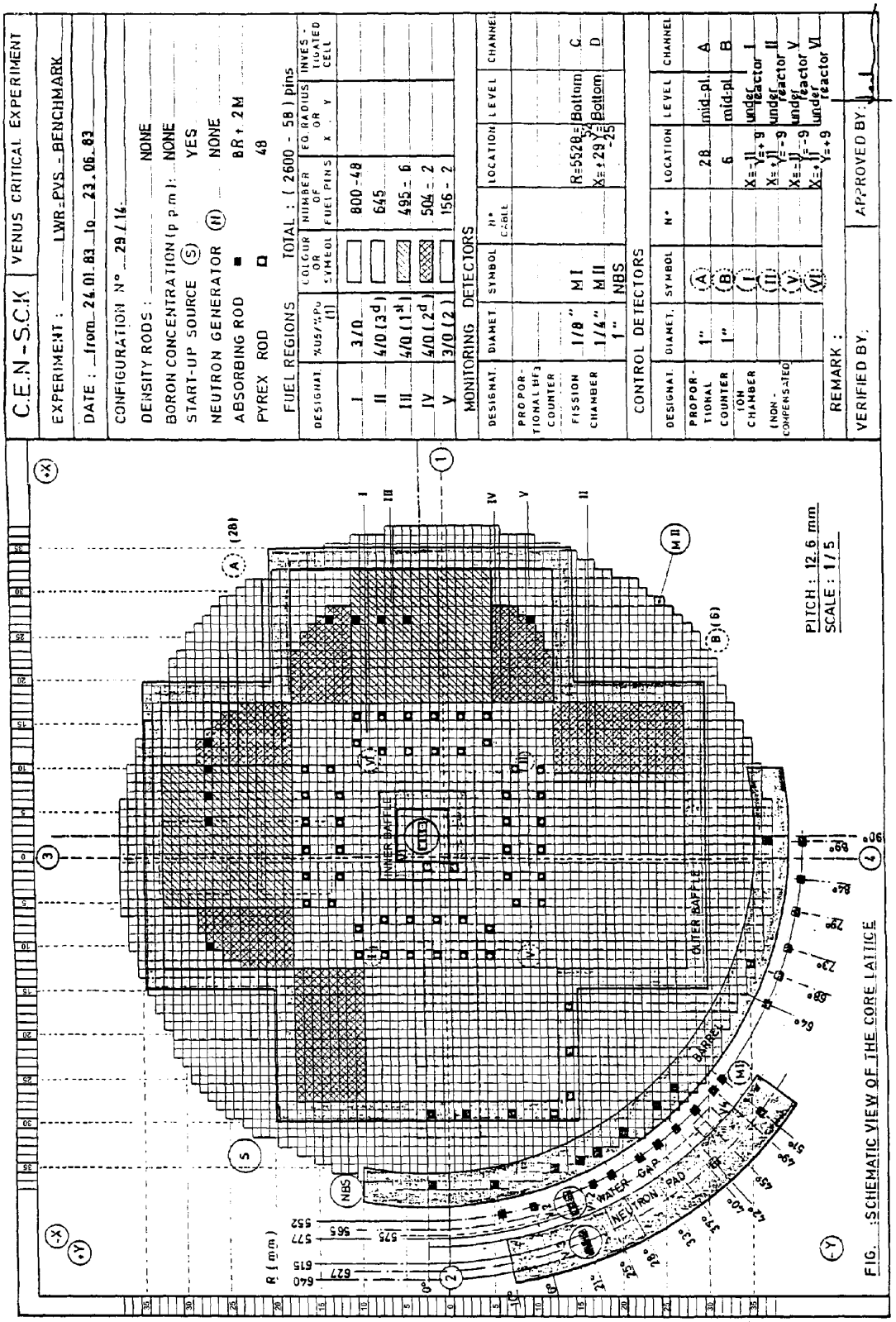

REMARKS: (1) Supply order of /0 fuel
(2) Out of specifications (0.25 < Bowing < 0.50 mm)

Figure 1.2.1. Core description: VENUS-1 configuration

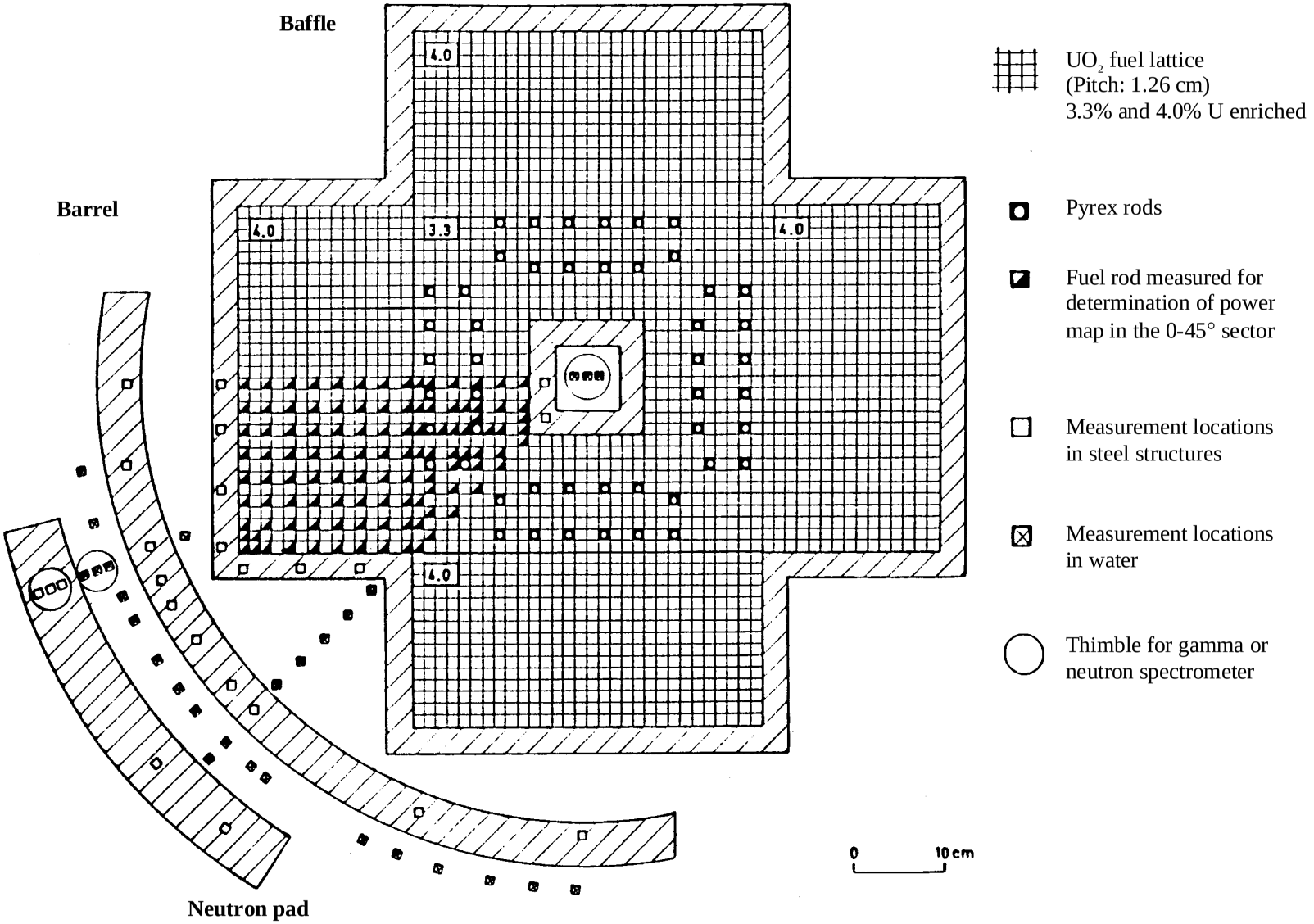

Figure 1.3. Top view of the VENUS core with the LWR-PVS benchmark experiment

SCK/CEN-Mol
VENUS critical facility

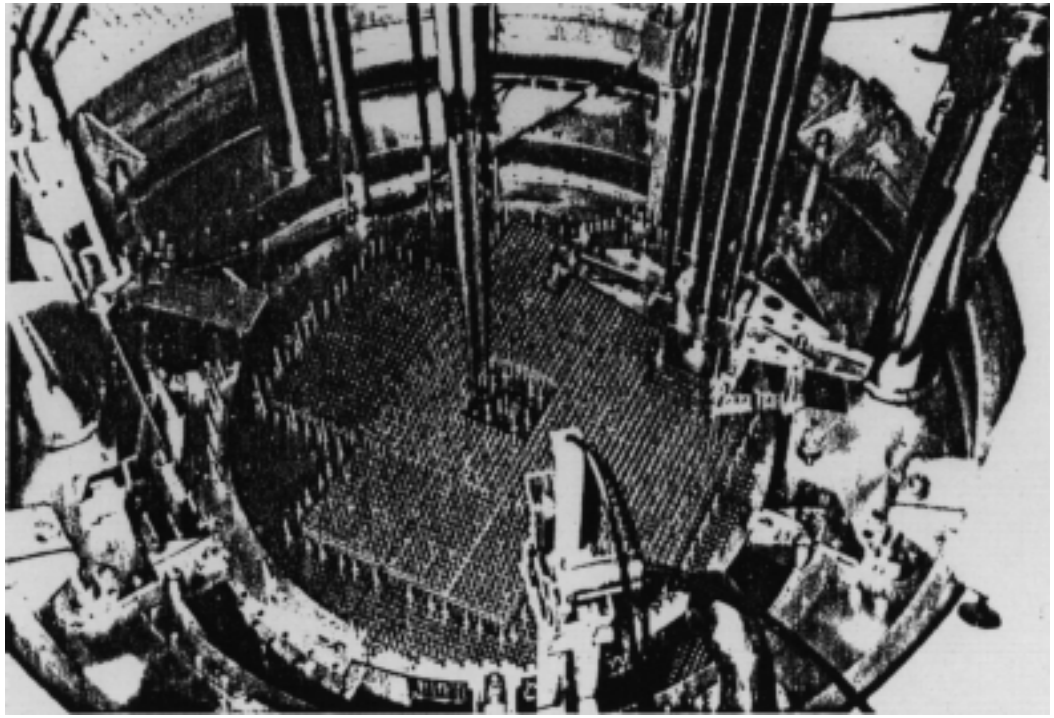

Figure 1.4. Core description (vertical cross-section

SCK/CEN-Mol
VENUS critical facility, LWR-PVS benchmark

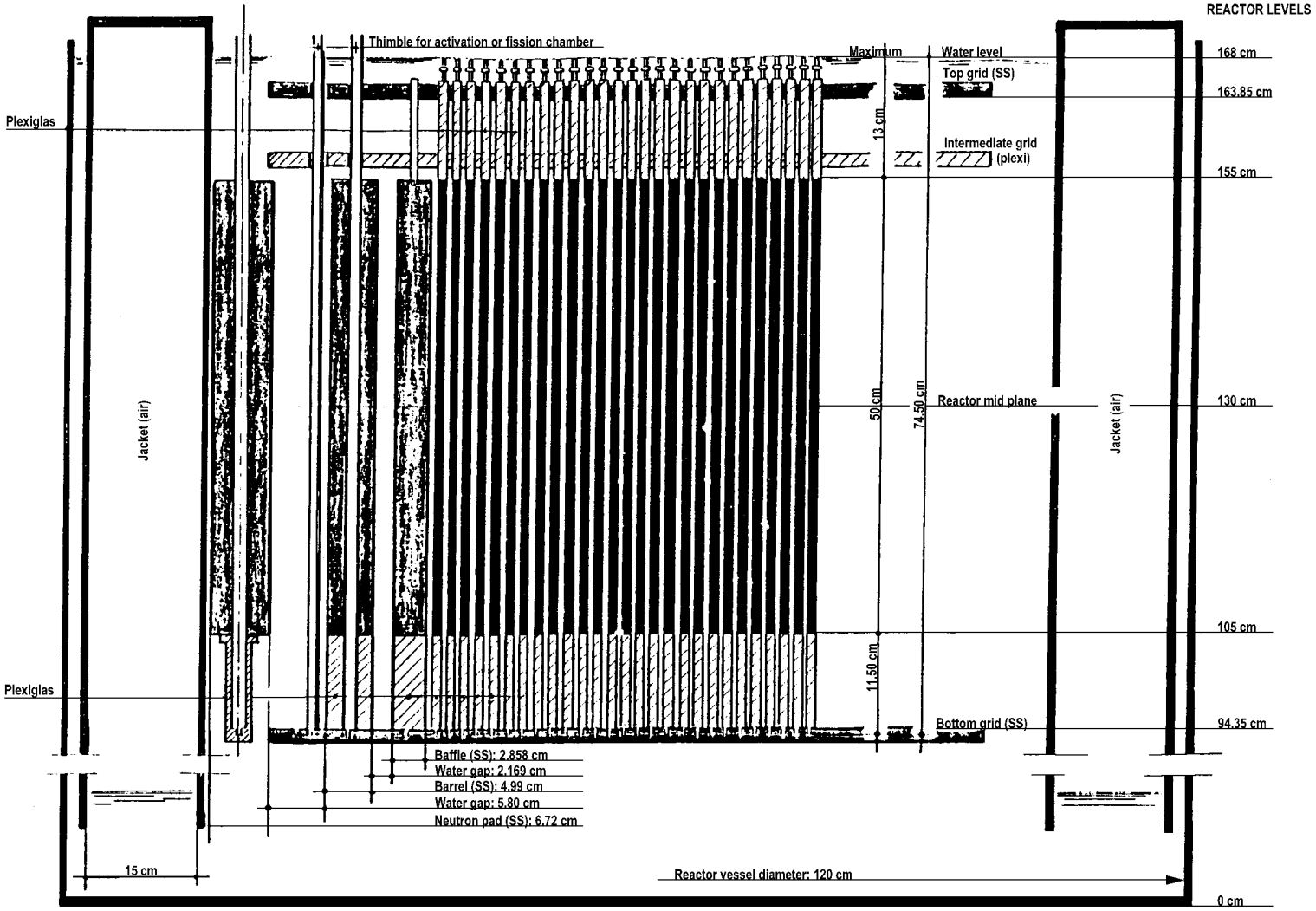

Figure 1.5. Core model (horizontal cross-section)

SCK/CEN-Mol
VENUS critical facility
LWR-PVS benchmark (1983)

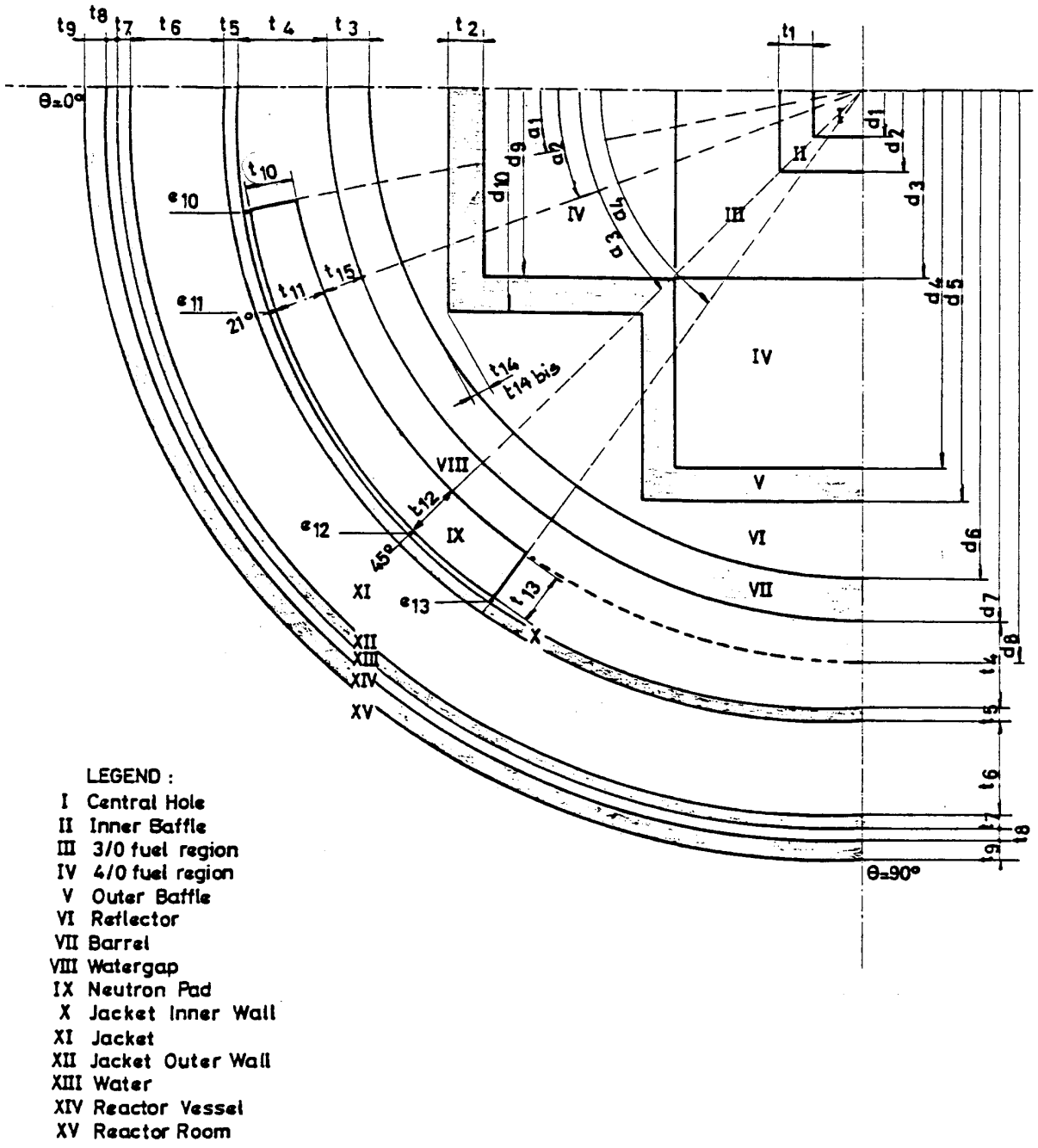

VENUS-1: Results of Experimental Determination of Relative Power Distribution and Absolute Level of Reference Power

(*Issued 20.03.84/updated 14.06.84*)

LWR-PV SURVEILLANCE DOSIMETRY IMPROVEMENT PROGRAMME: VENUS PWR CORE SOURCE AND AZIMUTHAL LEAD FACTOR EXPERIMENTS AND CALCULATIONAL TESTS

5.1. Power distribution (L. Leenders)

Fifty-six fuel rods (33 4/0-ones and 23 3/0-ones) were measured after an irradiation of 8 h at 90% of the VENUS maximum power. The data correspond to the gamma activity of ^{140}La (fission yields ~6%, energy ~1.6 MeV, effective half-life ~12.8 d).

The measured gamma activities were improved for decay, for self-shielding (different pellet geometries and inner flux depressions) and they were normalised to a core averaged fission rate of 1 fission/sec/cell (or to a total core fission rate of 2 552 fission/sec). A complete pin-to-pin power distribution has been obtained by an interpolation process.

Figure 1 shows the investigated region.

Figure 2 gives a complete map of the experimental power distribution. Underlined values are experimental data: $\varepsilon = \pm 1.1\%$ (1.7 σ). Values that are not underlined are interpolated: $\varepsilon = \pm 2\%$.

5.2. Absolute core power normalisation

The determination of the reference power level of the reactor and of the related fission source needed for neutron transport calculations relies upon:

1) The measurement of the relative pin-to-pin power distribution at the mid-plane level as reported in Section 5.1.; this distribution is normalised to a core averaged value of 1 fission/second per centimetre length of fuel rod.

2) The determination of the absolute fission rate in a VENUS fuel rod sample which has been used as monitor for the pin-to-pin power distribution measurements; this VENUS rod sample was irradiated in the BR1 thermal column synchronously with the reference power distribution irradiation of VENUS, performed on 8 June 1983. The run-to-run monitoring will allow to normalise all the experimental data on the reference nominal power level as determined for this run.

So far, results of absolute fission rate measurements obtained by four different methods are available.

5.2.1. Gamma scanning calibrated by foil activation (L. Leenders, L. Verbruggen, J. Lacroix)

The first method consists in measuring the absolute thermal neutron density inside the fuel rod sample irradiated in the BR1 thermal column, by means of activation foils (Dy, Au) inserted between

Figure 1. Radial power distribution

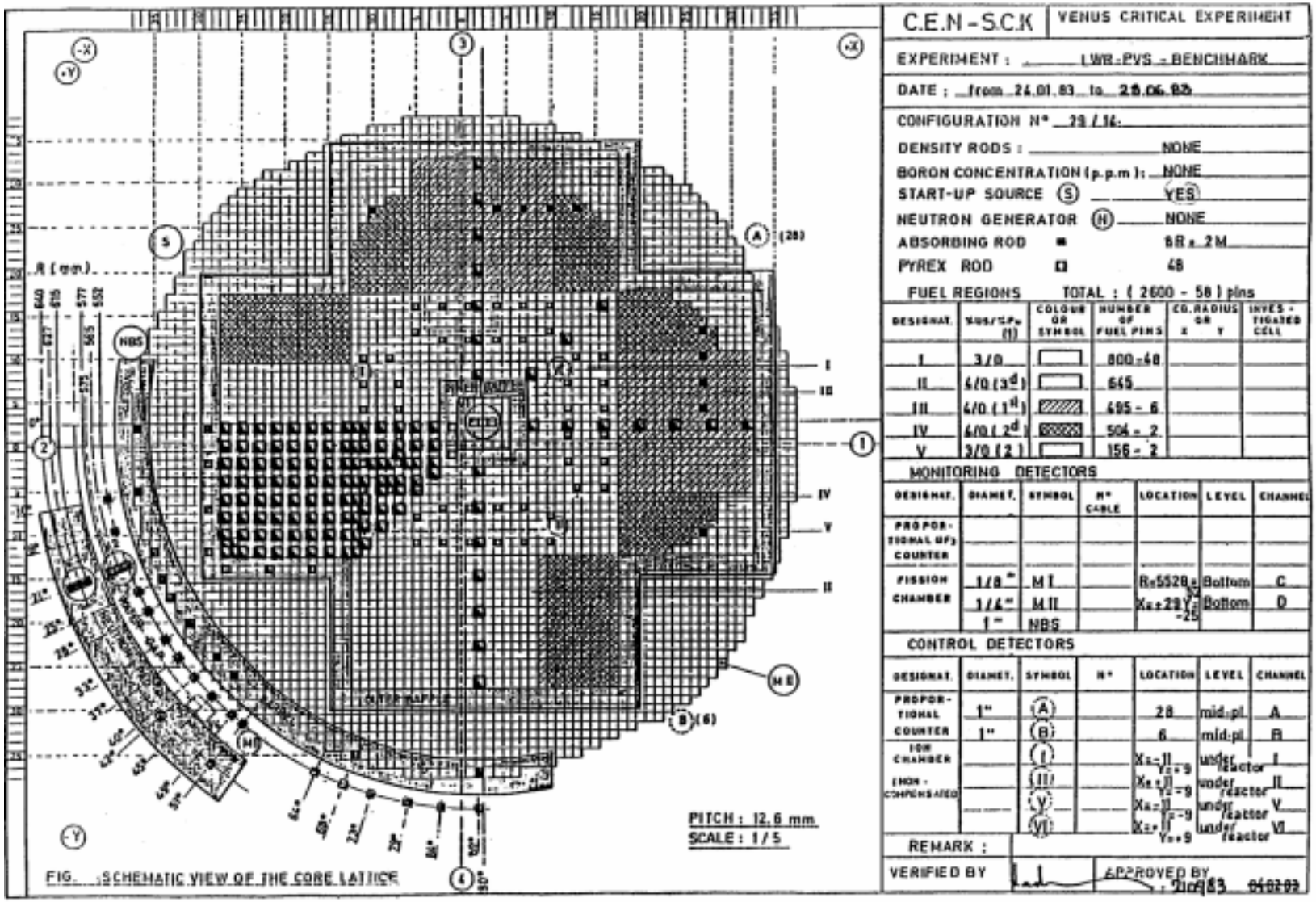

Figure 2. Radial power distribution

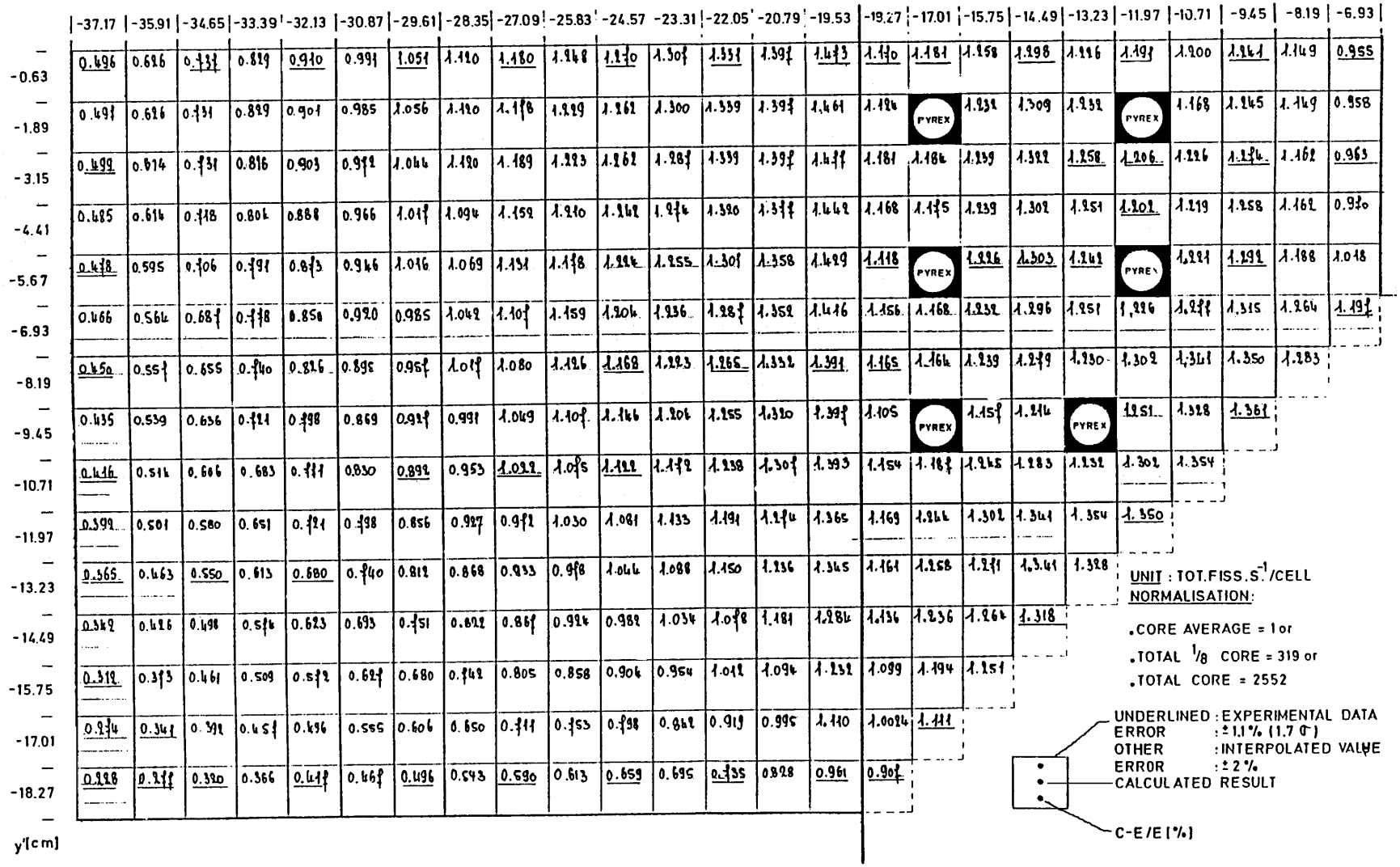

the pellets. Using the ^{235}U fission cross-section corresponding to the local Maxwellian neutron temperature, the ^{235}U fission density in the pellet stack can be calculated. The fuel pins irradiated in the VENUS are then measured on a gamma scanning installation (NaI crystal, measurement of the ^{140}La gamma peak at 1.6 MeV) with respect to the reference pin sample irradiated in BR1. A small correction related to the 1.6 MeV gamma self-shielding is applied to take into account the difference in the radial fission density depressions, in the pellets irradiated in VENUS (LWR lattice spectrum) and in the pellets irradiated in the well-thermalised BR1 spectrum. This fission density depression in both irradiation conditions has been measured through concentric annular foils, cut from dysprosium/ aluminium discs activated between the pellets. A correction was also applied to take into account the difference in the (^{140}Ba, ^{140}La) fission yields for ^{235}U and ^{238}U; this very small correction is based on VENUS cell calculations.

5.2.2. Gamma scanning calibrated by fuel pellet activation (L. Leenders, L. Verbruggen, J. Lacroix)

A second method consists in measuring directly the ^{140}La gamma activity of some of the pellets irradiated in the BR1 thermal column and/or in VENUS with a Ge-Li crystal calibrated by means of European Commission standard sources. For these measurements, the axis of the pellet coincides with the axis of the crystal. A gamma self-shielding correction is calculated taking into account the exact geometry and position of the pellet with respect to the crystal. The average fission density in the pellet is calculated from the measured activity, using the (^{140}Ba, ^{140}La) fission yield of 6.10% for ^{235}U, corrected for the ^{238}U contribution in the VENUS irradiated pellet.

5.2.3. Radiochemical analysis of fuel pellet (P. De Regge)

The radiochemical analysis was applied as a third method. After dissolution of the pellet, the gamma activities from ^{140}La, ^{141}Ce, ^{144}Ce and ^{103}Ru were measured on a Ge-Li crystal, different from the one used in the second method and calibrated with different standard source. Here again, appropriate fission yields were used, respectively 6.10, 5.84, 5.54 and 3.04% for ^{235}U, with corrections for the ^{238}U contribution.

5.2.4. Fission chambers (A. Fabry, E.D. McGarry)

Finally, the measurements performed with miniature ^{235}U fission chambers inserted vertically in water between fuel rods at several locations in the VENUS core allowed to determine the ^{235}U fission density in the neighbour rods. The fission chambers were calibrated in the BR1 reference thermal neutron induced ^{235}U fission spectrum. The determination of the fission density in the VENUS fuel requires in this case the knowledge of a “disadvantage factor” (^{235}U fission rate in fuel with respect to water). This disadvantage factor as well as the ^{238}U fission rate contribution were deduced from VENUS cell calculations.

5.3. Evaluation (L. Leenders, L. Verbruggen)

In order to judge the overall consistency of the four methods, the measured values were converted, using the relative power distribution, to give the fission density at the mid-plane level of the fuel pin located at position X = -5, Y = -5 (X′ = -94.5 mm, Y′ = -94.5 mm). This location was considered as it corresponds to a direct measurement of fuel pellets by *Radiochemical Analysis* (Section 5.2.3.). The results are summarised in Table 5.2.1.

The fission density as given in the table is the number of fissions per centimetre of fuel and per second at this location at the reference nominal power level of 100%.

Table 5.2.1. Consistency analysis

Method	Fission density (cm^{-1} sec^{-1})
1	$(2.88 \pm 0.06) \times 10^8$
2	$(2.78 \pm 0.02) \times 10^8$
3	$(2.83 \pm 0.06) \times 10^8$
4	$(2.76 \pm 0.08) \times 10^8$
Average and observed dispersion	$(2.81 \pm 0.06) \times 10^8$

For these individual results, the uncertainty margins correspond to the internal consistency as observed for each method, when applying different procedures, e.g. measuring the neutron flux by different foils or calibrations, using 4% and 3.3% ^{235}U fuel pellets, measuring several fission products in the radiochemical analysis, etc., thus disregarding the error on the basic data.

The dispersion added to the average value is simply the maximum observed deviation from method to method.

As this observed dispersion is of the same order of magnitude as the individual uncertainty margins, it may be concluded that the four methods are fully consistent.

5.4. Recommendation (L. Leenders, L. Verbruggen)

As the methods have been demonstrated to be consistent on one fuel pin location, they were now applied in such a way that each one gives the *best estimate* for *fission rate at the mid-plane level as averaged over the whole core (2 552 fuel pins) running at 100% power* (1.111 times the reference run, see Section 2).

For instance, for the gamma scanning (the first two methods), there were as many absolute power determinations as measured fuel pins (56 according to Section 2). In other words the final result practically does not depend on the relative power distribution but only on the monitor capsule calibration. These results are summarised in Table 5.4.1.

Table 5.4.1. Reference core average fission rate, available results

Method	Fission density (cm^{-1} sce^{-1})	Comment
1	2.13×10^8 (± 1.7 %) 2.15×10^8 (± 1.7 %)	56 measurements with one 4% monitor capsule 2 measurements with one 3.3% monitor capsule
2	2.06×10^8 (± 3.3 %) 2.12×10^8 (± 4.2 %)	56 measurements with one 4% monitor capsule 2 measurements with one 3.3% monitor capsule
3	2.08×10^8 (± 1.7 %)	2 pellet measurements
4	2.03×10^8 (± 3.2 %)	4 F.C. measurements

In this table the uncertainty margins correspond to the global relative errors established with a 90% confidence interval. As the errors are different according to the methods and to the amounts of measurements, the *weighted average value* is recommended as the *best estimate for the reference core average fission rate* (100% power):

$$2.10 \times 10^{8} (\pm 1.8\ \%) \text{ fiss. cm}^{-1} \text{ sec}^{-1}$$

The final uncertainty is the highest value as obtained in the three following ways:

- Deduced from the individual errors $\sigma^{i}_{90\%}$: $\sigma_{90\%} \cong \frac{1}{\sqrt{6}} \cdot \overline{\sigma}^{i}_{90\%}$.
- Deduced from the observed highest deviation: $\sigma_{90\%} \approx \frac{|\text{Max.}-\text{Min.}|}{2\sqrt{6}}$.
- Deduced from the observed standard deviation: $\sigma_{90\%} = \frac{t_{\text{student}}}{\sqrt{6}} \cdot \sigma$.

NB: Calculation of the reference power level

Starting from the fission density at the mid-plane level of an average fuel pin the total power is obtained by:

2.10×10^{8} cm^{-1} sec^{-1}
$\times$ Maximum axial/Axial average over the fuel height (0.768)
$\times$ Number of fuel rods (2552)
$\times$ Fuel length (50 cm)
$\times$ Number of Watt seconds per fission (3.20×10^{-11} for 200 MeV/fission)

The second factor is calculated with an extrapolated height of 64.1 cm corresponding to:

$$B_{ax}^{2} = 2\ 400 \times 10^{6} \text{ cm}^{-2}.$$

One has thus:

$$P = 2.10 \times 10^{8} \times 0.768 \times 2\ 552 \times 50 \times 3.2 \times 10^{-11} = 658 \text{ Watt}$$

VENUS-1: Results of Experimental Measurement of Vertical Bucklings in the Core and Outside

(*Issued 20.03.84*)

LWR-PV SURVEILLANCE DOSIMETRY IMPROVEMENT PROGRAMME: VENUS PWR CORE SOURCE AND AZIMUTHAL LEAD FACTOR EXPERIMENTS AND CALCULATIONAL TESTS

6.0. VENUS vertical bucklings (A. Fabry, L. Leenders, E.D. McGarry)

6.1. Vertical bucklings in the core (fuel activation)

Vertical bucklings in the core have been proven to be independent on the energy by scanning ^{235}U and ^{237}Np fission chambers (see Section 6.2).

In order to obtain vertical bucklings, representative of the core, six fuel pins (three 4/0 and three 3/0 ones) were measured axially by γ-scanning after an irradiation of 8 h at 90% of the VENUS maximum power. The data correspond to the gamma activity of the ^{140}La (fission yield ~6%, energy ~1.6 MeV, effective half-life ~12.8 d).

The measured gamma activities were improved for decay and analysed by a least square cosine fitting, which defines the extrapolated height of the reactor and the corresponding buckling.

Figure 6.1.1 shows the investigated fuel pins and Table 6.1.1 summarises the results.

As no significant geometrical dependence appears, it is proposed to adopt a unique vertical buckling for the fuel region of the VENUS mock-up.

$$B_{v,\,core} = (4.90 \pm 0.01)\ 10^{-2}\ cm^{-1}$$

or

$$B^2_{v,\,core} = (2400 \pm 12)\ 10^{-6}\ cm^{-2}$$

6.2. Vertical bucklings in the core and outside (fission chambers)

Vertical bucklings have been measured by scanning ^{235}U and ^{237}Np fission chambers in 17 locations from the central hole to neutron pad as illustrated in Figure 6.2.1.

For the measurements in the core, the investigated fuel pin was unloaded and replaced by an empty cladding tube in order to guide the fission chamber. The latter was surrounded by stainless steel in order to reduce the perturbation.

For the measurements in the stainless steel pieces and in the water, the fission chamber was surrounded by stainless steel and by Plexiglas, respectively.

The results are summarised in Table 6.2.1 and illustrated in Figure 6.2.2. It appears clearly that the thermal neutron vertical buckling remains constant inside and outside the reactor core, and the ^{235}U fission chamber results are in agreement with the value recommended from the fuel activations (see Section 6.1).

The fast neutron vertical buckling, given by ^{237}Np fission chambers, is also in agreement with the recommended value in the core, while it decreases as a function of the distance to the core as was the case for the PCA experiments.

In VENUS, the azimuthal buckling variation is "felt" as an effect of the distance to the core; as the variation is not very high it is recommended to adopt an average buckling per region as a function of the distance to the core:

Water reflector:	from 0 to ~16.7 cm	$B_{v,\ reflector} = (4.84 \pm 0.06)\ 10^{-2}\ cm^{-1}$
Barrel:	from 10 to ~19.3 cm	$B_{v,\ barrel} = (4.79 \pm 0.03)\ 10^{-2}\ cm^{-1}$
Water gap:	from 15.7 to ~24.8 cm	$B_{v,\ water\ gap} = (4.75 \pm 0.03)\ 10^{-2}\ cm^{-1}$
Neutron pad:	from 22.1 to ~31.3 cm	$B_{v,\ neutron\ pad} = (4.71 \pm 0.03)\ 10^{-2}\ cm^{-1}$

Figure 6.1.1. Axial buckling core by fuel activation (SCK/CEN)

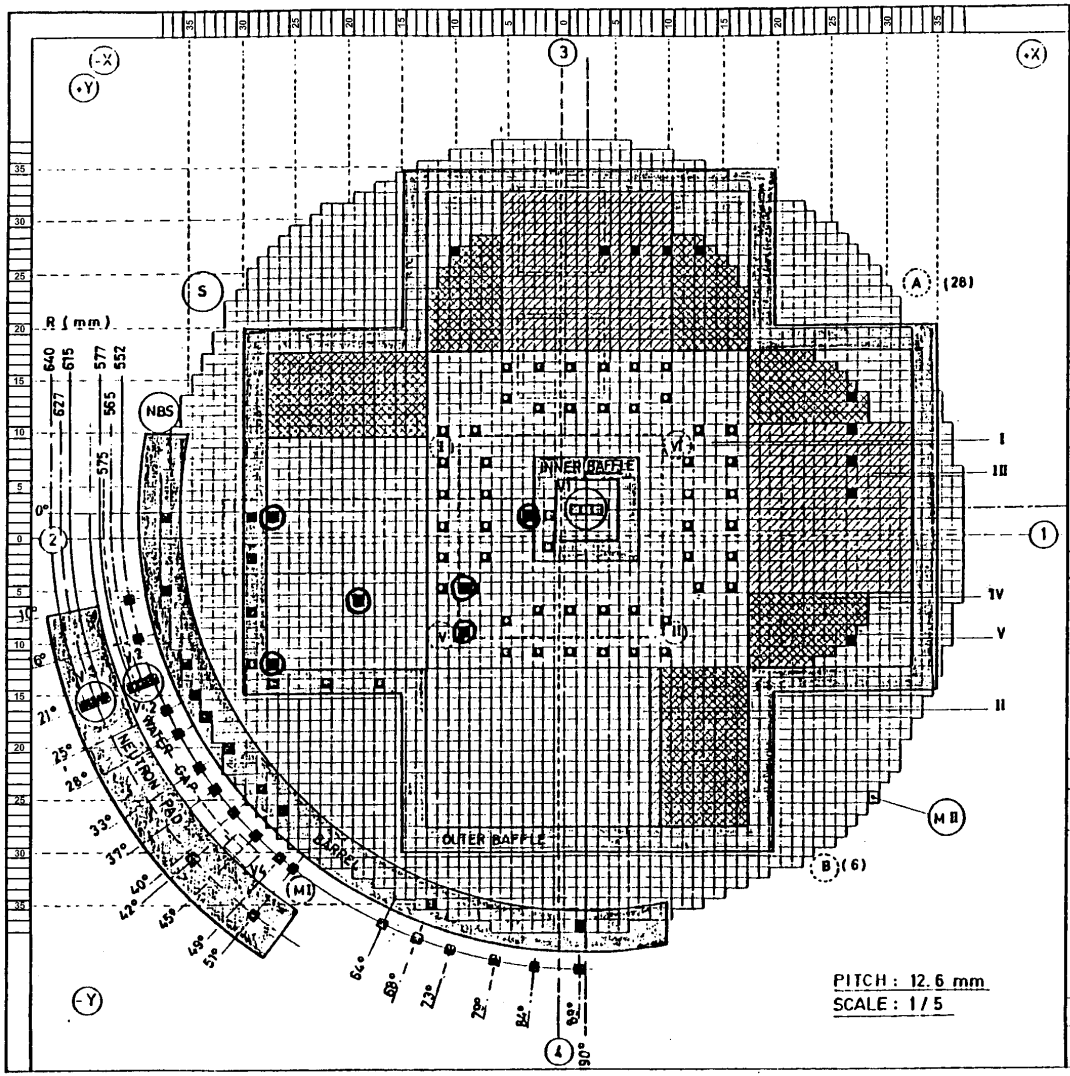

C.E.N-S.C.K	VENUS CRITICAL EXPERIMENT
EXPERIMENT :	LWR-PVS - BENCHMARK
DATE :	from 24.01.83 to
CONFIGURATION N°	29 / 14
DENSITY RODS :	NONE
BORON CONCENTRATION (p.p.m) :	NONE
START-UP SOURCE (S)	YES
NEUTRON GENERATOR (N)	NONE
ABSORBING ROD ■	8R + 2M
PYREX ROD ◘	48

FUEL REGIONS TOTAL : (2600 - 58) pins

DESIGNAT.	%US/%Pu (1)	COLOUR OR SYMBOL	NUMBER OF FUEL PINS	EQ. RADIUS OR X . Y	INVESTIGATED CELL
I	3/0		800-48		
II	4/0 (3d)		645		
III	4/0 (1st)		495 - 6		
IV	4/0 (2d)		504 - 2		
V	3/0 (2)		156 - 2		

MONITORING DETECTORS

DESIGNAT.	DIAMET.	SYMBOL	N° CABLE	LOCATION	LEVEL	CHANNEL
PROPORTIONAL BF3 COUNTER						
FISSION CHAMBER	1/8"	MI		R=552 θ=54	Bottom	C
	1/4"	MII		X=±29 Y=-25	Bottom	D
	1"	NBS				

CONTROL DETECTORS

DESIGNAT.	DIAMET.	SYMBOL	N°	LOCATION	LEVEL	CHANNEL
PROPORTIONAL COUNTER	1"	(A)		28	mid-pl.	A
	1"	(B)		6	mid-pl.	B
ION CHAMBER (NON-COMPENSATED)		(I)		X=-11 Y=+9	under reactor	I
		(II)		X=+11 Y=-9	under reactor	II
		(V)		X=-11 Y=-9	under reactor	V
		(VI)		X=+11 Y=+9	under reactor	VI

REMARK :

VERIFIED BY: APPROVED BY: 040283

REMARKS: (1) Supply order of 4/0 fuel
(2) Out of specifications (0l25 < Bowing < 0.50 mm)

Table 6.1.1. Vertical bucklings measured in the VENUS core by fuel activation

VENUS critical experiment – Mol
LWR-PVS benchmark, 1983

Issued 14/10/83
Unmodified 20/03/84

I. Region with 3/0 fuel

X,Y[(1)]	X′ [cm][(2)]	Y′ [cm][(2)]	Remark	Vertical extrapolation length [cm][(3)]	Axial buckling [10^{-6} cm^{-2}]
-3, +2	-6.93	-0.63	Side inner baffle	14.55 ± 0.15	2 369 ± 11[(4)]
-9, -5	-14.49	-9.45	Close to Pyrex	14.06 ± 0.17	2 406 ± 13
-9, -9	-14.49	-14.49	Centre 3/0 fuel	14.29 ± 0.22	2 388 ± 17

II. Region with 4/0 fuel

X,Y[(1)]	X′ [cm][(2)]	Y′ [cm][(2)]	Remark	Vertical extrapolation length [cm]	Axial buckling [10^{-6} cm^{-2}]
-19, -6	-27.09	-10.71	Centre 4/0 fuel	14.11 ± 0.19	2 401 ± 15
-27, +2	-37.17	-0.63	Side outer baffle	14.18 ± 0.19	2 397 ± 14
-27, -12	-37.17	-18.27	Corner outer baffle	13.98 ± 0.21	2 411 ± 15

(1) Co-ordinates with respect to the reactor grid, as used during the experiments.
(2) Co-ordinates with respect to the reactor centre, as used for the calculation model.
(3) Fuel length = 50 cm.
(4) Possible influence of the central hole, probably limited to the 44 rods being close to the inner baffle.

Figure 6.2.1. Axial buckling regions by mechanised fission chamber (NBS, SCK/CEN) (^{235}U and/or ^{237}Np)

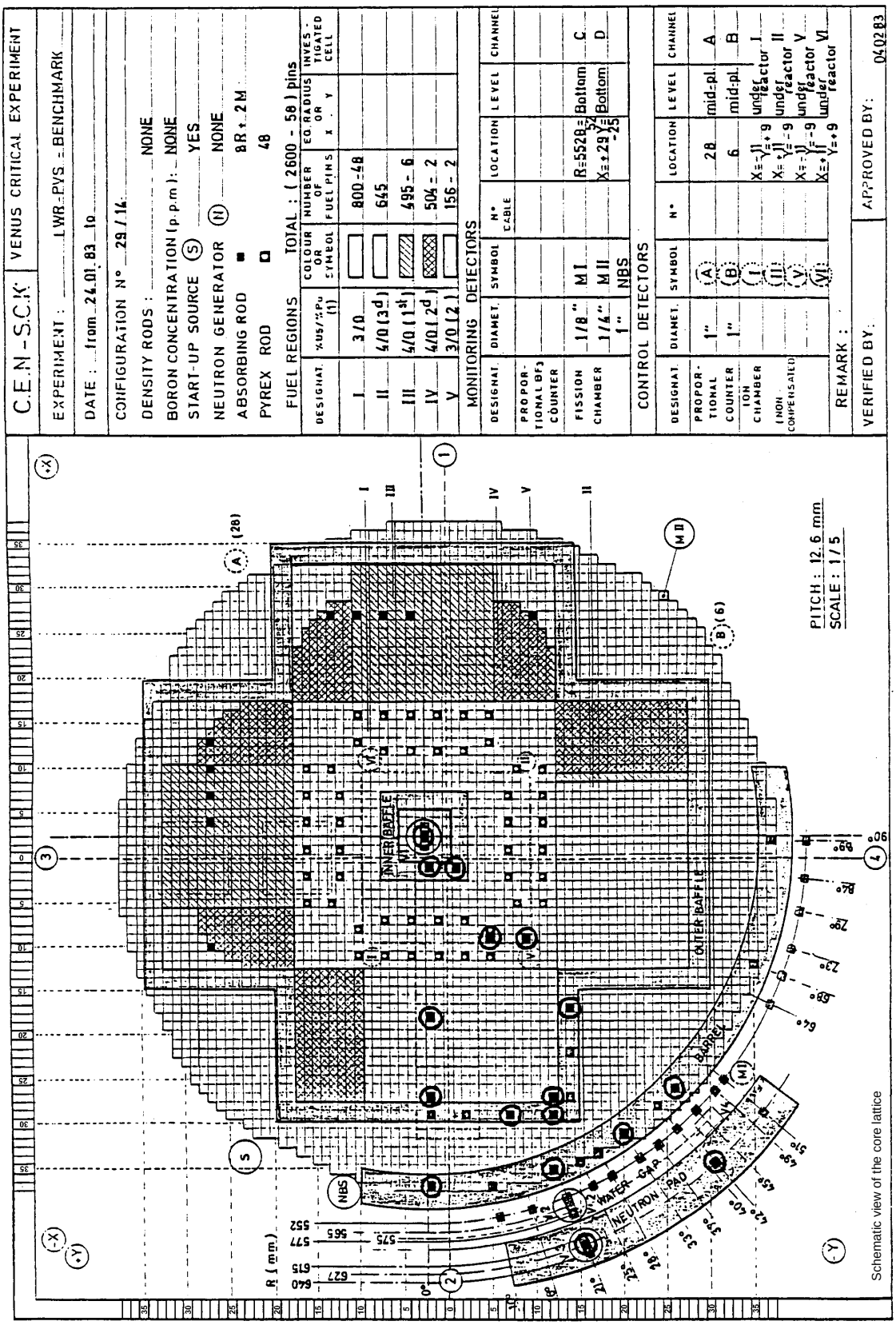

Schematic view of the core lattice

REMARKS: (1) Supply order of 4/0 fuel
(2) Out of specifications (0.25 < Bowing < 0.50 mm)

Figure 6.2.1. Vertical bucklings measured through the VENUS mock-up by fission chambers

VENUS critical experiment – Mol

Issued 20/03/84

Region	Co-ordinates			Remark	^{235}U fission chamber		^{237}Np fission chamber	
	X,Y (1)	X′ (cm) (2)	Y′ (cm) (2)		Extrap. length [cm] (3)	Buckling [10^{-6} cm^{-2}]	Extrap. length [cm] (3)	Buckling [10^{-6} cm^{-2}]
Central hole	+2.5, +2.5	0	0	Unique buckling with the weighted average data (4)	14.26 ± 0.20	2390 ± 15	14.23 ± 0.11	2392 ± 10
Inner baffle	-1, +2 -1, -1	-44.10 -44.10	-6.30 -44.10					
3/0 fuel	-9, -5 -9, -9	-144.90 -144.90	-94.50 -144.90					
4/0 fuel	-18, +2 -27, +2 -27, -12	-258.30 -371.70 -371.70	-6.30 -6.30 -182.70					
Outer baffle	-17, -14 -29, +7 -29, -12	-245.70 -396.80 -396.80	-207.90 -119.70 -182.70					
Barrel 0°	-37, +2	-497.70	-6.30	21°	–	–	14.81 ± 0.69	2350 ± 50
Barrel 21°	-35, -12	-472.50	-182.70	45°	14.36 ± 0.07	2383 ± 6	16.17 ± 0.19	2254 ± 13
Barrel 33°	-31, -20	-422.10	-283.50	weighted average data	14.14 ± 0.24	2399 ± 18	–	–
Barrel 45°	-26, -26	-359.10	-359.10					
Neutron pad		R = 627 R = 627	θ = 21 θ = 45	21°	14.19 ± 0.34	2396 ± 25	16.63 ± 0.89	2224 ± 59

(1) Co-ordinates with respect to the reactor grid, as used during the experiments.
(2) Co-ordinates with respect to the core centre, as used for the calculational model.
(3) Fuel length and reactor height = 50 cm.
(4) The traverses obtained from the central hole to the outer baffle are essentially the same both for ^{235}U and for ^{237}Np.

Figure 6.2.2. Measurements of VENUS neutron vertical leakage trends
(comparison with the PCA results)

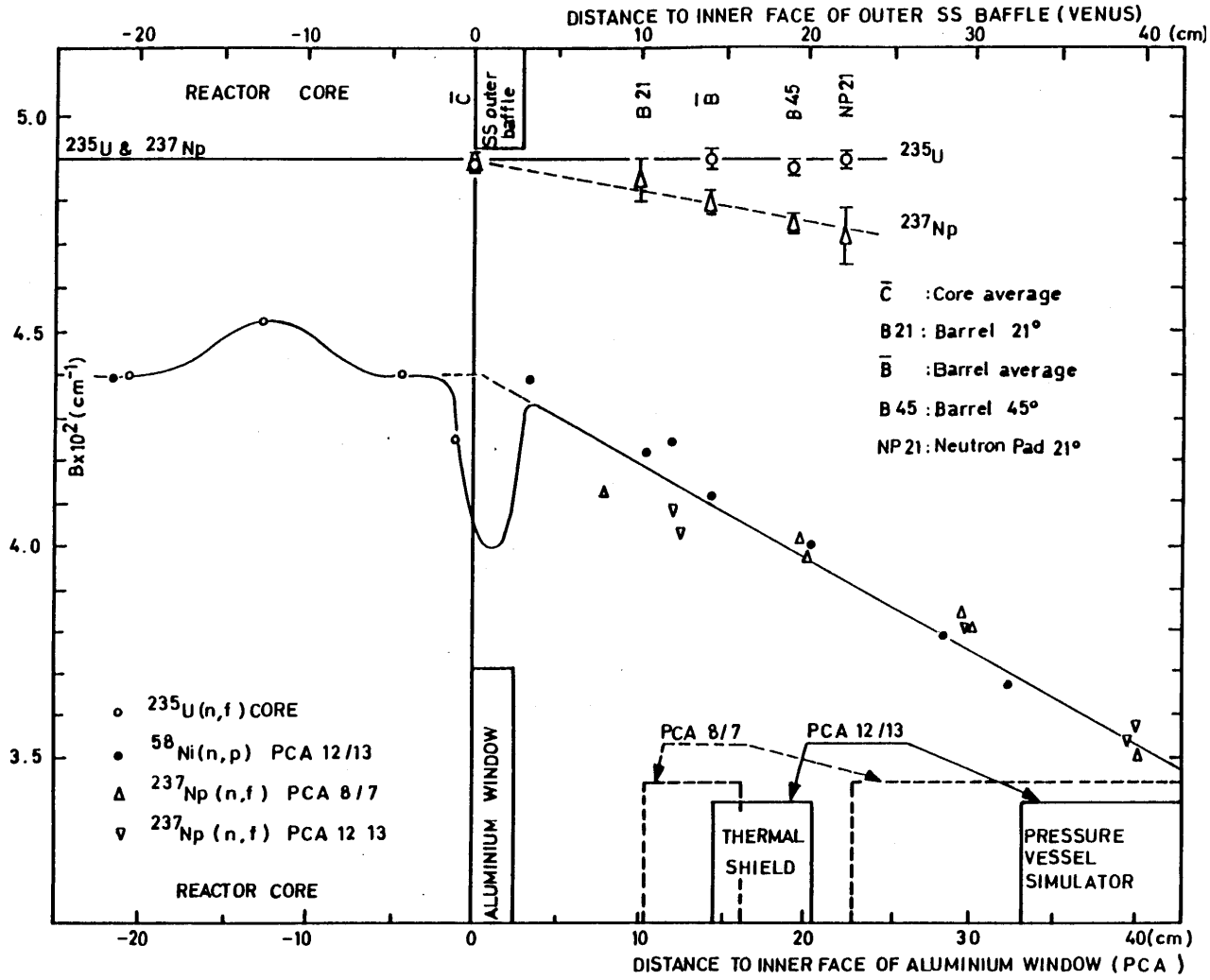

APPENDIX A

Benchmark specifications

A.2. VENUS-3

I. General comments

In this benchmark, which is a follow-up exercise to the recently completed VENUS-1 two-dimensional exercise, the goal is to test the current state-of-the-art three-dimensional methods of calculating neutron flux to reactor components against the measured data of the VENUS-3 critical experiment.

Similarly to the VENUS-1 benchmark, this is a "blind'" test, hence the measured values of the equivalent fission flux at specified VENUS-3 locations are not revealed to the participants *a priori*, but will be provided when benchmark results are analysed.

A complete specification of the VENUS-3 problem is given in the included report: *LWR-PVS benchmark experiment VENUS-3 (with partial length shielded assemblies) – Core description and qualification.* The information given fully specifies all geometry and material data required in developing the detailed computational model of the 1/4 fraction of the VENUS-3 reactor.

II. Co-ordinate systems

The fission flux measurement points as well as the reactor zones in which they are placed in the VENUS reactor are defined in tables below. The co-ordinates of the measurement points are given in three different co-ordinate systems:

- (x,y,z) co-ordinates with respect to the reactor grid (used in the experiments).
- (x,y,z) co-ordinates with respect to the core centre (for use in calculational model).
- (r,θ,z) co-ordinates with respect to the core centre (for use in calculational model).

The (x,y) or (r,θ) co-ordinates of all measurement points are given in Table 1 (similar to Table 1 provided with the VENUS-1 distribution package, however, with some measurement points different than in the VENUS-1 benchmark).

The origin of the (x,y) co-ordinate system with respect to reactor grid is located in the inner baffle at a point 2.5 pitches (1 pitch = 1.26 cm) to the left and 2.5 pitches below the geometric centre of the core. The south-west quadrant of the core to be considered in the calculations is thus defined by the ranges $-27 < x < +2$ and $-27 < y < +2$, where the limits represent cell centre-to-centre distances in units of pitches. Positions exterior to the core may also be located by extending the grid to include the outer baffle, core barrel and water (the baffles are 2.268 pitches thick).

* In this revised version of the benchmarck specification, modified points compared with the original version dated 11 July 1997 are in bold italic.

III. 3-D neutron source

The three-dimensional source input for calculations released to the NEA by H. Aït Abderrahim (SCK·CEN Mol, Belgium) is provided to participants in electronic form via e-mail. A description of the source format is given in the source file. It suffices to say that the source is given at 14 different vertical planes (each clearly defined in the source file). Each vertical plane consists of a 30×30 matrix of relative source values at (x,y) ($1 < x < 30$, $1 < y < 30$) positions defined in Figure 1 with respect to core centre (i.e. the centre of the central hole). The correspondence between this co-ordinate system and co-ordinate system with respect to reactor grid (defined in Section II above) is clearly given in Figure 1.

Not all source values were measured in the VENUS-3 experiment. The missing source values were interpolated at the NEA within the scope of the joint NEA/ORNL SINBAD project (H.T. Hunter, D.T. Ingersoll, R.W. Roussin, C.O. Slater, E. Sartori, I. Kodeli, "SINBAD – Shielding Integral Benchmark Archive and Database", Proc. ANS Topical Meeting on Radiation Protection and Shielding, Cape Cod, Massachusetts, April 1996). This is a valid procedure considering extremely regular core power distribution in VENUS-3 core.

The reference measured fission rate per core quadrant is 8.845×10^9 (±4%) and should be used as a multiplication factor for converting the provided normalised 3-D source values to the source at 100% power (the total fission rate value per quadrant was obtained from absolute measurements at several locations using ^{235}U miniature fission chambers; this measurement yielded a value of 5.652×10^{12} fissions per second per core quadrant which then was divided by 639 pins per quadrant yielding 8.845×10^9 fissions/sec/pin/quadrant).

IV. Results to be provided and their format

For the measurement points defined in Table 1 the "equivalent fission flux" and neutron fluxes at threshold energies $E_{th} > 1.0$ MeV and $E_{th} > 0.1$ MeV should be calculated and reported in Tables 2.1 through 3.2 given below. The "equivalent fission flux" is defined as a ratio of calculated reaction rate [three different reactions to be considered are defined in Tables 2.1 through 2.3] and the average dosimeter cross-section.

In the calculations, the participants are kindly requested to use the **IRDF-90 Version 2** dosimeter cross-section data in order to assure comparability between different results.

The following information should be included when reporting the results of the benchmark:

- Description of the calculations procedure (all important information about modelling assumptions and codes/methods used); if S_N method is used then the quadrature set order should be reported (a symmetric or not quadrature is used?), etc.
- Grid/mesh structure of the model (***including a picture of the geometrical model used***).
- The name and version of the point library neutron transport cross-section data and the energy group structure.
- Method/model used in cross-section collapsing.

- The name and version of the dosimeter cross-sections data.

- Any other information not listed above but judged by the participant as important in interpreting this benchmark should be included.

III. Optional calculations

Two additional but **optional** calculations are suggested:

1) The participants who wish are kindly invited to calculate the DPA using pre-calculated neutron spectra. Those DPAs should be reported in columns marked "**Optional DPA**" in Tables 2.1 through 3.2.

2) The participants who wish to perform the uncertainty analysis of their benchmark calculations are encouraged to do so as an additional option.

Table 1. (x,y) and (r,θ) co-ordinates of VENUS-3 measurement positions

No.	Measurement point zone	(x,y) co-ordinates with respect to reactor grid	(r,θ) in (cm,°) co-ordinates with respect to core centre	(x,y) in (cm,cm) co-ordinates with respect to core centre
1	Central hole	(+2.5,+2.5)		(0.,0.)
	Inner baffle			
2		(-1,+2)	(–,8.1°)	(-4.41,-0.63)
3		(-1,-1)	(–,45.0°)	(-4.41,-4.41)
	Outer baffle			
4		(-29,+2)	(–,0.9°)	(-39.69,-0.69)
5		(-29,-2)	(–,8.1°)	(-39.69,-5.67)
6		(-29,-7)	(–,16.8°)	(-39.69,-11.97)
7		(-29,-12)	(–,24.7°)	(-39.69,-18.27)
8		(-27,-14)	(–,29.2°)	(-37.17,-20.79)
9		(-22,-14)	(–,34.0°)	(-30.87,-20.79)
10		(-17,-14)	(–,40.2°)	(-24.57,-20.79)
	Core barrel			
11		(-37,+2)	(–,0.7°)	(-49.77,-0.63)
12		(-37,-5)	(–,10.8°)	(-49.77,-9.45)
13		(-35,-12)	(–,21.1°)	(-47.25,-18.27)
14		(-34,-15)	(–,25.6°)	(-45.99,-22.05)
15		(-33,-17)	(–,28.8°)	(-44.73,-24.57)
16		(-31,-20)	(–,33.9°)	(-42.21,-28.35)
17		(-28,-24)	(–,41.0°)	(-38.43,-33.39)
18		(-26,-26)	(–,45.0°)	(-35.91,-35.91)
19		(-12,-35)	(–,68.9°)	(-18.27,-47.25)
20		(+2,-37)	(–,89.3°)	(-0.63,-49.77)
	Water gap			
21		(-33,+2)	(–,0.81°)	(-44.73,-0.63)
	PLSA			
22		(-27,+2)	(–,0.97°)	(-37.17,-0.63)
23		(-27,+3)	(–,0.97°)	(-37.17,+0.63)
24		(-25,+3)	(–,1.04°)	(-34.65,+0.63)
25		(-23,+2)	(–,1.12°)	(-32.13,-0.63)
26		(-23,+3)	(–,1.12°)	(-32.13,+0.63)
27		(-27,-9)	(–,21.3°)	(-37.17,-14.49)
	3.3% fuel			
28		(-21,+2)	(–,1.22°)	(-29.61,-0.63)
29		(-19,+3)	(–,1.33°)	(-27.09,+0.63)
30		(-22,+0)	(–,5.82°)	(-30.87,-3.15)
31		(+2,***-23***)	(–,88.6°)	(-0.63,***-32.13***)

Table 2.1. Nickel equivalent fission fluxes at 100% power at inner and outer baffle locations: VENUS-3

Angle	Measure position	Axial level (cm)	^{58}Ni(n,p)	Flux at E > 0.1 MeV	Flux at E > 1.0 MeV	Optional DPA
8.1°	**Inner baffle** (-1,+2)	114.50 131.45 131.55 145.50				
45.0°	(-1,-1)	114.50 131.45 131.55 145.50				
0.9°	**Outer baffle** (-29,+2)	106.5 110.5 114.5 118.5 122.5 125.5 128.5 131.5 134.5 137.5 141.5 145.5 149.5 153.5				
8.1°	(-29,-2)	114.5 131.5 145.5				
16.8°	(-29,-7)	114.5 131.5 145.5				
24.7°	(-29,-12)	114.5 131.5 145.5				
29.2°	(-27,-14)	114.5 131.5 145.5				
34.0°	(-22,-14)	114.5 131.5 145.5				
40.2°	(-17,-14)	114.5 131.5 145.5				

Table 2.2. Nickel equivalent fission fluxes at 100% power at core barrel locations: VENUS-3

Angle	Core barrel position	Axial level (cm)	^{58}Ni(n,p)	Flux at E > 0.1 MeV	Flux at E > 1.0 MeV	Optional DPA
0.7°	(-37,+2)	106.5 110.5 114.5 118.5 122.5 125.5 128.5 131.5 134.5 137.5 141.5 145.5 149.5 153.5				
10.8°	(-37,-5)	114.5 131.5 145.5				
21.1°	(-35,-12)	106.5 110.5 114.5 118.5 122.5 125.5 128.5 131.5 134.5 137.5 141.5 145.5 149.5 153.5				
25.6°	(-34,-15)	114.5 131.5 145.5				
28.8°	(-33,-17)	114.5 131.5 145.5				
33.9°	(-31,-20)	114.5 131.5 145.5				
41.0°	(-28,-24)	114.5 131.5 145.5				

Table 2.2. Nickel equivalent fission fluxes at 100% power at core barrel locations: VENUS-3 (*cont.*)

Angle	Core barrel position	Axial level (cm)	^{58}Ni(n,p)	Flux at E > 0.1 MeV	Flux at E > 1.0 MeV	Optional DPA
45.0°	(-26,-26)	106.5				
		110.5				
		114.5				
		118.5				
		122.5				
		125.5				
		128.5				
		131.5				
		134.5				
		137.5				
		141.5				
		145.5				
		149.5				
		153.5				
68.9°	(-12,-35)	106.5				
		110.5				
		114.5				
		118.5				
		122.5				
		125.5				
		128.5				
		131.5				
		134.5				
		137.5				
		141.5				
		145.5				
		149.5				
		153.5				
89.3°	(+2,-37)	106.5				
		110.5				
		114.5				
		118.5				
		122.5				
		125.5				
		128.5				
		131.5				
		134.5				
		137.5				
		141.5				
		145.5				
		149.5				
		153.5				

Table 2.3. Nickel equivalent fission fluxes at 100% power at water gap locations: VENUS-3

Angle	Position	Axial level (cm)	^{58}Ni(n,p)	Flux at E>0.1 MeV	Flux at E>1.0 MeV	Optional DPA
	Water gap					
0.81°	(-33,+2)	106.5				
		110.5				
		114.5				
		118.5				
		122.5				
		125.5				
		128.5				
		131.5				
		134.5				
		137.5				
		141.5				
		145.5				
		149.5				
		153.5				

Table 2.4. Nickel equivalent fission fluxes at 100% power at PLSA* locations: VENUS 3

Angle	PLSA position	Axial level (cm)	^{58}Ni(n,p)	Optional Flux at E > 0.1 MeV	Optional Flux at E > 1.0 MeV	Optional DPA
0.97°	(-27,+3)	106.5 110.5 114.5 118.5 122.5 125.5 128.5				
0.97°	(-27,+2)	131.05 134.15 137.25 141.35 145.45 149.55 153.65				
1.04°	(-25,+3)	106.5 110.5 114.5 118.5 122.5 125.5 128.5 131.05 134.15 137.25 141.35 145.45 149.55 153.65				
1.12°	(-23,+2)	131.05 134.15 137.25 141.35 145.45 149.55 153.65				
1.12°	(-23,+3)	106.5 110.5 114.5 118.5 122.5 125.5 128.5				
21.3°	(-27,-9)	106.5 110.5 114.5 118.5 122.5 125.5 128.5				

** PLSA: Partial length shielded assembly*

Table 2.5. Nickel equivalent fission fluxes at 100% power at 3.3% fuel locations: VENUS-3

Angle	3.3% fuel position	Axial level (cm)	^{58}Ni(n,p)	Optional Flux at E > 0.1 MeV	Optional Flux at E > 1.0 MeV	Optional DPA
1.2°	(-21,+2)	106.05				
		110.15				
		114.25				
		118.35				
		122.45				
		125.55				
		128.65				
		131.75				
		134.85				
		137.95				
		141.05				
		145.15				
		149.25				
		153.35				
1.3°	(-19,+3)	106.05				
		110.15				
		114.25				
		118.35				
		122.45				
		125.55				
		128.65				
		131.75				
		134.85				
		137.95				
		141.05				
		145.15				
		149.25				
		153.35				
5.8°	(-22,+0)	106.05				
		110.15				
		114.25				
		118.35				
		122.45				
		125.55				
		128.65				
		131.75				
		134.85				
		137.95				
		141.05				
		145.15				
		149.25				
		153.35				

Table 2.5. Nickel equivalent fission fluxes at 100% power at 3.3% fuel locations: VENUS-3 (*cont.*)

Angle	3.3% fuel position	Axial level (cm)	^{58}Ni(n,p)	Optional Flux at E > 0.1 MeV	Optional Flux at E > 1.0 MeV	Optional DPA
88.6°	(+2,-***23***)	106.05 110.15 114.25 118.35 122.45 125.55 128.65 131.75 134.85 137.95 141.05 145.15 149.25 153.35				

Table 3.1. Indium equivalent fission fluxes at 100% power at inner baffle, outer baffle and water gap locations: VENUS-3

Angle	Position	Axial level (cm)	$^{115}In(n,n')$	Flux at E > 0.1 MeV	Flux at E > 1.0 MeV	Optional DPA
	Inner baffle					
8.1°	(-1,+2)	131.5				
45.0°	(-1,-1)	131.5				
	Outer baffle					
0.9°	(-29,+2)	106.5				
		110.5				
		114.5				
		118.5				
		122.5				
		125.5				
		128.5				
		131.5				
		134.5				
		137.5				
		141.5				
		145.5				
		149.5				
		153.5				
	Water gap					
0.8°	(-33,+2)	106.5				
		110.5				
		114.5				
		118.5				
		122.5				
		125.5				
		128.5				
		131.5				
		134.5				
		137.5				
		141.5				
		145.5				
		149.5				
		153.5				

Table 3.2. Indium equivalent fission fluxes at 100% power at core barrel locations: VENUS-3

Angle	Core barrel position	Axial level (cm)	$^{115}In(n,n')$	Flux at E > 0.1 MeV	Flux at E > 1.0 MeV	Optional DPA
0.7°	(-37,+2)	106.5				
		110.5				
		114.5				
		118.5				
		122.5				
		125.5				
		128.5				
		131.5				
		134.5				
		137.5				
		141.5				
		145.5				
		149.5				
		153.5				
10.8°	(-37,-5)	114.5				
		131.5				
		145.5				
21.1°	(-35,-12)	114.5				
		131.5				
		145.5				
25.6°	(-34,-15)	114.5				
		131.5				
		145.5				
28.8°	(-33,-17)	106.5				
		110.5				
		114.5				
		118.5				
		122.5				
		125.5				
		128.5				
		131.5				
		134.5				
		137.5				
		141.5				
		145.5				
		149.5				
		153.5				

Table 3.2. Indium equivalent fission fluxes at 100% power at core barrel locations: VENUS-3 (*cont.*)

Angle	Core barrel position	Axial level (cm)	$^{115}In(n,n')$	Flux at E > 0.1 MeV	Flux at E > 1.0 MeV	Optional DPA
33.9°	(-31,-20)	106.5				
		110.5				
		114.5				
		118.5				
		122.5				
		125.5				
		128.5				
		131.5				
		134.5				
		137.5				
		141.5				
		145.5				
		149.5				
		153.5				
41.0°	(-28,-24)	114.5				
		131.5				
		145.5				
45.0°	(-26,-26)	114.5				
		131.5				
		145.5				
68.9°	(-12,-35)	114.5				
		131.5				
		145.5				
89.3°	(+2,-37)	106.5				
		110.5				
		114.5				
		118.5				
		122.5				
		125.5				
		128.5				
		131.5				
		134.5				
		137.5				
		141.5				
		145.5				
		149.5				
		153.5				

Table 3.2. Aluminium equivalent fission fluxes at 100% power at various locations: VENUS-3

Angle	Position	Axial level (cm)	$^{27}Al(n,\alpha)$	Flux at E > 0.1 MeV	Flux at E > 1.0 MeV	Optional DPA
	Inner baffle					
45.0°	(-1,-1)	131.5				
8.1°	(-1,+2)	131.5				
	Outer baffle					
0.9°	(-29,+2)	114.5 131.5 145.5				
	Water gap					
0.8°	(-33,+2)	114.5 131.5 145.5				
	Core barrel					
0.7°	(-37,+2)	114.5 131.5 145.5				
10.8°	(-37,-5)	114.5 131.5 145.5				
21.1°	(-35,-12)	114.5 131.5 145.5				
25.6°	(-34,-15)	114.5 131.5 145.5				
28.8°	(-33,-17)	114.5 131.5 145.5				
33.9°	(-31,-20)	114.5 131.5 145.5				
41.0°	(-28,-24)	114.5 131.5 145.5				
45.0°	(-26,-26)	114.5 131.5 145.5				
68.9°	(-12,-35)	114.5 131.5 145.5				
89.3°	(+2,-37)	114.5 131.5 145.5				

Mol, September 1, 1988
FCP/VEN/01

LWR-PVS Benchmark Experiment VENUS-3
(with Partial Length Shielded Assemblies)

Core description and qualification

L. Leenders

1.1. General

The VENUS Critical Facility is a zero power reactor located at SCK·CEN, Mol (Belgium). This facility was built in 1963-1964, as a nuclear mock-up of a projected marine reactor so-called VULCAIN; hence the name VENUS which stands for "VULCAIN EXPERIMENTAL NUCLEAR STUDY".

In 1967, this facility was adapted and improved in order to study LWR core designs and to provide experimental data for nuclear code validation. A great flexibility was looked for, as well as an easy handling of the fuel pins, handled one by one, while a great precision of the results had to be achieved.

In 1980, additional material was purchased with a view to studying typical 17×17 PWR fuel assemblies. Such an adaptation is easy; only new reactor grids and small devices adapted to the new fuel geometry are necessary. In 1982, special stainless steel pieces were manufactured in order to build a mock-up of the pressure vessel internals representative of a three-loop Westinghouse power plant. These stainless steel pieces were delivered at the beginning of December 1982. Since this date, the facility has been used for three LWR-PVS benchmark experiments as follows:

- *VENUS-1*: This mock-up was aimed to check the calculation procedure for a standard LWR core, i.e. with fresh UO_2 fuel assemblies at the periphery. The VENUS-l core was made critical for the first time on 20 December 1982. The experimental programme was carried out from 26 January 1983 until 6 June 1986.

- *VENUS-2*: Between the possible solutions to reduce the lead factor at the PV, it is proposed to replace some fresh UO_2 fuel assemblies by burnt fuel assemblies at the most critical corners of the core periphery. For benchmark purposes, the VENUS-2 core was obtained by replacing the peripheral UO_2 fuel by a MOX fuel, actually simulating a two-cycle burnt UO_2 fuel (except for FP poisoning). The VENUS-2 core was made critical for the first time on 16 September 1986. The corresponding experimental programme was carried out from 6 October 1986 until 16 December 1987.

- *VENUS-3*: For some early built reactors, it is proposed to reduce the lead factor at the level of the PV horizontal welding by loading partial length shielded assemblies at the most critical corners of the core periphery (the shielded part is obtained by replacing part of the fuel length by a stainless steel rod). For benchmarking this improvement, the VENUS-3 core has been built with 3/0-SS rods at the periphery (the 3/0-SS rods are made of half a length of stainless steel and half a length of 3.3% ^{235}U enriched UO_2 fuel). The VENUS-3 core was made critical for the first time on 16 March 1988. The experimental programme started on 29 March 1988 and is planned to go on until the end of December 1988.

1.2. Description of the facility

The facility comprises a reactor shielded room and several associated facilities: the control room, the fuel room, the fuel storage, the gamma scanning device, the counting room and the plutonium laboratory. The shielded room is partly illustrated in Figure 1.1; under the floor, it contains:

1. The reactor vessel (~2.6 m^3).

2. The reactor grids (1 m diameter).

3. The safety neutron detectors.

4. The safety system (moderator fast dump).

5. The water and compressed air circuitries (not shown in the figure).

The working room (6, above the floor) gives a direct access to the reactor core for loading and unloading fuel pins or experimental thimbles. This room contains:

- The start-up neutron source.
- The reactor and health physics controls.
- The regulating rod or fission chamber mechanisms.
- The handling tools.

Due to the direct access to the fuel, the reactor is shut down when the shielded room is open. The neutron flux level in operation is limited to 1×10^9 nv, with a view to limiting the irradiation level of the core and the radioactivity of unloaded fuel pins.

1.3. Core design

The LWR-PVS benchmark experiment in VENUS is aimed at validating the analytical methods needed to predict the azimuthal variation of the fluence in the pressure vessel. The VENUS core was designed with the following objectives:

a) *It had to be representative of typical irradiation conditions of a modern PWR vessel*:

From exploratory calculations [Ref.1.1.], it appeared that a three-loop Westinghouse plant presents a higher azimuthal gradient of the fluence; this gradient has moreover a higher sensitivity to fuel pattern modification. For this reason, the VENUS mock-up had preferably to simulate the corner assembly environment of such a plant, i.e.:

- Core baffle thickness: 2.858 cm
- Reflector minimum thickness: 2.169 cm
- Core barrel thickness: 5.161 cm
- First water gap thickness: 5.952 cm
- Thermal shield thickness: 6.825 cm
- Second water gap thickness: 11.431 cm
- Pressure vessel thickness: 20.003 cm

b) *It had to fit the grid and the vessel geometries of VENUS*:

This led to a limitation of the core size and of the amount of simulated internals. In fact:

- The core is made of 16 "15 × 15" subassemblies, instead of "17 × 17" ones (the pin-to-pin pitch remains typical of the "17 × 17" subassembly).

- The second water gap and the pressure vessel are not simulated; a validation of the calculation up to the thermal shield was considered as acceptable; the complete simulation in the radial direction was indeed investigated in a slab geometry with the PCA mock-up.

- Except for the baffle and the reflector minimum thickness, the thicknesses have been somewhat reduced to fit the VENUS geometry.

c) The core size being defined by a) and b), the core loading was adjusted on the basis of preliminary calculations [Refs. 1.2 and 1.3] with the following objectives:

- A pure uranium core was preferred as being simpler both experimentally and analytically [Ref. 1.4].

- The gamma-heating experiments had to be performed with a low boron content, thus preferably without boron poisoning of the water [Ref. l].

- The radial power shape factor had to be as low as possible, in order to reach, in the different stainless steel pieces, fast flux levels high enough to perform accurate measurements.

- The azimuthal flux variations had to be as high a possible to allow a valuable test of the analytical methods.

- The PLSA benchmark had to be "representative" despite the significant scaling entailed by the smaller size of VENUS; by "representative" it is meant that an adequate testing is provided for all the sensitive aspects in a discrete-ordinates three-dimensional synthesis and superposition approach to an actual PWR/PLSA geometry.

- Finally, a quadrangular symmetry was desirable, each quadrant including both the PLSA fuel region and the unperturbed reference fuel region (for a full flux distortion and for an accurate calculation/experiment comparison).

All these objectives were attained with the actual core configuration as given in Figure 1.2.

Note: *Some mechanised absorbing rods, added far from the region of interest, help to adjust the reactivity balance from run to run.*

d) Preliminary calculations, carried out for VENUS-1, were useful to choose the measurement locations of interest. The 21° and 45° angles, which correspond to the maximum and minimum fast fluxes respectively, were provided with experimental holes. In particular, access holes are accommodated at 21° and at the centre with a view to performing neutron and gamma spectrometry.

Notes: The angular shape of the core barrel is such that both quadrant and octagonal symmetries are achieved with acceptable reflecting conditions (in stainless steel) at 0°, 45° and 90° respectively.

The angular shape of the thermal shield, so-called neutron pad was limited by the available space (it is moreover removable); the quadrant and octagonal symmetries are also achieved with reflecting conditions in water at 0° and 90° and with reflecting conditions in stainless at 45°. This geometry was moreover considered as representative of some Babcock & Wilcox designs.

1.4. Core description

Figure 1.2 gives an horizontal cross-section and Figure 1.3 a top view of the actual core. For experimental and analytical purposes, it should be regarded as a perfect symmetrical core reproducing four times the quadrant between 0° and 90°. The other quadrants are loaded with fuel pins "quasi" identical to the fuel pins of the first quadrant (due to fuel inventory limitations) and with some absorbing rods for critically balance adjustment. Starting from the centre, the core may be divided into 10 horizontal regions:

- The *central hole* (water).
- The *inner baffle* (stainless steel: 2.858 cm thick).
- The *4/0 fuel region*, this region contains stainless steel clad UO_2 rods, with 4% enriched uranium, the rods are typical of a "15×15" lattice (first generation of Westinghouse plants), they are loaded with the pin-to-pin pitch typical of the "17×17" lattice. Eleven Pyrex rods, typical of PWR poison clusters are loaded per quadrant.
- The *3/0 fuel region*, this region contains zircaloy clad UO_2 rods, two with 3.3% enriched uranium, in a "17×17" lattice; part of this region contents the PLSA rods.
- The *outer baffle* (stainless steel: 2.858 cm thick).
- The *reflector* (minimum thickness: 2.169 cm).
- The *barrel* (stainless steel: 4.99 cm thick).
- The *water gap* (water: 5.80 cm thick).
- The *neutron pad* (stainless steel, average thickness: 6.72 cm).
- The VENUS environment, i.e. the jacket (air filled), the reactor vessel (stainless steel) and the reactor room (air).

Figure 1.4 shows a vertical cross-section of the core. Vertically the core may be divided, from bottom to top, as follows:

- The VENUS room environment (air).
- The *lower filling* (water).

- The *reactor support* (water and stainless steel).
- The *bottom grid* (mainly stainless steel).
- The *lower reflector* (mainly water and Plexiglas); the reflector composition changes a little bit from one fuel region to another.
- The *active height* (fuel or stainless steel).
- The *upper reflector* (mainly water and Plexiglas), including the *intermediate grid* (mainly Plexiglas).
- The *upper grid* (mainly stainless steel).
- The *upper filling* (water and stainless steel).
- The VENUS room environment (air).

The figure shows clearly that, whatever the region is, the material of interest (i.e. fuel or stainless steel) is located from level 105 cm to level 155 cm (50 cm length). To ensure proper axial buckling conditions, both lower and upper axial reflectors are "quasi" infinite for all the regions (the effective extrapolation length is ~7 cm); where necessary water is replaced by Plexiglas.

These details could be important for the three-dimensional analytical model.

1.5. Qualified data on the core materials

- The core materials are qualified in several ways. For the stainless steels, for instance, the qualification is based on a comparison between the corresponding standard, the certificate delivered by the supplier and, at least, one analysis carried out by SCK·CEN. The adopted value is generally the average of the consistent data (if necessary a weighted average is made) and the given error is the range defined by the extreme values ($\varepsilon = \pm$ (Max.-Min.)/2).
- For most of the materials, there is at least one more sample for documentation or later cross-check.
- For the fuel cladding and the Pyrex tubes, the linear specific weight has been determined instead of the volume specific weight as the accuracy of checking the tube thickness is too small.
- The impurities of water were checked in the worst conditions, i.e. when the water resistivity reached its lowest value (450 kΩcm); the water temperature is the median value for the experimental period (from 18.03.88 to 29.03.88) and the range is defined by the extreme recorded values.
- For the VENUS internals being outside the LWR-PVS benchmark mock-up, no qualification was made so that average stainless steel characteristics are given.

The detailed qualification is given in work documents available at SCK·CEN. The results are as follows.

1.5.1. Central hole

1.5.1.1. Water composition

H_2O, impurities lower than given hereafter.

- Diluted oxygen: O 8.6 ppm (saturation for air-water contact)
- Detected impurities:

B	12 ppb (1.E-9 g/l) ~ ppm (weight)
Si	46
Mn	2.5
Fe	.7
Mg	5
Cu	5
Ca	75
Al	8
Sr	.5
Zn	25
V	5
Ag	2
Ba	15

- Non-detected impurities: Li, Zr, Ti, Be, Nb, Ga, Hf, Co, In, Bi, Ni, Pb, Cd, Te, P, Ge, W, Sb, Cr, Mo, Hg, As, Tl, Sn

1.5.1.2. Water temperature

- $(24.0 \pm 2.0)°C$

1.5.2. Inner baffle

1.5.2.1. Chemical composition: AISI 304 stainless steel

C	$(.059 \pm .020)$ w/o
Mn	$(1.651 \pm .053)$
P	$(.030 \pm .015)$
S	$(.013 \pm .013)$
Si	$(.285 \pm .129)$
Cr	$(16.370 \pm .327)$
Ni	$(8.720 \pm .185)$
Mo	$(.454 \pm .075)$
Co	$(.138 \pm .070)$
Fe	$(72.281 \pm .231)$

Check 100.001

Detected impurities: – < 10 ppm: Cd, Ta, Au, B
– < 100 ppm: Sm, Eu, Dy, Ir, Gd

Non-detected impurity: Cu

1.5.2.2. Specific weight

- (7.902 ± .002) g/cm^3

1.5.2.3. Bottom support

- Plexiglas (material not qualified)

1.5.3. 3/0 fuel pin (standard VENUS fuel pins)

1.5.3.1. Fuel composition

- UO_2

1.5.3.2. Fuel stoichiometry [O/U]

- 1.997 ± .005

1.5.3.3. Fuel isotopic composition of U

^{234}U (.029 ± .001) w/o
^{235}U (3.306 ± .010)
^{236}U (.016 ± .001)
^{238}U (96.649 ± .012)
Check 100.000

Total impurities: .8 ppm B equivalent in U

1.5.3.4. Fuel linear specific weight

- (5.40 ± .05) g/cm

1.5.3.5. Fuel diameter

- (.819 ± .002) cm

1.5.3.6. Fuel pellet length

- (.992 ± .040)

1.5.3.7. Fuel length

- (50.0 ± .1) cm

1.5.3.8. Cladding composition: Zircaloy 4

Sn (1.41 ± .06) w/o
Fe (.020 ± .01)
Cr (.10 ± .01)
O (.12 ± .01)
Zr (98.17 ± .06)
Check 100.00

Detected impurities: – < 1 ppm: B, Cd, U
– < 10 ppm: C1, Co, Cu, H, Mg, Mn, Ti, Zn
– < 50 ppm: Al, Hf, N, Nb, Ni, V, W, Au, Ir, Mo, Pb
– < 100 ppm: Ta, Si, Sm, Eu, Dy, Gd, Lu
– 146 ppm: C

1.5.3.9. Cladding linear specific weight

- (1.0627 ± .0004) g/cm

1.5.3.10. Cladding outer diameter

- (.950 ± .001) cm

1.5.3.11. Cladding inner diameter

- (.836 ± .001) cm

1.5.3.12. Cell pitch

- (1.260 ± .001) cm

1.5.3.13. Moderator

- Water, see Section 1.5.1

1.5.3.14. Bottom and top blanket composition: AISI 304 stainless steel

C .042 w/o
Mn 1.580
P .025
S .028
Si .460
Cr 18.200
Ni 8.600
Mo –

Co .120
Fe 70.945 (complement to 100)

Impurities: Not available

1.5.3.15. Bottom and top blanket linear specific weight

- 4.14 g/cm

1.5.3.16. Bottom and top blanket diameter

- (.820 ±.005) cm

1.5.3.17. Bottom and top blanket length

- (.50 ± .01) cm

1.5.3.18. Bottom reflector composition

- Plexiglas (not qualified)

1.5.3.19. Bottom reflector linear specific weight

- .627 g/cm

1.5.3.20. Bottom reflector diameter

- (.820 ± .005) cm

1.5.3.21. Bottom reflector length

- (8.0 ± .01) cm

1.5.3.22. Top reflector composition

- Plexiglas (not qualified)

1.5.3.23. Top reflector linear specific weight

- .587 g/cm

1.5.3.24. Top reflector diameter

- (.820 ± .005) cm

1.5.3.24. Top reflector length

- (7.57 ± .01) cm

Note: The top reflector is filling the intermediate reactor grid over 1.5 cm of its length.

1.5.3.25. Bottom stop composition, upper part Zircaloy 4, lower part AISI 304

Zircaloy 4 composition:	Sn (1.51 ± .03) w/o Fe (.22 ± .01) Cr (.12 ± .01) O (.13 ± .01) Zr 98.02 (complement to 100)
Detected impurities:	– < 1 ppm: B, Cd, Mg, U – < 10 ppm: C1, Co, Cu, H, Mn, Zn – < 50 ppm: Al, Mo, N, Nb, Ni, Pb, Si, Ti, V, W – < 100 ppm: Hf, Ta – 82 ppm: C
AISI 304 composition:	See Section 1.5.3.14

1.5.3.27. Bottom stop linear specific weight

- Upper part: 3.49 g/cm
- Lower part : 5.58 g/cm

1.5.3.28. Bottom stop diameter

- .950 cm

1.5.3.29. Bottom stop length

- Upper part: 1.25 cm
- Lower part: .90 cm

1.5.3.30. Top stop composition

- AISI 304 stainless steel (see Section 1.5.3.14)

1.5.3.31. Top stop linear specific weight

- 5.64 g/cm

1.5.3.32. Top stop diameter

- .950 cm

1.5.3.33. Top stop length

- 2.23 cm

Note: The top stop is assumed to end with the upper face of the upper reactor grid, the highest 1.45 cm of this stop is filling the hole of the upper reactor grid.

1.5.4. Pyrex pin

1.5.4.1. Pyrex composition: Corning glass code 7740

SiO_2	78.53 w/o
B_2O_3	(14.65 ± .15)
Al_2O_3	2.21
Fe_2O_3	.05
Na_2O	3.44
K_2O	1.13
Check	100.01

1.5.4.2. Isotopic composition of B

- ^{10}B: (19.775 ± .005) at %
- ^{11}B: (80.225 ± .005)

1.5.4.3. Pyrex outer diameter

- (.9048 ± .0043) cm

1.5.4.4. Pyrex inner diameter

- (.6058 ± .0031) cm

1.5.4.5. Pyrex linear specific weight

- (.7886 ± .0052) g/cm

1.5.4.6. Cladding composition: AISI 304 stainless steel

C (.03 ± .03) w/o
Mn (.87 ± .42)
Si (.29 ± .16)
Cr (18.40 ± .10)
Ni (9.50 ±- .50)
Mo (.07 ± .07)
Fe (70.84 ± 1.28)
Check 100.00

1.5.4.7. Cladding specific weight

- (7.9 ± .1) g/cm

1.5.4.8. Cladding outer diameter

- (.978 ± .005) cm

1.5.4.9. Cladding inner diameter

- (.940 ± .003) cm

1.5.4.10. Cell pitch

- (1.260 ± .001) cm

1.5.4.11. Moderator

- Water, see Section 1.5.1

1.5.4.12. Bottom and top blanket composition

- Aluminium (purity: 99.5% Al, not qualified)

1.5.4.13. Bottom and top blanket linear specific weight

- 1.83 g/cm

1.5.4.14. Bottom and top blanket diameter

- (.930 ± .005) cm

1.5.4.15. Bottom and top blanket length

- (.50 ± .01) cm

1.5.4.16. Bottom reflector composition

- Plexiglas (not qualified)

1.5.4.17. Bottom reflector linear specific weight

- .806 g/cm

1.5.4.18. Bottom reflector diameter

- (.930 ± .005) cm

1.5.4.19. Bottom reflector length

- (8.00 ± .01) cm

1.5.4.20. Top reflector composition

- Plexiglas (not qualified)

1.5.4.21. Top reflector linear specific weight

- .769 g/cm

1.5.4.22. Top reflector diameter

- (.930 ± .005) cm

1.5.4.23. Top reflector length

- (7.57 +- .01) cm

Note: The top reflector is filling the intermediate reactor grid over 1.5 cm of its length.

1.5.4.24. Bottom stop composition

- AISI 304 stainless steel

1.5.4.25. Bottom stop linear specific weight

- 5.03 g/cm (estimated)

1.5.4.26. Bottom stop diameter

- .978 cm

1.5.4.27. Bottom stop length

- 2.15 cm

1.5.4.28. Top stop composition

- AISI 304 stainless steel (not qualified)

1.5.4.29. Top stop linear specific weight

- 5.97 g/cm (estimated)

1.5.4.30. Top stop diameter

- .978 cm

1.5.4.31. Top stop length

- 2.23 cm

Note: The top stop is assumed to end with the upper face of the upper reactor grid. The highest 1.45 cm of this stop is filling the upper reactor grid.

1.5.5. 4/0 fuel pin (standard VENUS fuel pins, third delivery)

1.5.5.1. Fuel composition

- UO_2

1.5.5.2. Fuel stoichiometry [O/U]

- $2.00 \pm .01$

1.5.5.3. Isotopic composition of U

^{234}U (.031 ± .009) w/o
^{235}U (4.022 ± .008)
^{236}U (.023 ± .006)
^{238}U (95.924 ± .010)

Impurities: Not available

1.5.5.4. Fuel linear specific weight

- (6.39 ± .70) g/cm

1.5.5.5. Fuel diameter

- (.8926 ± .0005) cm

1.5.5.6. Fuel pellet length

- (1.114 ± .115) cm

1.5.5.7. Fuel length

- (50.0 ± .5) cm

1.5.5.8. Cladding composition: AISI 304 stainless steel

C (.040 ± .040) w/o
Mn (1.290 ± .030)
P (.020 ± .020)
S (.015 ± .015)
Si (.135 ± .003)
Cr (18.300 ± .400)
Ni (10.030 ± .200)
Mo (.132 ± .003)
Fe (70.038 ± .711)

Detected impurities: – < 10 ppm: Cd, Ta, Au, B, Co
– < 100 ppm: Sm, Eu, Dy, Ir, Gd

1.5.5.9. Cladding linear specific weight

- (.8855 ± .0007) g/cm

1.5.5.10. Cladding outer diameter

- (.978 ± .002) cm

1.5.5.11. Cladding inner diameter

- (.902 ± .004) cm

1.5.5.12. Cell pitch

- (1.260 ± .001) cm

1.5.5.13. Moderator

- Water, see Section 1.5.1

1.5.5.14. Bottom reflector composition

- Plexiglas (not qualified)

1.5.5.15. Bottom reflector linear specific weight

- .738 g/cm

1.5.5.16. Bottom reflector diameter

- (.89 ± .03) cm

1.5.5.17. Bottom reflector length

- (8.80 ± .02) cm

1.5.5.18. Top reflector composition

- Plexiglas (not qualified)

1.5.5.19. Top reflector linear specific weight

- .738 g/cm

1.5.5.20. Top reflector diameter

- (.89 ± .03) cm

1.5.5.21. Top reflector length

- (7.00 ± .02) cm

Note: The top reflector is filling the intermediate reactor grid over 1.5 cm of its length.

1.5.5.22. Bottom stop composition

- AISI 304 L stainless steel (not qualified)

1.5.5.23. Bottom stop linear specific weight

- 0.593 g/cm

1.5 5 24. Bottom stop diameter

- 0.978 cm

1.5.5.25. Bottom stop length

- 1.85 cm

1.5.5.26. Top stop composition

- AISI 304 L stainless steel (not qualified)

1.5.5.27. Top stop linear specific weight

- 0.636 g/cm

1.5.5.28. Top stop diameter

- .978 cm

1.5.5.29. Top stop length

- 3.3 cm

Note: The top stop is assumed to end with the upper face of the upper reactor grid, the highest 1.45 cm of this stops is filling the upper grid.

1.5.6. Outer baffle

- Stainless steel, see Section 1.5.2

1.5.7. Reflector

- Water, see Section 1.5.1

1.5.8. Barrel

1.5.8.1. Chemical composition: AISI 304 stainless steel

C .015 w/o
Mn (1.303 ± .430)
P .028
S .005
Si .513
Cr (18.464 ± .200)
Ni (10.199 ± .380)
Mo .474
Co .097
Fe (68.819 ± 1.010)
N .080
Check 99.997

Non-detected impurities: Cd, Sm, Eu, Dy, Ir, Gd, Ta, Cu, Au, B

1.5.8.2. Specific weight

- (7.9 ± .1) g/cm^3 (not qualified so far)

1.5.9. Water gap

- Water, see Section 1.5.1.

1.5.10. Neutron pad

1.5.10.1. Chemical composition: AISI 304 stainless steel

C .016 w/o
Mn (.830 ± .280)
P .026
S .004
Si .395
Cr (18.022 ± .030)
Ni (10.588 ± .360)
Mo .425
Co .196
Fe (69.498 ± .670)
Check 100.000

Non-detected impurities: Cd, Sm, Eu, Dy, Ir, Gd, Ta, Cu, Au, B

1.5.10.2. Specific weight

- $(7.9 \pm .1)$ g/cm^3 (not qualified so far)

1.5.11. Space between neutron pad and jacket

- Water, see Section 1.5.1

1.5.12. Jacket inner wall

1.5.12.1. Chemical composition: AISI 304 stainless steel (not qualified)

C $(.024 \pm 012)$
Mn $(1.168 \pm .270)$
P $(.025 \pm .003)$
S $(.008 \pm .005)$
Si $(.374 \pm .150)$
Ce (17.619 ± 1.047)
Ni $(9.836 \pm .934)$
Mo $(.452 \pm .024)$
Co $(.113 \pm .074)$
Fe (70.354 ± 1.963)
N $(.027 \pm .040)$
Check 100.000

1.5.12.2. Specific weight

- (7.9 ± 1) g/cm^3 (not qualified)

1.5.13. Jacket volume

- Air with 100% relative humidity

1.5.14. Jacket outer wall

- Stainless steel, see Section 1.5.12

1.5.15. Space between jacket and reactor vessel

- Water, see Section 1.5.1

1.5.16. Reactor vessel wall

- Stainless steel, see Section 1.5.12

1.5.17. Around the reactor vessel

- Dry air

1.5.18. Lower filling

- Water, see Section 1.5.1.2

1.5.19. Bottom support

1.5.19.1. Composition

- Water: 93.36 vol %
- Stainless steel: 6.64 vol %

1.5.19.2. Water composition

- See Section 1.5.1

1.5.19.3. SS composition

- AISI 304 not qualified, see Section 1.5.12.1

1.5.20. Bottom grid

1.5.20.1. Composition

- Water: 32.8 vol %
- Stainless steel: 67.2 vol %

Note: The bottom pin of the fuel pin is included in the bottom stop, which is assumed to be cylindrical and to be supported by the upper face of the bottom grid.

1.5.20.2. Water composition

- See Section 1.5.1

1.5.20.3. SS composition

- AISI 304 not qualified, see Section 1.5.12.1.

1.5.21. Lower reflector

The lower reflector is the region defined by the following borders:

a) The upper face of the bottom grid (for the inner part) and the upper face of the reactor support (for the outer part).

b) The fuel bottom and/or the stainless steel piece bottom.

c) The jacket inner wall.

Its composition varies according to the lateral region concerned (I to XI) as follows:

1.5.21.1. Below central hole (I)

- Water, see Section 1.5.1

1.5.21.2. Below inner baffle (II)

- Plexiglas (not qualified)

1.5.21.3. Below 4/0 fuel (III)

- See 4/0 fuel pin description, items 1.5.5.14-17 and 22-25
- Below Pyrex tube (III): see Pyrex pin description, items 1.5.4.12-19 and 24-27

1.5.21.4. Below 3/0 fuel (IV)

- See 3/0 fuel pin description, items 1.5.3.14-21 and 26-29

1.5.21.5. Below PLSA fuel (V)

- See SS-3/0 PLSA pin description, items 1.5.30.14-21 and 26-29 equivalent to 1.5.3.14-21 and 26-29

1.5.21.6. Below outer baffle (VI)

- Plexiglas (not qualified)

1.5.21.7. Below lateral reflector (VII)

- Water, see Section 1.5.1

1.5.21.8. Below barrel (VIII)

- Plexiglas (not qualified)

1.5.21.9. Below water gap (IX)

- Water, see Section 1.5.1

1.5.21.10. Below neutron pad (X)

- Water, see Section 1.5.1

1.5.21.11. Below space between pad and jacket (XI)

- Water, see Section 1.5.1

1.5.22 Intermediate grid

1.5.22.1. Composition

- Water: 63.4 vol %
- Plexiglas: 36.6 vol %

Note: The intermediate reactor grid is partially filled by the pins, such that water is partially replaced by Plexiglas and cladding tube.

1.5.22.2. Water composition

- See Section 1.5.1

1.5.22.3. Plexiglas composition

- Not qualified

1.5.23. Upper reflector

The upper reflector is the region defined by the following borders:

a) The fuel top and/or the stainless steel piece top.

b) The lower face of the upper grid.

c) The jacket inner wall. The reflector composition varies according to the lateral region concerned (I to XI) as follows:

1.5.23.1. Above central hole (I)

- Water, see Section 1.5.1*

1.5.23.2. Above inner baffle (II)

- Water, see Section 1.5.1*

1.5.23.3. Above 4/0 fuel (III)

- See 4/0 fuel pin description, items 1.5.5.18-21 and 26-29*
- Above a Pyrex tube (III): see Pyrex pin description, items 1.5.4.12-15, 20-23 and 28-31*

1.5.23.4. Above 3/0 fuel (IV)

- See 3/0 fuel pin description, items 1.5.3.14-17, 22-25 and 30-33*

1.5.23.5. Above PLSA fuel (V)

- See SS – 3/0 PLSA pin description, items 1.5.30.14-17, 22-25 and 30-33 equivalent to 1.5.3.14-17, 22-25 and 30-33*

1.5.23.6. Above outer baffle (VI)

- Water, see Section 1.5.1*

1.5.23.7. Above lateral reflector (VII)

- Water, see Section 1.5.1*

1.5.23.8. Above barrel (VIII)

- Water, see Section 1.5.1

1.5.23.9. Above water gap (IX)

- Water, see Section 1.5.1

---

* Takes into account the presence of Plexiglas in the water at the level of the intermediate reactor grid, as given in Section 1.5.22.

1.5.23.10. Above neutron pad (X)

- Water, see Section 1.5.1

1.5.23.11. Above space between pad and jacket (XI)

- Water, see Section 1.5.1

1.5.24. Upper grid

1.5.24.1. Composition

- Water: 63.4 vol %
- Stainless steel: 36.6 vol %

Note: This is the composition where no pin is loaded, in the loaded part the water is partially replaced by stainless steel due to the top stop of the pin (Regions III, IV and V).

1.5.24.2. Water composition

- See Section 1.5.1

1.5.24.3. SS composition

- AISI 304 not qualified, see item 1.5.12.1

1.5.25. Upper filling

- Water, see Section 1.5.1

1.5.30. SS-3/0 PLSA pin

1.5.30.1 to 13: Upper 3/0 fuel part

- Same data as Sections 1.5.3.1 to 13, except for Section 1.5.30.7 (fuel length)

1.5.30.7. Fuel length

- (25.00 ± .08) cm

1.5.30.14 to 33: Blankets, reflectors and stops

- Same data as Sections 1.5.3.14 to 33

Note: The following items are concerned with the lower SS-PLSA part

1.5.30.34. SS composition: AISI 304 stainless steel

C (.024 ± .012)
Mn (1.186 ± .160)
P (.025 ± .003)
S (.008 ± .005)
Si (.374 ± .150)
Cr (18.710 ± .120)
Ni (9.832 ± .370)
Mo (.183 ± .020)
Co (.105 ± .005)
Cd (.005 ± .005)
B (.005 ± .005)
Fe (69.538 ± 1.075)
Check 100.000

1.5.30.35. SS linear specific weight

- (4.138 ± .002) g/cm

1.5.30.36. SS diameter

- (.817 ± .002) cm

1.5.30.37. SS rod length

- (25.01 ± .02) cm

1.5.30.38 to 43

- Same data as Sections 1.5.3.8 to 13

1.6. Qualified data on the core geometry

The components of the mock-up were qualified in sizes during fabrication and before loading in the core, special attention was paid to the stainless steel thicknesses. Some data, particularly sensitive for the fast neutron depletion, were checked in the core as built: for instance, the minimum outer baffle-barrel distance, the water gap thickness and the azimuthal location of the neutron pad. All the recorded data were combined to describe the mock-up as given in Figures 1.5 and 1.6. Where no qualification was possible, the data were deduced from the fabrication specifications.

Notes: During the mounting, it was stated that the neutron pad did not take its designed azimuthal location, probably due to some machining mistake; it has been decided, on site, to adjust the V3 hole (foreseen at the highest azimuthal fast neutron flux and accommodated for spectrometry) at the angle 21.1°.

Up to the inner diameter of the neutron pad, all the components are concentric with respect to the core centre, they are defined by distances or radii d1 to d10, the VENUS internals (jacket and reactor vessel) are concentric with respect to a point located at X′ = -3.15 cm, Y′ = -3.15 cm in the core model, as a consequence their locations are no longer given by radii but by thicknesses t9 to t20 and the neutron pad has a variable thickness.

For the active height, the components are 50 cm high and the following data are given: LL = Lower Level, UL = Upper Level, h = height (see Figure 1.4); for other vertical regions, actually located from level 0 to 168 cm, the levels are given from bottom to top (see Figure 1.6).

The detailed qualification is given in work documents available at SCK·CEN, the data are as follows:

1.6.1. ***Central hole*** (I, Figures 1.5 and 1.6)

d1 = (3.442 ± .021) cm

1.6.2. ***Inner baffle*** (II, Figures 1.5 and 1.6)

d2 = (6.300 ± .013) cm
t1 = (2.858 ± .003) cm
LL II = (104.849 ± .032) cm*
UL II = (154.856 ± .036) cm*
h II = (50.006 ± .004) cm)*

1.6.3. ***4/0 Fuel region*** (III, Figures 1.5 and 1.6)

d3 = (18.900 ± .005) cm
t2 = (12.600 ± .005) cm
d4 = (26.460 ± .005) cm
t3 = (7.56 ± .005) cm
d11 = (18.900 ± .013) cm
LL III = (105.00 ± .05) cm*
UL III = (155.00 ± .55) cm*
h III = (50.0 ± .5) cm*

* Active height only!

1.6.4. 3/0 fuel region (IV, Figures 1.5 and 1.6)

d5 = (31.500 ± .005) cm
t4 = (5.040 ± .005) cm
d6 = (37.800 ± .013) cm
t5 = (11.34 ± .014) cm
d11 = (18.900 ± .013) cm
LL IV = (105.00 ± .05) cm*
UL IV = (155.00 ± .15) cm*
h IV = (50.0 ± .1) cm*

1.6.5. 3/0 – SS fuel region (V, Figures 1.5 and 1.6)

d6 = (37.800 ± .013) cm
t6 = (6.300 ± .014) cm
d11 = (18.900 ± .019) cm
LL V = (105.00 ± .05) cm (stainless steel bottom)*
ML V = (130.01 ± .07) cm (border SS-3/0 fuel)*
UL V = (155.01 ± .15) cm (3/0 fuel top)*
h SS-V = (25.01 ± .02) cm*
h 3/0-V = (25.00 ± .08) cm*

1.6.6. Outer baffle (VI, Figures 1.5 and 1.6)

d7 = (40.658 ± .021) cm
d12 = (21.758 ± .021) cm
t7 = (2.858 ± .003) cm
LL VI = (104.850 ± .033) cm*
UL VI = (154.850 ± .039) cm*
h VI = (50.000 ± .006) cm*

1.6.7. Reflector (VII, Figure 1.5, Section 1.6)

t15 (distance between baffle corner and barrel) = (2.169 ± .080) cm
t15 bis (idem, but taking account of broken corners = (2.251 ± .080) cm
d8 (barrel inner radius) = (48.283 ± 0.050) cm

1.6.8. Barrel (VIII, Figures 1.5 and 1.6)

d8 = (48.283 ± 0.050) cm
d9 = (53.273 ± .060) cm
t8 = (4.99 ± .01) cm

---

* Active height only!

LL VIII = (105.00 ± .06) cm*
UL VIII = (155.00 ± .16) cm*
h VIII = (50.0 ± .1) cm*

*1.6.9. **Water gap*** (IX, Figures 1.5 and 1.6)

t16 = (5.800 ± .060) cm

*1.6.10. **Neutron pad*** (X, Figures 1.5 and 1.6)

d10 = (59.073 ± .120) cm
t17 = (6.300 ± .030) cm
t18 = (6.690 ± .030) cm
t19 = (7.050 ± .030) cm
t20 = (6.900 ± .030) cm
a1 = (11.25 ± .25) cm
a2 = (21.10 ± .10) cm
a3 = 45º
a4 = (54.75 ± .25)º
LL X = (105.00 ± .26) cm*
UL X = (155.00 ± .16) cm*
h X = (50.0 ± .1) cm*

*1.6.11. **Space between neutron pad and jacket*** (XI, Figures 1.5 and 1.6)

e17 = (.3 ± .3) cm at 11.25º
e18 = (.3 ± .3) cm at 21.10º
e19 = (.332 ± .310) cm at 45º
e20 = (.3 ± .3) cm at 54.75º

*1.6.12. **Jacket inner wall*** (XII, Figures 1.5 and 1.6)

t9 = (11.80 ± .21) cm
t10 = .5 cm

Note: The inner radius of the jacket inner wall is (62.0 ± .15) cm with respect to a centre being at (X' = -3.15 cm, Y' = -3.15 cm) from the core centre, all the next internals are concentric with this jacket inner wall.

*1.6.13. **Jacket volume*** (XIII, Figures 1.5 and 1.6)

t11 = (15.0 ± .3) cm

---

* Active height only!

1.6.14. Jacket outer wall (XIV, Figures 1.5 and 1.6)

t12 = .5 cm

1.6.15. Space between jacket and reactor vessel (XIV, Figures 1.5 and 1.6)

t13 = (2.0 ± .3) cm

1.6.16. Reactor vessel wall (XVI, Figures 1.5 and 1.6)

t14 = 0.4 cm

1.6.17. Reactor room (XVII, Figures 1.5 and 1.6)

Infinite medium filled by air.

1.6.18. Lower filling (XVIII, Figure 1.6)

h0 = 0 cm
h1 = 83.45 cm
r18 = defined by jacket inner wall, see Section 1.16.12

1.6.19. Reactor support (XIX, Figure 1.6)

h2 = 92.85 cm
t19 = (9.40 ± .05) cm

1.6.20. Bottom grid (XX, Figure 1.6)

h3 = 94.35 cm
t20 = (1.50 ± .01) cm
r20 = (50.00 ± .01) cm

Note: The grid centre is at (X′ = -3.15 cm, Y′ = -3.15 cm) from the core centre.

1.6.21. Lower reflector (XXI, Figure 1.6)

h4 = 96.20 cm (upper end of bottom stop of 4/0 fuel pins)
h5 = 96.50 cm (upper end of bottom stop of other pins)
h6 = 104.50 cm (lower end of blanket for all the pins, except 4/0 fuel pins)
h7 = 105.0 cm (bottom active height)
r21 = defined by jacket inner wall, see Section 1.16.12

1.6.22. Intermediate grid (XXII, Figure 1.6)

k11 = 156.30 cm
h12 = 157.80 cm
t22 = 1.5 cm
r22 = (50.00 ± .01) cm

Note: The grid centre is at (X′ = -3.15 cm, Y′ = -3.15 cm) from the core centre.

1.6.23. Upper reflector (XXIII, Figure 1.6.)

h9 = 155.0 cm (top active height)
h10 = 155.5 cm (upper end of blanket for all the pins, except 4/0 fuel pins)
h13 = 162.0 cm (upper end of reflector in 4/0 fuel pins)
h14 = 163.07 cm (upper end of reflector in other pins)
r23 = defined by jacket inner wall, see item 1.16.12

1.6.24. Upper reactor grid (XXIV, Figure 1.6)

h15 = 163.85 cm
h16 = 165.30 cm
t = (1.45 ± .01) cm
r24 = (50.00 ± .01) cm

Note: The grid centre is at (X′ = -3.15 cm, Y′ = -3.15 cm) from the core centre.

1.6.25. Upper filling (XXV, Figure 1.6)

h17 = 168.0 cm (water level)

Note: h18 is the top of both the jacket and the reactor vessel, h18 = 170.8 cm.
h8 is the mid-plane of the reactor active height, h8 = 130.0 cm.

1.7. References

[1.1] LWR Pressure Vessel Surveillance Dosimetry Improvement Program Review Meeting, NBS, Maryland, 26-30 October 1981: Exploratory calculations carried out at Westinghouse, S. Anderson in co-operation with G. Guthrie (HEDL).

[1.2] VENUS-3 PLSA Conceptual Design Considerations SCK·CEN Note AF/sa 380/87-02, 2 February 1987, A. Fabry.

[1.3] Design Studies of VENUS-3, a Benchmark Experiment of PLSA Calculational Procedures to be Performed in the VENUS Critical Facility at Mol.

[1.4] LWR Pressure Vessel Surveillance Dosimetry Program, “Activities, Status and Scheduling”, 29 March-2 April 1982.

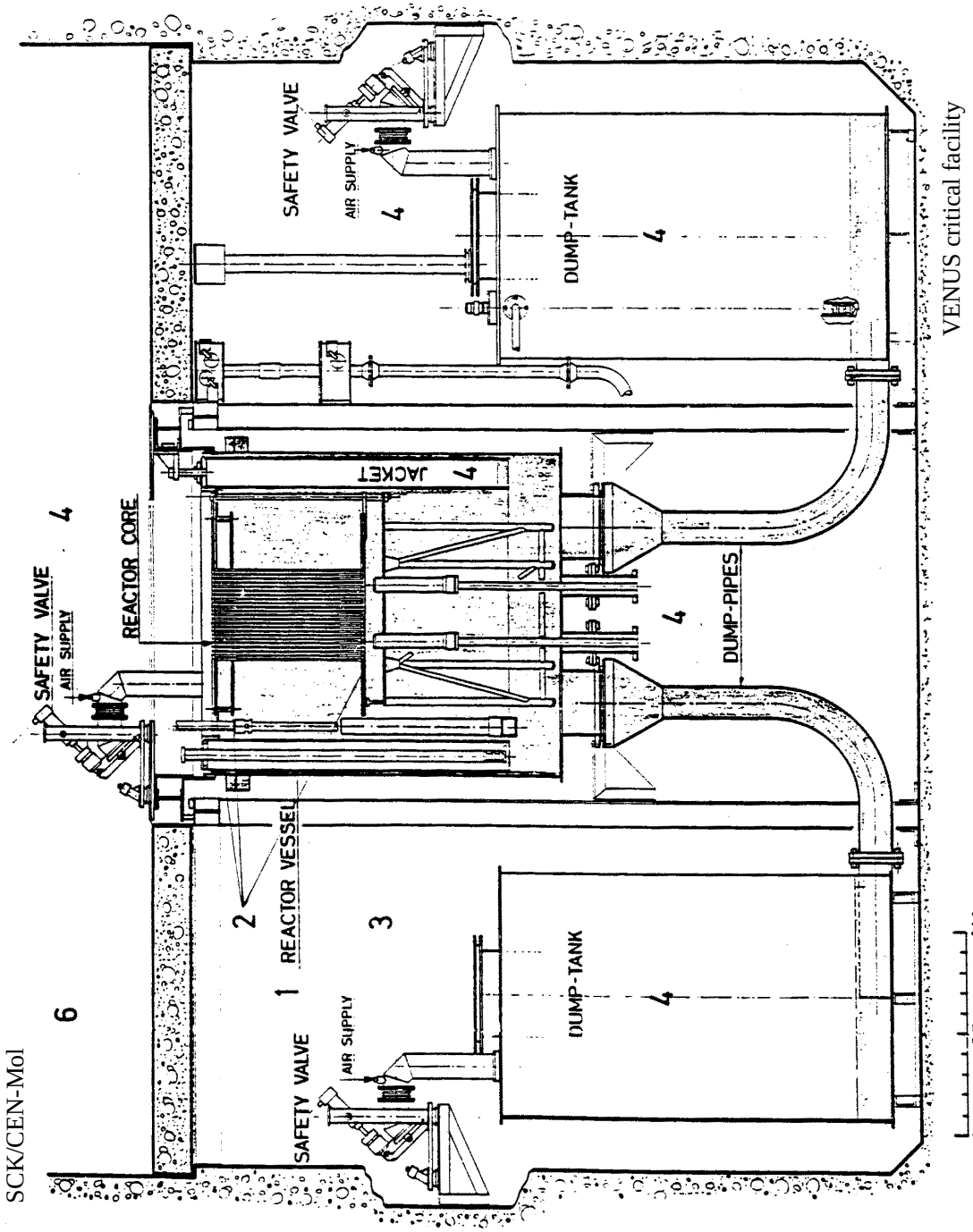

Figure 1.1. Vertical cross-section of the facility

Figure 1.2. Core description (horizontal cross-section)

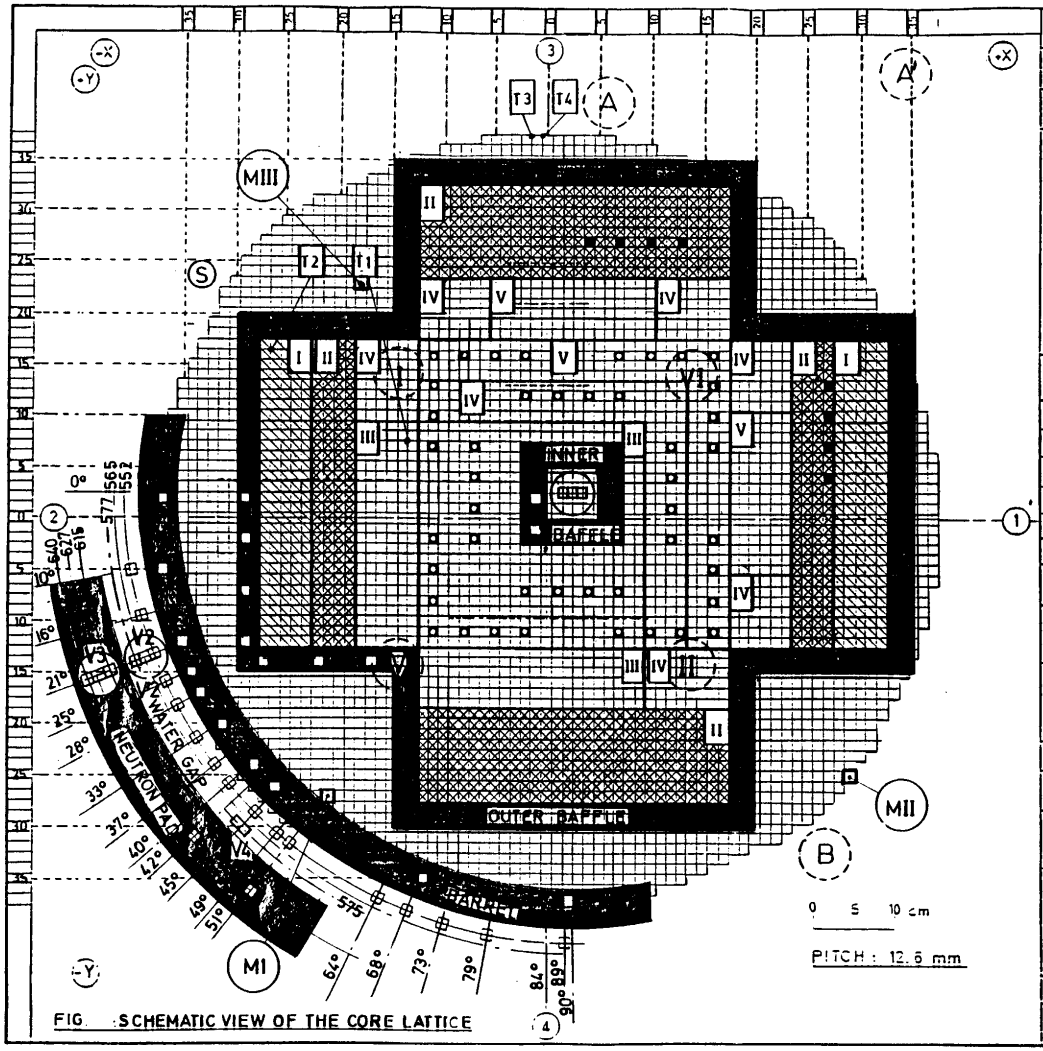

C.E.N - S.C.K | VENUS CRITICAL FACILITY

EXPERIMENT : VENUS-3 : LWR - PVS - BENCHMARK (PLSA)

DATE : from 28 03 88 to

CONFIGURATION N° 31 / 08

DENSITY RODS : NONE

BORON CONCENTRATION (p.p.m.) : NONE

START-UP SOURCE (S) YES

NEUTRON GENERATOR (N) NONE

ABSORBING ROD ■ 8R Level ≈ 3/4 fuel height

PYREX ROD □ 44

FUEL REGIONS TOTAL : (2600 - 52) PINS

DESIGNAT.	%US/%Pu	COLOUR OR SYMBOL	NUMBER OF FUEL PINS	EQ. RADIUS OR X . Y	INVESTIGATED CELL
I	SS-3/0		300		
II	3/0		780-8		
III	4/0 (3)		648-17		
IV	4/0 (2)		456-12		
V	4/0 (1)		416-15		

MONITORING DETECTORS

DESIGNAT.	DIAMET.	SYMBOL	N° CABLE	LOCATION x/y	LEVEL	CHANNEL
PROPORTIONAL BF_3 COUNTER						
FISSION CHAMBER	1/8" ^{5}U	MI	-	-21 / -27	Bottom	C
	1/4" ^{5}U	MII	-	+29 / -25	Bottom	E
	1mm ^{5}U	MIII	-	-18 / +23	Mid. pl.	Nim-rack

CONTROL DETECTORS

DESIGNAT.	DIAMET.	SYMBOL	N°	LOCATION	LEVEL	CHANNEL
PROPORTIONAL COUNTER	1"	(A)		wall	-	A
	1"	(B)		6	Bottom	B
ION CHAMBER (NON-COMPENSATED)		(I)		-	under reactor	log I
		(II)		-		log II
		(V)		-		lin V
		(VI)		-		lin VI

REMARK : k_{eff} = 1 for water at 1680 mm & R_2 ≈ 1400 mm

VERIFIED BY. APPROVED BY:

REMARKS : (1) First delivery (2) Second delivery (3) Third delivery

Issued : 28.03.88

88 / B3235 / 65503

Figure 1.3. Top view of the VENUS core with the LWR-PVS benchmark experiment

SCK/CEN-Mol
VENUS critical facility

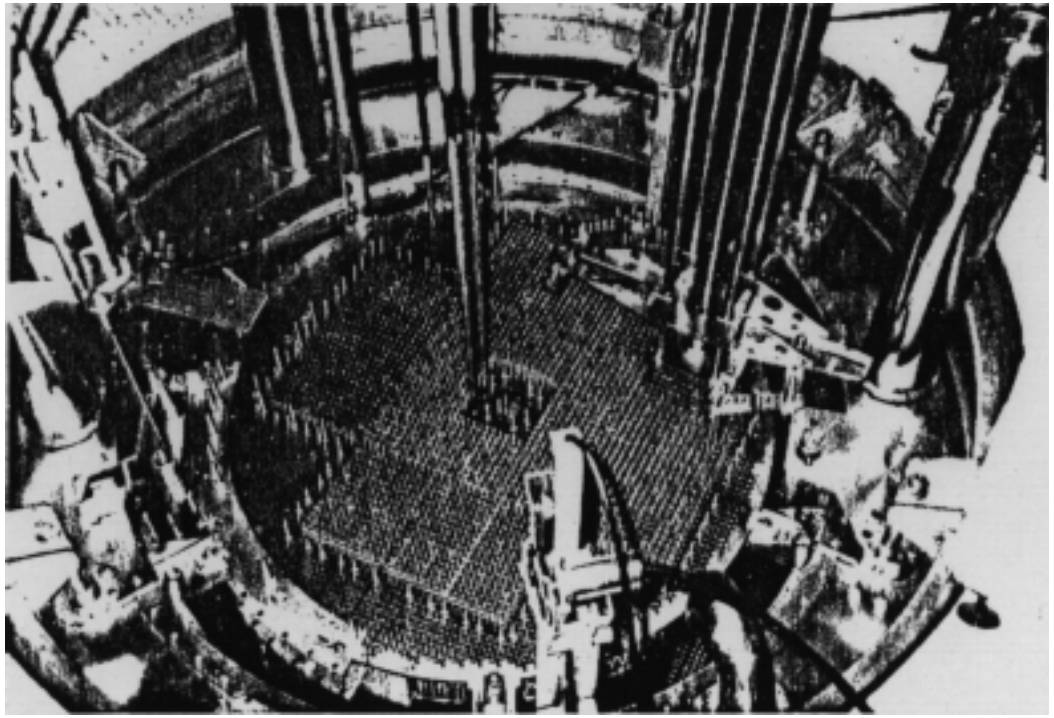

Figure 1.4. Core description (vertical cross-section)

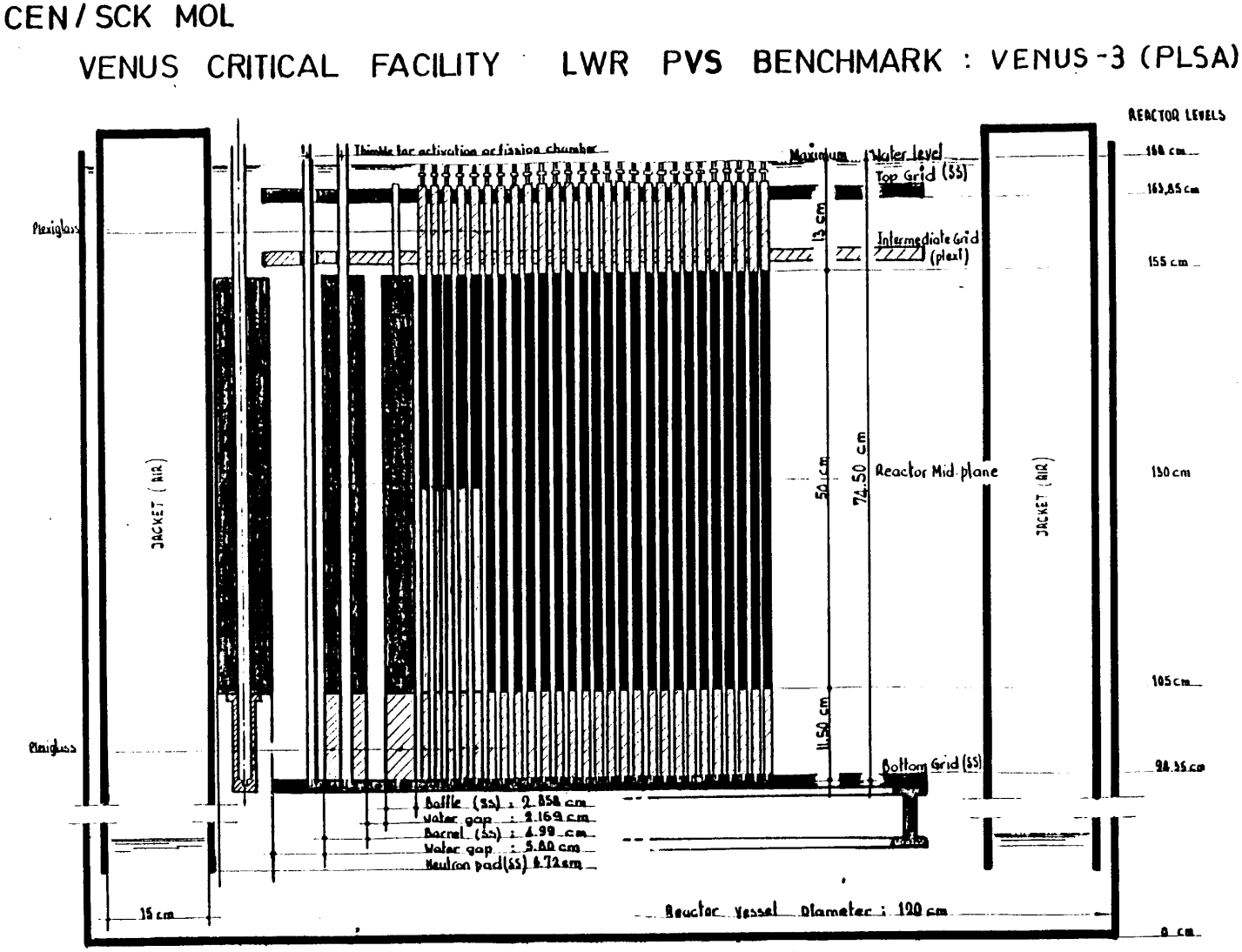

Figure 1.5. Core model (horizontal cross-section)

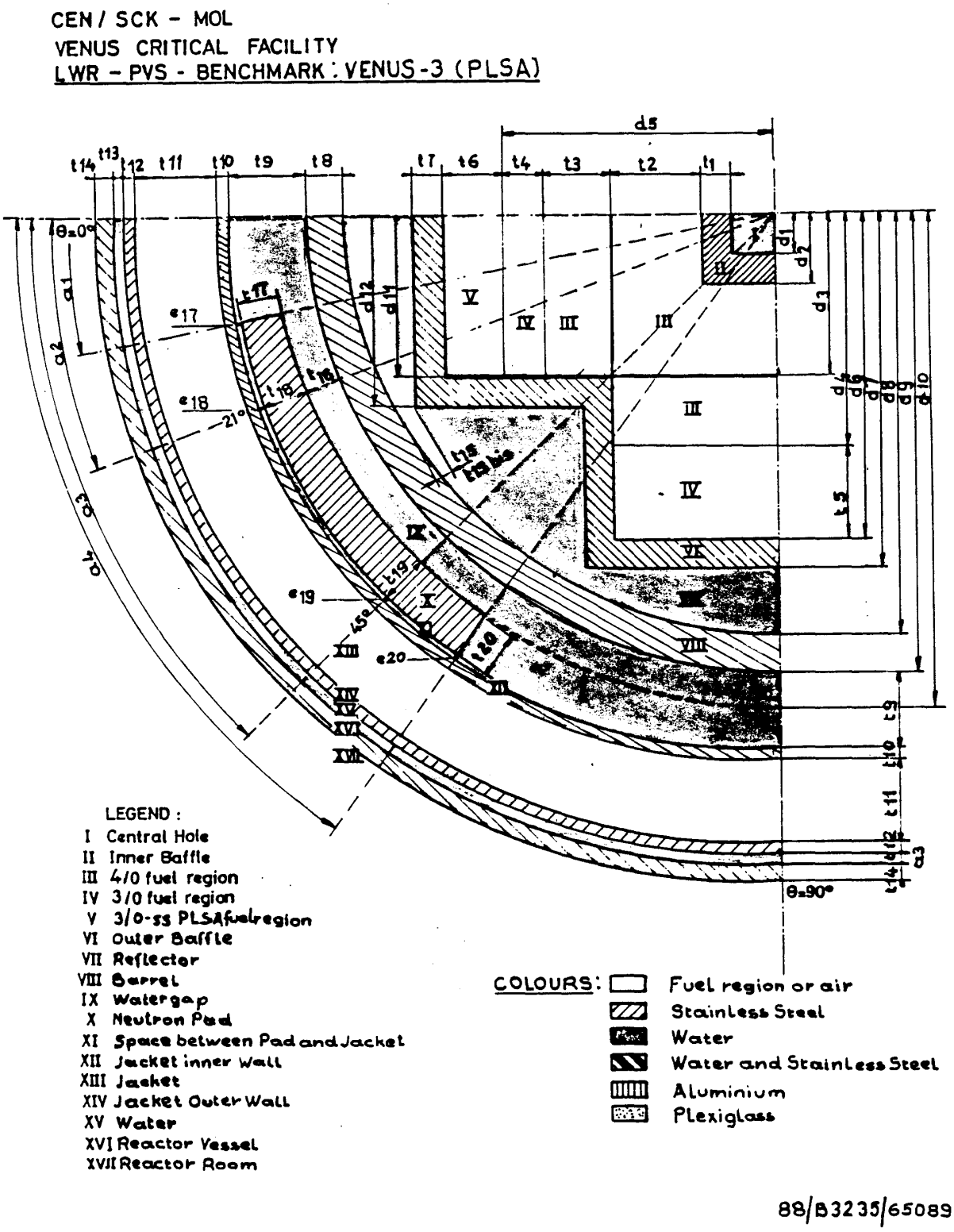

Figure 1.6. Core model (vertical cross-section)

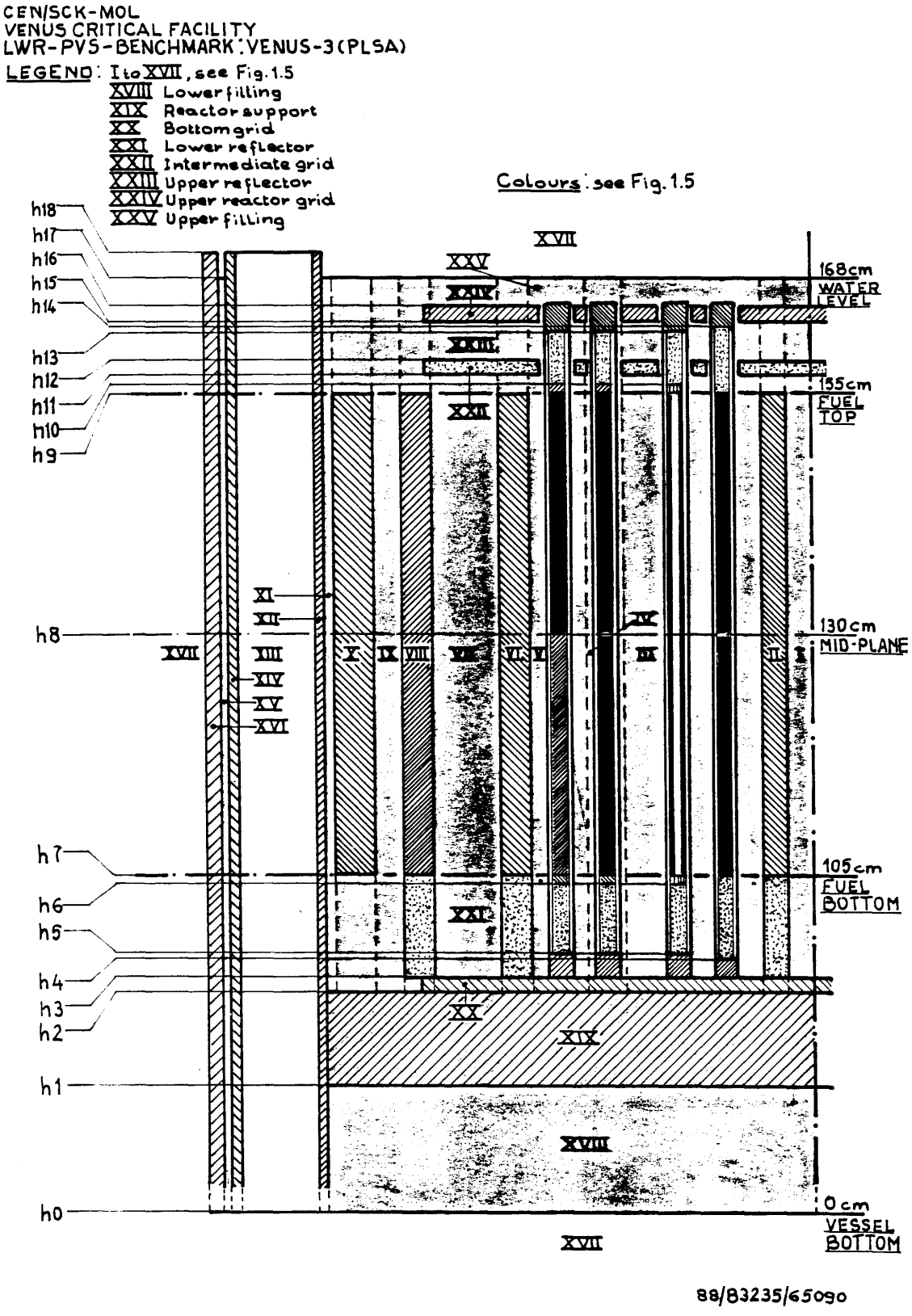

APPENDIX B

Calculation details supplied by participants

B.1. VENUS-1

1.0 Author: J. Koban

Organisation: SIEMENS AG Power Generation Group (KWU)
Postfach 3220
D-91050 Erlangen, Germany

1.1 Transport method and modelling assumptions

S_N method using DOT 4.2, (r,θ) geometry, S_8 quadrature set, 1/8 core model, 165 radial and 98 azimuthal meshes.

1.2 Transport cross-sections

For DOT 4.2 calculations a 100 neutron energy group library was used. This library was obtained by collapsing the 175 group EURLIB-VI/N175 (based on the ENDF/B-VI Rev.2 library).

The EURLIB-VI/N175 was generated using the NJOY-91 code system. The energy group boundaries are identical to that of the VITAMIN-J group structure. The generation of the group data was based on the usual energy weighting: above 2.12 MeV fission spectrum weighting was used, between 2.12 MeV and 0.414 eV 1/E weighting was used, and below 0.414 eV maxwellian weighting was used. The final 100 energy group library used in DOT 4.2 calculations has an energy group structure identical to that of EURLIB 4 library.

1.3 Neutron source

For the spectral shape of the neutron source for the whole core the ^{235}U fission spectrum based on ENDF/B-VI was adopted.

1.4 Axial leakage treatment

The vertical buckling for the DOT input was evaluated for each zone from the data given in the NEA benchmark specifications. All diffusion coefficients D were assumed to be 1 cm. For thermal neutrons DB^2 = 2.400E-3 1/cm was used in all zones. For neutrons at energies above thermal the following data were used:

All zones up to the outer baffle:	DB^2 *= 2.40E-3 1/cm*
Reflector, barrel, and 2nd water gap:	DB^2 *= 2.30E-3 1/cm*
Neutron pad, 3rd water gap, and jacket inner wall:	DB^2 *= 2.21E-3 1/cm*
Jacket volume (air) up to reactor vessel wall:	DB^2 *= 2.12E-3 1/cm*

** Corrected on 11/01/99*

1.5 Response functions and fission averaged data

Equivalent fission fluxes are defined as ratios of calculated reaction rates and the ^{235}U fission spectrum averaged dosimeter cross-section. The basic data for dosimeter cross-sections were 620 group data given in IRDF-90 Version 2 data file. These data were collapsed to 100 energy group structure

(the same as in DOT calculations and using weighting techniques described above). The ^{235}U fission spectrum averaged dosimeter cross-sections were calculated using the ENDF-B/VI ^{235}U fission spectrum and the 100 group dosimeter cross-sections. The calculated average dosimeter cross-sections are given below:

Reaction ^{235}U fission spectrum averaged dosimeter cross-section

Reaction	Cross-sections (mbarn)
$^{58}Ni(n,p)^{58}Co$	105
$^{115}In(n,n')^{115m}In$	185.2
$Rh(n,n')^{115m}Rh$	702.7
$^{238}U(n,f)$	304.3
$^{237}Np(n,f)$	1 349

1.6 Comments/special references

Flux-DPA conversion factors were taken from DPA-ASTM (Kocherov, McLaughlin, The International Reactor Dosimetry File (IRDF 90), IAEA-NDS-141 Rev.2, October 1993).

2.0 Author: H. Aït Abderrahim

Organisation: SCK•CEN
Fuel Research Unit
200 Boeretang
B-2400 Mol, Belgium

2.1 Transport method and modelling assumptions

The LEPRICON code system was used to calculate the ex-core neutron flux distribution. This code system is based on the 2-D DORT 4.3 code and the 1-D ANISN. The DOTSYN module is used to synthesise a 3-D flux map ϕ (R,θ,Z) starting from two 2-D DORT flux maps (R,θ) and (R,Z) and one 1-D ANISN map ϕ (R).

The VENUS-1 simulation did not make use of the DOTSYN module, as the incorrect locations were at the core mid-plane. A DORT (R,θ) calculation with a very fine meshing 165 R × 66 θ for a 45° sector was performed. The S_8 full symmetric quadrature and a P_3 approximation were adopted.

2.2 Transport cross-sections

The 56 group ELXSIR Library based on ENDF/B-V Rev. Mod. 3 was used to generate by means of the GIP module the macroscopic cross-section set used for this calculation. The new evaluation of Y. Fu for the Fe inelastic cross-section, included in this library, was used.

2.3 Neutron source

The experimental (x-y) source distribution was used as input in the DOTSOR module to generate the S(R,θ) source distribution corresponding to the meshing of the DORT (R,θ) run. The ENDF/B-V ^{235}U fission spectrum was adopted as energy distribution of the source.

2.4 Axial leakage treatment

The axial leakage was taken into account by a DB^2 correction where the zone wise B^2 were used and the D values were derived for each material and each energy group using the $\Sigma_{transport}$ ($D = 1/3\ \Sigma_{transport}$).

2.5 Response functions and fission averaged data

The ENDF/B-V dosimetry file included in the ELXSIR library was used to derive the reaction rate and were divided by the fission averaged cross-sections given in the following table to derive equivalent fission fluxes:

Average dosimeter cross-section for reaction (barn)

^{58}Ni(n,p)	0.1053
^{115}In(n,n′)	0.1795
^{103}Rh(n,n′)	–
^{238}U(n,f)	0.3048
^{237}Np(n,f)	1.3479

2.6 Comments/special references

3.0 Author: F. Wasastjerna

Organisation: Tech. Res. Centre of Finland
VTT/ENE
PL 1604
FIN-02044 VTT Tekniikantie 4C, Finland

3.1 Transport method and modelling assumptions

DORT (r,θ). Quadrature either S_8 or S_{16}. 41 or 91 radial, 28 or 60 azimuthal mesh intervals. A series of calculations using different approximations was performed.

Case	Groups	Library	P_kS_n	Mesh	Source
0 (routine)	17	BUGLE-80	P_3S_8	coarse	5*5 assemblies
1	47	BUGLE-80	P_3S_8	coarse	5*5 assemblies
2	47	BUGLE-93	P_3S_8	coarse	5*5 assemblies
3	47	BUGLE-93	P_7S_{16}	coarse	5*5 assemblies
4	47	BUGLE-93	P_7S_{16}	semi-fine	5*5 assemblies
5	47	BUGLE-93	P_7S_{16}	semi-fine	pinwise
6 (high precision)	47	BUGLE-96T	P_7S_{16}	semi-fine	pinwise

DORT version 2.8.14, in all calculations the (r,θ) option was used with azimuthal mesh set to 28×1.607 deg (coarse mesh) and 60×0.75 deg (semi-fine mesh).Radial mesh: the interior baffle was cylindricised conserving the volume of steel and water. The interface between the two core zones of different enrichment was also cylindricised conserving the volume of the inner (3/0) fuel region.

From the barrel outward, the material zones fit naturally into the (r,θ) geometry, so no geometrical approximations were made there. At the Pyrex rod cell locations, the fuel pin cell fraction was frequently about 0.5, and in no mesh interval did it drop below 0.25. Consequently, all intervals with a fuel pin-cell fraction between 0.25 and 0.75 were filled with a mixture of 50% Pyrex rod cell and 50% fuel pin-cell. Those fuel cells with a fuel pin-cell fraction above 0.75 were considered to contain unperturbed fuel pin-cells.

At the outer surface of the core, all mesh intervals with a fuel pin-cell fraction above 0.5 were considered to contain fuel, and the remainder were filled with baffle steel. The outer surface of the exterior baffle was determined by looking at the interval thickness of the baffle in each azimuthal interval. The number of mesh intervals containing steel was then chosen to reproduce this radial thickness as close as possible. For the coarse mesh this was done for each azimuthal interval. For the semi-fine mesh, azimuthal intervals in which the inner surface of the baffle (the outer surface of the core) were located at the same radial mesh boundary were grouped together and the location of the baffle outer surface was also the same for the whole group.

3.2 Transport cross-sections

BUGLE-80, BUGLE-93 or BUGLE96T, P_3 or P_7. Either condensed to 17 groups or left at 47 groups.

3.3 Neutron source

"Harwell 1975" spectrum (a Watt spectrum), with or without a spatial approximation involving lumping the pins together into 5×5 "bundles" with the source specified at the centre and corners of each bundle.

3.4 Axial leakage treatment

DB^2 correction in DORT, using D values calculated for each group and material by the cross-section manipulation program TOPICS. D values of steel used in air gap.

3.5 Response functions and fission averaged data

IRDF-90 Version 2 and ENDF/B-VI dosimetry cross-sections, collapsed to 47 groups or one group (fission spectrum weighted in the latter case) by INTERSIG.

DPA cross-sections

Three different DPA cross-sections were initially included in the cross-section file: an old set and more recent sets based on ASTM and EURATOM data, both completed with NUREG/CR-5530 data at low energies. The EURATOM data were used in calculations.

3.6 Comments/special references

4.0 Authors: G. Hehn, A. Sohn, M. Mattes and G. Pfister

Organisation: IKE University of Stuttgart
Postfach 801140
D-70550 Stuttgart, Germany

4.1 Transport method and modelling assumptions

We applied the S_N method with the two-dimensional transport code DORT 3.1 in $S_{12}P_5$ approximation. Since for power reactors cylindrical geometry is the first choice, we also used cylindrical co-ordinates in the benchmark calculation with 93 r-meshes and 53 theta meshes within a core quadrant (denoted as Case 6). Special care was taken to model the outer fuel pins, the control rods and the outer rectangular baffle. For checking, a second calculation (denoted as Case 7) was performed with Cartesian co-ordinates (62 x-meshes and 62 y-meshes), too. Since we intended to analyse the benchmark results in great detail with the help of colour graphics, we could not use variable space meshing to reduce the mesh number. For the flux extrapolation model the theta-weighted approximation was selected. The pointwise flux convergence was everywhere better than 1.0E-4.

4.2 Transport cross-sections

Since two-dimensional transport calculations are performed easily for the configuration of VENUS-1, a multi-group library VIT-J had been used with a 175 neutron energy group comprising 105 groups above 0.1 MeV. For comparison the routinely applied few group library BUGLE-96 has 47 neutron groups with 26 groups above 0.1 MeV. Likewise the angular moments have been increased from the usually applied P_3-approximation to P_5-approximation. The multi-group library VIT-J of IKE/Stuttgart has a group structure identical to VITAMIN-J and is based on the point data of ENDF/B-VI for all isotopic components of stainless steel and on JEF-2.2 data for the other elements.

4.3 Neutron source

For the standard fluence calculation in cylindrical geometry we had to transfer the relative pin power distribution, specified in Cartesian co-ordinates, into the cylindrical mesh system with strict conservation of the source strength. The number of neutrons per fission and the fission spectrum were taken for the dominating thermal fission of ^{235}U. For both two-dimensional calculations in cylindrical and Cartesian co-ordinates the neutron source rate had been normalised to 3.264E+11 n/cm s in the total core quadrant.

4.4 Axial leakage treatment

The axial neutron leakage is described by the term DB^2 in diffusion theory, which is a good approximation for the core region. But the diffusion term overestimates the lateral leakage outside the core, where diffusion theory is no longer applicable. We applied several variations of the leakage term in DORT3.1. With group and zone dependent DB^2 we got the predicted underestimation of the measured reaction rates, which becomes worse with growing distance to the core. Without any axial leakage B = 0 we achieved overestimation everywhere and with D = 1 arbitrarily and zone dependent B2 the results were in between. This shows the inherent uncertainty of two-dimensional neutron fluence calculations in reactor technology and for two-dimensional specification and calculation of benchmarks as well.

4.5 Response functions and fission averaged data

The activation cross-sections were taken from IRDF-90 Version 2. There are large differences between the inelastic scattering cross-section of the reaction $^{103}Rh(n,n')^{103m}Rh$ given in IRDF-90 Version 2 and in the response function of BUGLE-96. Likewise the DPA cross-section of iron has changed up to +20% from the old iron data in ASTM-82 contained in IRDF-90 Version 2 to the updated iron data of ENDF/B-VI. For determining the equivalent fission flux the following fission spectrum averaged reaction cross-sections (in barn) were used in both libraries IRDF-90 Version 2 and BUGLE-96:

	VIT-J	**BUGLE-96**
^{58}Ni	0.1053	0.1070
^{115}In	0.1853	0.1802
^{27}Al	0.7279E-03	0.7821E-03
^{103}Rh	0.7031	0.1194
^{238}U	0.3046	0.3073
^{237}Np	1.3498	1.3305

4.6 Comments/special references

The benchmark calculations for the two-dimensional VENUS-1 experiment performed in cylindrical and Cartesian geometries represent "high precision" calculations concerning $S_{12}P_5$ approximation with energy resolution of the 175 multi-group library VIT-J. The spatial meshes were taken form the VENUS-3 modelling with the consequence that the mesh centres and the detector positions do not coincide everywhere, requiring two-dimensional interpolation (linear) of the reaction rates calculated. It has been shown that "routine" calculations can be restricted to S_8P_3 approximation with changes in the results of ±1%. But the inherent deficiency of two-dimensional neutron fluence calculations remains unresolved concerning proper treatment of axial leakage in ex-core layers up to the pressure vessel and also concerning proper integration of axial power variation in the fuel rods for detector positions with growing distances to the core. More details are summarised in the IKE report:

- G. Hehn, A. Sohn, M. Mattes, G. Pfister, "IKE Calculations of the OECD/NEA Benchmarks VENUS-1 and VENUS-3 for Computing Radiation Dose to Reactor Pressure Vessel and Internals", IKE, Stuttgart, IKE 6 NEA 2,133 p., Dec. 1997.

5.0 Authors: M. Pescarini, M.G. Borgia and R. Orsi

Organisation: ENEA – Centro Ricerche "E. Clementel"
Via Martiri di Montesole, 4
I-40129 Bologna, Italy

5.1 Transport method and modelling assumptions

A simulation of the VENUS-1 benchmark experiment was performed at ENEA Bologna using the two-dimensional discrete ordinates transport code DORT-3.1 included in the DOORS-3.1 modular system of ORNL deterministic codes.

Three S_8-P_3 DORT-3.1 fixed source calculations have been performed in plane and polar geometry:

- Plane geometry calculation (113 x-meshes × 113 y-meshes) for 1/4 of the VENUS-1 reactor configuration.

  The DORT-3.1 code was used in the (X,Y) plane geometry option with 113 mesh intervals in both the X and Y directions. In particular, a 66.0 cm × 66.0 cm square region was described in the geometrical model, taking into account the quarter of the VENUS-1 reactor configuration containing the barrel, the neutron pad and the jacket inner wall. The jacket outer wall and the external regions beyond the jacket outer wall were not included in the geometrical model since it was considered that they can only slightly affect the calculated results in the 34 measurement positions. A standard fixed source calculation with one outer iteration was performed in the S_8-P_3 approximation using a fully symmetrical quadrature set and bypassing the fission calculation. For the pointwise flux convergence criterion the value 1.0E-4 was assumed while for the flux extrapolation model the theta-weighted approximation was selected. The BUGLE-96 library permits, if necessary, to take into account the thermal upscattering reactions: in the present case no upscattering was considered. The plane geometry was preferred in this fixed source calculation for two reasons. The first is that an accurate description of the core and of the baffle was considered more important than an accurate description of the barrel and of the neutron pad. The second is that the use of the original neutron distributed source in (x,y) Cartesian co-ordinates avoids manipulations to transform the original neutron source in (r,θ) co-ordinates, possibly compromising the accuracy of the original data.

- Plane geometry calculation (162 x-meshes × 163 y-meshes) for 1/4 of the VENUS-1 reactor configuration.

- Polar geometry calculation (172 r-meshes × 143 theta-meshes) for 1/4 of the VENUS-1 reactor configuration.

- Each detector position is placed in the centre of the corresponding plane or polar spatial mesh and no interpolation technique is used to obtain the results in all the calculations.

- Fully symmetrical directional quadrature sets are used.

- The theta-weighted approximation for the flux extrapolation model is introduced.

- The fission calculation is bypassed.
- The same neutron vertical leakage treatment is introduced in all the calculations.
- The same pointwise flux convergence criterion is assumed (1.0E-4) in all the calculations.
- The two plane geometry calculations differ exclusively for the total number of spatial meshes.
- The same cross-section working library obtained from the ENDF/B-VI based DLC-185/ BUGLE-96 (47 n + 20 gamma energy groups) shielding library is used in all the calculations.
- The upscattering cross-sections are not used in the thermal neutron energy region.
- Two different dosimetry data files are utilised in each calculation to obtain the dosimetric results: ENDF/B-VI BUGLE-96 and IRDF-90 Version 2.
- Two different flux weightings of the dosimeter cross-sections, from both the dosimetry data files, are used to obtain the results in the steel zones: the flat weighting and the 1/4 T pressure vessel weighting. The flat flux weighting is used for the results in the water zones.

5.2 Transport cross-sections

The cross-sections used in the transport calculations, the detector response functions and the ^{235}U fission spectrum were obtained from the DLC-185/BUGLE-96 (47 neutron + 20 gamma-ray energy groups) shielding library based on the ENDF/B-VI Release 3 data file. No cross-section collapsing was performed.

5.3 Neutron source

In the geometrical model adopted, 1/4 of the total number (2 552) of the fuel cells of the VENUS-1 core configuration is considered. The value of the normalisation factor is 3.2584E+11 and corresponds to the VENUS-1 reactor at the full power. It is obtained as follows:

$$\text{Normalisation Factor} = 3.2584E{+}11 = 2.10E{+}8 \times 2.432 \times 638$$

where 2.10E+8 is the number of fissions per second and per centimetre length of the average fuel rod; 2.432 is the ENDF/B-VI proposed value for ν (^{235}U), the average number of neutrons emitted per ^{235}U fission; 638 is the number of fuel cells corresponding to 1/4 of the total number of fuel cells in the VENUS-1 core configuration.

5.4 Axial leakage treatment

The DORT-3.1 code permits to insert a DB^2 correction by energy group and by spatial region to take into account the vertical leakage of neutrons. On the basis of the experimental vertical buckling values obtained for the VENUS-1 experiment, the following strategy was decided. Since it was reported that the thermal buckling has approximately the same value in both the in-core (including external baffle) and the ex-core regions, the reported value B^2 = 2.401E-3 cm^2 was assumed in both regions together with the water thermal diffusion coefficient value D_{th} = 0.159 cm to obtain the DB^2

correction. For the in-core fast buckling the same previous B^2 = 2.401E-3 cm^2 value was assumed together with the water fast diffusion coefficient value D_f = 1.13 cm. For the ex-core region, the DB^2 correction was obtained using a single B^2 = 2.278E-3 cm^2 value for the fast buckling together with the previously reported value D_f = 1.13 cm of the water fast diffusion coefficient. The previous fast buckling B^2 value for the ex-core region was obtained performing an arithmetic average on the ex-core experimental buckling values reported specifically for only four ex-core zones: the so-called water reflector, barrel, water gap and neutron pad zones. This strategy was decided since these four values are only slightly different from one another. The neutrons of energy above 0.414 eV, belonging to the groups 1-45 in the BUGLE-96 group structure, were considered "fast". Below this energy threshold (groups 46-47), neutrons were considered "thermal". This threshold was selected on the basis of the information on the thermal buckling measurements coming from ^{235}U fission chambers, having the upper limit of the response energy range at 0.22 eV. The nearest increasing energy limit in the BUGLE-96 group structure is 0.414 eV and for this reason this energy limit was selected as the upper thermal energy threshold.

5.5 Response functions and fission averaged data

The response functions used for the $^{58}Ni(n,p)$, $^{115}In(n,n')$, $^{103}Rh(n,n')$, $^{238}U(n,f)$ and $^{237}Np(n,f)$ detectors are available in the BUGLE-96 ENDF/B-VI and IRDF-90 Version 2 dosimetry files with two different weightings: a standard flat weighting and a 1/4T pressure vessel (PV) weighting for the steel regions. It was decided to use the response functions of the first type for the detectors in the water measurement positions while the response functions of the second type were used for the detectors in the steel measurement positions. In fact the neutron spectrum in the 1/4T PV position (few centimetres of neutron penetration depth in the PV steel) is believed to be very similar in shape to those obtained in the measurement positions located in the steel regions of the VENUS-1 experiment, where the neutrons have to cross a similar steel thickness. In addition, the standard flat weighting was used, as a term of comparison, also in the steel measurement positions. In the BUGLE-96 library report it is not indicated from which dosimetric file the response functions are obtained but it is reported that they come from the updated ENDF/B-VI data files.

The "equivalent fission fluxes" corresponding to the five detector results were obtained dividing the calculated reaction rates ("activities") by the corresponding following values of the ^{235}U fission spectrum averaged dosimeter cross-sections. These average cross-sections were calculated using the specific values of the detector cross-sections and of the ^{235}U fission spectrum contained in the BUGLE-96 library:

Detector	Averaged cross-sections (barns)			
	BUGLE-96 ENDF/B-VI		IRDF-90 V.2	
	Flat weighting	1/4T PV weighting	Flat weighting	1/4T PV weighting
$^{58}Ni(n,p)$	0.1070	0.1062	***0.1072***	0.1065
$^{115}In(n,n')$	0.1802	0.1797	***0.1865***	0.1856
$^{103}Rh(n,n')$	0.1195	0.1196	***0.7068***	0.7055
$^{238}U(n,f)$	0.3073	0.3055	***0.3074***	0.3064
$^{237}Np(n,f)$	1.3305	1.3275	***1.3555***	1.3546

DPA calculation

Neutron damage-energy cross-sections (barns × eV) for the ENDF/B-VI Fe-56 data file were produced in the 47 neutron group structure of the BUGLE-96 library, using the HEATR module of the NJOY-94.66 data processing system. The groupwise damage-energy cross-sections were processed using the GROUPR module of NJOY at the temperature of 300 K with total self-shielding (background cross-section = 1.0E-6 barns). The weighting function inserted in GROUPR was derived from the 1/4T PV weighting spectrum used to process the cross-sections of the steel nuclides for the BUGLE-96 library. The conversion to the DPA cross-sections (barns) was obtained multiplying the damage-energy cross-sections by the factor 0.8/2Ed, where Ed, the energy required to displace an iron atom from its lattice position, was assumed equal to 40.0 eV. The total displacement rates per atom (DPA × s^{-1}) at the various measurement positions were obtained summing up the group displacement rates per atom of all the 47 groups.

5.6 Comments/special references

The equivalent fission flux results are practically equivalent with both the dosimetry data files except for the ^{103}Rh(n,n′)^{103m}Rh dosimeter: the ENDF/B-VI BUGLE-96 ^{103}Rh(n,n′) data produce unacceptable results.

Negligible differences in the equivalent fission flux results are obtained in the steel zones using the two different dosimeter cross-section weightings from both the dosimetry data files ENDF/B-VI BUGLE-96 and IRDF-90 Version 2.

The iron displacement rates are calculated with ENDF/B-VI ^{56}Fe DPA cross-sections and the total displacement rates are obtained summing up the contributions from all the 47 neutron groups (thermal neutron groups included) of the BUGLE-96 library.

The calculated results for the ^{237}Np(n,f) and the ^{238}U(n,f) dosimeters do not contain the contributions of the thermal neutron groups below 0.41 eV, since cadmium filters have been used during the measurements.

The accuracy of the equivalent fission flux results, obtained with the IRDF-90 Version 2 standard reference dosimetry file, for the two fine spatial mesh plane and polar calculations No. 2 and No. 3 are reported.

Plane geometry calculation (162 x-meshes × 163 y-meshes): equivalent fission flux results

- ^{58}Ni(n,p) accuracy within 10%
- ^{115}In(n,n′) accuracy within 20%
- ^{103}Rh(n,n′) accuracy within 15%
- ^{238}U(n,f) accuracy within 10%
- ^{237}Np(n,f) accuracy within 15%

Polar geometry calculation (172 r-meshes × 143 theta-meshes): equivalent fission flux results

- ^{58}Ni(n,p) accuracy within 10%
- ^{115}In(n,n′) accuracy within 15%
- ^{103}Rh(n,n′) accuracy within 15%
- ^{238}U(n,f) accuracy within 5%
- ^{237}Np(n,f) accuracy within 10%

The accuracy required (within 20%) is reached for all the detectors in each measurement position with both the fine mesh calculations. The most accurate global results (within 15%) are obtained with the polar geometry calculation No. 3.

6.0 Author: Rob van der Stad

Organisation: NRG
Nuclear Analysis Group
B.U. Nuclear Energy
Postbus 1
NL-1755 ZG Petten, The Netherlands

6.1 Transport method and modelling assumptions

The calculations are performed with MCNP4A using the EJ2-MCNP library based on JEF2.2. The calculations are performed in a 1/4 core with a fuel height of 50 cm plus a water reflector at the top of 13 cm and at the bottom of 11.5 cm.

6.2 Transport cross-sections

6.3 Neutron source

6.4 Axial leakage treatment

MCNP can only perform calculations in a finite geometry.

6.5 Response functions and fission averaged data

The average dosimeter cross-sections (calculated using the IRDF-90 Version 2 data) are given in the table below:

Average dosimeter cross-section for reaction (barn)

^{58}Ni(n,p)	0.1069
^{115}In(n,n′)	0.1855
^{103}Rh(n,n′)	0.7035
^{238}U(n,f)	0.3039
^{237}Np(n,f)	1.3411

6.6 Comments/special references

7.0 Author: J.M. Paratte

Organisation: Paul Scherrer Institute
CH-5232 Villigen, Switzerland

7.1 Transport method and modelling assumptions

Transport calculations performed using the code BOXER. Same method as described in the following report (p.49ff):

Computing Radiation Dose to Reactor Pressure Vessel and Internals, NEA/NSC/DOC(96)5.

Geometry

The reactor and its internals were subdivided in 60×60 rectangular meshes. Dimension of the meshes: ~ 1 cell pitch, with some reduction to modelise the baffles (inner and outer). At the interfaces between different cylindrical zones, the materials were mixed according to their respective volume within a mesh (10 different mixtures are used for the barrel and also 10 for the neutron pad). The dimensions of the neutron pad were extended to fill the outer space.

Energy range

- Upper limit at 15 MeV.
- 36 groups above 1 MeV.
- 44 groups above 0.1 MeV.

Only one quarter of the core was calculated, with reflective boundary conditions on two sides.

7.2 Transport cross-sections

7.3 Neutron source

Normalisation of the fluxes:

The fluxes were calculated using as source directly the numbers given as “numbers of fission per cell”. This method introduces three errors:

1) The number of fissions has to be multiplied by nu (the number of neutrons per fission) to get the neutron source.

2) The number of fissions is given per cell. What is needed is the number per cm^3, the fluxes are then too high by a factor of pitch**2.

3) The total number of fissions in the core is: ft = 2.1E+8/(cm $\times$ sec) (as given).

The fluxes from BOXER were then multiplied with the following factor:

$$fac = xnu \times ft/(cp^2)$$

- xnu: number of neutrons per fission = 2.4609 (only one value was used because the difference between the two different cells of the core is very small: outer cells: xnu = 2.4622, inner cells: xnu = 2.4582)
- ft = 2.1E+8 fissions/(cm×sec)
- nbc: number of cells in the core = 2552
- cp: cell pitch = 1.26 cm
- fac becomes then: fac = 3.2552E+8 neutrons/(cm^3×sec)

The mesh fluxes were interpolated to obtain the flux at given point P.

$$\text{Interpolation function: } f(x,y) = c0 + c1 \cdot x + c2 \cdot y + c3 \cdot x \cdot y$$

The interpolation parameters c0, c1, c2 and c3 were obtained through a least square fit on the nine meshes next to the point P.

The "equivalent fission fluxes" (EFF) were calculated according to the formula:

$$EFF = \text{sum}(g = 1,G)(\text{sigma}(g) \times \text{phi}(g)) / \text{sum}(g = 1,G)(\text{sigma}(g) \times \text{chi}(g))$$

- sigma(g): microscopic cross-section of the nuclide considered [barn]
- phi(g): normalised flux
- chi(g): fission spectrum of ^{235}U

7.4 Axial leakage treatment

A buckling of 2.4E-3 cm^2 was taken into account.

7.5 Response functions and fission averaged data

7.6 Comments/special references

8.0 Authors: Bok Ja Moon and Hae Ryong Hwang

Organisation: Korea Power Engineering Co.(KOPEC)
Yusong, Taejon, Korea

8.1 Transport method and modelling assumptions

S_N method using DORT (Version 2.8.14) was used. The reactor was assumed to have quadrant symmetry and the quadrant reactor was modelled using XY and RΘ co-ordinates. The central water hole, inner and outer baffle, core, barrel and neutron pad were modelled and the structures beyond the neutron pad were excluded in the modelling. The 104×93 meshes were used for DORT XY model and the 92×122 meshes were used for DORT RΘ model. Finer meshes were given to the regions containing dosimeters. All dosimeters were assumed to be point detectors without surrounding structures and the reaction rates were calculated using the fluxes at the corresponding detector position. S_8 quadrature set was used with Legendre polynomial P_5 for cross-section expansion.

8.2 Transport cross-sections

The macroscopic cross-sections for the DORT calculation were calculated using BUGLE-96 library and GIP code.

8.3 Neutron source

The measured pin power distribution was used as the source term. The pin power distribution was given as the values normalised to the core average value of 1 fission/sec/pin. The reference core average fission rate was given as 2.10×10^8 [fissions/cm/sec/pin] at the mid-plane level. The neutron spectrum was obtained from ^{235}U fission spectrum in BUGLE-96 library and 2.432 neutrons released per fission event was adopted.

8.4 Axial leakage treatment

Since all the neutron responses were measured at the mid-plane, the fluxes calculated using XY and RΘ co-ordinates were corrected to reflect the axial flux distribution. The buckling approximation and synthesis method were used for this calculation.

Buckling approximation

In buckling approximation, the mid-plane flux is calculated using DB^2 coefficients. The diffusion coefficients D, in DB^2, were calculated from the expression:

$$D_{z,g} = \frac{1}{3\sum_{tr}^{z,g}}$$

where: $D_{z,g} \equiv$ diffusion coefficient for group g in zone z

$\sum_{tr}^{z,g} \equiv$ macroscopic transport cross-section for group g in zone z

But:

$$\sum_{tr}^{z,g} = \sum_{T}^{z,g}(P_0) - \frac{1}{3}\sum_{g'}\sum_{g\to g'}^{z,g}(P_1)$$

where: $\sum_{T}^{z,g}(P_0) \equiv$ total macroscopic cross-section associated with the P_0 component

$\sum_{g'}\sum_{g\to g'}^{z,g}(P_1) \equiv$ macroscopic scattering cross-section associated with the P_1 component

The DB^2 coefficients were calculated using the measured vertical buckling factors in each region and diffusion coefficients calculated above. The DB^2 coefficients were entered in the DORT XY calculation by zone and group and the normalisation factor based on the mid-plane power level was calculated as:

$$\begin{aligned} XNF_{XY} &= 2.10 \times 10^8 \times 2.432 \times 2\,552/4 \\ &= 3.258 \times 10^{11} \text{ neutrons/cm/quarter core} \end{aligned}$$

where: measured fission density = 2.10×10^8 [fissions/cm/sec/pin]
number of neutrons per fission = 2.432 neutrons
number of fuel rods in the quadrant core = 2 552/4 pins

The fluxes at each dosimeter were calculated as the interpolated ones from the fluxes of neighbouring meshes.

Calculation using synthesis method

In the synthesis method, a three-dimensional flux representation is constructed by synthesising calculations of lower dimensions. For the calculation of mid-plane fluxes, the two-dimensional XY or RΘ calculation with core average power is performed and then axial factor at the mid-plane is multiplied using the expression:

$$\Phi_g^{mid}(x,y) = \Phi_g(x,y,z=130 \text{ cm}) = \Phi_g(x,y) \times \frac{\Phi_g(r,z=130 \text{ cm})}{\Phi_g(r)}$$

or:

$$\Phi_g^{mid}(r,\theta) = \Phi_g(r,\theta,z=130 \text{ cm}) = \Phi_g(r,\theta) \times \frac{\Phi_g(r,z=130 \text{ cm})}{\Phi_g(r)}$$

where z = 130 cm is the height of the mid-plane. The normalisation factor for DORT XY or RΘ calculation was calculated based on the core average power as follows:

$$XNF_{XY,R\Theta} = 2.1 \times 10^{8} \times 2.432 \times 2\,552/4 \times 0.768$$
$$= 2.502 \times 10^{11} \text{ neutrons/cm/quarter core}$$

where 0.768 is mean to peak axial power.

The axial flux distribution was calculated using two-dimensional RZ flux normalised to one-dimensional radial flux. The 92 × 28 meshes were applied to the two-dimensional RZ mode. The axial flux distribution was calculated. The same material zone numbers with those of first azimuthal mesh in RΘ calculation were assigned. The radial sources were calculated as azimuthally integrated values from RΘ source distribution and the axial source distribution was assigned as cosB(z-130), where B is measured vertical buckling in the core and 130 cm is the height of the mid-plane. The normalisation factor was calculated as follows:

$$XNF_{RZ} = 2.10 \times 10^{8} \times 2.432 \times 2\,552 \times 0.768 \times 50$$
$$= 5.005 \times 10^{13} \text{ neutrons/core}$$

where 50 is the active core height.

The one-dimensional radial flux was calculated using DORT RZ calculation with unit axial height. The radial mesh intervals and source were the same with those of RZ calculation and the normalisation factor was calculated as follows:

$$XNF_{R} = 2.10 \times 10^{8} \times 2.432 \times 2\,552 \times 0.768$$
$$= 1.001 \times 10^{12} \text{ neutrons/cm/core}$$

The calculated axial factors for each structure were applied to the fluxes obtained from DORT XY and RΘ calculations.

8.5 Response functions and fission averaged data

The necessary dosimetry cross-sections were taken from response functions in BUGLE-96 library. But for Rh-detector, the dosimetry cross-sections were taken from IRDF-90 Version 2 and generated using NJOY-97 code system. The equivalent fission flux for dosimeter d is defined as a ratio of calculated reaction rate and the average dosimeter cross-section. Thus, it can be calculated as follows:

$$\Phi_{eq}^{d} = \sum_{g} \sigma_{r}^{d}(E_g)\phi(E_g) \Big/ \sum_{g} \sigma_{r}^{d}(E_g)\chi(E_g)$$

where: $\sigma_{r}^{d}(E_g) \equiv$ reaction cross-section of g^{th} energy group for dosimeter d

$\phi \equiv$ neutron flux from DORT output

$\chi \equiv {}^{235}U$ fission spectrum

The average dosimeter cross-sections were calculated using reaction cross-section and ^{235}U fission spectrum in BUGLE-96 library. The calculated average dosimeter cross-sections are as follows in the table below:

Average dosimeter cross-section

Reactions	Average dosimeter cross-section(barn)
^{58}Ni(n,p)^{58}Co	0.1070 (BUGLE-96)
^{115}In(n,n′)	0.1802 (BUGLE-96)
^{238}U(n,f)	0.3070 (BUGLE-96)
^{237}Np(n,f)	1.3300 (BUGLE-96)
^{103}Rh(n,n′)	0.7057 (IRDF-90 v2 using NJOY97)

The DPA values were calculated as follows:

$$dpa/\text{sec} = \sum_g \sigma_d\left(E_g\right)\phi\left(E_g\right)$$

where: $\sigma_d\left(E_g\right) \equiv$ displacement cross-section

$\phi \equiv$ neutron flux from DORT output

The displacement cross-section is the group collapsed data from the data in ASTM E693-94.

8.6 Comments/special references

The results at the following tables were obtained based on the detector positions given in the fifth column((x,y) in (cm,cm)) at Table 1 in the VENUS-1 benchmark specification (refer to "NEA/NSC/DOC(96)25"). Because we found some mismatches between the fourth and fifth columns, we had to select only one column. We found a minor mistake at the first detector position on the exterior baffle. We think the correct position is (-39.69,-0.63) not (-39.69,-0.69).

The Rh(n,n′) reaction consists of two paths, one of which has an intermediate isomeric state of ^{104}Rh and the other reaction path goes directly to ^{104}Rh. The Rh response function in the BUGLE-96 library seems to have a problem. Therefore, the Rh response function in IRDF-90 v.2 was used.

The photo-fission effect was not corrected for ^{238}U and ^{237}Np dosimeters.

For the ^{237}Np detectors, the reaction rate was integrated from 1 to 45 groups in BUGLE-96 library because of Cd cut-off energy.

We performed the gamma heating analysis also and want to discuss the gamma heating analysis besides neutron flux.

9.0 Authors: Masahide Suzuki[1], Kazuaki Kosako[2] and Yukio Sakamoto[1]

Organisation: JAERI[1], Sumitomo Atomic Energy Industries[2]
Japan

9.1 Transport method and modelling assumptions

S_N method using DORT code, (r,θ) geometry, S_{16} quadrature set and P_5 Legendre order, 1/4 core model, 109 radial and 90 azimuthal meshes.

9.2 Transport cross-sections

For DORT calculations an 86 neutron energy group library was used. This library was generated using the nuclear data processing system NJOY94 from JENDL-3.2, with energy weighting (fission spectrum + 1/E + Maxwellian). The macroscopic cross-sections were produced by TRANSX-2 code to consider the self-shielding correction.

9.3 Neutron source

The ^{235}U fission spectrum was obtained from the Watt formula for the spectral shape of the neutron source:

$$N(E) = 0.453*\exp(-E/0.965)*\sinh(\sqrt{2.29*E})$$

Pin power distribution in the r-theta model was determined the source strength from area of pin cells in the r-theta mesh. The source neutron emission rate was normalised to 3.255E+11 in 1/4 core and full power.

9.4 Axial leakage treatment

DORT calculation was used the DB^2 correction values by energy group and by spatial region to take into account the vertical leakage of neutron. The zone buckling values were obtained from the VENUS-1 experiment report. The diffusion coefficient values were calculated by groups and regions from cross-section data.

9.5 Response functions and fission averaged data

The activation cross-sections were generated by NJOY94 based on IRDF-90 Version 2. The fission spectrum averaged dosimetry cross-sections were calculated from the 86 group activation cross-section and ^{235}U fission spectrum.

Reaction	$^{58}Ni(n,p)$	$^{115}In(n,n')$	$^{103}Rh(n,n')$	$^{238}U(n,f)$	$^{237}Np(n,f)$
Cross-section (barn)	0.1027	0.1823	0.6951	0.2985	1.3372

9.6 Comments/special references

DPA cross-sections were generated by NJOY94 and KERMAP code based on JENDL-3.2.

10.0 Authors: A.F. Albornoz and E.M. Lopasso

Organisation: Centro Atómico Bariloche (CAB)
(8400) San Carlos de Bariloche, Río Negro
Argentina

10.1 Transport method and modelling assumptions

The VENUS-1 experiment was modelled in r-θ geometry and calculated with the DORT transport code. S_8-P_3 transport calculations were based on nuclear data taken from the BUGLE-96 library. Equivalent fission flux at the measured positions were obtained combining the calculated spectra with detector cross-sections taken from the IRDF-90 Version 2 library.

The neutron flux distribution in the VENUS-1 system was calculated in R-θ geometry with the DORT transport code. Even though the core geometry and the provided neutron source suggest a X-Y modelling for the system, a R-θ model was choose in order to test the same calculation chain we apply to our power plants. An S_8 symmetrical quadrature was used, together with a P_3 Legendre expansion for cross-sections. The system was modelled as a 45° angular sector with reflective boundary conditions both at 0° and 45°. A vacuum boundary condition was set at the external radial boundary, at R = 84.82 cm and at R = 53.27 cm. A point flux convergence criteria for all energy groups equal to 10^{-3} was requested in the calculations but, due to the outer iterations needed to converge the thermal fluxes, fluxes of energy greater than 0.1 MeV were effectively calculated with a convergence criteria equal to 10^{-4}.

Two different DORT inputs were prepared. The first one was intended to calculate the neutron flux at all positions outside the core, including the outer baffle positions. In this model ("outer model"), no special care was taken to represent the central hole, the Pyrex pins and the fuel 3/0 region. The second one ("inner model") was specially prepared to calculate the neutron flux at the measurement positions located at the central hole and at the inner baffle. This model was extended just to the barrel region, where a void boundary condition was set up.

Final mesh structures consisted of the same 63 azimuthal intervals in the two models, together with 220|235 radial intervals (variable radial meshing) for the outer model, and 253 radial intervals (fixed radial meshing) for the inner one. Then, resulting mesh size from the central hole up to the neutron pad region was between 0.16 cm and 0.36 cm, depending on the material zone traversed. Special care was taken to model the outer baffle border in both models. Once the azimuthal discretisation was fixed, radial intervals were chosen so that the outer baffle border was represented as accurately as possible.

10.2 Transport cross-sections

Nuclear data were taken from the 47 neutron group BUGLE-96 library. The energy spectrum of neutrons born in the core was assumed to be that of pure ^{235}U. This spectrum was taken from the BUGLE-96 library. Cross-section sets with and without upscattering were used in calculations, but no significant difference was found in the requested activities when comparing results from both sets. Final results were calculated by using the infinitely diluted cross-section set in BUGLE-96, with the upscattering data retained in thermal groups.

Some comparisons between results from this calculation and others that used the different self-shielded sets in BUGLE-96, show differences within 1% in almost all points, reaching a maximum of 3% in the calculated ^{237}Np activity at the measure positions in the water gap II zone.

10.3 Neutron source

The fixed source distribution in the adopted R-θ geometry was calculated from the provided relative power distribution, by means of an auxiliary code. For each R-θ mesh, this code determines its source density by calculating areas with the help of the Monte Carlo method. The grids (the X-Y grid that defines the fuel zone and the R-θ grid adopted for DORT calculations) were superposed, and the contribution from X-Y pins to R-θ meshes was determined.

For each DORT mesh the code randomly "throws" inside a pre-defined amount of sampling points, uniformly distributed, and determines how many points lie inside each pin of the fuel grid (see Figure 1 below). If N_T is the total amount of points, N_i are the points that lie inside pin i, and S_i is the source density for that pin, the source density for the DORT mesh is calculated as:

$$S_{M_j} = \frac{1}{N_T} \sum_i N_i \cdot S_i$$

For the DORT mesh M_1, the sum involves pins P_1, P_2, P_3, and P_4.

Figure 1. Scheme showing how a R-θ grid is superposed to the X-Y grid

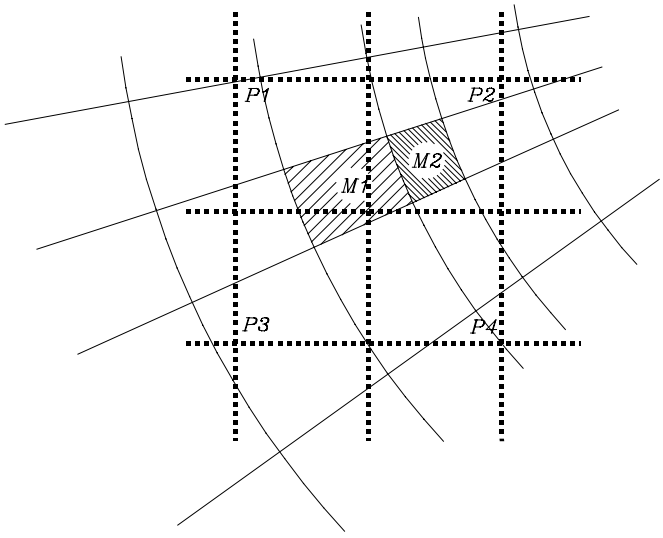

The program detects the situation for DORT mesh M_2, for which only one pin contributes (pin P_2 in the example), and does not perform the Monte Carlo calculation. This is because the source density of the DORT mesh is, exactly, the source density of the pin. If a DORT mesh has no intersections in the fuel region, a null source density is assigned.

Because the calculation is made by sampling, it is necessary to perform several independent runs to improve the determination. The source density for each DORT mesh is calculated from the mean value of several independent calculations using the above equation, and the involved error is reported.

The desired accuracy is defined by the user. The minimum and the maximum amount of independent runs are also specified. In our case, an error lower than 1% in the total source was achieved.

When a DORT mesh has a small coincidence with a pin, the source error from that pin could be important, as it is the situation in pin P_4 and mesh M_1 in the example. However, if other pins are present in a large proportion (as are pins P_1, P_2 and P_3 in the example), the total error in the source will not be significant. If the source in pins P_1, P_2 and P_3 in the example were zero, then the error would be large due to the single contribution of pin P_4. In this situation the program detects the problem and automatically increases the number of sampling points in the DORT mesh. Nevertheless, the contribution of this mesh to the total source will be small, and so will the error in total source.

Concerning the source normalisation, a reference core average fission rate at 100% power equal to 2.1×10^8 fiss/cm/pin/s was used. A value of $\bar{\nu} = 2.43$ neutrons per fission was used. So, the total source density in the fuel region was equal to 3.21×10^8 n/cm^3/s^1.

10.4 Axial leakage treatment

Buckling correction was made by using the DB^2 input option available in DORT. Buckling data for each material zone were taken from the provided documentation. Values of the diffusion coefficient for each material zone and for each energy group were calculated from data in BUGLE-96 library as $D_g = 1/3\Sigma_{tr,g}$. The transport cross-section ($\Sigma_{tr,g}$) was, in turn, calculated as: $\Sigma_{tr,g} = \Sigma_{t,g} - \Sigma_{s1,g}/3$.

Factor 3 in the denominator of the above equation corresponds to the fact that all terms in the Legendre expansion of BUGLE-96 cross-sections include the 2l+1 factor. So, $\Sigma_{s1,g}$ in the equation is the sum over all energy groups of the $\Sigma_{s1,g\rightarrow g'}$ matrix in BUGLE-96. For all the zones behind the neutron pad (jacket walls, jacket volume, reactor vessel and water gaps), the buckling correction was not done.

10.5 Response functions and fission averaged data

Response cross-sections were taken from the IRDF-90 Version 2 library. For the displacement per atom (dpa) cross-section, the set corresponding to iron in steel, ASTM standard, was taken. Cross-sections at the 47 group energy structure were obtained by expanding the calculated spectrum to the 640 groups of the IRDF-90 structure with the BLOWUPJR code. This 640 group spectrum was then used to collapse the detector cross-sections taken from IRDF-90 with the X333 code. Both spectrum expansion and cross-section collapsing were performed at seven different measurement positions: central hole (measurement position #1); inner baffle (#2); outer baffle (#8); barrel (#15); water gap II (#23); neutron pad (#29); and water gap I (#32). When these different 47 group cross-section sets were used to calculate reaction rates, no significant differences were found in the results. Nevertheless, these seven cross-section sets were used to calculate the corresponding activities at all measurement points. At each measurement zone, the same set for all points in that zone was used.

Equivalent fission flux is defined as the ratio of the calculated reaction rates and the average detector cross-section. Equivalent fission fluxes are used for comparison instead of reaction rates because their use removes some of the dependence of the calculated reaction rates on the dosimeter cross-sections, and the resulting comparisons tend to become better measures of the accuracy of the transport calculations themselves.

The average cross-sections were calculated by weighting the detector cross-section with the ^{235}U fission spectrum (ENDFB-V evaluation), also present in the IRDF-90 package. When the BUGLE-96 ^{235}U fission spectrum was used to perform this same average cross-section calculation, the calculated values were all within 1% difference with the previous ones. The so calculated ^{235}U fission spectrum averaged cross-sections are:

Calculated ^{235}U fission spectrum averaged cross-section for all the dosimeters used

Reaction	Average cross-section (barn)
$^{58}Ni(n,p)$	0.1067
$^{115}In(n,n')$	0.1854
$^{103}Rh(n,n')$	0.7000
$^{238}U(n,f)$	0.3045
$^{237}Np(n,f)$	1.3437
Dpa Fe – ASTM	862.88

10.6 Comments/special references

Fluxes and energy spectra at the measure positions were interpolated from the calculated mesh fluxes, by weighting the fluxes at the four neighbouring positions with a factor equal to the square of the inverse distance between the mesh centre and the measure point.

It is a common practice to cover the ^{238}U and ^{237}Np detectors with a cadmium sheet, in order to suppress thermal contribution to measured activity both from the detector itself and from fissile impurities. This is why the calculated cumulative energy response for ^{237}Np, both with and without a cadmium cover, was considered. In the case of the ^{238}U dosimeters, the contribution from energies below 0.1 MeV is negligible. Thus, for the ^{238}U dosimeter, there is no difference between considering or not the cadmium cover in the response calculation.

The current CAB methodology used to calculate equivalent fission fluxes for different dosimeters at the measurement positions of the VENUS-1 experiment produced an average calculation to experiment ratio (C/E) equal to 0.95 ± 0.07 (1σ).

A very good agreement is obtained for all dosimeters at the core positions but, the further the detectors are from the core, the lower the C/E ratio. This general behaviour seems to indicate that the buckling correction is not good enough to represent axial leakage in small systems as the VENUS one.

APPENDIX B

Calculation details supplied by participants

B.2. VENUS-3

1.0 Author: Ivo Kodeli (consultant)

Organisation: OECD NEA
Le Seine St. Germain
12, Bd. des Iles
F-92130 Issy-les-Moulineaux, France

1.1 Transport method and modelling assumptions

The calculation was performed using TORT [3] three-dimensional discrete ordinates transport code, PC version. The following model was chosen:

- S_N approximations: S_4-P_1 and S_8-P_3.
- Slab (xyz) geometry.
- Variable space mash with max. 51 x, 52 y, and 22 z intervals.

Modelling approximations

The materials composing upper and lower reflectors (zones XXI and XXIII) were smeared in homogenous zones. The same was done for bottom, intermediate and upper grids (zones XX, XXII, XXIV). Coarse mesh was used in these regions.

The central hole dimensions were changed to 3.442 × 3.78 cm (the actual dimensions are 3.442 × 3.442 cm).

The primary objective of the study was to perform the sensitivity and uncertainty analysis. The above approximations were considered reasonable for these studies.

1.2 Transport cross-sections

47 neutron energy group library BUGLE-96 [4] was used.

1.3 Neutron source

The VENUS-3 power distribution was fully measured only at two (out of 14) axial levels [5]: at the axial level corresponding to the mid-plane of the lower PLSA part of the core loading and at the one corresponding to the mid-plane of the upper part of the core loading. In addition to the two XY radial distributions, the full axial power distribution was measured at 374 fuel pin locations, out of the total of 639 fuel pins comprised in the 1/4 of the reactor core.

In order to establish a complete 3-D map of the power distribution in the VENUS-3 core, an extrapolation procedure based on the RECOG-ORNL code [6] was used. (See Appendix 2 for more details.)

The neutron source distribution is expressed in units of fissions per pin per second, arbitrarily normalised to a core averaged power of one fission per second per active fuel pin. Since there are 639 active pins (including those in the PLSA) in a quadrant of the core, and 2.432 neutrons per

thermal fission, this normalisation is equivalent to 639 fissions per second summed over the quadrant. This arbitrarily normalised source was converted to 100% VENUS-3 power as the measured reaction rates refer to this value. The multiplication factor was calculated as:

$$N = No \times 2.432/(Vol \times 639) = 2.7099E + 8$$

where: No = 5.652E + 12 fissions per second per core quadrant, corresponding to 100% power
Vol = $50 \times 1.26 \times 1.26$ cm^3 (fuel pin volume)

1.4 Response functions and fission averaged data

The detector activation cross-sections were taken from the BUGLE-96 library, processed to 47 neutron groups from IRDF-90 Version 2. The reaction rates were divided by the fission spectrum. The averaged cross-sections are:

Detector	Averaged cross-section (barns)
^{27}Al(n,α)	7.323E-04
^{58}Ni(n,p)	0.1063
^{115}In(n,n′)	0.1797

1.5 Comments/special references

Sensitivity/uncertainty analysis

The transport methods combined with sensitivity analysis have proved very useful in order to establish reliable safety margins for the measured and calculated values, as well as to determine to what extent the benchmark experiment is representative of the real nuclear reactor environment.

The SUSD3D code system [7], which can also perform three-dimensional sensitivity/uncertainty analysis, was used. SUSD3D requires direct and adjoint angular fluxes or moments calculated by an S_N code. The direct and adjoint transport calculations were performed using the TORT code, as described previously.

The cross-section covariance matrices from ENDF/B-VI (iron cross-sections) ENDF/B-V (hydrogen and oxygen) evaluations were used. For the detector response functions the covariance matrices were taken from IRDF90 Version 2, included in the ZZ-VITA.-J/COVA/EFF (NEA 1264/04 package) [8] in the processed multi-group format.

Uncertainties due to the ENDF/B-V neutron fission source spectrum used were calculated assuming the uncertainties of 1.2% in the parameter A of the Watt distribution function, and of 5.9% in the parameter B. The sensitivities were therefore expressed as the product of the adjoint fluxes and the sensitivity functions (derivatives) of the Watt spectrum distribution with respect to the parameters A and B [9].

The uncertainties of the detector responses in the VENUS-3 core barrel location due to the uncertainties in the neutron source energy and space distributions, detector activation cross-sections and transport cross-sections are summarised in the table below:

Source of uncertainty		Uncertainty (%)			
		ϕ > 1 MeV	^{27}Al(n,α)	^{58}Ni(n,p)	^{115}In(n,n′)
Fission spectrum		4.4	12	6.5	4.4
Source space distribution		~ 1.5 - 4%			
Absolute power		4			
Response function		0	1.4	2.5	2.2
Cross-sections	H	1.9	1.1	1.4	1.6
	O	0.6	1.6	0.7	0.5
	Fe	2	5	2.5	2.1
Total		**~ 7**	**~ 14**	**~ 9**	**~ 8**

It can be observed that the calculated standard deviations (1σ ~ 10%) agree well with the observed discrepancies between the calculations and the measurements.

By comparing the VENUS-3 sensitivity and uncertainty analysis with similar ones performed in the scope of the reactor pressure vessel surveillance [10], the representativity of VENUS-3 with respect to the real reactor environment can be determined. Figures 1 and 2 present the sensitivity profiles of the fast neutron flux in the VENUS-3 core barrel to hydrogen, oxygen (Figure 1) and iron (Figure 2) cross-sections, compared to the sensitivity profiles corresponding to the fast neutron flux in the PW reactor surveillance capsules. The sensitivity profiles for the hydrogen and oxygen cross-sections are similar in both cases (similar water thickness in both cases), but VENUS-3 is not very sensitive to iron cross-sections (see Figure 2 – low sensitivity to iron cross-sections as compared to the PWR surveillance capsules).

The primary use of VENUS-3 is therefore for testing of the three-dimensional computational tools and models.

More information on this analysis can be found in [11].

Figure 1. Sensitivity profiles of Φ > 1 MeV in a PWR surveillance capsule and in VENUS-3 core barrel to the iron cross-sections

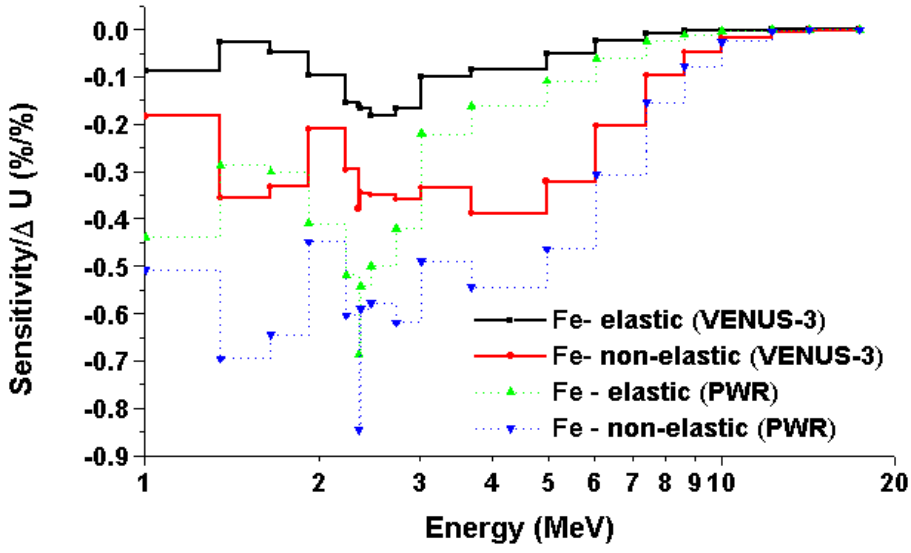

Figure 2. Sensitivity profiles of Φ > 1 MeV in a PWR surveillance capsule and in VENUS-3 core barrel to hydrogen and oxygen cross-sections

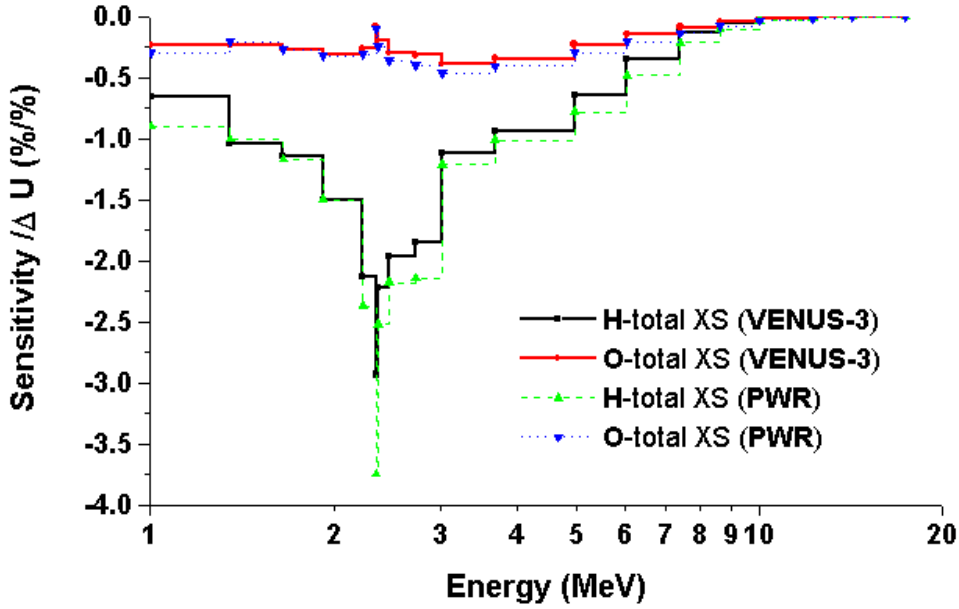

REFERENCES

[1] P. D'Hondt, *et al.*, "Contribution of the VENUS Engineering Mock-Up Experiment to the LWR-PV Surveillance", Proc. 7th ASTM-EURATOM Symposium on Reactor Dosimetry, Strasbourg, France, 27-31 August 1990.

[2] L. Leenders, "LWR-PVS Benchmark Experiment VENUS-3", FCP/VEN/01 Report, Sept. 1988.

[3] Radiation Shielding Information Center, Oak Ridge, TN (1993).

[4] W.A. Rhoades, R.L. Childs, "TORT-DORT: Two- and Three-Dimensional Discrete Ordinates Transport, Version 2.7.3, RSIC-CCC-543, ORNL Group Cross-Section Library for LWR Applications Based on ENDF/B-VI Release 3", ANS Rad. Prot. & Shielding Topical Meeting, Falmouth, MA (April 1996).

[5] J.E. White, *et al.*, "BUGLE-96: A Revised Multi-Group Cross-Section Library for LWR Applications Based on ENDF/B-VI Release 3", ANS Rad. Prot. & Shielding Topical Meeting, Falmouth, MA (April 1996).

[6] H. Ait Abderrahim, VENUS-3 3-D Power Distribution, private communication.

[7] C.L. Begovich and N.M. Larson, “A User’s Manual for the Pattern Recognition Code RECOG-ORNL”, ORNL/CSD/TM-21 (1977).

[8] I. Kodeli, “Progress on Computational Tools for 3-D Sensitivity and Uncertainty Analysis”, OECD NEA Seminar on 3-D Deterministic Radiation Transport Computer Programs Features, Applications and Perspectives, Paris, 2-3 December 1996.

[9] G.C. Panini, I. Kodeli, “ZZ-VITA.-J/COVA/EFF – Covariance Data Library”, NEA DB, NEA 1264/04 package (1996).

[10] I. Kodeli, “Etudes des incertitudes sur la fluence dans les cuves des REP. Ajustement des Données de base”, Note CEA-N-2749 (1994).

[11] I. Kodeli, J.C. Nimal, “Assessment of Uncertainties for PWR Pressure Vessel Surveillance – French Experience”, *Trans. Am. Nucl. Soc*., Vol. 74, 1996.

[12] I. Kodeli, E. Sartori, “Use of Benchmark Experiments Database for Pressure Vessel Dosimetry”, Proc. 1998 ANS Radiation Protection and Shielding Division Topical Conf., Nashville, Tennessee, p. I-287 (April 1998).

2.0 Authors: J. Manuel Perlado, Jaime Marián and J. García Sanz

Organisation: CSN – UNESA – DENIM – CIEMAT – TECNATOM, Spain
VENUS Spanish Agreement on Reactor Vessel Fluence Calculations and Computer Simulation of Microscopic Damage Effects
Produced by: Instituto de Fusión Nuclear (DENIM)/E.T.S.I.I./
Universidad Politécnica de Madrid (UPM, Spain)

2.1 Transport method and modelling assumptions

The Monte Carlo methodology has been chosen at DENIM to broach the problem and the Los Alamos National Laboratory general-purpose MCNP4B Monte Carlo transport code has been used to perform all calculations concerning the benchmark. It was originally installed on a DIGITAL ALPHA STATION 200 workstation where the first calculations were realised, but afterwards it was installed on a more powerful HP X-Class EXEMPLAR with 16 processors. All relevant calculations have been run on the latter, whereas cross-section processing and geometry plotting is still carried out on the former. Standard Monte Carlo techniques such as importance and energy cut-offs have been used in diverse runs and the performance of the code has been optimised by means of variance reduction techniques such as weight windows or the use of the adjoint function as well. The full three-dimensional description including the neutron pad, water gap, jacket and the reactor vessel has been modelled. The geometry is divided into volumetric cells that are bounded by algebraic surfaces. In the model figured out at DENIM for the VENUS-3 geometry, 139 cells defined by 75 bounding surfaces were required to describe the whole simulated reactor in detail. The code provides a plotting tool itself that is helpful to visualise and debug geometry errors. The intermediate and upper grids have been considered concentric instead of eccentric. We have thoroughly followed the specifications provided in documents sent by NEA ("LWR-PVS Benchmark Experiment VENUS-3", FCP/VEN/01, Mol (Sept. 1988)). Some fuel rods and their corresponding reflector radii have been adjusted to have the same values *always inside the tolerances specified in the documentation.* Several simplifying hypotheses have been considered when describing some structural elements belonging to the reactor. Particularly the bottom, intermediate and top grids have been modelled to be composed of an homogeneous mixture of steel or Plexiglas and water rather than a heterogeneous grating structure surrounded by water. Densities of bottom and top stops of 4/0 fuel have been modified in accordance with more realistic data for they are clearly inconsistent in the geometry specifications document (FCP/VEN/01). The composition of the barrel has been that in 1.5.8.1 (page 20) of the document, between the reflector and the water gap (it has been clearly missed). Plexiglas has been considered as $(CH)_n$. We have set the jacket volume to be void. Inconsistencies have been observed in the description of the so-called AISI 304 stainless steel, for eight different compositions of this material were given for the many elements that it is part of.

2.2 Transport cross-sections

ENDF/B-VI processed using NJOY 94.105 and the DLC-189/MCNPXS code package, both in MCNP-suitable ACE format (pointwise cross-sections).

2.3 Neutron source

2.4 Response functions and fission averaged data

IRDF-90 Version 2. This library has been processed at DENIM using NJOY 91.118 and the ACER module for ^{58}Ni(n,p), ^{115}In(n,n′), ^{27}Al(n,α). The calculation of the average dosimetry cross-section for the different reactions to be used in the computation of the equivalent fission flux, according with NEA communications and common uses in dosimetry, has been performed weighing the dosimetry library with the ^{235}U fission spectrum given in the NJOY code system. The values are:

Reaction	Averaged cross-section (barn)
^{58}Ni(n,p)	0.105
^{115}In(n,n′)	0.185
^{27}Al(n,α)	0.72 E-03

2.5 Comments/special references

The results for the indium equivalent fission fluxes are different between transport and dosimetry values. The reason is that those of dosimetry include the total inelastic cross-section, and those in transport ONLY include the inelastic cross-section to the first excited state. Some of the requested points have been skipped because they do not belong to the south-west quadrant specified in the benchmark (–,+3). In addition, the point (–,+23), which is identified as 3/0 fuel position, corresponds to a 4/0 fuel pin according to the given data. All those points have not been included in the results; however, the symmetric points were computed and not added here.

3.0 Authors: Bok Ja Moon and Hae Ryong Hwang

Organisation: Korea Power Engineering Co. (KOPEC)
Yusong, Taejon, Korea

3.1 Transport method and modelling assumptions

- Codes used: GIP – macroscopic cross-section calculation/TORT three-dimensional discrete ordinate transport code.
- Geometry model: xyz model ($56 \times 45 \times 20$).
- Assign almost 1 pin to 1 mesh for each vertical plane.
- S_8 order used, Legendre Polynomial: P_5.
- Modelled above and below active core as air and then applied vacuum boundary condition.

Geometry

The structures beyond the neutron pad such as air jacket, vessel, etc., are excluded because those structures have negligible effect on the responses of the dosimeters located at the inner regions of the neutron pad. A reflector region of the coolant at room temperature (24°C) is assumed above and below the active core and a vacuum boundary condition is applied to the top and bottom boundaries.

Calculational methods

1) DORT XZ and DORT X transport calculations with a multi-channel synthesis method.
2) TORT XYZ transport calculation.

XYZ model consists of ($56 \times 45 \times 26$) meshes. The same XY mesh intervals are assigned to the DORT and TORT calculations to minimise differences arising from discretisation.

3.2 Transport cross-sections

The DLC-185/BUGLE-96 multi-group cross-section library based on ENDF/B-VI is used. (47 neutron/20 gamma-ray group cross-section: same energy group structure as BUGLE-80.)

3.3 Neutron source

The measured three-dimensional pinwise source distribution is used as the source for the transport calculations. Not all values were measured, and missing ones were interpolated by the NEA. The source distribution is normalised to 5.652×10^{12} (fission/sec/quadrant), the reference measured fission rate, at 100% power and 2.432 neutrons/thermal fission are used.

For the DORT calculations, the one- and two-dimensional pinwise source distributions are calculated from the measured three-dimensional source distribution using:

$$Pxy_{ij}^{above} = \sum_{k=8}^{14} P_{ijk} \frac{\Delta z_k}{25}$$

$$Pxy_{ij}^{below} = \sum_{k=1}^{7} P_{ijk} \frac{\Delta z_k}{25}$$

$$Pxz_{ik}^{above} = \sum_{j=1}^{J_i} P_{ijk} \frac{1}{J_i}\Bigg|_{k=8-14}$$

$$Pxz_{ik}^{below} = \sum_{j=1}^{J_i} P_{ijk} \frac{1}{J_i}\Bigg|_{k=1-7}$$

$$Px_{i}^{above} = \sum_{k=8}^{14}\sum_{j=1}^{J_i} P_{ijk} \frac{1}{J_i}\frac{\Delta z_k}{25}$$

$$Px_{i}^{below} = \sum_{k=1}^{7}\sum_{j=1}^{J_i} P_{ijk} \frac{1}{J_i}\frac{\Delta z_k}{25}$$

where 25 is the half height of the VENUS-3 reactor in cm, P_{ijk} is the measured relative 3-D source distribution and J_i is the number of fuel rods in ith x-direction. The axial nodes from 1st to 7th node correspond to the sources lying below the mid-plane and the nodes from 8th to 14th node correspond to the sources lying above the mid-plane.

The normalisation factors for the 1-D and 2-D calculations are obtained as follows:

$$XNF_{xz}^{above} = 5.652 \times 10^{12} \times 2.432 \times \frac{\sum_{ij} Pxy_{ij}^{above}}{\sum_{ij} Pxy_{ij}^{above} + \sum_{ij} Pxy_{ij}^{below}} \text{ (neutrons/sec/upper quadrant)}$$

$$XNF_{xz}^{below} = 5.652 \times 10^{12} \times 2.432 \times \frac{\sum_{ij} Pxy_{ij}^{below}}{\sum_{ij} Pxy_{ij}^{above} + \sum_{ij} Pxy_{ij}^{below}} \text{ (neutrons/sec/upper quadrant)}$$

Some XY mesh intervals do not match with the fuel rod pitch because they are determined considering not only the fuel rod pitch, but also baffle thickness. To obtain the source for a mesh, each mesh interval is divided into subintervals and the subinterval powers are summed considering area fraction. The subinterval power is determined as the power of the pin located at the centre of the subinterval. One XY mesh is divided into 20×20 subintervals.

The TORT calculation has the advantage of directly obtaining the 3-D flux distribution with one transport calculation. However, the extensive input needed for the TORT calculation, along with the transformation of the pinwise source distribution to the TORT mesh structure, requires additional computer manipulations.

As the vertical TORT mesh boundaries correspond to the node boundaries of the measured source distribution, the assignment of the pinwise powers to the individual mesh intervals for each XY plane is done using the same method as in the DORT calculation.

The normalisation factor for the TORT calculation is obtained as follows:

$$XNF = \frac{5.652 \times 10^{12} \times 2.432}{\sum_{ijk} P_{ijk} \Delta x_i \Delta y_j \Delta z_k} \text{ (neutrons/sec/cc)}$$

3.4 Response functions and fission averaged data

The equivalent fission flux for dosimeter d is defined as a ratio of calculated reaction rate and the average dosimeter cross-section. Thus it can be calculated as follows:

$$\phi_{eq}^{d} = \sum_{g} \sigma_g^d \phi_g \Big/ \sum_{g} \sigma_g^d \chi_g$$

where σ_g^d : g^{th} group reaction cross-section for dosimeter *d*
ϕ_g : g^{th} group neutron flux from DORT or TORT output
χ_g : g^{th} group ^{235}U fission spectrum

Dosimeter cross-sections taken from the BUGLE-96 library were used. The average dosimeter cross-sections are as follows:

Reactions	**Average cross-section (barn)**		**C/E**
	Calculation	Experiment	
$^{58}Ni(n,p)^{58}Co$	0.1070	0.1085	0.99
$^{115}In(n,n')^{115m}In$	0.1802	0.1903	0.95
$^{27}Al(n,\alpha)^{27}Na$	0.782E-3	0.706E-3	1.11

The DPA values were calculated as follows:

$$dpa/\text{sec} = \sum_{g} \sigma_d\left(E_g\right)\phi\left(E_g\right)$$

where: $\sigma_d\left(E_g\right) \equiv$ displacement cross-section
$\phi \equiv$ neutron flux from DORT or TORT output

The displacement cross-section is the group collapsed data from the data in ASTM E693-94.

Some dosimeters are not positioned in the modelled core quadrant, and the flux for these dosimeters is calculated at the quarter symmetry locations in the modelled quadrant. All dosimeters are assumed to be point detectors without surrounding structures and the reaction rates are calculated using the linearly interpolated fluxes at the corresponding detector position.

3.5 Comments/special references

The synthesising calculation using DORT (2-D) provides unsatisfactory results for the dosimeters located far from the selected azimuthal angle for the DORT XZ model.

TORT calculation shows a good agreement within 10% with the experimental data and gives consistent results for all regions and all dosimeters. Three-dimensional calculations are recommended for the analysis of reactors with strong axial or azimuthal heterogeneity.

The detector positions given in fifth column ((x,y) in (cm,cm)) at Table 1 and axial levels at Tables 2-4 in the VENUS-3 benchmark specification “NEA/NSC/DOC(97)12” were used. The results at detector position (+2,+23) are replaced with the data at the detector position (+2,-23) according to NDB/98/1327/cem.

4.0 Authors: W. Hofmann and J. Koban

Organisation: SIEMENS AG Power Generation Group (KWU)
D-91050 Erlangen, Germany

4.1 Transport method and modelling assumptions

Methods and input data

The neutron transport calculations were performed by the use of the three-dimensional S_N code TORT [4]. The (x,y,z) geometry option and full symmetrical S_8 quadrature sets were used.

Geometry

The geometrical model was limited to a core quadrant.

The boundary conditions chosen in the calculational model are reflected at the left and inside boundary and vacuum at the right, outside, bottom and top boundary. The assumption of the vacuum boundary condition outside the reactor pressure vessel will not influence the results of the calculated neutron flux densities at the measurement points drastically because the outermost measurement points are within the core barrel. In axial direction the positions of all measurement points are within the active core height (105-155 cm) so that the vacuum boundary conditions within the lower filling zone at z = 83.45 cm and at the upper surface of the upper filling zone (z = 168 cm) again will not have significant influence on the calculational results at the measurement positions.

The numbers of x-meshes and y-meshes in the geometrical model are the same: IM = JM = 55. The meshes were chosen in the equidistant manner given by the pins (1.26 cm). The z-meshes within the active core (105 cm up to 155 cm) were chosen identical with the 14 axial meshes of the relative source distribution provided by the NEA. Below the active core (83.45 cm up to 105 cm) a total of 10 meshes and above the active core (155 cm up to 168 cm) a total of 8 meshes were used.

Because of the meshes chosen no interpolations between the results of TORT meshes were necessary in order to get the results at the measurement positions. In x- and y-direction the midpoints of the TORT meshes are identical with the measurement points. In the axial direction the deviations between TORT mesh midpoints and z co-ordinates of the measurement points are always smaller than 1 cm, and in most cases the z co-ordinates are identical. Therefore interpolation procedures between neighbouring meshes were not necessary in order to get the calculational results at the measurement points.

4.2 Transport cross-sections

For the TORT calculation a collapsed version of the 175 neutron energy group library EURLIB-VI/N175 [5] was used, based on ENDF/B-VI Rev. 2 nuclear data [6]. The EURLIB VI/N175 library was generated by the use of the NJOY-91 [7] program system. The energy group boundaries are identical to that of the VITAMIN-J [8] group structure. The generation of the group data was based on the usual energy weighting, meaning above 2.12 MeV fission spectrum weighting, in the intermediate energy region down to 0.414 eV 1/E, and Maxwellian weighting in the thermal energy region. In order to reduce the number of energy groups to an acceptable level for three-dimensional

neutron transport calculations, the resulting 175 group library was collapsed by the use of the usual energy weighting procedure. The result was a 100 neutron energy group cross-section library with an energy group structure that is identical to that of the EURLIB 4 library [9].

The macroscopic cross-section library that was finally used for each material zone of the TORT calculational model was generated by multiplying the number densities of the materials and the microscopic cross-section data and by summing up over all nuclides. The number densities used in the calculation were generated from the input data given in [3].

4.3 Neutron source

The neutron source input data for the TORT calculation are the following:

- ^{235}U fission spectrum normalised to 1.0.
- Pin by pin relative source distribution for 14 axial zones provided by the NEA.

The source normalisation factor XNF, which is only a multiplication factor in the TORT code, was calculated in the following manner:

Total neutron source per core quadrant and per second:

5.652E12 fissions/quadrant/s $\times$ 2.43 neutrons/fission = 1.373E 13 neutrons/quadrant/s

Average neutron source per cm^3 of the active core:

1.373E 13 neutrons/quadrant/s / 4.774E4 cm^3 = 2.876E 8 neutrons/cm^3/s

Unnormalised neutron source per core quadrant calculated by the TORT code from the pin by pin input data provided by the NEA: 5.09E 4 neutrons/quadrant/s. From this TORT output value we can calculate:

5.09E 4 neutrons/quadrant/s / 4.774E 4 cm^3 = 1.066 neutrons/cm^3/s

What we need, as shown above, is an average neutron source term of 2.876E 8 neutrons/cm^3/s. That means the TORT input value for XNF is 2.876E 8 / 1.066 = 2.697E 8.

4.4 Response functions and fission averaged data

The equivalent fission flux is defined as the ratio of the calculated reaction rate and the ^{235}U fission spectrum averaged dosimeter cross-section. Equivalent fission fluxes were calculated for the measurement points for three different dosimeter materials. The basic data for the dosimeter cross-sections are the 620 group data given in the IRDF/90, Version 2 [10] nuclear data file. The cross-section data were collapsed to the 100 energy group structure of the neutron transport calculation. Again the usual cross-section weighting technique was used. The 100 group cross-section data for each dosimeter are input data (response functions) of the TORT code. Therefore the TORT output file already includes the reaction rates for each geometrical mesh and dosimeter in question.

The ^{235}U fission spectrum averaged dosimeter cross-sections were calculated by the use of the ENDF/B6 ^{235}U fission spectrum [5] and the 100 group dosimeter cross-sections which, as mentioned above, are included in TORT input data as response functions. The calculated ^{235}U fission spectrum averaged dosimeter cross-sections are listed below:

Dosimeter reaction	^{235}U fission spectrum averaged dosimeter cross-section (mbarn)
$^{27}Al(n,\alpha)^{24}Na$	0.72
$^{58}Ni(n,p)^{58}Co$	105
$^{115}In(n,n')^{115m}In$	185.2

For the DPA calculation the flux-DPA conversion factors were taken from [10] (DPA-ASTM).

4.5 Comments/special references

[1] R.P. Rulko, NDB/96/0891/rr, 15 July 1996:

a) VENUS-1: Two-Dimensional Benchmark on Ex-Core Dosimetry Computations NEA/NSC/DOC(96)25.

b) VENUS-1: Description of Geometry and Composition of Different Materials.

c) VENUS-1: Results of Experimental Determination of: Relative Power Distribution and Absolute Level of Reference Power.

d) Results of Experimental Measurement of Vertical Bucklings in the Core and Outside.

[2] Attachment to the letter of J. Koban to Dr. R.P. Rulko, dated 24 April 1997:

a) VENUS-1: Two-Dimensional Benchmark on Ex-Core Dosimetry Computation, J. Koban, SIEMENS AG Power Generation Group, D-91050 Erlangen, Germany, April 1997.

[3] R.P. Rulko, NDB/97/1182/rr, 16 July 1997:

a) "VENUS-3 Three-Dimensional Benchmark on Ex-Core Dosimetry Computations", NEA/NSC/DOC(97)12.

b) "LWR-PVS Benchmark Experiment VENUS-3 (with Partial Length Shielded Assemblies) – Core Description and Qualification", FCP/VEN/01. Mol, 1 Sept. 1988.

[4] Rhoades, Childs, TORT-DORT Two- and Three-Dimensional Discrete Ordinates Transport Code, Version 2.7.3, RSIC CODE PACKAGE CCC-543, ORNL, Oak Ridge, Tennessee, 1993.

[5] M. Mattes and G. Hehn, EURLIB-VI/N175, Neutronenwirkungsquerschnitts-Bibliothek in VITAMIN-J-Struktur basierend auf, Kerndaten von ENDF/B-VI, IKE 6-FB-72, Universität Stuttgart, Juni 1995.

[6] P.F. Rose, ENDF/B-VI Summary Documentation. BNL-NCS-17541 (ENDF-201), 4th Edition, October 1991.

[7] R.E. MacFarlane, D.W. Muir, The NJOY-91 Nuclear Data Processing System, Version 91, LA-12740-M, October 1994.

[8] E. Sartori, Standard Energy Group Structures for Cross-Section Libraries for Reactor Shielding, Reactor Cell and Fusion Neutronics Applications: VITAMIN-J, ECCO-33, ECCO-2000 and XMAS, JEF/DOC-315, June 1991.

[9] Cagliotti, 120-Group Coupled Neutron and Gamma Data Library, European Community Commission, EURATOM, CCR-Ispra, Ispra, April 1978.

[10] Kocherov, McLaughlin, “The International Reactor Dosimetry File (IRDF 90)”, IAEA-NDS-141, Rev. 2, October 1993.

5.0 Authors: G.Hehn, A.Sohn, M. Mattes and G. Pfister

Organisation: IKE University of Stuttgart
Postfach 801140
D-70550 Stuttgart, Germany

5.1 Transport method and modelling assumptions

The main effort of the benchmark study had been devoted to "high precision" calculations and "routine" type calculations of the strongly three-dimensional VENUS-3 facility with the aim to clarify the precision and practicability achievable today by neutron fluence calculations for reactor pressure vessel and reactor internals in real three-dimensional geometry. We applied the S_N method with the three-dimensional transport code TORT 3.1 in S_8P_3 and $S_{12}P_5$ approximations. Since for power reactors cylindrical geometry is the first choice, we used also cylindrical co-ordinates in the benchmark calculation with 93 and 71 r-meshes, 53 theta meshes and 62 z-meshes within a core quadrant. Special care was taken to model the outer fuel pins, the control rods and the outer rectangular baffle. For checking a second calculation was performed with Cartesian co-ordinates (62 x-meshes, 62 y-meshes and 62 z-meshes), too. Since we intended to analyse the benchmark results in great detail with the help of colour graphic, we could not use variable space meshing to reduce the mesh number. For the flux extrapolation model the theta-weighted approximation was selected. The pointwise flux convergence was better than 1.0E-4 everywhere.

5.2 Transport cross-sections

For "high precision" calculations the multi-group library VIT-J of IKE had been used with 175 neutron energy groups similar to VITAMIN-J comprising 105 groups above 0.1 MeV. VIT-J is based on the point data of ENDF/B-VI for all isotopic components of stainless steel and on JEF 2.2 data for the other elements. For "routine" calculations the few group cross-sections of BUGLE-96 had been applied with 47 neutron groups totally and 26 groups above 0.1 MeV. Normally P_3 approximation of the scattering cross-sections is good enough, but checks have also been made with P_5 approximation.

5.3 Neutron source

For the standard fluence calculation in cylindrical geometry we had to transfer the relative pin power distribution, specified in Cartesian co-ordinates, into the cylindrical mesh system with strict conservation of the source strength. The number of neutrons per fission and the fission spectrum were taken for the dominating thermal fission of ^{235}U. For all three-dimensional calculations in cylindrical and Cartesian co-ordinates the neutron source rate had been normalised to 1.554E+3 n/s in the total core quadrant.

5.4 Response functions and fission averaged data

The activation cross-sections were taken from IRDF-90 Version 2 and BUGLE-96 respectively. The DPA cross-section of iron has changed up to +20% from the old iron data in ASTM-82 contained in IRDF-90 Version 2 to the updated iron data of ENDF/B-VI, which were used. For determining the equivalent fission flux the following fission spectrum averaged reaction cross-sections were used in both libraries IRDF-90 Version 2 and BUGLE-96:

	Fission averaged reaction cross-section (barn)	
	IRDF-90 V.2	BUGLE-96
^{58}Ni	0.1053	0.1070
^{115}In	0.1853	0.1802
^{27}Al	0.7279E-03	0.7821E-03

5.5 Comments/special references

For the three-dimensional benchmark VENUS-3 six different runs were performed with the code TORT 3.1:

- Case 1a: P_3S_8-sym., 93 r-meshes, 53 theta-meshes, 62 z-meshes, energy group structure of VIT-J up to group 105/0.1 MeV.

- Case 1b: P_3S_8-sym., 93 r-meshes, 53 theta-meshes, 62 z-meshes, energy group structure of VIT-J up to group 175/thermal.

- Case 2: P_3S_8-sym., 62 x-meshes, 62 y-meshes, 62 z-meshes, energy group structure of VIT-J up to group 105/0.1 MeV.

- Case 3: P_3S_8-sym., 93 r-meshes, 53 theta-meshes, 62 z-meshes, energy group structure of BUGLE-96 up to group 26/0.1 MeV.

- Case 4: P_3S_8-sym., 71 r-meshes, 53 theta-meshes, 62 z-meshes, energy group structure of VIT-J up to group 105/0.1 MeV.

- Case 5: P_5S_{12}-sym., 71 r-meshes, 53 theta-meshes, 62 z-meshes, energy group structure of VIT-J.

6.0 Authors: R.C.L. van der Stad and A. Hogenbirk

Organisation: NRG, FAI (Fuel, Actinides and Isotopes)
P.O. Box 25
NL-1755 ZG Petten
(Former: ECN, BU Nuclear Energy)

6.1 Transport method and modelling assumptions

NRG participated in this benchmark using the general purpose Monte Carlo software package MCNP version 4B [1] with the JEF2.2 based EJ2-MCNP cross-section library [2] generated at NRG with NJOY91.118+. MCNP is a general-purpose, continuous-energy, time-dependent, coupled neutron-photon-electron Monte Carlo transport code system. MCNP uses a general geometry description through which virtually all 3-D geometries can be modelled.

All details of the upper and lower reactor grids and all details in the top and bottom of the rods, as far as they were given in [3], were modelled explicitly. Some data of minor importance were missing from the benchmark specification such as the exact composition of Plexiglas and the exact composition of the steel in the reactor grid and in the steel water mixture. Realistic values from other sources were taken in order to be able to complete the model.

The calculations were performed in a 1/4 core, full 3-D geometry. In the real VENUS-3 core some measurement positions were located in one of the other three quadrants of the core. In our calculations we have used the corresponding location in the modelled quadrant.

6.2 Transport cross-sections

NRG has used the EJ2-MCNP continuous energy cross-section data library based on the JEF2.2 evaluated nuclear data file. This MCNP nuclear data library was generated at NRG with NJOY91.118+.

6.3 Neutron source

A “normalised pin power density” was supplied by the OECD. From this density a fixed neutron source distribution for MCNP can be deduced. In the MCNP fixed source calculations a standard Watt’s fission spectrum was taken for the energy distribution of the source neutrons.

Additionally, in Section 6.2 the results are shown when the source is calculated by MCNP instead of using the supplied pin power density. The source is calculated by MCNP in a “k_{eff} calculation”. This last method appears to reproduce the experimental data better than when the measured pin power distribution is used.

6.4 Response functions and fission averaged data

For the calculation of the reaction rates and equivalent fission fluxes, cross-sections from the IRDF90 Version 2 library were processed for use in MCNP. An additional MCNP library with DPA cross-sections was used with DPA cross-sections originating from the JEF2.2 evaluation.

Table 1 shows the average dosimeter cross-sections calculated with MCNP using IRDF90 Version 2 dosimeter cross-sections. The second column shows the average dosimeter cross-sections calculated with MCNP and the third column the values found in the reports [NUREG/CR-5338, ORNL/TM-11106] which were probably used by the experimentalists. For further discussion see Section 6.1.

Table 1. Average dosimeter cross-sections calculated with MCNP

	$<\sigma_{Reaction}>_{\phi f}$	
Reaction	MCNP (mBarn)	NUREG/CR-5338, ORNL/TM-11106 (mBarn)
^{58}Ni(n,p)	106.9	108.5
^{115}In(n,n′)	185.5	190.3
^{27}Al(n,α)	0.719	0.706

In the calculation of the average dosimeter cross-section of inelastic scattering reactions it is important to consider the correct excited state. We have used for ^{115}In(n,n′) and ^{103}Rh(n,n′) only the first excited state which is the correct procedure.

6.5 Comments/special references

Remark to the normalisation to the equivalent fission flux

The equivalent fission flux is just a reaction rate divided by a constant called the average dosimeter cross-section and is defined as follows:

$$\text{Equivalent fission flux} = \frac{\sigma_R \phi}{\langle \sigma_R \rangle_{\phi f}} \tag{1}$$

with the average dosimeter cross-section ($\langle \sigma_R \rangle_{\phi f}$) defined as:

$$\langle \sigma_R \rangle_{\phi f} = \frac{\int dE \sigma_R(E) \phi_f(E)}{\int dE \phi_f(E)} \tag{2}$$

with: ϕ = the spectrum calculated in the transport calculation
$\langle \sigma_R \rangle$ = the reaction cross section (some threshold reaction or fission reaction
ϕ_f = the fission spectrum

The average dosimeter cross-section is equal to the fission spectrum averaged reaction cross-section so it depends only on the dosimeter cross-sections (data library) and the (constant) fission spectrum used in the code. Within an experimental set-up or in a transport code system it is a constant. Experimenters measure reaction rates directly and then use this constant to normalise their experimental values. The benchmark contributors were asked to calculate the average dosimeter cross-sections with their own codes and use this value in the normalisation. This procedure could introduce a shift of the calculated results with respect to the experimental results, which does not originate from the transport calculation but just from a normalisation.

Table 1 shows the average dosimeter cross-sections calculated with MCNP using IRDF90.2 dosimeter cross-sections. The second column shows the average dosimeter cross-sections calculated with MCNP and the third column displays the values found in the reports [NUREG/CR-5338, ORNL/TM-11106] which were probably used by the experimenters. Comparisons of the values show differences of about 2%. These differences cause a small shift in the equivalent fission flux of 2% that does not originate from the transport calculation but just from a normalisation. In our opinion it would have been better to compare the reaction rates directly with the experimental data without introducing a shift due to normalisation.

VENUS-3 results using the source from a $k_{effective}$ calculation

The overall experimental error aimed at in the VENUS experiment was 20%. The experimental uncertainty in the determination of reaction rate of $^{58}Ni(n,n')$ is typically of the order of 5%. The experimental error in the pin power profile (source) and geometry is estimated to be of the order of 10%. Assuming that the benchmark specification is realistic, the contribution to the uncertainty in the calculated equivalent fission flux due the error in the pin power profile can by eliminated by calculating the source with MCNP in a $k_{effective}$ calculation.

This section shows an additional set of results using the source from a $k_{effective}$ calculation.

Figure 1 shows a comparison of the axial profile of the calculated ^{58}Ni equivalent fission flux expressed as the C/E ratio for measurement position (-29,+2) in case the neutron source was derived from the pin power distribution and in case the neutron source was calculated by MCNP itself. It shows that the underestimation at the top and bottom of the fuel clearly present in the results of the fixed source calculation, reduces in the results in the k_{rmeff} calculation. The small discrepancy which is still present at the outermost part of the fuel region could be due to the simplification made in the benchmark specification concerning the upper and lower reflector. The upper and lower reflector is specified as a homogeneous mixture of steel and water (lower reflector), Plexiglas and water (upper reflector).

Figure 1. Comparison of the ratio of the calculated and experimental results in case the source is derived from the benchmark specification provided pin power (MCNP fixed source calculation) or in case the source is calculated by MCNP (MCNP $k_{effective}$ calculation)

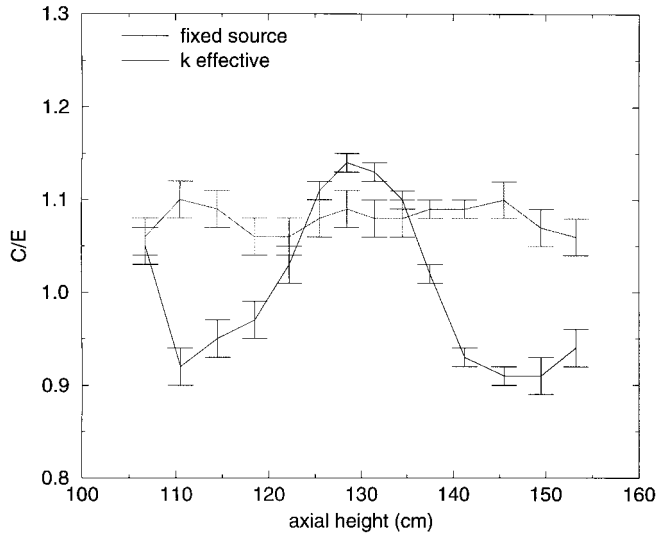

Tables 2-5 show the MCNP VENUS-3 results as the ratio to the experimental values (C/E) in case the neutron source was calculated by MCNP itself.

Table 2. C/E ^{58}Ni inner and outer baffle locations ($k_{effective}$ calculation)

z[cm] z[cm]	(-1,+2) 2	(-1,-1) 3	(-29,+2) 4	(-29,-2) 5	(-29,-7) 6	(-29,-12) 7	(-27,-14) 8	(-22,-14) 9	(-17,-14) 10
106.7			1.07						
110.5			1.00						
114.5	0.99	1.03	1.01	1.04	1.07	1.04	0.96	1.03	1.02
118.5			1.14						
122.2			0.92						
125.5			1.01						
128.5			1.02						
131.5	1.02	1.00	1.02	1.11	1.02	1.10	1.01	1.03	1.03
134.5			1.08						
137.5			1.06						
141.2			1.00						
145.5	1.08	1.05	1.00	1.13	1.03	1.12	1.02	1.05	1.06
149.5			1.06						
153.2			1.08						

Table 3. C/E ^{58}Ni core barrel locations ($k_{effective}$ calculation)

z[cm] z[cm]	(-37,+2) 11	(-37,-5) 12	(-35,-12) 13	(-34,-15) 14	(-33,-17) 15	(-31,-20) 16	(-28,-24) 17	(-26,-26) 18	(-12,-35) 19	(+2,-37) 20
106.7	1.18		1.12					1.08	1.06	1.25
110.5	1.12		1.03					0.99	1.02	0.99
114.5	1.17	1.03	0.97	1.05	1.08	0.88	1.03	0.93	1.07	1.04
118.5	1.00		1.06					1.06	1.11	1.08
122.2	1.05		1.00					1.10	1.02	1.11
125.5	1.00		1.00					0.92	1.01	1.02
128.5	1.01		1.03					1.03	1.11	1.12
131.5	1.09	1.12	1.08	1.04	1.03	0.92	1.03	1.07	0.99	1.10
134.5	1.17		1.00					1.03	1.04	1.07
137.5	1.01		1.09					1.06	1.08	1.07
141.2	1.06		1.00					1.05	1.00	1.09
145.5	1.08	1.13	1.04	1.08	1.09	0.94	1.02	1.08	1.13	0.98
149.5	1.05		0.97					1.12	0.98	1.10
153.2	1.19		1.10					1.14	1.04	1.05

Table 4. C/E ^{58}Ni water gap locations, PLSA locations and 3.3% fuel locations ($k_{effective}$ calculation)

z[cm] z[cm]	(-33,+2) 21	(-27,+2) 22+23	(-25,+3) 24+25	(-23,+2) 26	(-27,-9) 27	(-21,+2) 28	(-19,+3) 29	(-22,+0) 30	(+2,+23) 31
106.7	0.86	0.94	0.94	0.99	1.03	1.06	1.09	1.06	1.46
110.5	1.05	1.01	1.00	0.99	0.97	1.03	1.04	1.10	1.39
114.5	1.00	1.02	1.04	1.00	1.11	1.07	1.05	1.09	1.37
118.5	1.01	1.00	1.07	1.04	1.23	1.06	1.05	1.06	1.35
122.2	0.94	1.07	1.03	1.00	1.06	1.08	1.03	1.06	1.33
125.5	0.98	1.07	1.03	0.98	1.11	1.04	1.02	1.08	1.38
128.5	1.03	1.07	1.05	0.98	3.07	1.01	1.06	1.09	1.36
131.5	1.00	1.10	1.13	1.05		1.07	1.09	1.08	1.35
134.5	1.07	1.11	1.10	1.06		1.06	1.09	1.08	1.36
137.5	1.00	1.06	1.08	1.11		1.10	1.09	1.09	1.36
141.2	1.09	1.07	1.06	1.08		1.08	1.08	1.09	1.35
145.5	1.03	1.06	1.11	1.07		1.08	1.05	1.10	1.34
149.5	1.11	1.05	1.06	1.11		1.04	1.05	1.07	1.32
153.2	1.16	1.05	1.04	1.14		1.10	1.09	1.06	1.37

Table 5. C/E ^{115}In inner and outer baffle locations, water gap locations and core barrel locations ($k_{effective}$ calculation)

z[cm] z[cm]	(-1,+2) 2	(-1,-1) 3	(-29,+2) 4	(-33,+2) 21	(-37,+2) 11	(-37,-5) 12	(-35,-12) 13	(-34,-15) 14	(-33,-17) 15	(-31,-20) 16	(-28,-24) 17	(-26,-26) 18	(-12,-35) 19	(+2,-37) 20
106.7			1.07	0.90	1.10				0.94	1.00				1.04
110.5			0.96	1.06	1.01				1.01	0.99				0.97
114.5			1.01	0.97	1.08	0.99	0.97	1.02	1.00	0.99	1.00	0.98	1.03	1.04
118.5			1.07	0.99	1.01				1.05	1.04				1.07
122.2			0.93	1.00	1.06				0.98	1.00				1.05
125.5			1.01	1.03	1.03				1.02	1.01				1.02
128.5			1.03	1.03	1.05				1.02	1.05				1.07
131.5	0.98	0.98	1.02	1.05	1.07	1.04	1.05	1.04	0.98	1.02	1.00	1.01	0.97	1.08
134.5			1.04	1.08	1.08				1.02	1.05				1.06
137.5			1.03	1.01	1.01				1.03	1.09				1.02
141.2			1.00	1.04	1.02				1.02	1.04				1.02
145.5			1.01	1.02	1.07	1.03	1.01	1.01	1.03	1.01	1.00	1.02	1.06	1.01
149.5			1.03	1.05	1.01				0.98	0.99				0.99
153.2			1.01	1.04	1.11				1.03	0.98				1.05

REFERENCES

[1] "MCNP – A General Monte Carlo N-Particle Transport Code, Version 4B", J.F. Briesmeister, ed., Report LA-12625-M, Los Alamos National Laboratory, March 1997.

[2] A. Hogenbirk, "EJ2-MCNPlib – Contents of the JEF2.2 Based Neutron Cross-Section Library for MCNP4A", Report ECN-I--95-017, Netherlands Energy Research Foundation ECN, May 1995.

[3] L. Leenders, "LWR-PVS Benchmark Experiment VENUS-3", FCP/VEN/01, SCK•CEN, Mol, Belgium, September 1988.

7.0 Authors: A. Haghighat[1], G. Sjoden[2] and H. Aït Abderrahim[3]

Organisation: [1]Penn State University
Nuclear Engineering Program
231 Sackett Building
University Park, PA 16802

[2]USAF Academy
Dept. of Mathematical Sciences
USAF Academy, CO 80840

[3]SCK•CEN
Fuel Research Unit
Boeretang 200
2400 Mol, Belgium

7.1 Transport method and modelling assumptions

For this benchmark, we use the PENTRAN (Parallel Environment Neutral-Particle TRANsport) code system. This code system includes PENTRAN, which is a 3-D Cartesian parallel S_N code [1], the PENMSH [2] and PENINP [3] codes, which are pre-processing codes, and the PENDATA [4] and PENPRL [5] codes, which are post-processing codes. PENMSH is a 3-D Cartesian-based mesh generator, PENINP automatically generates a PENTRAN input file using PENMSH output files, PENDATA gathers flux distributions from output files generated in a parallel environment, and PENPRL determines flux values at arbitrary points using a 3-D linear interpolation approach.

Model development

Using PENMSH, a 3-D discrete model is developed. This model represents a quadrant of the VENUS-3 facility with a radial size of 65.573 cm × 65.573 cm and an axial size of 70 cm. Axially, it represents the core (50 cm height) and the upper and lower reflectors (10 cm height each). Radially, it extends to the pressure vessel.

Based on the PENTRAN meshing methodology, using PENMSH, we have partitioned the physical model into 196 coarse meshes including four axial and 7×7 radial meshes per axial mesh. These coarse meshes are partitioned with different grid densities, resulting in a total of 84 784 fine meshes. Figure 1 shows the mesh (material) distribution for the first three axial coarse meshes corresponding to the lower reflector, lower half of the core and upper half of the code. The fourth (top) axial coarse mesh (not shown) represents the top reflector, which is the same as the first (lowest) axial coarse mesh.

Quadrature set

An S_8 level-symmetric quadrature set is used.

Differencing scheme

PENTRAN has an adaptive differencing strategy [1] that includes the linear diamond, directional theta-weighted (DTW) [6] and exponential directional weighted (EDW) [7] schemes. For this simulation, the code automatically used either DTW or EDW depending on the flux gradient. (The weight parameter for the upgrade from DTW to EDW is 0.96.) To improve the accuracy of flux distribution across the coarse meshes with different grid densities, PENTRAN uses the Taylor Projection Mesh Coupling (TPMC) algorithm [8], which performs a linear interpolation for projection of the fluxes at the interfaces of the coarse meshes.

Acceleration

For this simulation, we have used only the "system rebalance" method. We are planning to examine the simplified multi-grid scheme [9]. Obviously, this only affects the computational time.

Parallel parameters

PENTRAN is capable of performing full phase space (space, energy and angle) domain decomposition. For this modelling, we consider four spatial and eight angular sub-domains processed on 32 processors of the DOD IBM SP2 computer (see Section 7.5). Further studies are underway to examine other decomposition strategies with different numbers of processors.

7.2 Transport cross-sections

Twenty-six group, P_3, cross-sections were prepared for eight material mixtures using the BUGLE-96 library. This library includes 47 neutron groups and 20 gamma groups. The eight mixtures are: i) water; ii) inner and outer baffles; iii) 4.0% enriched fuel rods, iv) 3.3% enriched fuel rods, v) the stainless steel region of the partial length assemblies; vi) neutron pad; vii) bottom and top reflectors; and viii) Pyrex rods.

7.3 Neutron source

The three-dimensional relative source distribution (with 30×30 radial and 14 axial meshes) prepared by the OECD is projected onto the x-y-z mesh (described in Section 7.2), using the PENMSH code. For this projection, PENMSH uses a nearest neighbour approach in the x-y plane and a linear average along the z-axis. The original source distribution is given for a variable mesh distribution axially, while we have projected the source onto a uniform fine-mesh interval. The use of the uniform mesh may introduce a few per cent variation in the flux values at the top and bottom of the core. This issue is being investigated further.

For the spectrum, ENDF/B-VI ^{235}U spectrum is collapsed based on the 47-group BUGLE-96 energy group structure. Table 1 gives the 26-group spectrum used for this calculation. Based on a total fission source of 1.375×10^{12} (fission neutrons/sec/quadrant), the flux distribution is normalised. Using a reference measured fission rate of 5.652×10^{12} (fission/sec/quadrant), this total fission source is determined and an average number of neutrons per fission ν of 2.43.

7.4 Response functions and fission averaged data

Reaction cross-sections for Ni(n,p), In(n,n′) and Al(n,α) were obtained from the BUGLE-96 library. The 26-group DPA cross-sections are obtained from the 56-group ELXSIR library. Table 2 gives the DPA cross-sections. Table 3 gives the averaged reaction cross-sections for the three reactions.

7.5 Comments/special references

Wall-clock time and flux distribution

This transport calculation (84 784 spatial meshes, 26 groups, P_3 anisotropic scattering, and an S_8 quadrature set) was performed on 32 processors of the DoD IBM SP2 in one hour and forty minutes. As a sample, Figure 2 shows the flux distribution for Group 1. This figure clearly demonstrates the effect of partial length assemblies that result in an asymmetric flux distribution.

For further information, you may consult http://gracie.psu.edu/~haghigha/venus3.html.

SP2 computer

For this work, we used the IBM SP2 (“Osprey”) at the DoD Major Shared Resource Centre at CEWES (Waterways Experiment Station, US Army Corps of Engineers, Vicksburg, Mississippi). All nodes are the “wide” SP2 nodes with 1 GB memory each and a clock-cycle of 135 MHz. For further information on Osprey, see http://www.wes.hpc.mil/hardware.

Ongoing studies

We are examining other domain decomposition strategies on different numbers of processors. Further, we are estimating the effect of a more accurate representation of the axial distribution of the source.

Acknowledgements

A major portion of this work by A. Haghighat was performed during his sabbatical leave at the SCK•CEN, Mol, Belgium. The first and second authors express appreciation for the SP2 time awarded by the Department of Defense (DoD) High Performance Computing and the Major Shared Resource Centres at ASC and CEWES.

REFERENCES

[1] G.E. Sjoden and A. Haghighat, "PENTRAN – Parallel Environment Neutral-Particle TRANsport Version 4.33", Manual, Nuclear Engineering Program, Penn State University, University Park, Sept. 1996.

G.E. Sjoden and A. Haghighat, "PENTRAN – A 3-D Cartesian Parallel S_N Code with Angular, Energy, and Spatial Decomposition", Proceedings of the Joint International Conference on Mathematical Methods and Supercomputing in Nuclear Applications, Vol. II, 1267-1276, Saratoga Springs, NY, 6-10 Oct. 1997.

[2] A. Haghighat, "PENMSH Ver. 2, A 3-D Cartesian Mesh Generator", Manual, Nuclear Engineering Program, Penn State University, University Park, Dec. 1998.

[3] A. Haghighat, "PENINP, A Code for Automatic Preparation of PENTRAN Input", Manual, Nuclear Engineering Program, Penn State University, University Park, August 1998.

[4] G.E. Sjoden, "PENDATA, A Code for Gathering Flux Distributions from PENTRAN Parallel Outputs", Nov. 1996.

[5] A. Haghighat, "PENPRL, A Code for Evaluating Flux Values at any Arbitrary Position Using a 3-D Linear Interpolation", Internal Report, Nuclear Engineering Program, Penn State University, Nov. 1998.

[6] B. Petrovic and A. Haghighat, "New Directional θ-Weighted S_N Differencing Scheme and Reduction of Estimated Pressure Vessel Fluence Uncertainty", *Reactor Dosimetry*, H. Abderrahim and H. Nolthenius, eds., World Scientific Publishing Co., March 1998.

[7] G.E. Sjoden and A. Haghighat, "The Exponential Directional Weighted (EDW) S_N Differencing Scheme in 3-D Cartesian Geometry", Proceedings of the Joint International Conference on Mathematical Methods and Supercomputing in Nuclear Applications, Vol. I, 553-562, Saratoga Springs, NY, 6-10 Oct. 1997.

[8] G.E. Sjoden and A. Haghighat, "Taylor Projection Mesh Coupling Between 3-D Discontinuous Grids for S_N", *Trans. Am. Nucl. Soc*., Vol. 74, 178-179, June 1996.

[9] G.E. Sjoden and A. Haghighat, "Simplified Multigrid Acceleration in the PENTRAN 3-D Parallel Code", *Trans. Am. Nucl. Soc*., Vol. 75, 152-154, Nov. 1996.

Table 1. Source spectrum for the VENUS-3 simulation

Group number	Average energy (eV)	Spectrum
1	0.158E+08	4.07795E-05
2	0.132E+08	1.76675E-04
3	0.111E+08	1.06617E-03
4	0.930E+07	2.52880E-03
5	0.801E+07	5.72671E-03
6	0.674E+07	1.64209E-02
7	0.552E+07	3.14454E-02
8	0.432E+07	8.24265E-02
9	0.335E+07	7.71631E-02
10	0.287E+07	4.36253E-02
11	0.260E+07	4.57588E-02
12	0.242E+07	1.96213E-02
13	0.236E+07	3.80720E-03
14	0.229E+07	2.38459E-02
15	0.208E+07	7.16329E-02
16	0.179E+07	7.01179E-02
17	0.150E+07	8.82348E-02
18	0.118E+07	1.14124E-01
19	0.912E+06	6.27792E-02
20	0.782E+06	2.72309E-02
21	0.675E+06	4.68272E-02
22	0.553E+06	3.76472E-02
23	0.433E+06	4.22244E-02
24	0.333E+06	2.19475E-02
25	0.240E+06	3.14420E-02
26	0.147E+06	1.65354E-02

Table 2. DPA cross-sections obtained from the ELXSIR library

Group number	Average energy (eV)	Cross-section (barn)
1	0.158E+08	0.292E+04
2	0.132E+08	0.268E+04
3	0.111E+08	0.244E+04
4	0.930E+07	0.221E+04
5	0.801E+07	0.209E+04
6	0.674E+07	0.195E+04
7	0.552E+07	0.179E+04
8	0.432E+07	0.159E+04
9	0.335E+07	0.137E+04
10	0.287E+07	0.127E+04
11	0.260E+07	0.129E+04
12	0.242E+07	0.117E+04
13	0.236E+07	0.110E+04
14	0.229E+07	0.104E+04
15	0.208E+07	0.105E+04
16	0.179E+07	0.791E+03
17	0.150E+07	0.823E+03
18	0.118E+07	0.579E+03
19	0.912E+06	0.330E+03
20	0.782E+06	0.560E+03
21	0.675E+06	0.352E+03
22	0.553E+06	0.293E+03
23	0.433E+06	0.392E+03
24	0.333E+06	0.206E+03
25	0.240E+06	0.203E+03
26	0.147E+06	0.141E+03

Table 3. Fission spectrum weighted averaged response cross-sections

Reaction	Average cross-section (barn)
^{58}Ni(n,p)	0.1079
^{115}In(n,n′)	0.1793
^{27}Al(n,α)	0.7765E-03

Figure 1. Mesh distribution for the VENUS-3 model

Purple = water, yellow = stainless steel, dark green = 4.% enriched fuel, light green = 3.3% enriched fuel, brown = stainless steel (partial length assembly), red = bottom reflector, dark red = stainless steel (neutron pad)

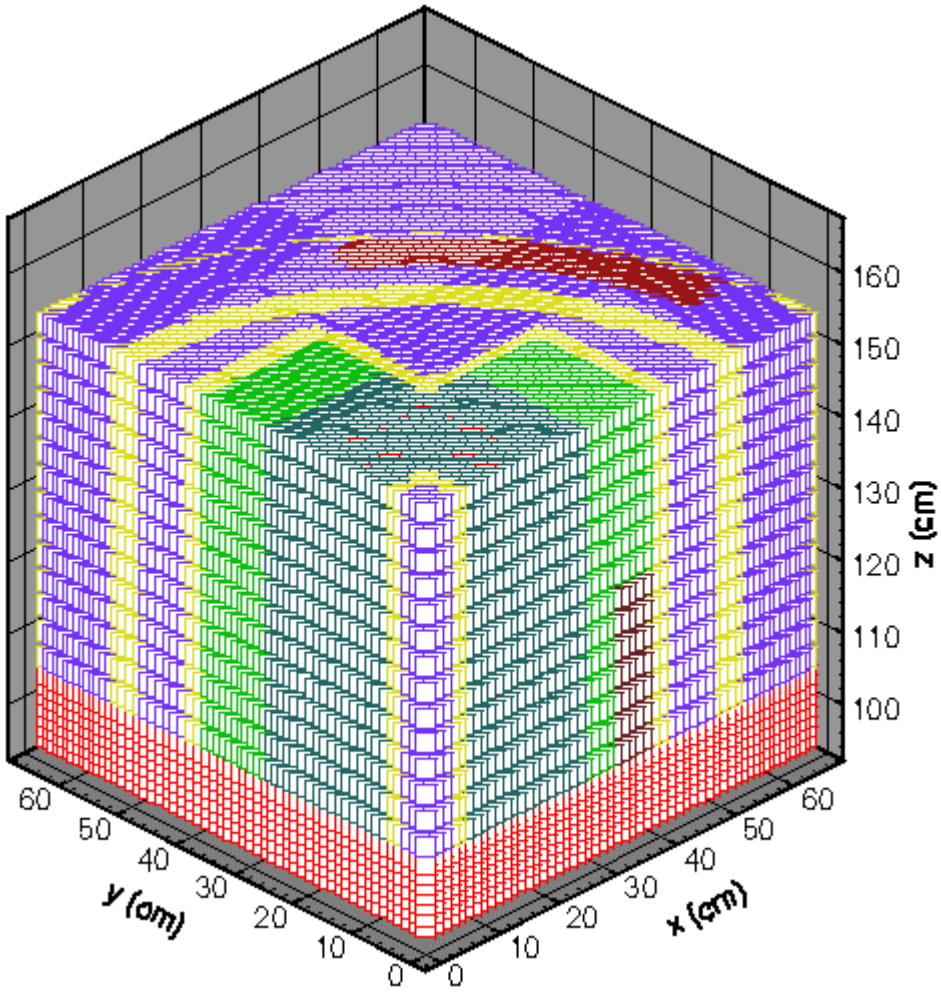

Figure 2. Group 1 flux distribution projected on the spatial mesh

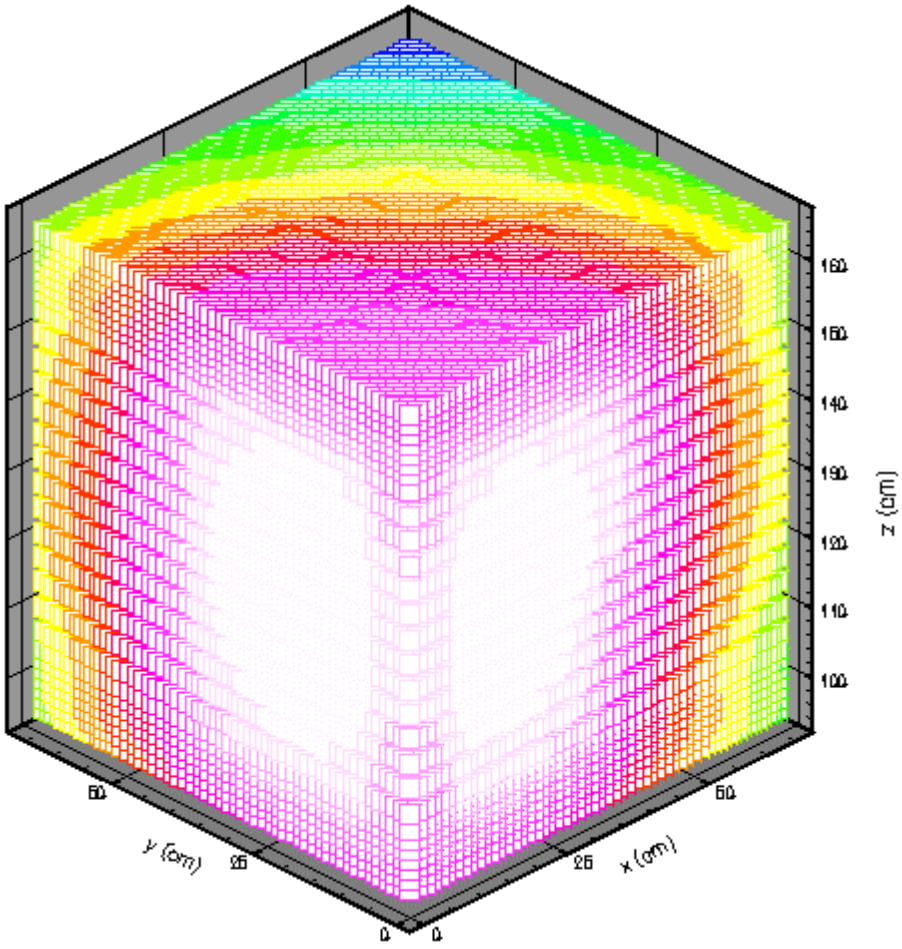

This appendix is based on the report "Analysis of the VENUS 3 Experiments" (August 1989, NUREG/CR-5338, ORNL/TM-11106) prepared by R.E. Maerker.

8.0 Author: R.E. Maerker

Organisation: Oak Ridge National Laboratory
USA

8.1 Transport method and modelling assumptions

The flux superposition synthesis model was used to estimate neutron transport in 3-D by combining the results of several lower dimensional calculations. For lower dimensional calculations, 2-D DOT 4 and 1-D ANISN codes were used. The X-Y geometry was set up using the variable mesh option available in 2-D discrete ordinates transport code DOT 4: 65 X intervals and between 36 and 101 Y intervals. The X-Z description employed a fixed mesh of 77 Z intervals along with the previously established 65 X intervals. The X geometry was used in ANISN, a 1-D discrete ordinates transport code, rather than in the 1-D mode available in DOT 4.

DOT 4: S_6P_3
ANISN: S_8P_3

8.2 Transport cross-sections

Cross-sections used in the transport calculations as well as in the calculation of the dosimetry responses were based on the ELXSIR library which is part of the LEPRICON system. The iron cross-sections were based on Mod 3 of ENDF/B-V. Flux calculations were extended down through group 38 (0.098 MeV) which is adequate to cover the range of responses for all dosimetry anticipated.

8.3 Neutron source

Both measured and interpolated source distribution data were used to produce a complete pin-by-pin radial distribution at two levels (114.05 cm and 145.5 cm) and a complete pin-by-pin radial distribution at all 14 levels between 105-155 cm for all pin locations in the west-by-south-west octant of the core lying to the left of the 45° direction. Further interpolation had to be performed at times by ORNL to cover some locations in the left half of the bottom arm and in the core interior that lie to the right of this direction. It is assumed that the source distribution in the lower left quadrant of the core is identical to that in each of the remaining quadrants, i.e. any source perturbations caused by the core barrel and neutron pad are neglected.

8.4 Response functions and fission averaged data

Dosimeter reaction	$^{58}Ni(n,p)^{58}Co$	$^{115}In(n,n')^{115m}In$	$^{27}Al(n,\alpha)^{24}Na$
^{235}U fission spectrum averaged dosimeter cross-section (mbarn)	108.5	190.3	0.706

8.5 Comments/special references

LIST OF CONTRIBUTORS

Analysis of results	*Secretariat*
G. Hehn, IKE (Germany) B.C. Na, OECD/NEA (France)	B.C. Na, OECD/NEA (France)

Benchmark participants

VENUS-1

J. Koban, Siemens (Germany)	R. van der Stad, NRG (The Netherlands)
H.Aït Abderrahim, SCK•CEN (Belgium)	J.M. Paratte, PSI (Switzerland)
F. Wasastjerna, VTT/ENE (Finland)	B.J. Moon, KOPEC (Korea)
G. Hehn, IKE (Germany)	H.R. Hwang, KOPEC (Korea)
A. Sohn, IKE (Germany)	M. Suzuki, JAERI (Japan)
M. Mattes, IKE (Germany)	K. Kosako, SAEI (Japan)
G. Pfister, IKE (Germany)	Y. Sakamoto, JAERI (Japan)
M. Pescarini, ENEA (Italy)	A.F. Albornoz, CAB (Argentina)
M.G. Borgia, ENEA (Italy)	E.M. Lopasso, CAB (Argentina)
R. Orsi, ENEA (Italy)	

VENUS-3

I. Kodeli (consultant), NEA (France)	A. Sohn, IKE (Germany)
J.M. Perlado, DENIM (Spain)	M. Mattes, IKE (Germany)
J. Marián, DENIM (Spain)	G. Pfister, IKE (Germany)
J. García Sanz, DENIM (Spain)	R. van der Stad, NRG (The Netherlands)
B.J. Moon, KOPEC (Korea)	A. Hogenbirk, NRG (The Netherlands)
H.R. Hwang, KOPEC (Korea)	A. Haghighat, PSU (USA)
W. Hofmann, Siemens (Germany)	G. Sjoden, USAFA (USA)
J. Koban, Siemens (Germany)	H. Aït Abderrahim, SCK•CEN (Belgium)
G. Hehn, IKE (Germany)	R.E. Maerker, ORNL (USA)